NASA CONTRACTOR REPORT

NASA CR-1230

NASA CR-123

$C.1$

ANALYTICAL AND EXPERIMENTAL STUDY OF THE DYNAMICS OF A SINGLE-TUBE COUNTERFLOW BOILER

by H. L. Hess, J. R. Hooper, and S. L. Organ

ANALYTICAL AND EXPERIMENTAL STUDY OF THE DYNAMICS

OF A SINGLE-TUBE COUNTERFLOW BOILER

By H. L. Hess, J. R. Hooper, and S. L. Organ

FOREWORD

This report was prepared by the Pratt & Whitney Aircraft Division of United Aircraft Corporation, East Hartford, Connecticut, to describe work conducted during the period from June 28, 1966 to August 27, 1967 in fulfillment of Contract NAS3-9420, A Boiler Dynamics Investigation. This contract consisted of a study of the transient response characteristics of a single-tube counterflow boiler. This boiler was designed to simulate one of the tubes of a typical boiler for a Rankine-cycle space powerplant.

Both analytical and experimental investigations were conducted. The experimental investigations were performed using a facility designed and built by Pratt & Whitney Aircraft which used water as the working fluid and was designed to simulate many fluid flow and heat transfer aspects of a space power conversion system.

The analytical work described in this report was performed by H. L. Hess, J. R. Hooper, and D. Reitsma, while the experimental work was performed by J. R. Hooper and S. E. Organ. Technical management was provided by H. G. Hurrell and technical assistance by A. A. Schoenberg and P. A. Thollot of the Lewis Research Center, National Aeronautics and Space Administration.

ABSTRACT

An analytical and experimental study of a single-tube counterflow boiler was conducted. The boiler geometry simulated one of the tubes of a typical boiler for a Rankine-cycle space powerplant.

Steady-state, frequency-response, and step-response tests were conducted using water as the working fluid. The frequency-response and step-response tests were conducted by perturbing the boiling-fluid flow rate at the inlet to the boiler. Experimental transfer functions were obtained from the frequency-response test results.

A linearized analysis of the boiler dynamics was performed to derive a theoretical expression for the boiling-fluid exit pressure transfer function. A comparison was made between the theoretical and experimental transfer functions.

TABLE OF CONTENTS

TABLE OF CONTENTS (Cont'd)

LIST OF FIGURES

LIST OF FIGURES (Cont'd)

LIST OF TABLES

I. SUMMARY

An experimental and analytical investigation was conducted to study the steady-state and dynamic characteristics of a single-tube counterflow boiler. The purpose of the investigation was to determine the factors influencing the dynamic stability of this type of boiler and to provide information useful for developing dynamic stability criteria. The boiler was designed to simulate one tube of a typical Rankine-cycle space powerplant boiler. It was constructed and tested under this contract. The tests were performed on an experimental facility which simulated a nuclear Rankine-cycle power system. Water was employed as the working fluid in all three loops of the test system to facilitate testing. Three types of tests were performed: steady-state, frequency-response, and step-response. These tests showed how the steady-state and dynamic performance of the boiler varied as a function of the primary system variables. The steady-state tests also provided information useful in formulating an analysis of the boiler dynamics, while the frequency-response tests provided experimental data with which to evaluate the theoretical predictions of this analysis.

The experimental investigation indicated that the factors having strong influence on the boiler dynamics are reflected in the conditions of the boiling fluid at the boiler exit. During the testing three types of exit conditions were observed:

1) Dry superheated vapor
2) A nonequilibrium mist containing superheated vapor and liquid droplets,
3) A mist containing saturated vapor and liquid droplets.

In general, as the exit conditions changed in the direction from dry superheated vapor to wet saturated conditions, the result was a lower amplitude and a greater phase lag in boiler pressure and temperature responses, when perturbed at a given frequency by the boiling-fluid flow rate. General conclusions relating this frequency-response characteristic to dynamic stability were precluded by the presence of several pronounced resonances. The frequency-response tests did indicate, however, that instabilities arising from dynamic interactions between the boiler and the feed system could present a potential problem. This resulted from the fact that the amplitude of the frequency response of the boiler inlet pressure was relatively large at the 180-degree phase lag point for several test conditions. One such unstable condition was observed during the testing. In addition a second unstable condition was also observed during the testing. This instability can probably be attributed to dynamic interactions occurring within the boiler itself.

A linearized analysis of the boiler dynamics was performed. The result was an expression for the transfer function between the exit pressure and the inlet flow rate of the boiling fluid. This expression indicated that there were at least 22 different parameters that were significant in describing the dynamic behavior of the boiler. Agreement was found between the trends displayed by the experimental data and the theoretical predictions of the analysis. However, close

quantitative agreement between the theory and the experimental data, particularly in the frequency range where 180-degree phase lag occurs, was not obtained. Further development of the analysis appears desirable in order to develop a more useful analytical tool for predicting the stability of the dynamic interactions between the boiler and feed system.

II. INTRODUCTION

Instabilities in boiling systems are very common and have been observed for many years. Unstable conditions in a Rankine-cycle powerplant can seriously impair the performance of the system and can, in some cases, cause actual destruction of equipment. Nuclear Rankine-cycle space powerplants such as SNAP-8, must operate continuously for 10,000 hours in deep space without a failure. As a consequence, the detrimental effects of unstable boiler operation cannot be tolerated by such a system. In the development of these powerplants, it is therefore desirable to be able to predict the stability of the boiler in the early design stages. This requires a fundamental understanding of both the causes of boiler instabilities and the physical processes involved.

A review of the literature on boiler stability, Reference 1*, indicates that many different types of instabilities have been observed. In general, these instabilities are very complex in nature and very difficult to analyze. Reference 1 indicates that the task of fully understanding boiler instabilities is still in its early stages.

An important class of boiler instabilities results from the dynamic characteristics of the boiler. These instabilities can result from dynamic interactions between the boiler and other components of the powerplant such as the boiler feed system. These instabilities can also result from dynamic interactions between the thermal and hydraulic processes occuring within the boiler itself. The work presented in this report studied the dynamic characteristics of a boiler having a geometry typical of the type employed in Rankine-cycle space powerplants. The purpose of the study was to provide fundamental information that would be employed in the development of methods for predicting the dynamic stability of this type of boiler.

The work performed under this contract followed both experimental and analytical approaches. A single-tube counterflow boiler employing a flow geometry which simulated one of the tubes of a typical space powerplant boiler was designed and constructed. The boiler was tested on an experimental facility which simulated a nuclear Rankine-cycle system. Water was used as the working fluid to facilitate testing. Three types of tests were performed: steady-state, frequency-response, and step-response.

The use of frequency-response techniques is based on the hypothesis that for small-amplitude disturbances the boiler, which is a non-linear device, can be treated as a linear element. The dynamics of the boiler can then be studied in

---

*See Page 92 for numbered list of references

terms of the manner in which it responds to small-amplitude perturbations imposed on the controllable variables. Since most boiler instabilities manifest themselves in the form of hydraulic disturbances, the boiling-fluid flow rate at the inlet to the boiler was selected as the variable to be perturbed. Frequency-response techniques have previously been employed successfully in the study of once-through boilers. These techniques were used in studies conducted at the NASA Lewis Research Center [2,3].

In the analytical approach a simplified linearized analysis of the dynamics of the boiler was performed. The result was a theoretical expression for the transfer function between the exit pressure and the inlet flow rate of the boiling fluid. A comparison was made between the frequency response predicted by this theoretical expression and the experimental frequency-response test results.

III.   TEST APPARATUS AND OPERATING PROCEDURES

The tests were conducted on a highly-instrumented boiler designed to simulate a single tube of a typical boiler for a nuclear Rankine-cycle space powerplant. The boiler was of a counterflow configuration and employed swirl flow-inducing devices typical of space powerplant boilers. However, unlike space power-plant boilers, the test boiler was of a single-tube construction. This was done to eliminate the type of boiler instabilities that result from multitube configurations.

The boiler was operated as part of a test system designed to simulate a nuclear Rankine-cycle powerplant. Water rather than a liquid metal was used as the working fluid to facilitate testing. This test system is a modified form of the transient simulator used in previous NASA contracts and described in Reference 4.

This section contains a detailed description of the boiler and its internal instrumentation, a description of the test rig including its instrumentation and controls, and a discussion of the operating procedures employed during both the steady-state and the dynamic tests.

A.   Description of Boiler

The construction of the boiler is shown in Figure 1. The boiler employed a single-tube counterflow configuration. The boiler tube and shell were fabricated from dimensionally selected 316 stainless-steel tubing. The boiler tube had an outside diameter of 0.625 inch and a wall thickness of 0.035 inch, while the boiler shell had an outside diameter of 0.875 inch and a wall thickness of 0.049 inch. The overall heat-transfer length was 10 feet.

Spacers on the boiler tube allowed it to be accurately centered in the shell during assembly. Machined fittings were employed at each end of the boiler. At the boiling-fluid exit both boiler and shell tubes were brazed to the fitting. At the inlet end the shell was brazed to the fitting, but the boiler tube was sealed with an O-ring packing nut arrangement which allowed for expansion and contraction of the boiler tube during operation.

The heating fluid was pressurized water which flowed through the annular passage between the boiler tube and the shell. Water was also used as the boiling fluid. As the boiling fluid entered the boiler tube, a swirl-flow pattern was induced by a close-fitting spirally-machined plug inserted into the inlet end of the boiler tube. The purpose of the swirl-flow pattern was to increase the heat-transfer coefficient of the boiling fluid. After the boiling fluid left the plug, a spirally-wound wire brazed inside the boiler tube maintained the swirl-flow pattern over the remaining length of the boiler.

The boiler employed extensive internal instrumentation to permit measurement of the axial temperature profiles of both the heating and boiling fluids. Fine wire thermocouples were mounted in the heating-fluid passage, the spiral-flow passage formed between the machined plug and the boiler tube, and along the tube axis downstream of the plug. The thermocouples used to measure the boiling-fluid temperature downstream of the plug were mounted on a probe of 0.250 inch outside diameter which was spaced concentrically with the axis of the boiler tube.

The positions of the spirally-machined plug and the thermocouple probe inside the boiler are shown in Figure 1. The following paragraphs present a more detailed description of the plug, the probe, and the boiler instrumentation. A discussion of thermal and hydraulic calculations employed in the design of this boiler is presented in Appendix 1.

1. Spiralled Plug Insert

A photograph of the spirally-machined plug insert is shown in Figure 2. The plug was fabricated from 316 stainless-steel stock. The plug length was 2.15 feet while the pitch of the spiral was 0.4 inch. The width of the spiral thread was 0.040 inch. The tolerance between the plug and the tube was held to within 0.002 inch to maintain a fit that would prevent leakage around the spiral thread.

A 0.310-inch passage was gun drilled through the spiralled-plug insert to carry the leads of the instrumentation. This passage was sealed at the downstream end by a cylindrical plug induction-brazed in place. This cylindrical plug was located one inch from the end of the passage to provide a centering recess for the thermocouple probe (see Figure 1). A tube of 0.375 inch outside diameter two feet long was brazed to the other end of the passage to act as a conduit for the instrumentation leads. An instrumentation junction block was attached to the end of this conduit as shown in Figure 2. Sealing between the conduit and the boiler tube was obtained by use of the heat exchanger tee shown in Figure 2. The heat exchanger tee also provided the inlet fitting for the boiling-fluid flow.

Instrumentation for the spiralled-plug insert consisted of eight thermocouples and a pressure tap. The thermocouples were positioned at equal lengths along the spiral path while the pressure tap was located near the downstream end of the insert. The holes drilled through the wall of the spiralled-plug insert to accommodate the thermocouples were inclined at an angle of 40 degrees from the axis of the insert, to avoid sharp bends that might break the thermocouple leads.

BOILING FLUID INLET

INSTRUMENTATION LEAD CONDUIT

HEAT EXCHANGER TEE

BRONZE PACKING NUT

END FITTING

"O" RING SEAL

PASSAGE TO CARRY INSTRUMENTATION LEADS

10 FT

2.16 FT.

HEATING FLUID EXIT

BOILER SHELL

BOILER PLUG INSERT

INDUCTION BRAZED PLUG

BOILER TUBE TO SHELL SPACER

0.067 SPIRALLY WOUND WIRE BRAZED TO BOILER TUBE I.D.

THERMOCOUPLE PROBE

THERMOCOUPLE PROBE TO BOILER TUBE SPACER

HEATING FLUID INLET

END FITTING

0.020 EXPOSED JUNCTION THERMOCOUPLE

BOILER TUBE

BOILING FLUID EXIT

HEAT EXCHANGER TEE

TABLE OF BOILER TUBE DIMENSIONS

BOILER SHELL 0.875"OD 0.049" WALL
BOILER TUBE 0.625"OD 0.035" WALL
BOILER PROBE 0.250"OD 0.049" WALL
INSTRUMENTATION LEAD CONDUIT
  0.375OD 0.035" WALL
HEATER LOOP INLET TO BOILER
  0.500"OD 0.049" WALL
HEATER LOOP EXIT FROM BOILER
  0.625"OD 0.049" WALL

Figure 1   Sectional View of Boiler

Preceding Page Blank

2. Thermocouple Probe

The thermocouple probe was a nine-foot length of 316 stainless-steel tubing with an outside diameter of 0.250 inch and a wall thickness of 0.049 inch. Five thermocouples were mounted along the length of the thermocouple probe in the manner shown in Figure 1. The thermocouple junctions protruded into the fluid stream while the thermocouple leads were conducted along the inside of the probe. The holes for the thermocouples were drilled at an angle of 40 degrees from the probe axis.

Spacers were brazed to the probe at two-foot intervals. These spacers insured that the probe would be centered inside the boiler tube. One end of the probe was braze sealed. This end fitted into the centering recess of the plug. The length of the probe that projected into the boiler was 7.85 feet. Sealing between the boiler tube and the probe was accomplished by using a heat exchanger tee. The heat exchanger tee also provided the exit fitting for the boiling-fluid flow.

3. Boiler Instrumentation

Instrumentation was provided to measure the internal temperature distribution of the heating fluid and the boiling fluid. Provision was also made to measure the pressure of the boiling fluid at one location inside the boiler. Temperatures inside the boiler were measured with 0.020-inch chromel-alumel sheathed thermocouples. The wire diameter of the thermocouple was 3-4 mils. Two types of immersion thermocouples were used: one type where the junction was sealed within the sheath, and another type where the junction was exposed directly to the fluid. The exposed type of thermocouple provided a much faster response to changes in temperature.

In the boiler shell there were 20 immersion thermocouples with sealed junctions to measure the temperature of the heating fluid. Thermocouple positions are presented in Table 1, Appendix 4. The immersion length of the thermocouples was 0.250 inch. The thermocouple junction was centered in the annular passage between the boiler tube and the shell. A stainless-steel sheath having an outside diameter of 0.050 inch extended from the shell to the junction block of the thermocouple to protect the thermocouples from damage. Brazing was used to secure the thermocouples in position.

In the boiler tube there were thirteen exposed junction thermocouples to measure the boiling fluid temperature. Eight were located in the plug and five in the thermocouple probe (see Table 1 for the exact locations). In the plug the thermocouple wire was bent along the contour of the spiral passage and centered in the passage. This provided sufficient immersion depth to eliminate conduction errors. The probe thermocouples were also bent in the direction

Preceding Page Blank

of the boiler axis for the same purpose. Because of the nature of the exposed junction thermocouples they could not be brazed in position. Instead, they were sealed and positioned with a high-temperature resin. The thermocouple leads were brought out through the probe and plug and attached to junction blocks welded to the ends of the conduit tubes. This method prevented unnecessary movement and subsequent leakage around the junctions. These thermocouples installed inside of the boiler were very effective in measuring temperature distributions of both fluids. The temperature distributions provided a clear indication of the processes occurring within the boiler as discussed in Section IV below.

A static-pressure tap was located near the downstream end of the spiralled-plug insert in an effort to measure the static pressure of the boiling fluid in this region. The tap was approximately 0.016 inch in diameter. Hypodermic tubing with an outside diameter of 0.020 inch was used to connect the tap with a fitting on the instrumentation junction block shown in Figure 2. A tube 0.250 inch in outside diameter was used to connect this fitting with a Heise Bourdon-tube gage located in the control room. This pressure tap, however, did not provide satisfactory measurements. It took such an extremely long time to respond to changes in the system pressure that it could not be employed even for steady-state measurements. This problem may have resulted from plugging of the hypodermic tubing or from the small inside diameter of the tubing itself.

B. Description of Test System

The test system was originally designed to simulate a nuclear Rankine-cycle space powerplant. It was composed of three separate fluid loops; the heater loop, the power loop, and an open coolant loop. Heat was added to the system by an electrical heater and removed from the system by the use of city water. The working fluid in all loops was water.

The test system was provided with controls that were capable both of holding the conditions of the steady-state tests within close tolerances, and imposing the perturbations required by the dynamic tests. The test system was also provided with instrumentation which had both the accuracy and the fast response required by the two types of tests.

Figure 3 is a photograph showing the boiler mounted on the test stand as well as some of the power-loop instrumentation. The test system is shown schematically in Figure 4 and is described in detail in the following paragraphs.

1. Description of Fluid Loops

Heater loop - This was a liquid loop which transferred energy from an electrical heat source to the boiler shell. Pressurization of the loop allowed

11
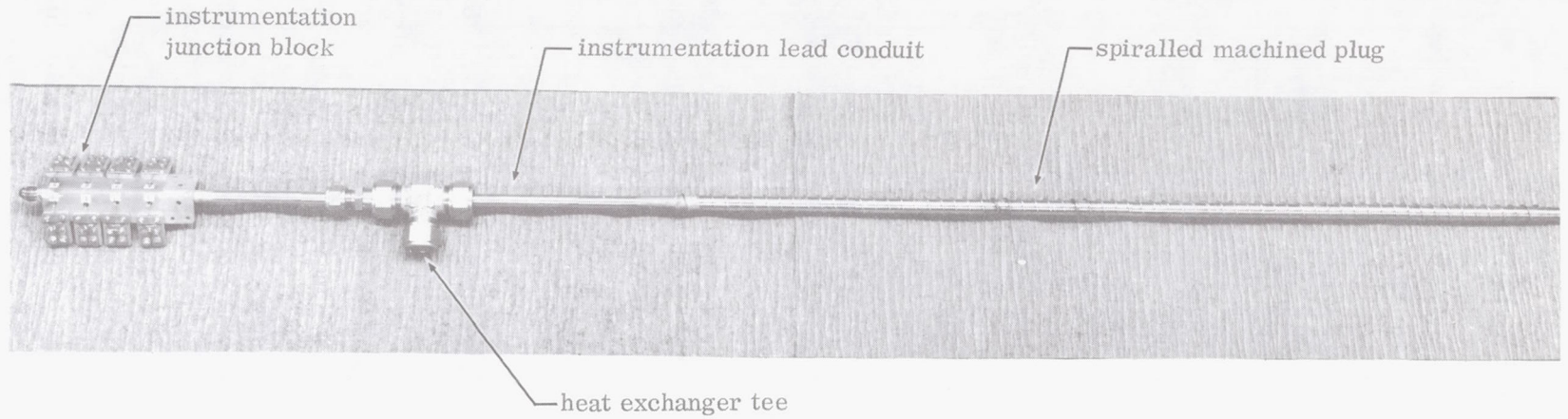
Figure 2   Photograph of Spiralled Plug Insert   X-23889
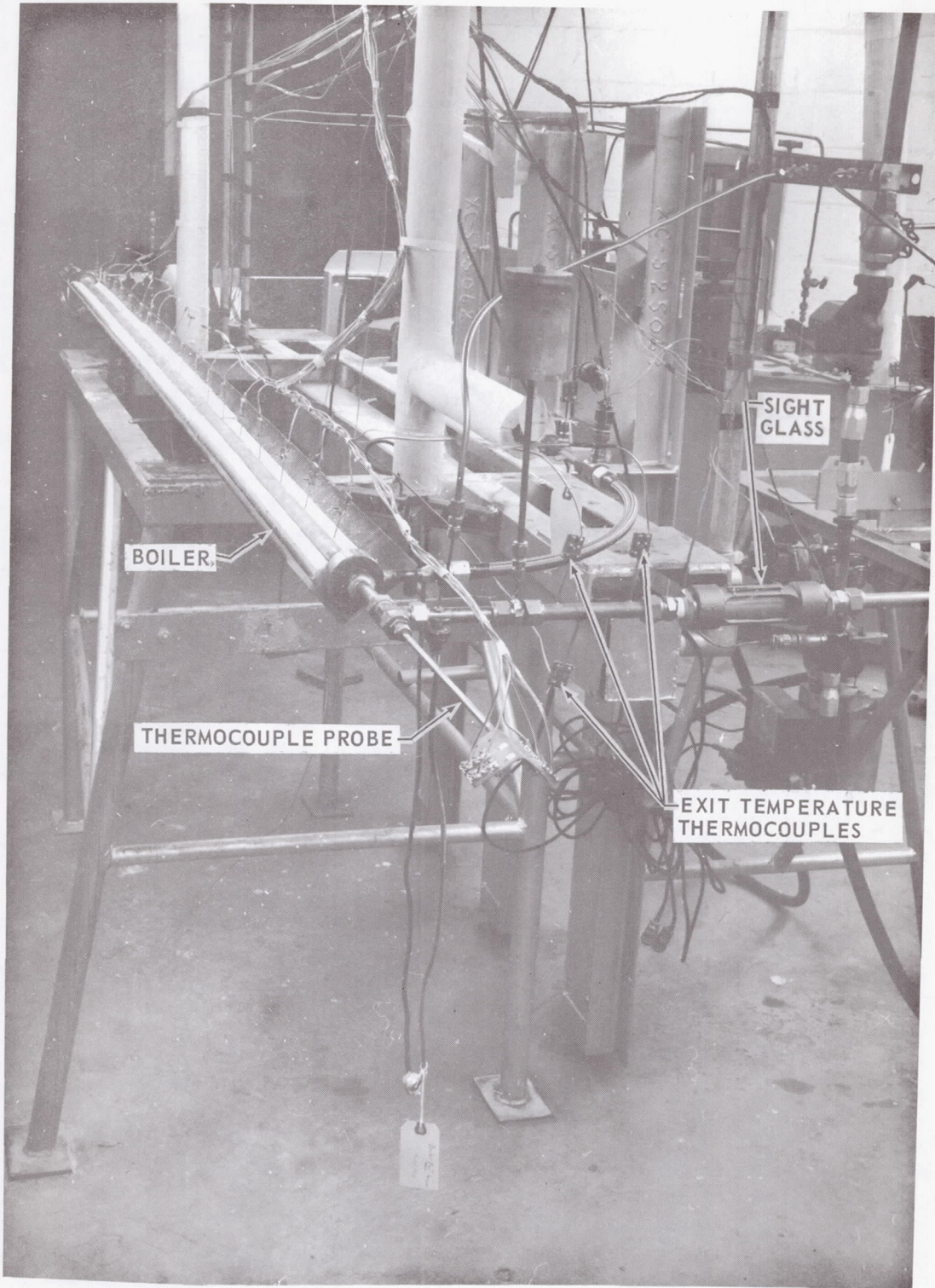
Figure 3   Photograph of Test System   X-23893
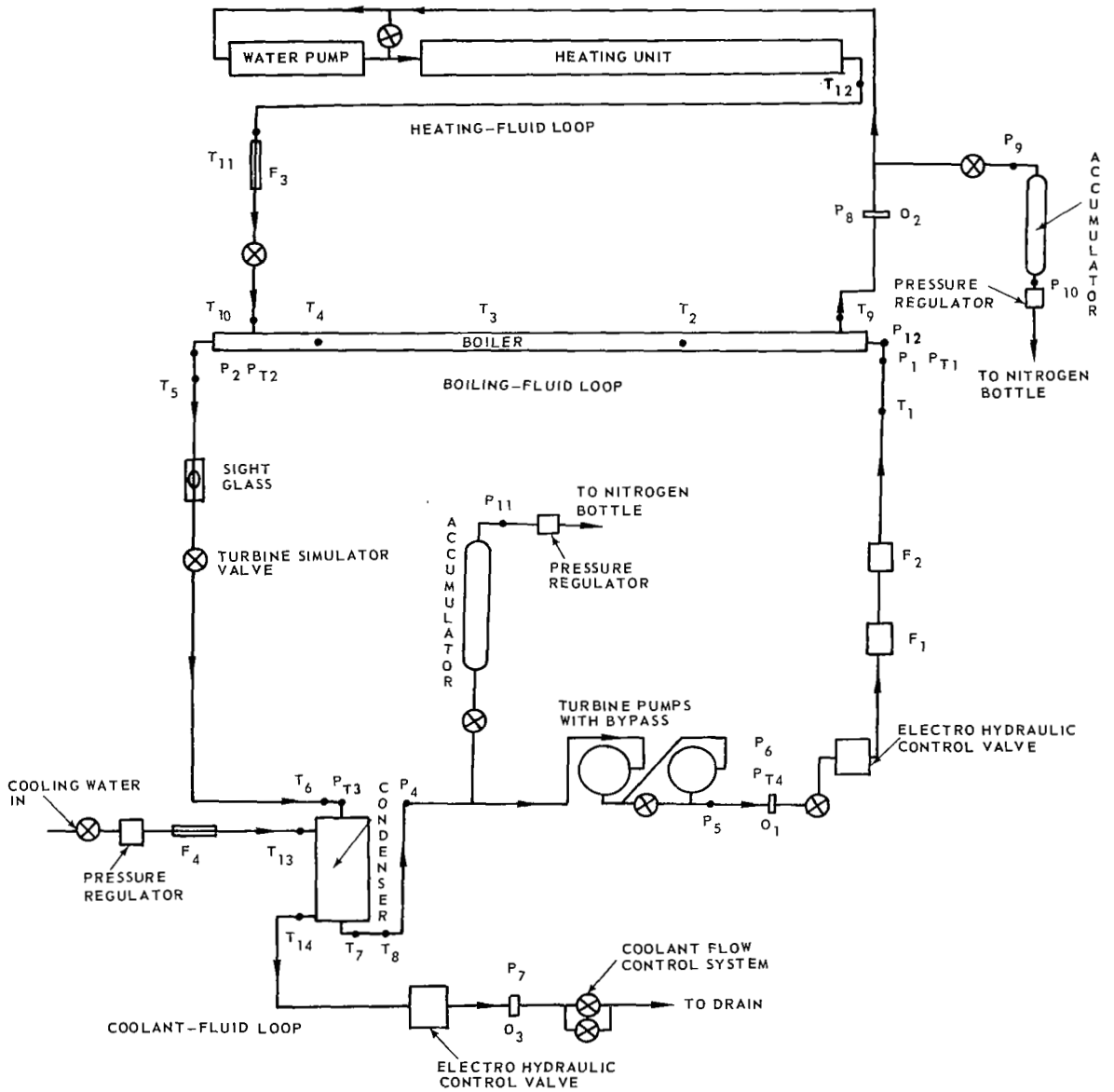
Figure 4 Schematic Diagram of Test System

temperatures of 450°F to be reached without vaporization of the fluid. The electrical heat source used is shown in Figure 5. It consisted of 19 calrods 0.496 inch in diameter and six feet long, distributed in circular patterns and encased in Schedule 40 stainless-steel pipe. The pumping power for the heater loop was provided by a Dean Brothers centrifugal pump. A bypass valve around the pump assisted in flow regulation.

Power Loop - This was a two-phase loop in which the boiling fluid was evaporated and recondensed. The fluid was vaporized in the boiler and then passed through a valve which simulated the choked-flow condition and pressure-drop characteristics of flow through a turbine. However, the valve extracted no energy from the system. The fluid then entered a condenser where it was condensed and subcooled. The condensed fluid was returned to the boiler through two Aurora Model B-4-7 turbine pumps connected in series. Flow control in this loop was maintained using a bypass around one of the pumps and an electrohydraulic valve. The bypass permitted control of the pressure-versus-flow characteristics of the pump system. The electrohydraulic valve permitted feedback control of the inlet flow to the boiler.

Coolant Loop - This was an open loop which extracted heat from the boiling fluid by coolant water flowing over the condenser tubes. The coolant water was supplied to this loop directly from the city water supply. The condenser was a single Ross RCF-7M300-8C8 heat exchanger mounted in a vertical position. Both the boiling fluid and the coolant fluid entered at the top of the unit. The boiling fluid flow was downward through 56 condensing tubes. Baffles in the coolant side directed the coolant flow across the condensing tubes. Boiler-inlet temperature was controlled by adjusting the coolant-loop flow rate.

   2. Rig Instrumentation

Rig instrumentation consisted of temperature, pressure, and flow-sensing devices. Thermocouples were used for temperature measurement; pressure transducers and Bourdon-tube gages for pressure measurements; and turbine-type flowmeters for flow measurements. All instrument locations are shown in the schematic diagram of Figure 4 and identified in Table 2. This table contains a description of each instrument, its accuracy and response time. The instrumentation employed in the dynamic testing was selected to have response times sufficiently fast to detect all significant effects.

Temperatures were measured with chromel-alumel sheathed thermocouples with sealed junctions. These thermocouples were installed with an immersion depth of 10-12 diameters to minimize measurement errors. All rig thermocouples were installed in duplicate. One permitted visual readings through a Brown model 156 readout potentiometer. The other was connected to the recording oscillograph through a thermocouple translator.

19 CALROD HEATER
ELEMENTS
0.496" DIA.

3.5" 3"

FLUID
OUT

2"

70"

HEATER LOOP
FLUID IN
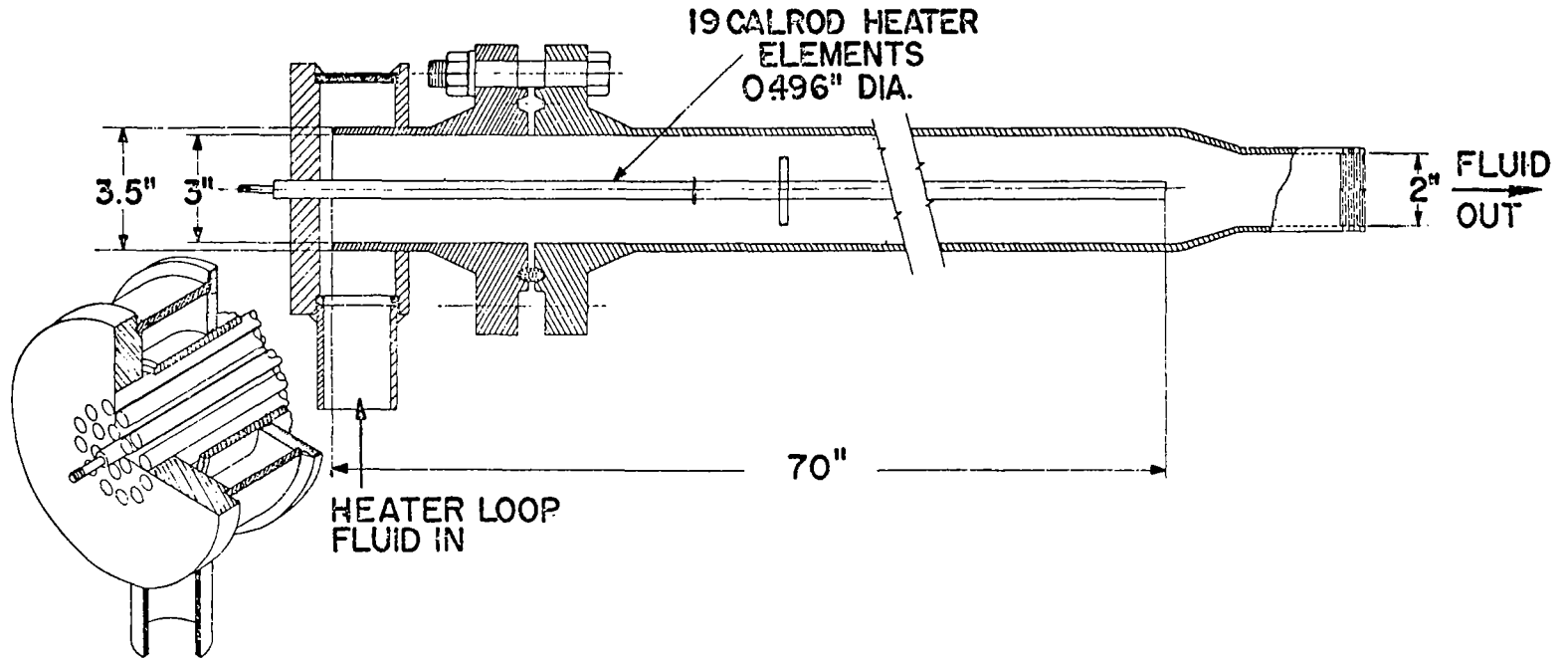
Figure 5   Calrod Heater

Measurements of the boiling-fluid pressure were made using both Bourdon-tube gages and strain-gage type pressure transducers. The Bourdon-tube gages were used for the steady-state measurements. The pressure at the inlet and exit to the boiler were made using Heise Bourdon-tube gages. These gages had an accuracy of ± 0.1 percent of full range and were mounted in the control room at the same height as the pressure taps to reduce gravitational effects. Due to the length of the lines from the pressure taps to the gages, valves were provided at the pressure taps to shut off these lines during the dynamic testing. This prevented these lines from acting as accumulators which might alter the system dynamics. All Bourdon-tube gages were calibrated periodically to insure their accuracy.

Pressure sensing during the dynamic tests was accomplished with strain-gage pressure transducers. The signal from the transducer was fed into preamplifiers which in turn were connected to the recording oscillograph. At the boiler exit the strain-gage face of the transducer was mounted flush with the boiler exit tube. This resulted in virtually no lag between the time a boiling-fluid pressure change occurred and the time it was sensed by the transducer. In mounting all other transducers, the length of line between the fluid and the strain-gage face was kept as short as rig mounting permitted, to maximize the response of the sensing unit.

Flow measurement in the power loop was taken with two Potter Model 60-4115 microflowmeters connected in series. One of these flowmeters provided the feedback signal for the electrohydraulic control valve. It also provided the signal source for the flowmeter frequency counter used to make visual readings during the steady-state tests. The second flowmeter was connected through a preamplifier to the recording oscillograph. Both flowmeters were calibrated over the operating flow range of the test system.

Turbine-type flowmeters were also used in the coolant and heater loops. Signals from these flowmeters were linked through a preamplifier to the recording oscillograph. In addition, these flowmeters were connected through a switching arrangement to a flowmeter frequency counter for visual readings. The switching arrangement allowed the flow in both loops to be monitored during rig operation. These flowmeters were calibrated in the operating range and corrected for temperature when necessary.

A Jacoby-Tarbox sight glass was mounted in the line between the boiler and the turbine simulator valve to permit visual inspection of the condition of the vapor leaving the boiler.

3. Control Systems

Control of flow, temperature, and pressure was necessary for operation of the rig. Hand valves and electrohydraulic valves were employed for flow control. Regulation of electrical power input to the heater and regulation of coolant flow provided the methods of temperature control. Pressures were regulated by the use of accumulators and the turbine simulator valve.

The flow rate in the heater loop was set by the bypass valve on the heater-loop pump. Fine adjustment was accomplished manually by the use of a Jenkins stainless-steel steam valve located at the heater-loop inlet to the boiler.

Flow in the power loop was controlled by an Annin electrohydraulic feedback control valve. The complete unit consisted of an Annin flow control valve, a hydraulic actuator with a Moog Model 73-167 servo valve, and an Annin electronic controller. Flow was set by adjusting a reference voltage. It was maintained by electronically comparing the reference to a feedback voltage produced by a turbine flowmeter upstream of the valve. Differences between these voltages resulted in an error signal. Changes in the valve position were then determined by the integral of the error signal over time. In the external control mode an external reference signal was fed into the controller. In the case of frequency-response tests, the external signal was generated by a Wavetek frequency generator. With this unit sinusoidal frequencies as low as 0.0015 cps could be fed into the controller.

The temperature of the boiling fluid at the inlet to the boiler was controlled by regulating the flow in the coolant loop. A feedback control system employing an electrohydraulic valve in the coolant loop was originally used to control this temperature. However, since this temperature responded very slowly to the system dynamics, it was found that adequate control could be obtained manually. This was done using a 0.5-inch gate valve in parallel with a 27-turn needle valve. A pressure regulator upstream of the flowmeter and condenser prevented pressure fluctuations due to city water demand changes.

The temperature of the heating fluid entering the boiler was controlled with a West Model JSB-6 controller which regulated the electrical power into the heater. This unit provided proportional control over a limited range of variation. It consisted of a photocell circuit connected to a meter reading the output of a thermocouple which was located in the exit line from the heater. Magnetic amplifiers increased the output of the photoelectric circuit to a large saturable-core reactor which directly controlled the power input to the calrods in the heater.

Pressure regulators on the heater loop and power loop controlled the system preload. System pressure level was varied by increasing or decreasing the nitrogen pressure to the accumulator bladders. The boiler exit pressure was set by changing the position of the turbine simulator valve.

C. Operation of Test System

The following paragraphs describe the operation of the test system in performing the steady-state, frequency-response, and step-response tests required under the contract. The discussion includes a description of the startup, test, and shutdown procedures for the different types of tests.

1. Steady-State Test Procedures

a. Startup

At the beginning of each week of testing, the heater and power loops were recharged with a fresh inventory of distilled deareated water to minimize the accumulation of contaminants and dissolved gasses in the working fluids.

At the beginning of each day of steady-state testing, the test system was started and the following nominal operating condition was established:

Nominal Operating Condition

boiling-fluid flow rate	45 lb/hr
boiling-fluid inlet temperature	140°F
boiling-fluid exit pressure	65 psia
heating-fluid flow rate	770 lb/hr
heating-fluid inlet temperature	410°F

Data was then recorded at this condition and compared with the results of previous tests at this same condition to determine if the boiler was performing properly.

b. Steady-State Tests

After the boiler performance at the nominal operating condition was checked, steady-state testing was initiated. These tests were performed at the 34 operating points presented in Table 3.

As can be seen in Table 3, each steady-state test condition was specified by constant values of the following primary variables: boiling-fluid flow rate W, boiling-fluid inlet temperature T_{in}, heating-fluid flow rate W_H, heating-fluid

inlet temperature $T_{H\,in}$, and either boiling-fluid exit pressure P_{out}, or the setting of the turbine simulator valve. The following tolerances were applied to these variables in holding a specific test condition.

boiling-fluid flow rate	±0.5 lb/hr
boiling-fluid inlet temperature	±4°F
boiling-fluid exit pressure	±0.5 psi
heating-fluid flow rate	±1.8%
heating-fluid inlet temperature	±1°F

After a test condition was established in the system, a period of approximately 30 minutes was taken to allow a steady state to be achieved. Data was then taken in the following manner. First a short oscillograph recording was made of the variables listed in Table 4. Then all temperature, pressure, and flow measurements were read manually. Finally a second oscillograph was made. A comparison between the two oscillograph recordings made it possible to determine if a steady state existed while the data was being read.

The following criteria were used in judging the acceptability of a test point:

1) Primary variables held within the specified tolerances,

2) Existence of steady state as indicated by the oscillograph recordings, and

3) System heat balances that checked within 7 percent.

c. Shutdown

After a series of steady-state tests was completed, the nominal operating conditions were re-established and the data checked to determine if the boiler performance had deteriorated during the course of the testing. Electric power to the heater was then cut while the fluids continued to be circulated through the loops until the system cooled off. At the end of each week of testing, the system was completely drained to permit preventive maintenance to be performed.

2. Dynamic Test Procedures

Dynamic testing included both frequency-response and step-response tests. These tests were performed at 21 operating conditions specified by the NASA project manager and presented in Table 5.

a. Startup

The startup procedures described for the transient tests were identical to those described above for the steady-state tests. After the boiler performance had been checked at the nominal operating condition, the operating condition was set for the transient tests and a period of approximately 30 minutes was allowed for a steady state to be achieved.

b. Step-Response Tests

Once steady state was achieved, the step-response tests were performed in the following manner. The boiling-fluid flow rate was suddenly increased by approximately 12 percent of its original value while the other primary variables were held constant. The system was then allowed to come to equilibrium. A continuous oscillograph recording was made of the variables listed in Table 4 during the initial step change, and for a period of approximately 30 seconds thereafter. Additional short oscillograph recordings were made at intervals of 1, 2, 3, 5 and 15 minutes until steady state had been achieved.

The system was brought back to the original operating condition. After steady state had been restored, the same procedure was repeated except that the boiling-fluid flow rate was suddenly decreased by 12 percent of its original value.

c. Frequency-Response Tests

After the step-response tests had been completed, the system was returned to the initial operating condition and frequency-response tests were initiated. The frequency-response tests were conducted by imposing a sinusoidal perturbation on the boiling-fluid flow rate while holding the other primary variables constant. This was done by feeding a sinusoidal signal from a Wavetek Model 112 frequency generator into the electronic feedback controller of the electrohydraulic valve in the power loop. The amplitude of this perturbation was approximately ±6 percent of the steady-state value.

Frequency-response tests were run for each operating condition between frequencies of 0.003 and 1.0 cycle per second. At each frequency a period of at least twice the period of oscillation was allowed before the data was recorded. An oscillograph recording was made of the variables listed in Table 4 for a period of two oscillations. A new frequency was set and the procedure repeated until the required number of frequencies was tested.

d. Shutdown

After a series of frequency-response tests was completed, the test system was shut down using the same methods described above for the steady-state tests.

IV. STEADY-STATE CHARACTERISTICS OF BOILER

Steady-state tests were performed to determine how the overall boiler perform-
ance changed as a function of the primary variables, and to study the important
processes occurring within the boiler. The resulting information served a
number of functions. It gave data with which to evaluate the parameters re-
quired for calculating the theoretical transfer function. It gave information as
to the actual physical processes occurring within the boiler with which to
compare the mathematical model used in the theoretical analysis of the boiler
dynamics, and it gave an insight into the boiler operating characteristics which
was useful in interpreting the frequency-response test results.

The steady-state tests were performed in accordance with the procedures de-
scribed in Section III above. These tests were performed at the 34 operating
conditions listed in Table 3. Each condition is defined by constant values of
the following primary variables.

> boiling-fluid flow rate W
> boiling-fluid inlet temperature T_{in}
> heating-fluid flow rate W_H
> heating-fluid inlet temperature $T_{H\,in}$
> boiling-fluid exit pressure P_{out}, or turbine
> simulator valve setting

The test conditions were selected so that each of the primary variables was
varied about the nominal operating condition described in Section III above.
This nominal condition was selected on the basis of preliminary tests to provide
a condition typical of that encountered in Rankine-cycle space powerplants.

The results of these tests indicate that the boiler performance can be cate-
gorized by the condition of the boiling fluid at the exit. Over the operating
range studied, three types of boiling-fluid exit conditions were observed:

1) Dry superheated vapor,
2) Superheated vapor with saturated liquid, and
3) Saturated vapor with saturated liquid.

The second condition is a nonequilibrium condition. Its existence was deter-
mined by the visual observation of liquid droplets in the superheated vapor
stream and by the fluctuation in the temperature measurements which resulted
when these droplets impinged on the thermocouples at the boiling-fluid exit.

By studying the axial temperature distributions measured inside the boiler, it was possible to discern three different regions within the boiler where different modes of heat transfer from the tube wall to the boiling-fluid predominated:

1) A subcooled region,
2) A boiling region, and
3) A nonequilibrium-superheated region.

This section contains a detailed discussion of three different regions of the boiler. The manner in which the primary variables affect these profiles is then related to the changes observed in the overall boiler performance.

A. Regions within Boiler

The temperature measurements made within the boiling-fluid and heating-fluid streams were plotted against the axial distance from the boiling-fluid inlet for each steady-state test condition. Using these temperature distributions and employing heat balances on sections of the boiler, it was possible to estimate the variation of boiling-fluid quality with axial distance in the two-phase regions.

Typical examples of these temperature and quality distributions are shown in Figures 6 through 9. The different regions of the boiler are apparent from the changes in the slopes of the temperature and quality profiles. For example, it can be seen that the boiling-fluid temperature increases rapidly in the subcooled region as it is heated to its saturation temperature. The slope of the heating-fluid temperature is not very steep, however, indicating a relatively low heat flux. Therefore the primary mode of heat transfer to the boiling fluid is forced convection, although some subcooled boiling may take place.

The saturation temperature is reached at the pinch point where bulk boiling commences. This is the primary mode of heat transfer in the boiling region. The high rate of heat transfer achieved in this region is indicated by the relatively steep slope of the heating-fluid temperature.

In the boiling region, saturation conditions exist and the boiling-fluid temperature is dependent upon the pressure. As a consequence the boiling-fluid temperature is observed in Figures 6 through 9 to decrease with length, due to the
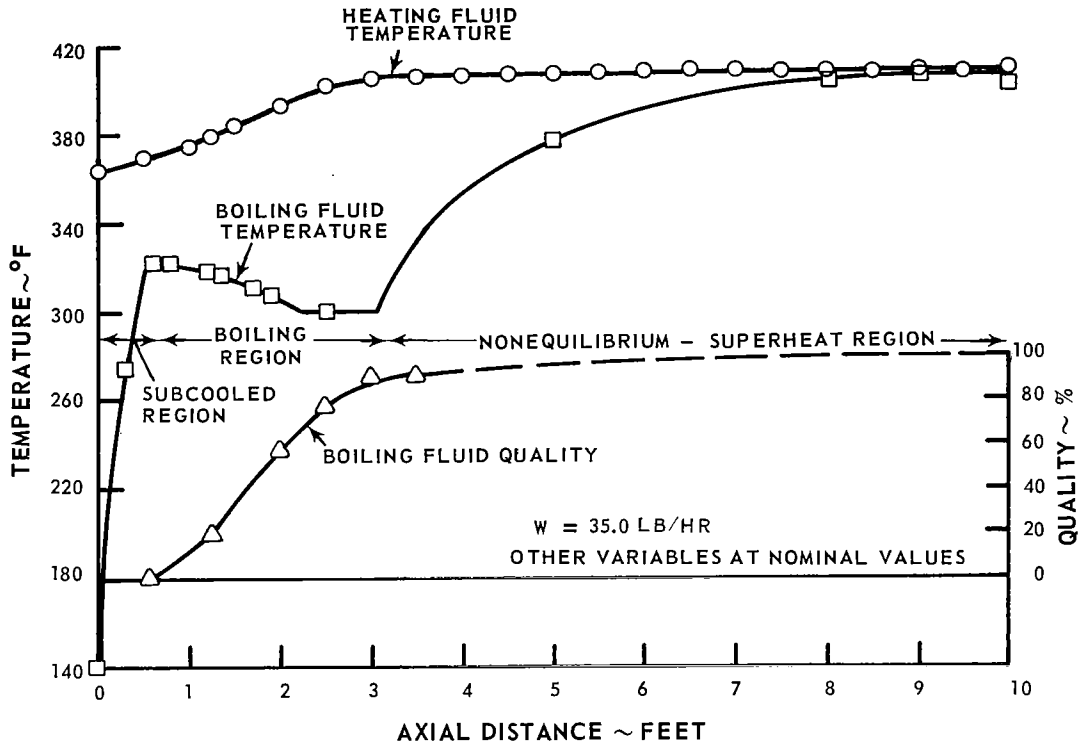
Figure 6 Steady-State Test Results. Temperature and Quality Profiles at Boiling-Fluid Flow Rate of 35. 0 lb/hr
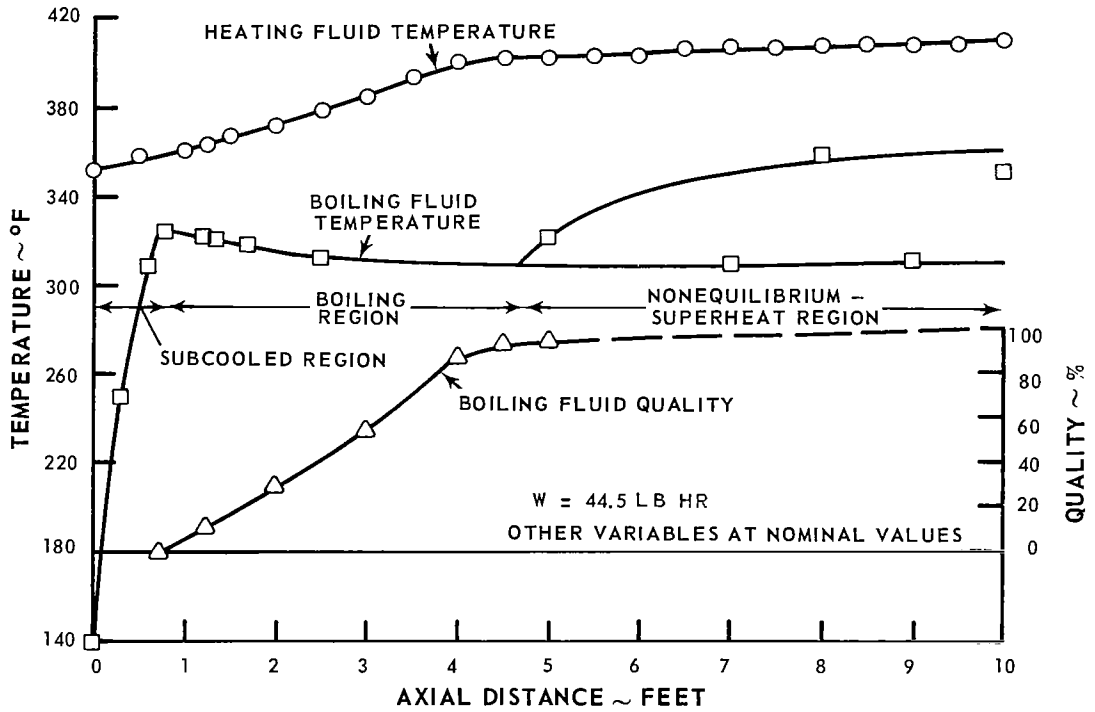
Figure 7 Steady-State Test Results. Temperature and Quality Profiles at Boiling-Fluid Flow Rate of 44. 5 lb/hr

24
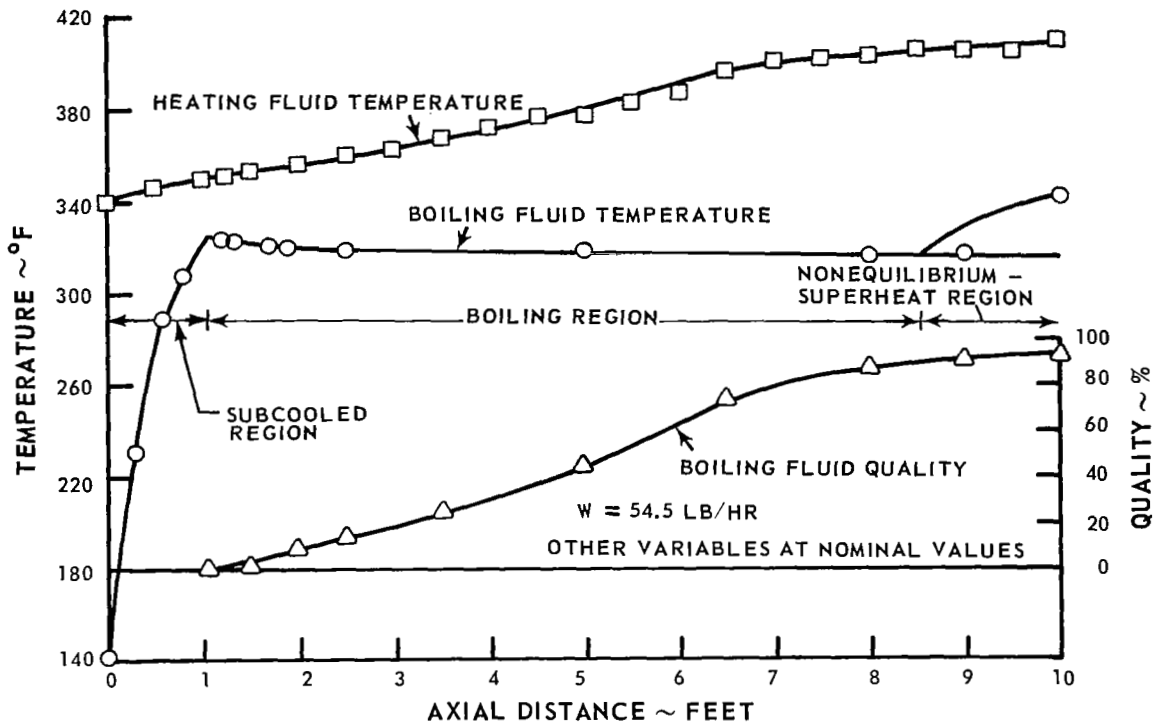
Figure 8 Steady-State Test Results. Temperature and Quality Profiles at Boiling-Fluid Flow Rate of 54.5 lb/hr
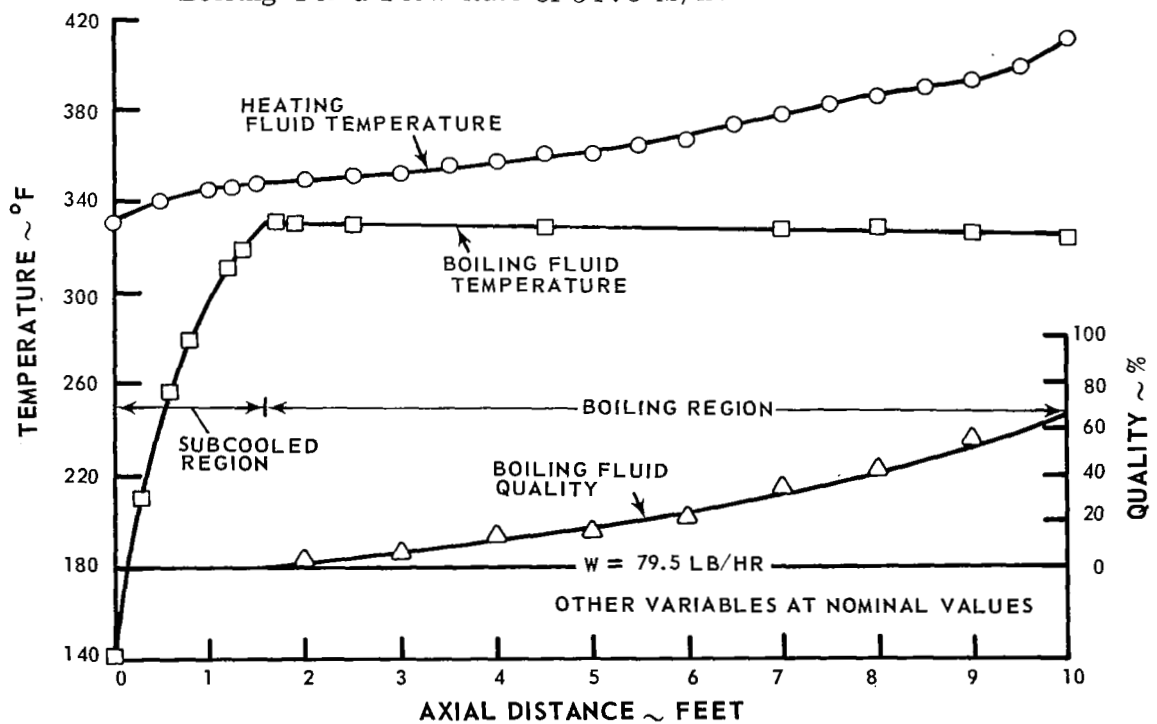
Figure 9 Steady-State Test Results. Temperature and Quality Profiles at Boiling-Fluid Flow Rate of 79.5 lb/hr

decrease in boiling-fluid pressure caused by frictional losses. The steeper slope of the boiling-fluid temperature over the first portion of the boiling region is caused by the boiling fluid flowing through the spiral passage formed by the machined plug, where frictional losses are higher. The boiling fluid is vaporized as it passes through the boiling region, as shown by the increase of quality with length. At a quality of approximately 90 percent, before the evaporation process has been completed, the boiling fluid enters the non-equilibrium-superheat region. In this region, the temperature of the vapor is observed to rise above the saturation temperature and the vapor becomes superheated. However, since the evaporation process was not completed when the boiling fluid entered this region, droplets of saturated liquid can be found dispersed in the superheated vapor. This results in a nonequilibrium state.

Since the evaporation process has not been completed before the vapor becomes superheated there is no clearly defined boundary between the boiling region and the nonequilibrium region, although for purposes of analysis it has been found necessary to define such a boundary. The criteria employed in defining this boundary are discussed in detail in Appendix 3.

Several modes of heat transfer are active in the nonequilibrium-superheat region:

1) Transfer of the heat from the tube wall to the vapor by forced convection,
2) Conduction of heat from the vapor to the liquid droplets, and
3) Transfer of heat by conduction from the tube wall to droplets impinged on the wall.

The low rate of heat transfer indicated by the shallow slope of the heating-fluid temperature in this region indicates that the primary mode of heat transfer is by the forced convection of the vapor.

For the condition illustrated in Figure 6, W=35 lb/hr, the evaporation process is completed shortly after the boiling fluid enters the nonequilibrium-superheat region. This is shown by the fact that none of the thermocouples in this region registered the saturation temperature. The boiling fluid emerges at a temperature only slightly below the heating-fluid inlet temperature and superheated by 117°F. The nonequilibrium effects that occur in this region become more pronounced at higher boiling-fluid flow rates.

The effect of boiling-fluid flow rate on the three regions of the boiler can be seen by comparing Figures 6 through 9 which represent flow rates of 35.0, 44.5, 54.5 and 79.5 lb/hr, respectively. As can be seen, increasing the

boiling-fluid flow rate tends to increase the lengths of the subcooled and boiling regions, while the length of the nonequilibrium-superheat region decreases until the region disappears.

As the boiling-fluid flow rate increases, the evidence of the nonequilibrium effects becomes more noticeable. Figure 7 shows that at 44.5 lb/hr two thermocouples register the saturation temperature, indicating the presence of droplets close to the boiler exit. However, heat balances and visual observation indicate that for this condition the evaporation process is completed before the fluid leaves the boiler. Therefore it leaves as a dry superheated vapor.

Figure 8 indicates at 54.5 lb/hr that the evaporation process has not been completed before the fluid leaves the boiler. As a consequence the boiling-fluid emerges in a nonequilibrium state containing 7 percent saturated liquid and 93 percent vapor superheated by 35°F.

Figure 9 indicates that at a flow rate of 79.5 lb/hr the nonequilibrium-superheat region has disappeared. No superheating of the vapor is observed. The boiling-fluid emerges in a saturated condition at a quality of 65 percent.

B. Effect of Primary Variables on Boiler Performance

The steady-state test data describing the overall performance of the boiler is summarized in Tables 6 through 10. In addition, curves of this data are presented in Figures 10 through 20 to illustrate the effect the primary variables have on boiler performance. The following paragraphs discuss the effect that each of these primary variables has on the performance of the boiler.

1. Effect of Boiling-Fluid Flow Rate

The manner in which the performance of the boiler varies with the boiling-fluid flow rate W is illustrated in Figures 10 and 11. Figure 10a shows the effect of varying W on the different regions of the boiler. The subcooled length L_{SC} and the boiling length L_B represent the axial locations of the boundaries between the regions as measured from the boiling fluid inlet. Figure 10a further illustrates the fact that as W is increased both the subcooled and boiling regions increase in size while the nonquilibrium-superheat region decreases until it disappears.

Figure 10c describes the condition of the boiling fluid at the exit. For boiling-fluid flow rates between 30 and 45 lb/hr, it can be seen that the vapor leaves in a dry superheated condition. Between 45 and 65 lb/hr, however, the exit quality drops below 1.0 while the vapor is still superheated, indicating the co-existence of liquid and superheated vapor in a nonequilibrium state. Above 65 lb/hr saturation conditions exist. There is no vapor superheat and the exit quality is less than one.

a) Subcooled Length L_{SC} and Boiling Length L_B vs W
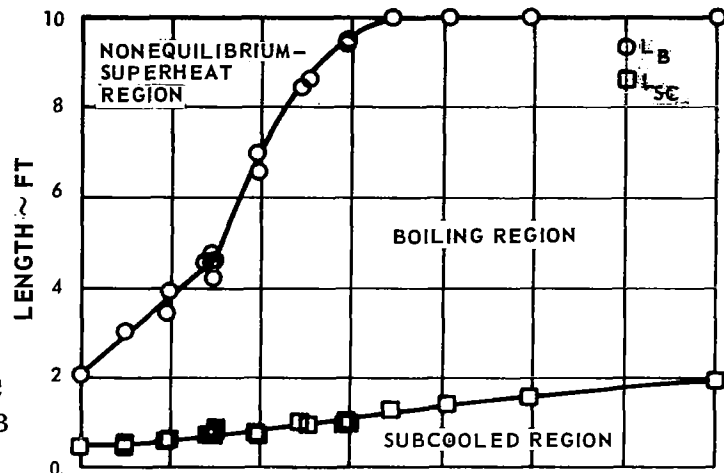
b) Boiling-Fluid Exit Temperature T_{out} vs W
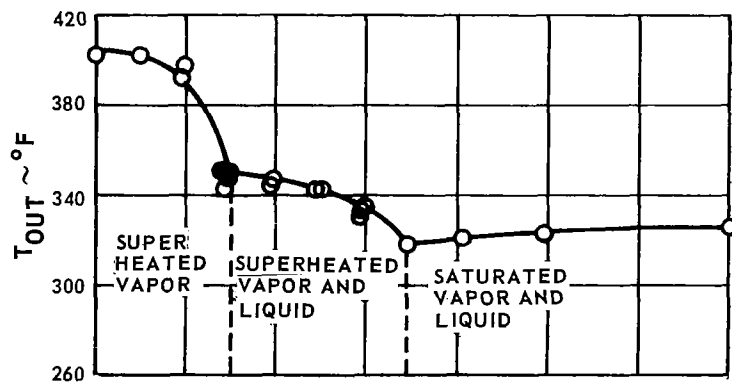
c) Boiling-Fluid Superheat ΔT_{SH} and Exit Quality X_e vs W

Figure 10 Steady-State Test Results. Variation of Boiler Performance with Boiling-Fluid Flow Rate

$W_H = 770$ lb/hr $T_{H\ in} = 410°F$ $T_{in} = 140°F$ T.S. valve at nominal setting

28

Figure 10b indicates that the condition of the boiling-fluid at the exit is also reflected in the boiling-fluid exit temperature, since this data exhibits a different curvature for each different exit condition.

Figure 11a illustrates the variation of the boiling-fluid exit pressure P_{out} with W. When the boiling fluid emerges in a dry superheated condition P_{out} is related to flow rate and temperature and pressure through the following relation for flow through a choked restriction.

$$\frac{W \sqrt{T_{out}}}{P_{out}} = \frac{A \text{ choked}}{\sqrt{\frac{\gamma}{R}\left(\frac{2}{\gamma+1}\right)^{\frac{\gamma+1}{\gamma-1}}}} \qquad (1)$$

For a given turbine simulator valve setting, this equation indicates that the parameter $W\sqrt{T_{out}}/P_{out}$ is approximately constant for a limited range of temperature variation. Also, it can be seen that for a limited range of temperature variation, P_{out} is approximately proportional to W. However, when liquid is intermixed with the vapor, Equation (1) no longer holds and the parameter $W\sqrt{T_{out}}/P_{out}$ becomes a function of exit quality X_e. The variation of this parameter with X_e for the condition where the turbine simulator valve setting was held constant is illustrated in Figure 12. The strong departure of the curve in Figure 11a from linearity above 60 lb/hr results from the large percentage of liquid in the flow.

One of the more significant effects of varying W on boiler performance is illustrated in Figure 11b where boiling-fluid pressure drop ΔP_B is plotted as a function of W. The negative slope in the curve exhibited for flows between 30 and 85 lb/hr is of particular interest in studying the stability of multitube boilers. This negative slope characteristic can lead to the static type of boiler instability, discussed in Section VI below, when the pressure at the exit of the boiling tube is independent of flow rate. This can occur in a multitube boiler where the pressure in the exit header is insensitive to the flow fluctuations in the individual tubes.

The negative slope exhibited in the ΔP_B curve is the result of a very complex interaction between the boiler geometry, the hydrodynamics of the flow in the three different regions, and the shift in the location of the boundaries of these regions as W is varied. An excellent discussion of the factors influencing ΔP_B and the manner in which they interact to produce the negative pressure gradient can be found in Reference 5. The mathematical analysis presented in this reference has shown very good agreement with the boiling-fluid pressure drop data presented in this section, as shown in Figures 5 and 6 of the reference.
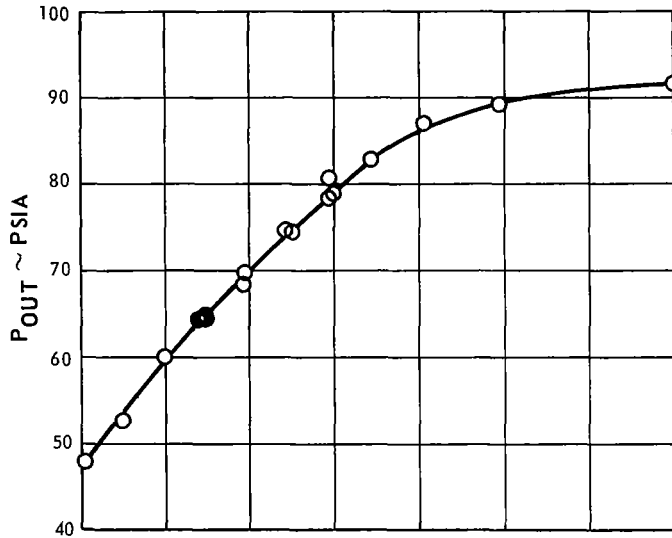
a) Boiling-Fluid Exit Pressure vs W
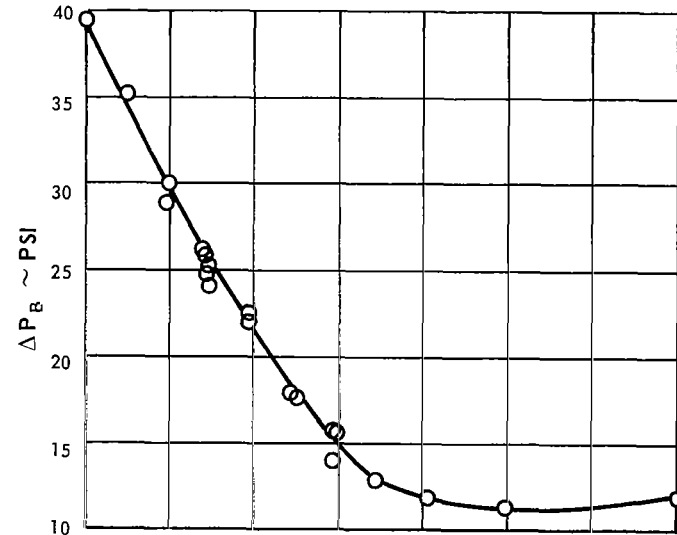
b) Boiling-Fluid Pressure Drop vs W
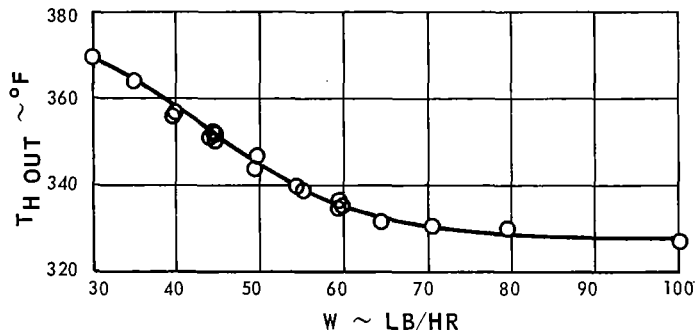
c) Heating-Fluid Exit Temperature vs W

d) Pinch-Point Temperature Difference vs W
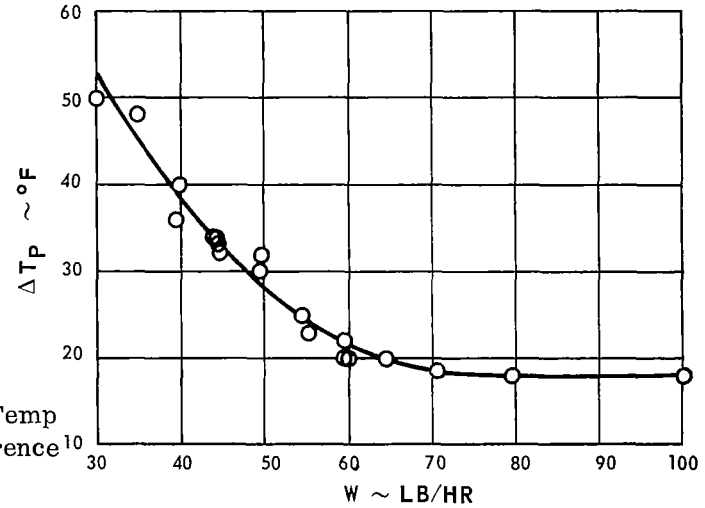
Figure 11 Steady-State Test Results. Variation of Boiler Performance with Boiling-Fluid Flow Rate

W_H = 770 lb/hr $T_{H\ in}$ = 410°F T_{in} = 140°F   T.S. valve at nominal setting

$$\text{CHOKED FLOW PARAMETER} \quad W\sqrt{\dfrac{T_{OUT}}{P_{OUT}}} \sim \dfrac{IN^2\sqrt{^\circ R}}{HR}$$

Figure vertical axis values: 34, 30, 26, 22, 18

Horizontal axis (X_e): 0.5, 0.6, 0.7, 0.8, 0.9, 1.0
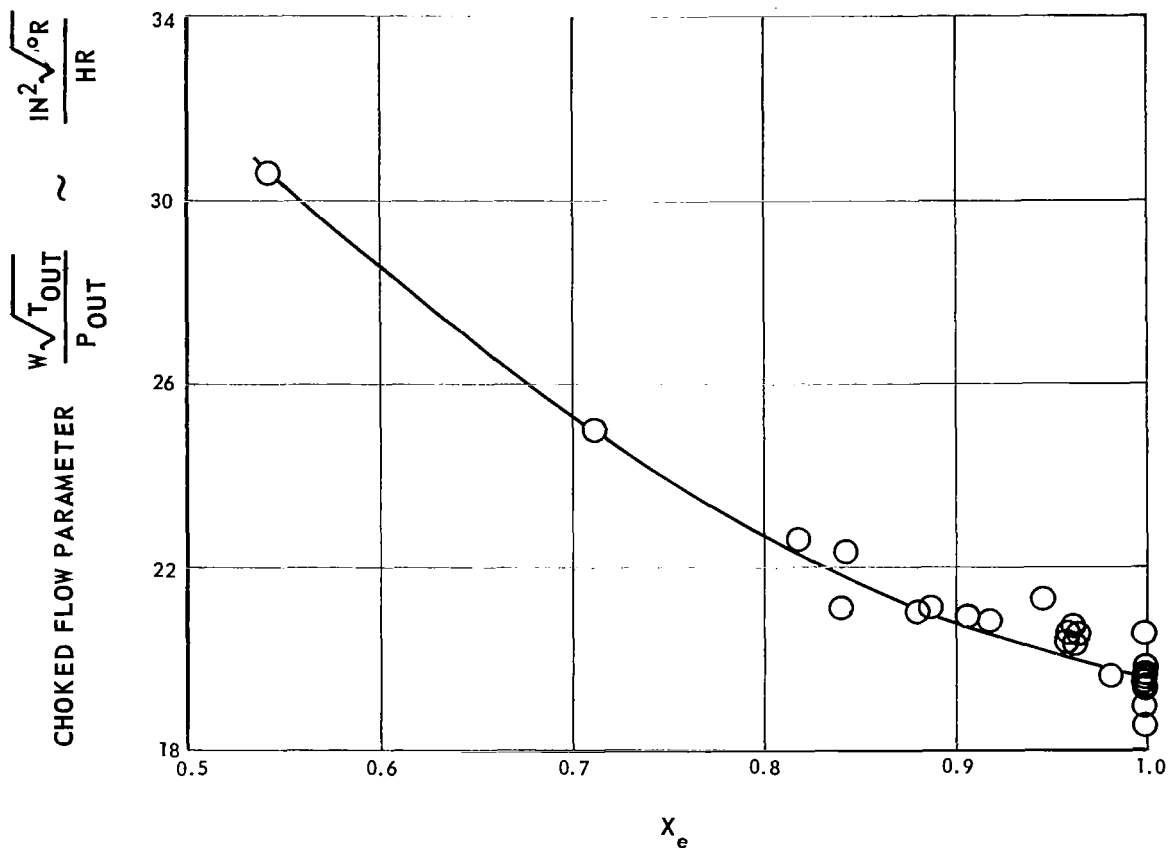
Figure 12   Variation of Choked-Flow Parameter with Boiling-Fluid Exit Quality X_e

The variation of the heating-fluid exit temperature $T_{H\ out}$ and the pinch-point temperature difference ΔT_p with W is shown in Figures 11c and 11d respectively. Both decrease with W until saturated exit conditions are reached at 65 lb/hr. Beyond this point they are relatively insensitive to W. These effects can be explained in the following manner. At flow rates below 65 lb/hr, Figure 10a shows that a portion of the superheat region is replaced by boiling region as the flow rate is increased. Since the heat-transfer coefficient is much higher in the boiling region than in the nonequilibrium-superheat region, the result is an increase in heat transfer over this length. Therefore, additional energy is removed from the heating fluid as the flow rate is increased and $T_{H\ out}$ decreases.

At flow rates above 65 lb/hr, bulk boiling exists as far as the boiler exit. Most of the heat transfer in the boiler occurs in the boiling region. The heat transfer coefficient in this region is relatively insensitive to changes in W. As Figure 10a shows, only small changes occur in the length of the boiling region at flow rates above 65 lb/hr. As a result the heat-transfer area and the heat-transfer coefficient are essentially constant in the boiling region. Under these conditions as the boiling-fluid flow rate is increased above 65 lb/hr, the energy removed from the boiling-fluid remains nearly constant which results in the small observed change of $T_{H\ out}$.

2. Effect of Varying Heating-Fluid Flow Rate

The effects of varying the heating-fluid flow rate W_H are illustrated in Figures 13 and 14. The primary effect of increasing the heating-fluid flow rate is to increase the heat-transfer rate in the boiling and subcooled regions. This is seen by the rapid decrease in the length of the boiling and subcooled regions as shown in Figure 13a.

The rise in the heat-transfer rate as W_H is increased results from increases in both the heat-transfer coefficient and the average heating-fluid temperature. The rise in the average heating-fluid temperature results from a decrease in the difference between $T_{H\ in}$ and $T_{H\ out}$ as W_H is increased, while the total heat transferred remains approximately constant. This is seen in the increased $T_{H\ out}$ shown in Figure 14c. The resulting increase in temperature difference between the heating and boiling fluids at the pinch point is shown by the curve of pinch-point temperature difference, Figure 14d.

As the length of the boiling region diminishes, Figure 13a indicates a corresponding increase in the length of the nonequilibrium-superheat region. This results in a drying out of the vapor and an increase in the superheat. This is shown in Figure 13c where it can be seen that for values of W_H between 400 and 770 lb/hr, the boiling fluid emerges in the nonequilibrium condition with ΔT_{SH} constantly increasing. Above the nominal value of 770 lb/hr, dry superheated vapor is produced. The lengthening of the nonequilibrium-superheat region is also the primary factor influencing the increase in ΔP_B shown in Figure 14b.

3. Effect of Varying Heating-Fluid Inlet Temperature

The effects of varying the heating-fluid inlet temperature $T_{H\ in}$ are illustrated

a) Subcooled Length L_{SC} and Boiling Length L_B vs W_H

b) Boiling-Fluid Exit Temperature vs W_H

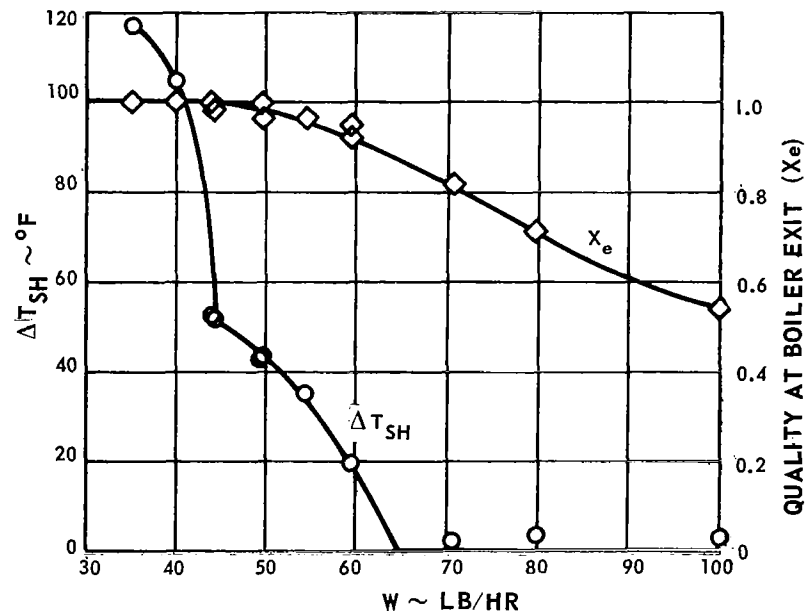c) Boiling-Fluid Super-heat ΔT_{SH} and Exit Quality X_e vs W_H
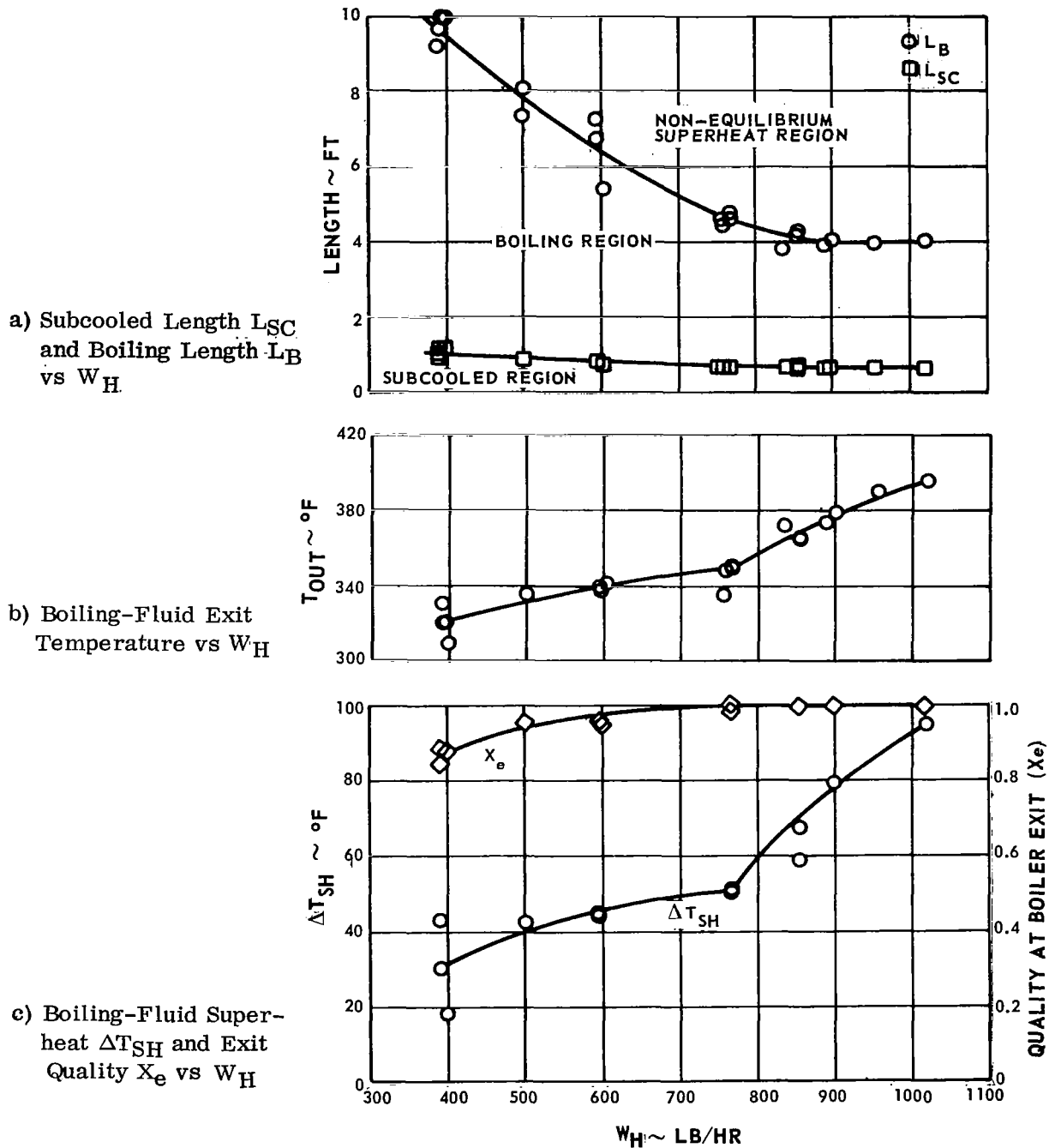
Figure 13 Steady-State Test Results. Variation of Boiler Performance with Heating-Fluid Flow Rate

W = 45 lb/hr $T_{H\,in}$ = 410°F T_{in} = 140°F   T.S. valve at nominal setting

a) Boiling-Fluid Exit
Pressure vs W_H

b) Boiling-Fluid Pres-
sure Drop vs W_H

c) Heating-Fluid Exit
Temperature vs W_H

d) Pinch-Point Temp-
erature Difference
vs W_H
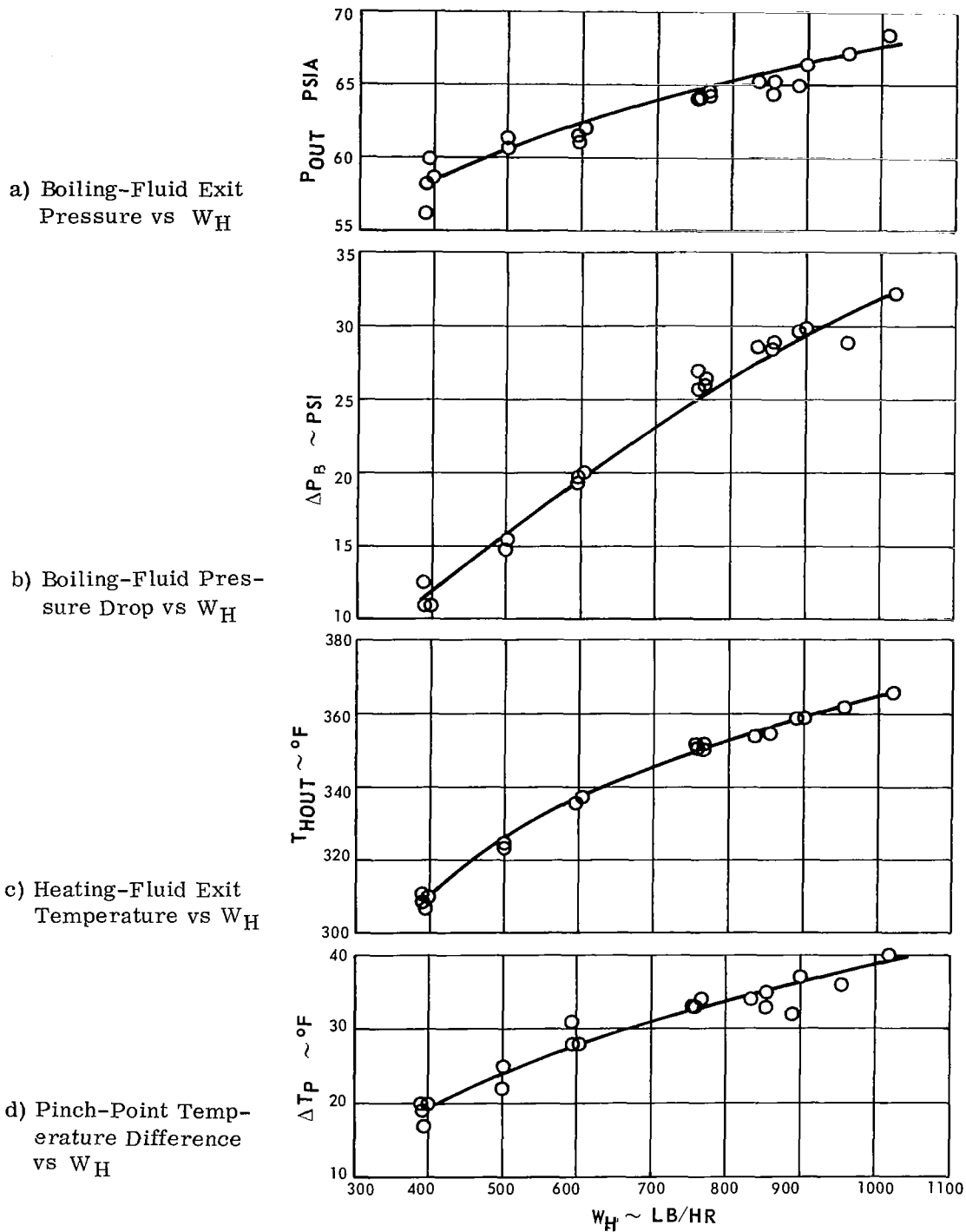
Figure 14 Steady-State Test Results. Variation of Boiler Performance with
Heater-Fluid Flow Rate

$W = 45$ lb/hr $T_{H\,in} = 410°F$ $T_{in} = 140°F$ T.S. valve at
nominal setting

in Figures 15 and 16. As can be seen by comparing these figures with Figures 13 and 14, the effect on boiler performance of increasing $T_{H\ in}$ is very similar to that obtained by increasing W_H. This is because the primary effect of increasing $T_{H\ in}$ is to increase the temperature difference between the two fluids, thereby increasing the heat transfer rates along the length of the boiler. This is shown by the decrease in the length of the boiling region in Figure 15a and by the increases in $T_{H\ out}$ and ΔT_p shown in Figures 16c and 16d respectively.

The variation in the exit conditions of the boiling fluid with $T_{H\ in}$ is shown in Figure 15c. For values of $T_{H\ in}$ between 360 and 410°F the vapor is dry. The increases in X_e and ΔT_{SH} with $T_{H\ in}$ result from the increase in the length of the nonequilibrium-superheat region shown in Figure 15a, as well as the higher heat-transfer rates resulting from the higher temperature differences between the two fluids.

The increase in boiling-fluid pressure drop ΔP_B with $T_{H\ in}$ shown in Figure 16b is due primarily to the increase in the length of the nonequilibrium-superheat region.

4. Effect of Varying Boiling-Fluid Exit Pressure

The effect of varying the boiling-fluid exit pressure P_{out} is illustrated in Figures 17 and 18. The effect of varying P_{out} is the reverse of the effect of varying $T_{H\ in}$. As P_{out} is increased, the saturation temperature of the boiling-fluid increases, decreasing the temperature difference between the two fluids. This results in reduced heat-transfer rates. The greatest percentage reduction in heat-transfer rates occurs in the vicinity of the pinch point, where the temperature difference between the two fluids is the smallest. These effects can be seen by the increase in length of the boiling region with an increase in P_{out} as shown in Figure 17a, and the decrease in ΔT_p with an increase in P_{out} shown in Figure 18c.

The variation in the exit conditions of the boiling fluid with P_{out} is shown in Figure 17c. As can be seen for values of P_{out} below the nominal value of 65 psia, the boiling-fluid emerges in a dry superheated condition. Above 65 psia nonequilibrium conditions exist until saturation conditions are approached at

a) Subcooled Length L_{SC} and Boiling Length L_B vs $T_{H in}$

b) Boiling–Fluid Exit Temperature vs $T_{H in}$

c) Boiling–Fluid Superheat ΔT_{SH} and Exit Quality X_e vs $T_{H in}$

Figure 15   Steady-State Test Results.   Variation of Boiler Performance with Heating-Fluid Inlet Temperature
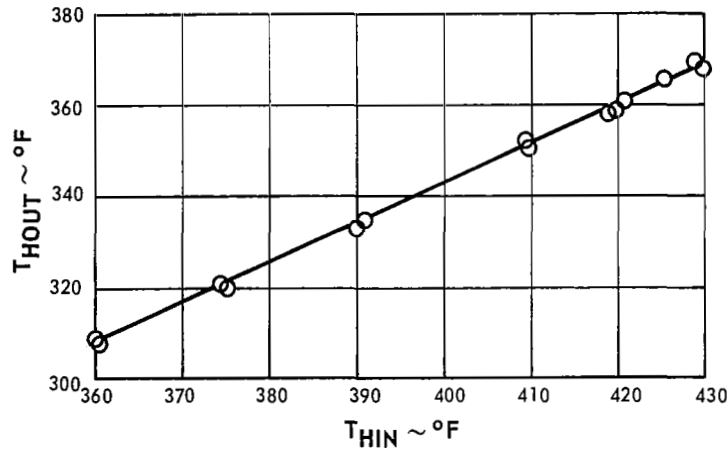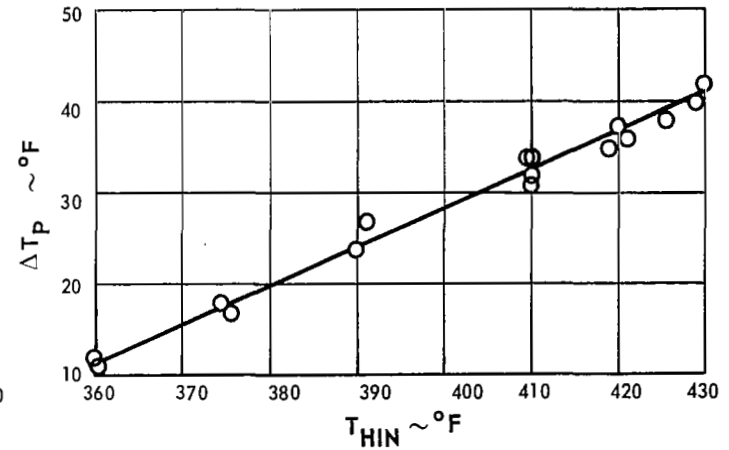
W   = 45 lb/hr W_H = 770 lb/hr T_{in} = 140 °F   T.S. valve at nominal setting

Figure 16 Steady-State Test Results. Variation of Boiler Performance with Heating-Fluid Inlet Temperature

$W = 45 \text{ lb/hr}$ $W_H = 770 \text{ lb/hr}$ $T_{in} = 140°F$ T.S. valve at nominal setting

a) Subcooled Length L_{SC} and Boiling Length L_B vs P_{out}

b) Boiling-Fluid Exit Temperature vs P_{out}

c) Boiling-Fluid Superheat ΔT_{SH} and Exit Quality X_e vs P_{out}
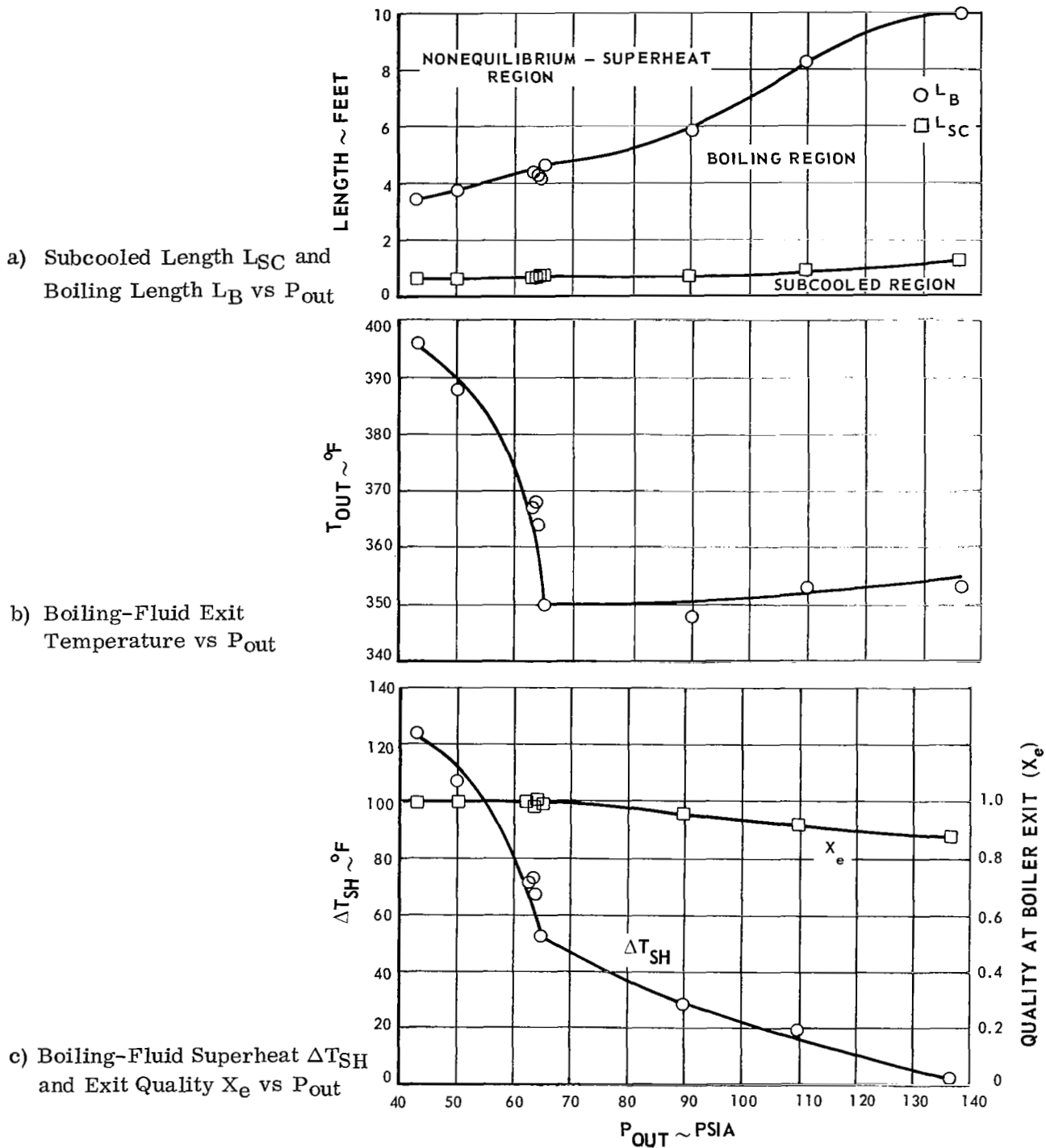
Figure 17 Steady-State Test Results. Variation of Boiler Performance with Boiling-Fluid Exit Pressure $\quad$ W = 45 lb/hr $\quad$ W_H = 770 lb/hr $\quad$ T_{in} = 140°F $\quad$ $T_{H\ in}$ = 410°F

a) Boiling-Fluid Pressure
   Drop vs P_{out}
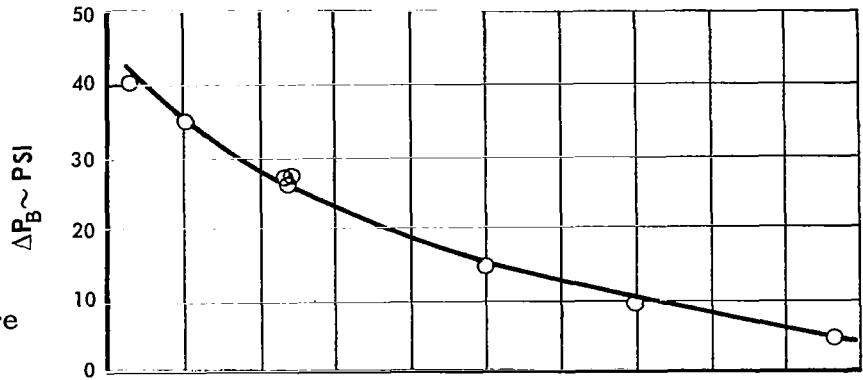
b) Heating-Fluid Exit
   Temperature vs P_{out}

c) Pinch-Point Temperature
   Difference vs P_{out}

$\Delta P_B \sim PSI$

$T_{HOUT} \sim °F$

$\Delta T_P \sim °F$

$P_{OUT} \sim PSIA$
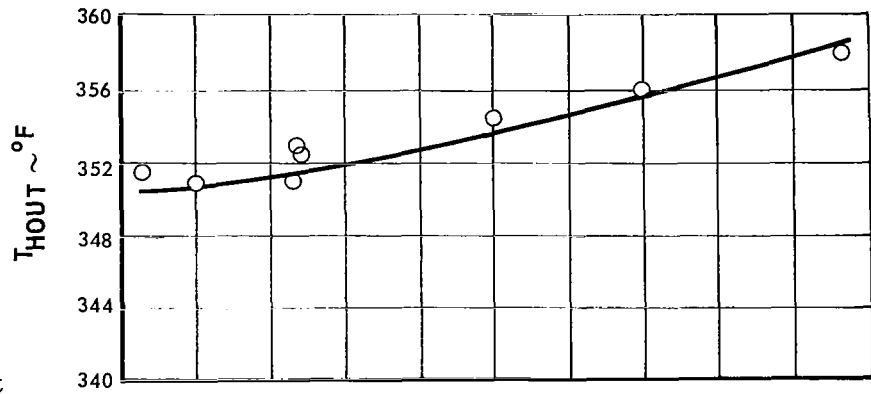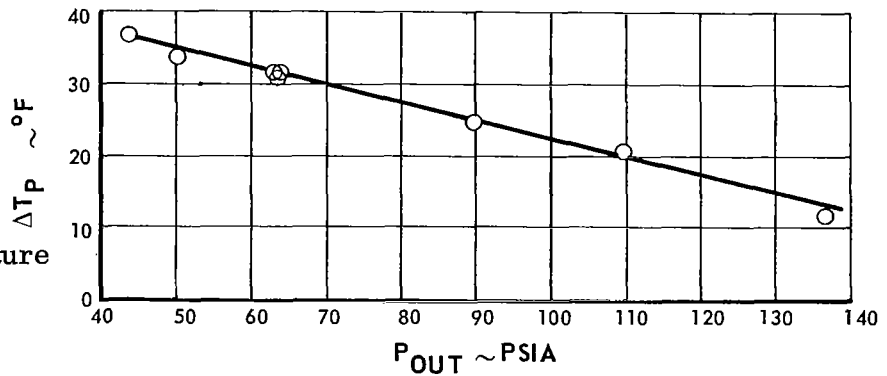
Figure 18 Steady-State Test Results. Variation of Boiler Performance with
          Boiling-Fluid Exit Pressure
          $W = 45$ lb/hr $W_H = 770$ lb/hr $T_{in} = 140°F$ $T_{H\,in} = 410°F$

137 psia. The decrease in X_e and ΔT_{SH} results from the reduction in the length of the nonequilibrium region shown in Figure 17a, and the reduced heat-transfer rates caused by the reduction in the temperature difference.

The decrease in ΔP_B with increasing values of P_{out} shown in Figure 17b results primarily from the reduction in the length of the nonequilibrium-superheat region. An increase in the vapor density also contributes.

5. Effect of Varying Boiling-Fluid Inlet Temperature

The effects of varying the boiling-fluid inlet temperature are shown in Figures 19 and 20. Almost all of the performance parameters are relatively independent of T_{in}. However, as T_{in} nears 200°F and approaches the saturation temperature of the boiling fluid, some increase in T_{out} and ΔT_{SH} is observed. This occurs because the principal effect of changing the inlet temperature is to change the subcooled length. Since the subcooled length involves only a relatively small portion of the heat-transfer area in the boiler, the steady-state boiler performance is little affected. However, since a large part of the fluid mass in the boiler resides in the subcooled region, a larger effect on the dynamic characteristics may be produced.

C. Summary of Steady-State Characteristics

The steady-state test results indicate that the principal effect of increasing W on boiler performance is the negative slope observed over a portion of the boiling-pressure-drop curve and the transition in boiling-fluid exit conditions from dry superheated vapor to wet saturated vapor. The principal effect of increasing W_H is an increase in the heat-transfer rate in the boiling region and subcooled region, caused by a higher heat-transfer coefficient and a higher average-temperature-difference between the boiling and heating fluids. Similarly increasing $T_{H\ in}$ raises this temperature difference, increasing the heat-transfer rate in the boiling region and subcooled region. Increasing P_{out} has the reverse effect, since an increase of pressure raises the saturation temperature and decreases this temperature difference. Boiler performance is relatively insensitive to changes in T_{in}.

In evaluating this data it should be remembered that these experiments were performed using water, where the heat transfer coefficient of the heating fluid is considerably less than that of the boiling fluid in the boiling region. The heat transfer coefficient of the heating fluid is, therefore, the controlling factor in determining the overall heat transfer coefficient for this region. The sensitivity of boiler performance to changes in the primary variables may be different for typical space power boilers which employ metallic working fluids. In this case the heat transfer coefficients of both boiling and heating fluids in the boiling region are of equal magnitude.

a) Subcooled Length L_{SC}
   and Boiling Length L_B vs T_{in}

b) Boiling-Fluid Exit
   Temperature vs T_{in}

c) Boiling-Fluid Superheat ΔT_{SH}
   and Exit Quality X_e vs T_{in}
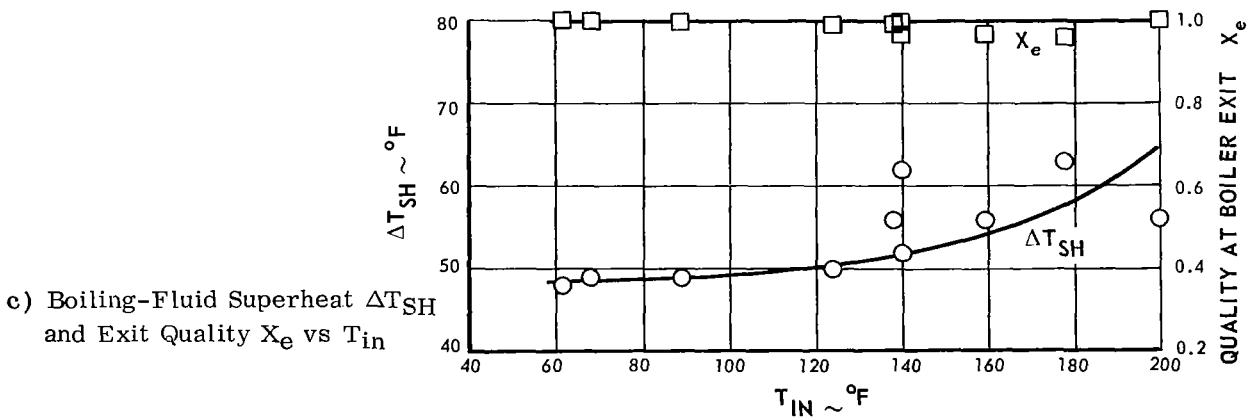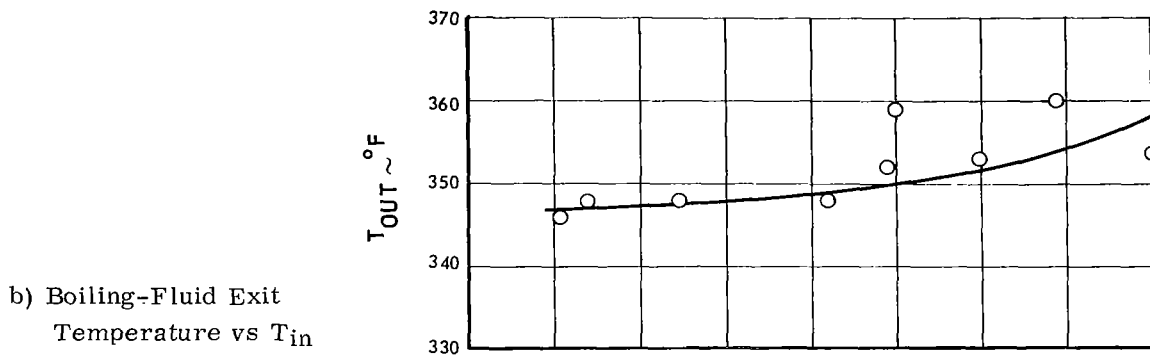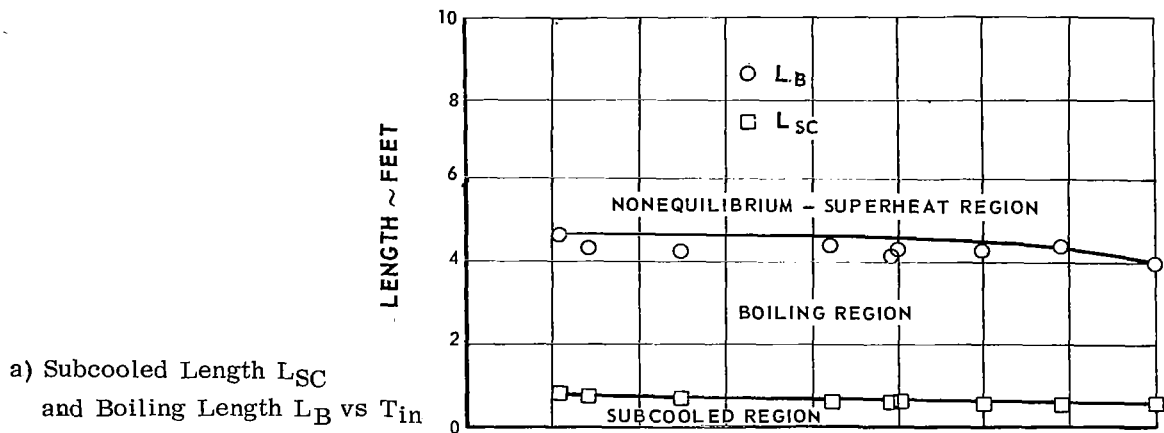
Figure 19   Steady-State Test Results.   Variation of Boiler Performance with
   Boiling-Fluid Inlet Temperature
   W = 45 lb/hr W_H = 770 lb/hr   T.S. valve at $T_{H\,in}$= 410°F
                                             nominal setting
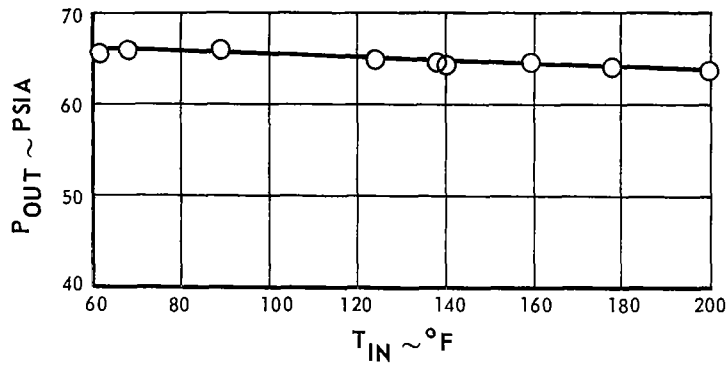
a) Boiling-Fluid Exit Pressure vs T_{in}
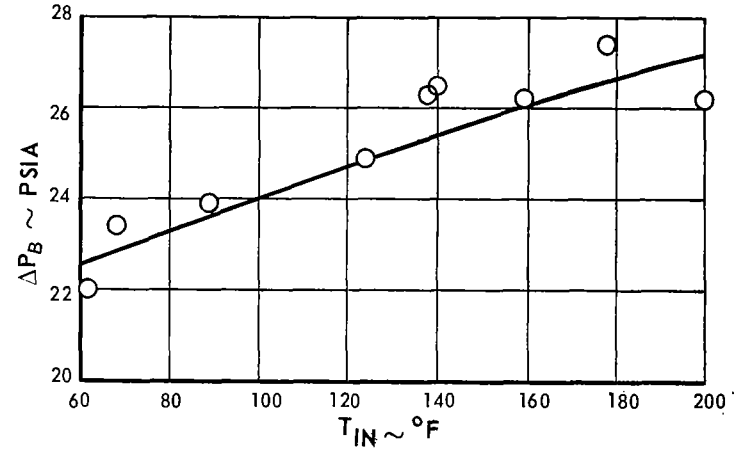
b) Boiling-Fluid Pressure Drop vs T_{in}
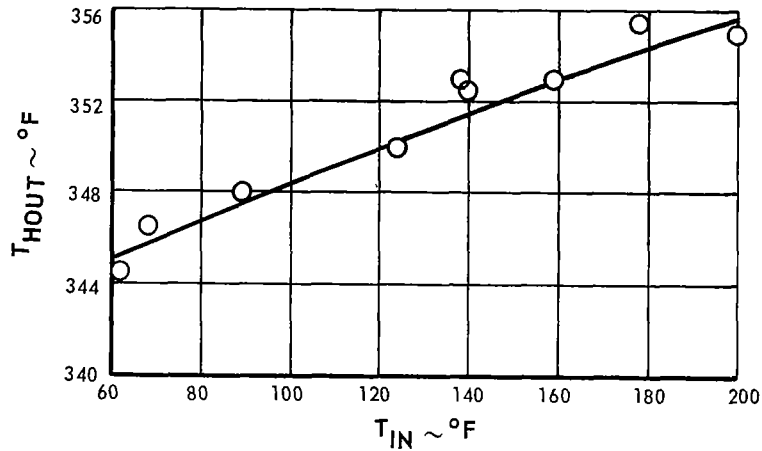
c) Heating-Fluid Exit Temperature vs T_{in}
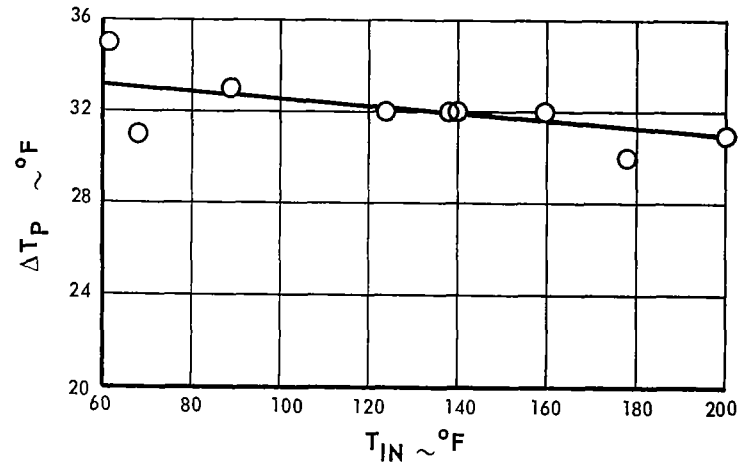
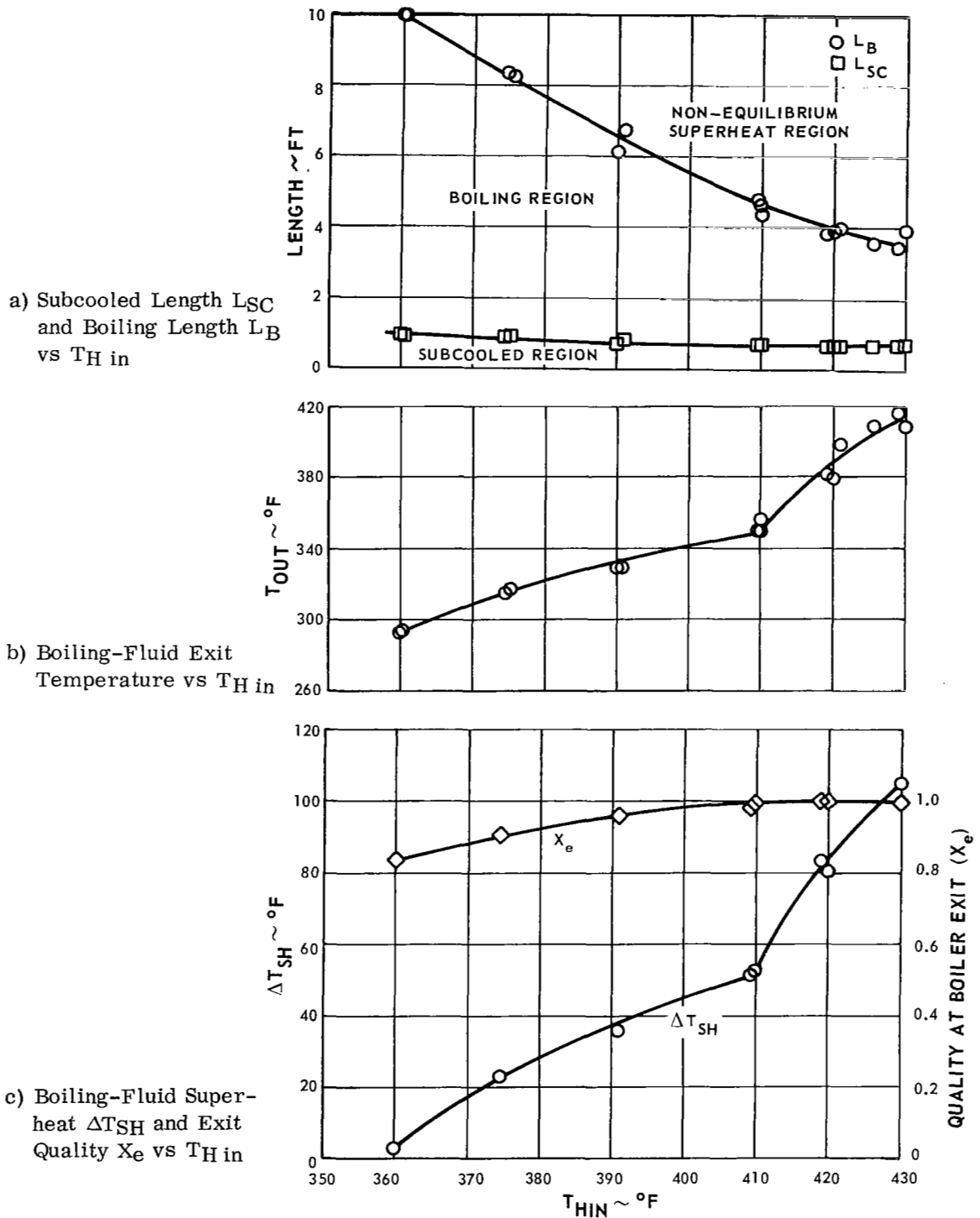d) Pinch-Point Temperature Difference vs T_{in}
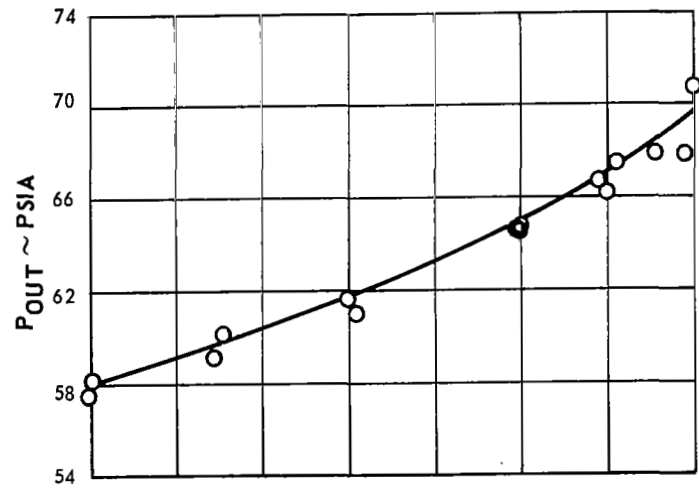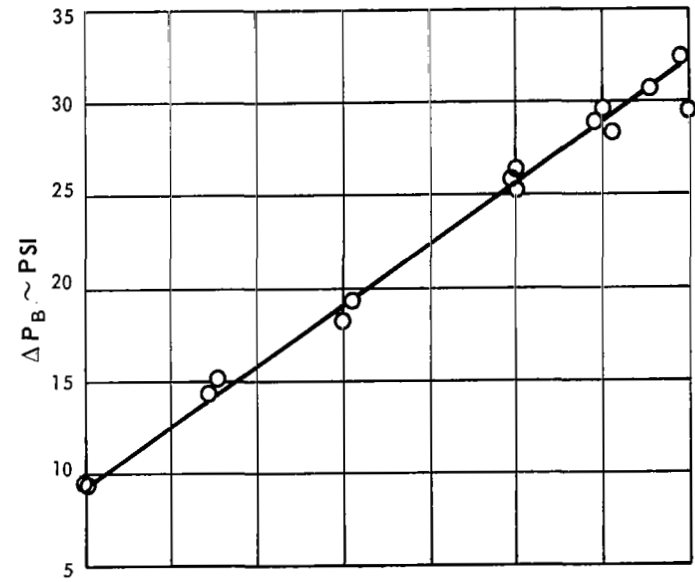
Figure 20   Steady-State Test Results. Variation of Boiler Performance with
Boiling-Fluid Inlet Temperature T_{in}
$W = 45$ lb/hr $W_H = 770$ lb/hr   T.S. valve at nominal setting $T_{H in} = 410°F$

V. DYNAMIC CHARACTERISTICS OF BOILER

Frequency-response and step-response tests were conducted at 21 operating conditions. The purpose of these tests was to determine how the dynamic response characteristics of the boiler are affected by changes in the primary variables. This was done to gain greater insight into the factors involved in the stability of boiler operation for Rankine-cycle space powerplants.

The 21 operating conditions selected for testing are listed in Table 5. Each condition is defined by constant values of the following primary variables.

> mean boiling-fluid flow rate W
> boiling-fluid inlet temperature T_{in}
> heating-fluid flow rate W_H
> heating-fluid inlet temperature $T_{H\ in}$
> mean boiling-fluid exit pressure P_{out}, or turbine simulator
>   valve setting

These conditions were selected so that each of the primary variables was varied individually about the nominal operating point while the other primary variables were held constant at their nominal values. This section describes the results of the dynamic tests conducted at these conditions.

A. General Characteristics of the Frequency Response of the Boiler

The frequency-response tests were conducted by perturbing the boiling-fluid flow rate sinusoidally about a mean value as described in Section III above. The purpose of these tests was to determine how the transfer functions of the boiler are affected by the primary variables. In addition the transfer function for the boiling-fluid exit pressure obtained from this data provided an experimental basis for judging the theoretical transfer function presented in Section VII of this report. The frequency-response tests were conducted over a frequency range between 0.003 and 1.0 cycle per second. During the tests the variables listed in Table 4 were recorded as a function of time on film using a CEC Model T5-119 oscillograph recorder.

1. Linearity of Boiler Response

The amplitude of the perturbations in the boiling-fluid flow rate was kept small, approximately 6 percent of the mean value, to reduce nonlinear effects. This technique was successful since the variables generally responded in a linear manner. This can be seen in Figure 21a which is a reproduction of one of the

oscillograph recordings. Both the temperature and pressure traces appear as well defined sinusoids in response to the sinusoidal perturbation of boiling-fluid flow rate. The test results shown in Figure 21a were obtained at a heating-fluid flow rate of 840 lb/hr, a condition which produced dry superheated vapor at the boiler exit.

A nonlinear response of the boiling-fluid exit temperature T_{out} did appear as boiling-fluid exit conditions were shifted from those of a dry superheated vapor to the nonequilibrium and wet saturated exit conditions discussed in Section IV above. This type of response can be seen in the nonsinusoidal shape of the T_{out} trace in Figure 21b. The test result shown in Figure 21b was obtained at a boiling exit pressure of 130 psia, a condition which produced a nonequilibrium mixture of superheated vapor and liquid droplets at the boiler exit ($\Delta T_{SH} \approx 5°F$, $X_e \approx 0.88$). The fluctuations in the trace of T_{out} result from the liquid droplets impinging on the thermocouple.

The pressure responses shown in Figure 21b are fairly linear as indicated by their sinusoidal shape. Irregularities superimposed on the sinusoids are probably the result of the passage of the liquid droplets through the choked turbine simulator valve. Nonlinear pressure responses were found only when the boiling fluid emerged in a wet saturated condition. When these non-linear responses did occur, they were observed only at frequencies below 0.005 cps.

2. Experimental Frequency Responses

Experimental frequency responses to pertubations in boiling-fluid flow rate were determined at each test condition for the following variables.

1) boiling-fluid inlet pressure P_{in}
2) boiling-fluid exit pressure P_{out}
3) boiling-fluid exit temperature T_{out}
4) heating-fluid exit temperature $T_{H\ out}$

For each frequency tested at a given operating condition, the amplitudes and phase lags were determined using data read from the oscillograph recordings. For each operating condition, the amplitudes were normalized by dividing the amplitude read from the oscillograph recordings by the amplitude that resulted when the power-loop flow rate was changed by the same amount at zero frequency (i.e., the steady-state variation).

The normalizing data is presented in Table 11. It was obtained by taking steady-state data at two values of W above and two values below the mean value $\overline{W}$. The resulting values of P_{in}, P_{out}, T_{out} and $T_{H\ out}$ were plotted
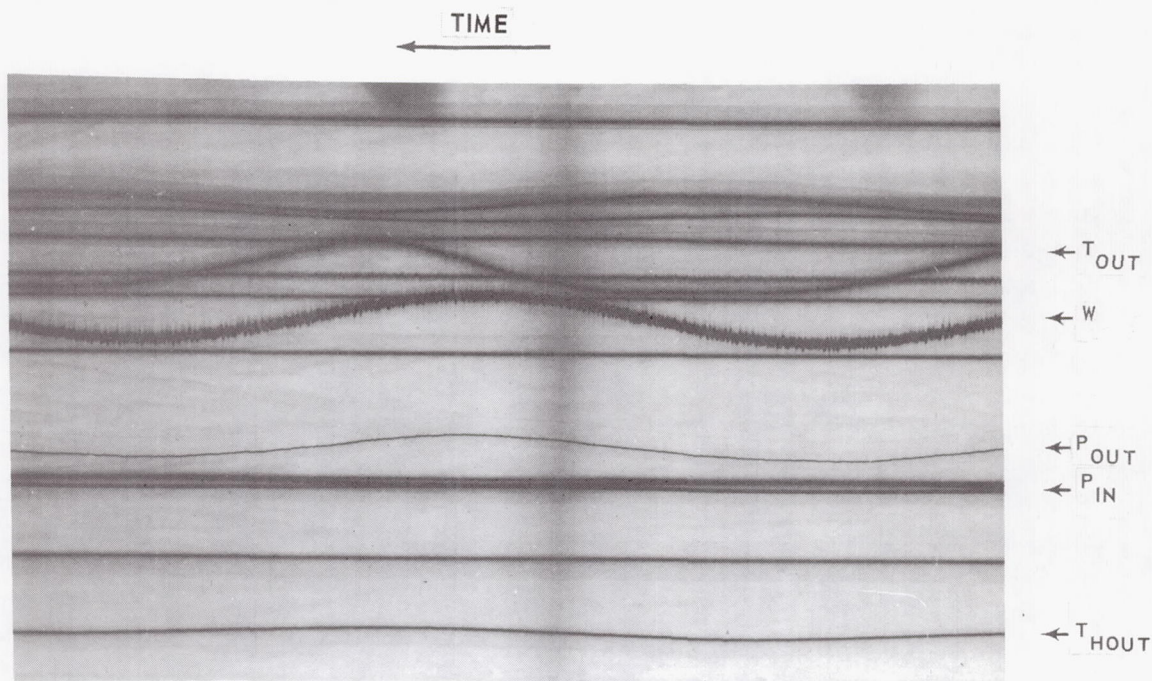
a) Typical Linear Response (obtained at W_{HL} = 840 lb/hr, Frequency = 0.009 cps)
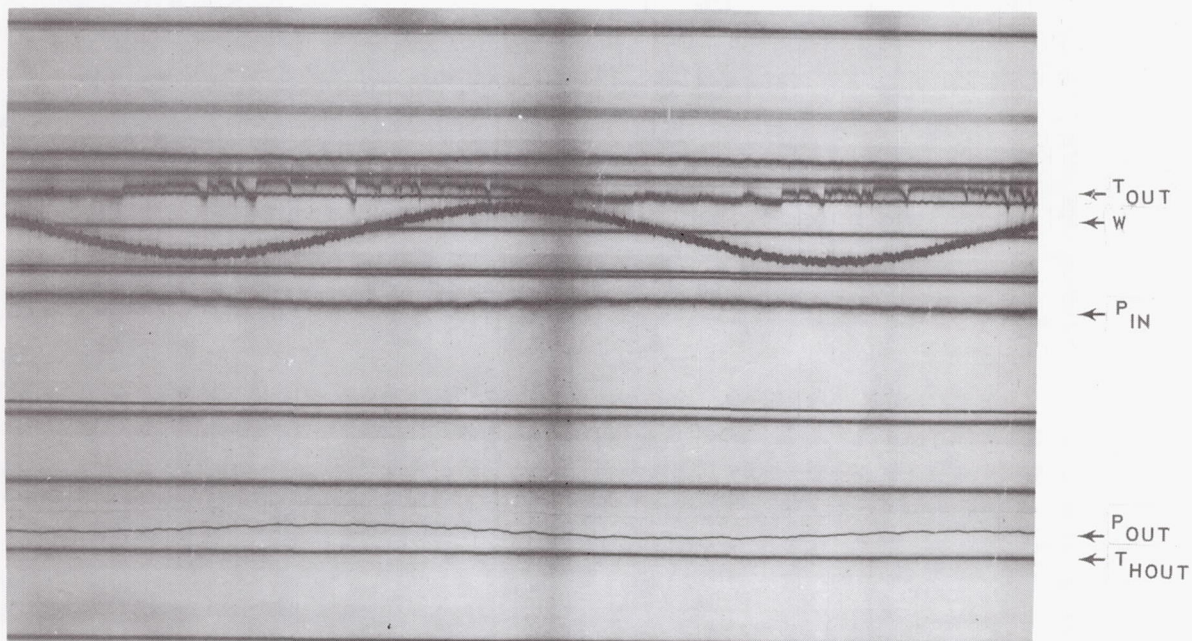
b) Typical Nonlinear Response of T_{out} (obtained at P_{out} = 130 psia, Frequency = 0.01 cps)

Figure 21   Oscillograph Recordings Illustrating the Linearity of the Frequency-
Response Tests

as functions of W and a straight line was drawn through the points for each variable. The amplitude at zero frequency was taken as the slope of this straight line.

The experimental frequency responses were plotted in the form of Bode diagrams as shown in Figures 23 through 32. In general the normalized amplitudes presented in these figures are observed to attenuate from values near 1.0 at a frequency of 0.003 cps to extremely low values in the frequency range between 0.1 and 0.3 cps. The normalized amplitude of the heating-fluid exit temperature T_{Hout} frequency response displays a resonance at the higher frequencies. At several test conditions the frequency responses of the boiling-fluid inlet and exit pressures also displayed resonances. However, in no case did any of the resonances display normalized amplitudes greater than 0.6.

Since high amplitude resonances in the frequency responses of the boiling-fluid inlet and exit pressures can have an important influence on hydrodynamic stability, additional scanning type tests were performed at the operating conditions which displayed resonances in these frequency responses. The purpose of these tests was to determine if there were any very high amplitude resonances either between the data points displayed in Figures 23 through 32 or at frequencies higher than those originally tested. These tests were conducted at closely spaced intervals in the frequency range between 0.2 and 2.0 for the conditions indicated on Table 5. In order to permit instant visual determination of a high amplitude resonance, the signals from the inlet and exit pressure transducers were fed directly into an oscilloscope rather than the oscillograph recorder. However, in the course of these tests no very high amplitude resonances were found.

B. Effect of Primary Variables on Boiler Frequency Response

In examining the frequency-response test data, it appears possible to relate the effects of the primary variables on the frequency response to the condition of the boiling fluid at the exit of the boiler. In almost every instance, the normalized amplitude and the phase lag for each frequency response are observed to shift to the left of the Bode diagrams as any of the primary variables is varied, so that the exit conditions change in the direction from dry superheated vapor to wet saturated conditions. In general, this results in a lower amplitude and a greater phase lag at a given frequency. This can be seen by making a side-by-side comparison of the Bode diagrams presented in Figures 23 through 32. This is further illustrated in Figure 22 for the variation of the boiling-fluid flow rate.

W, lb/hr		ΔT_{SH}	X_e
○	35	117	1.00
△	45	52	1.00
□	55	33	0.95
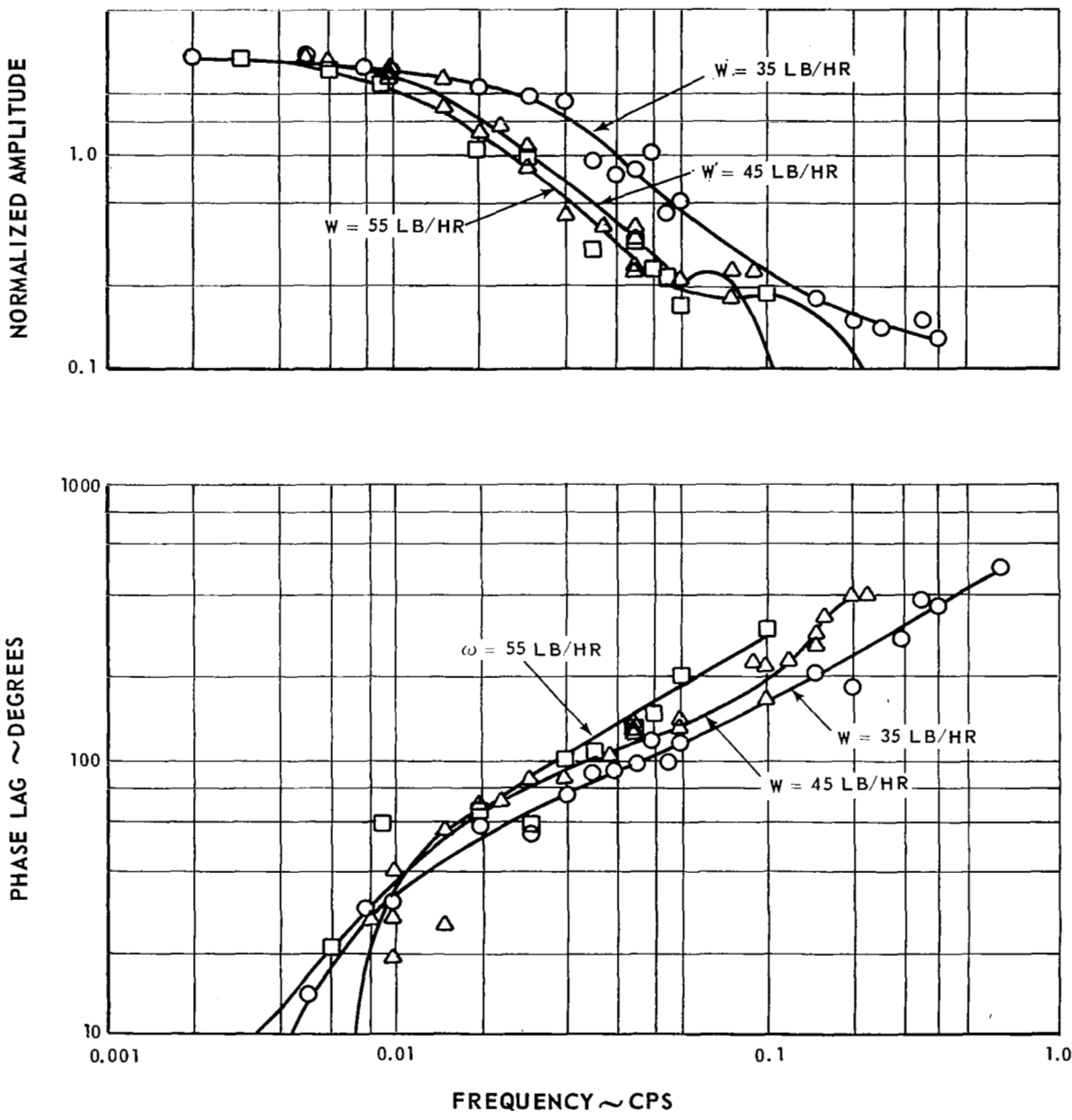
Figure 22   Effect of Boiling-Fluid Flow Rate on P_{out} Frequency Response

The following paragraphs discuss specific characteristics of the experimental frequency-response curves as functions of each primary variable.

1. Effect of Boiling-Fluid Flow Rate

The frequency response for various values of the mean boiling-fluid flow rate, $\overline{W}$ are shown in Figures 23 and 24. The individual graphs are arranged in the order of increasing values of $\overline{W}$ with the 35 lb/hr case representing a dry superheated boiling-fluid exit condition and the 65 lb/hr case representing a wet saturated exit condition.

At a mean boiling-fluid flow rate of 35 lb/hr, Figure 23 shows that the P_{in} frequency response has a normalized amplitude above 3.0 in the middle frequency range. The amplitude then attenuates rapidly to a very low value at 0.25 cps. Two sharp resonances are then found in the frequency range between 0.25 and 1.0 cps. One of these resonances occurs near the frequency of the 180-degree phase lag and may be responsible for the unstable boiler operation observed at flow rates below 30 lb/hr. This is discussed further in Section VI of this report.

As $\overline{W}$ is increased to 45 lb/hr, these sharp resonances are observed to disappear. As $\overline{W}$ is further increased and the boiling-fluid exit conditions become wet (i.e. $X_e < 1.00$), these two resonances reappear at the middle and higher frequencies. In addition, the maximum value of the normalized amplitude curve is observed to decrease towards 1.0 as $\overline{W}$ is increased above 35 lb/hr.

At a mean boiling-fluid flow rate $\overline{W}$ of 35 lb/hr, the normalized amplitude of the P_{out} frequency response does not exhibit the sharp resonances shown by the P_{in} frequency response. As $\overline{W}$ is increased, the normalized amplitude curve of the P_{out} frequency response does not exhibit the sharp resonances shown by the P_{in} frequency response. As $\overline{W}$ is increased, the normalized amplitude curve of the P_{out} frequency response shifts to the left and a slight resonance develops at the

The normalized amplitude of the $T_{H\ out}$ frequency response displays a resonance at all values of $\overline{W}$. As $\overline{W}$ is increased the normalized amplitude curve is observed to shift to the left while the resonance becomes more pronounced.

The normalized amplitude of the T_{out} frequency response is observed to attenuate much more rapidly than the normalized amplitudes of the other frequency responses for values of $\overline{W}$ between 35 and 45 lb/hr. At flow rates above 45 lb/hr, the boiling-fluid exit quality dropped below 1.0 and the response of T_{out} became nonlinear as discussed above. It was not possible to determine a frequency response for T_{out} under these conditions.
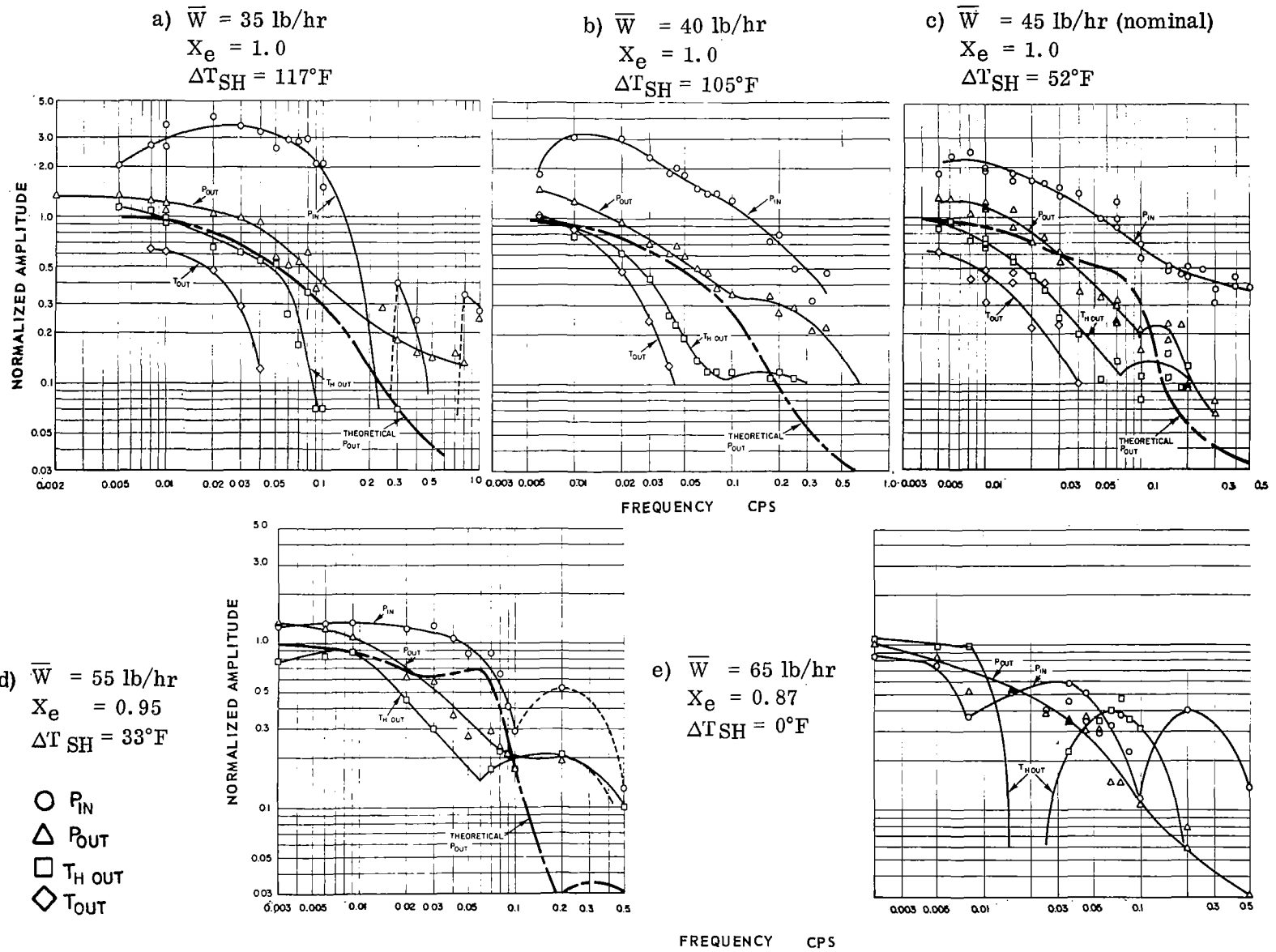
Figure 23   Frequency Response Test Results. Normalized Amplitude vs Frequency at Various Boiling-
Fluid Flow Rates. T_{in} = 140°F, W_H = 770 lb/hr, T.S. valve at nominal setting, $T_{H\ in}$ = 410°F

a) $\overline{W}$ = 35 lb/hr
X_e = 1.0
ΔT_{SH} = 117°F

b) $\overline{W}$ = 40 lb/hr
X_e = 1.0
ΔT_{SH} = 105°F

c) $\overline{W}$ = 45 lb/hr
X_e = 1.0
ΔT_{SH} = 52°F

d) $\overline{W}$ = 55 lb/hr
X_e = 0.95
ΔT_{SH} = 33°F

e) $\overline{W}$ = 65 lb/hr
X_e = 0.87
ΔT_{SH} = 0°F

O P_{IN}
△ P_{OUT}
□ $T_{H\ OUT}$
◇ T_{OUT}
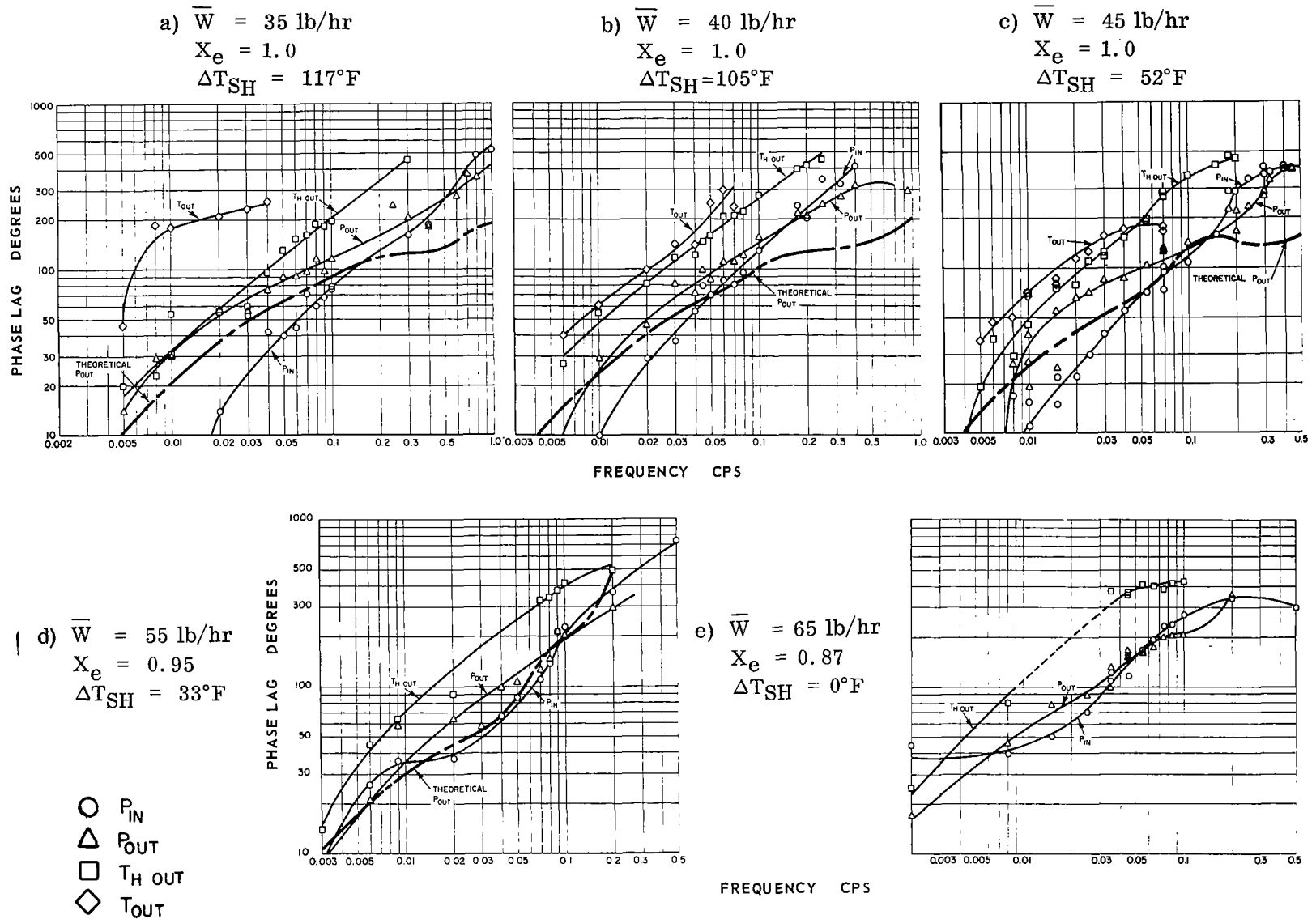
Figure 24   Frequency Response Test Results. Phase Lag vs Frequency at Various Boiling-Fluid
Flow Rates. T_{in} = 140°F, W_H = 770 lb/hr, T.S. valve at nominal setting, $T_{H\ in}$ = 410°F

As $\overline{W}$ is increased from 35 lb/hr the phase lag of the T_{out} frequency response shifts to the right as can be seen by comparing Figure 24a to 24c. This is the principal exception found to the general tendency of both normalized-amplitude and phase-lag curves to shift to the left as boiling-fluid exit conditions change from dry superheated vapor towards wet saturated conditions.

In conducting the frequency-response tests at a mean boiling-fluid flow rate of 35 lb/hr an unusual phenomenon was observed which has not yet been explained. At a single frequency near 3.0 cps the level of the boiling-fluid exit pressure was observed to drop drastically and then remain constant with time. In addition no further fluctuations in exit pressure were observed on the oscillograph recording in response to the sinusoidal perturbations of boiling-fluid flow rate.

2. Effect of Heating-Fluid Flow Rate

The frequency responses for various values of the heating-fluid flow rate W_H are shown in Figures 25 and 26. The individual graphs on these figures are arranged in order of decreasing value of the heating-fluid flow rate, with the 1000 lb/hr case representing a dry superheated boiling-fluid exit condition and the 400 lb/hr case representing a wet nonequilibrium exit condition.

In comparing the frequency responses at the different conditions shown in these figures a general tendency of both normalized-amplitude and phase-lag curves to shift to the left as W_H is decreased can be seen. This corresponds to a change in boiling-fluid exit conditions from dry superheated vapor to wet nonequilibrium conditions.

The normalized amplitude of the P_{in} frequency response exhibits no resonances. The normalized amplitude of the P_{out} frequency response exhibits a slight resonance only in the immediate region of the nominal operating condition of 770 lb/hr. The normalized amplitude of the T_{Hout} frequency response develops a resonance at a heating fluid flow rate of 840 lb/hr. This resonance becomes more pronounced as heating-fluid flow rate is decreased, producing nonequilibrium conditions at the boiling fluid exit.

An interesting phenomenon was observed while testing at the 400 lb/hr condition. When perturbing the boiling-fluid flow rate at a frequency of 0.085 cps, P_{in} and P_{out} responded at a frequency of 0.24 cps, a harmonic of the input frequency, while the other variables responded at the input frequency. This type of response may be related to an area of unstable operation also discovered while testing at the 400 lb/hr condition, which is discussed further in Section VI below.

a) W_H = 1000 lb/hr
X_e = 1.00
ΔT_{SH} = 93°F

b) W_H = 840 lb/hr
X_e = 1.0
ΔT_{SH} = 68°F

c) W_H = 770 lb/hr
X_e = 1.00
ΔT_{SH} = 52°F

d) W_H = 600 lb/hr
X_e = 0.98
ΔT_{SH} = 46°F

e) W_H = 400 lb/hr
X_e = 0.88
ΔT_{SH} = 31°F

○ P_{IN}

△ P_{OUT}

□ $T_{H\ OUT}$

◇ T_{OUT}
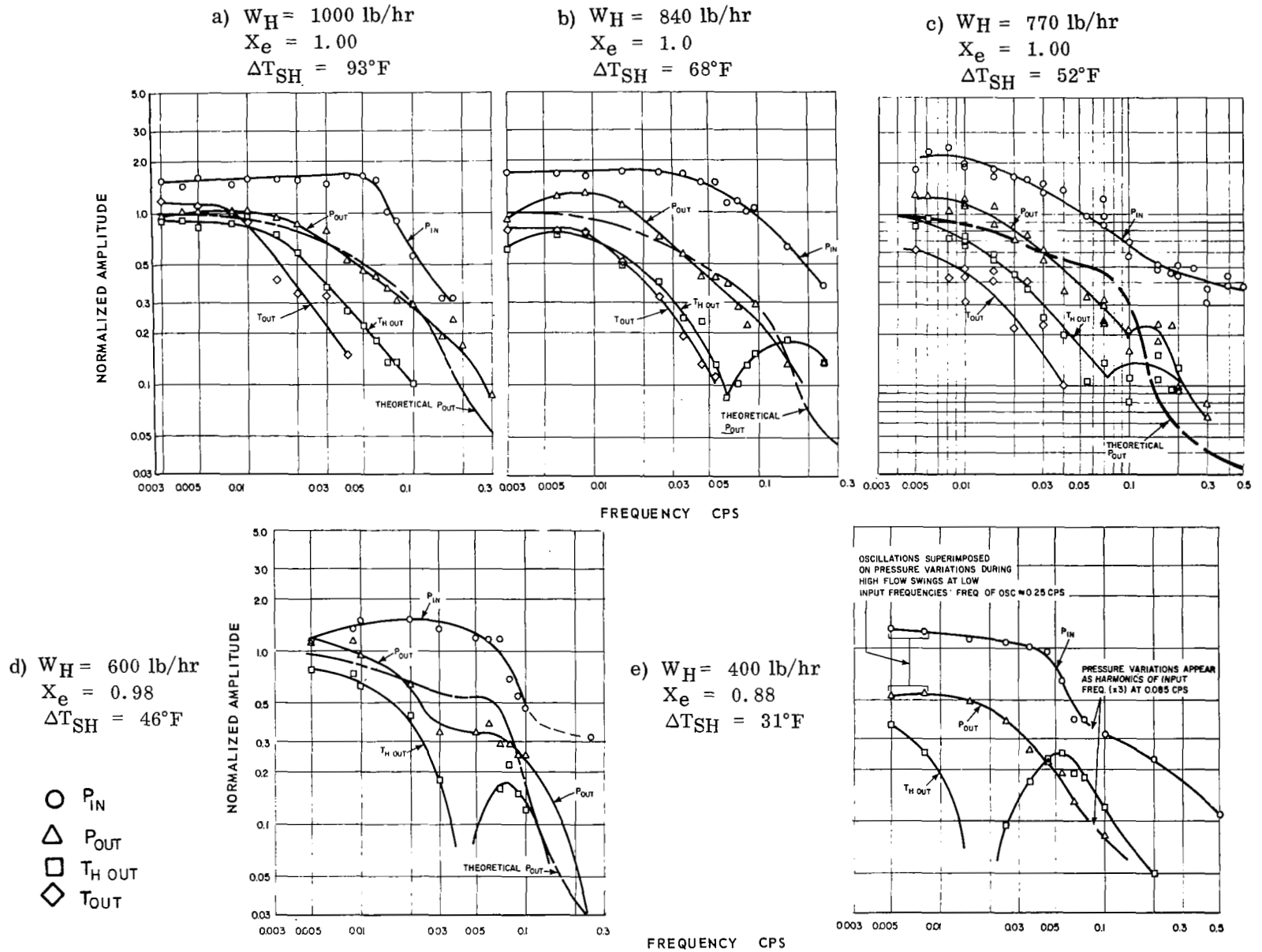
Figure 25   Frequency Response Test Results. Normalized Amplitude vs Frequency at Various Heating-Fluid Flow Rates. W = 45 lb/hr, $T_{H\ in}$ = 410°F, T_{in} = 140°F, T.S. valve at nominal setting
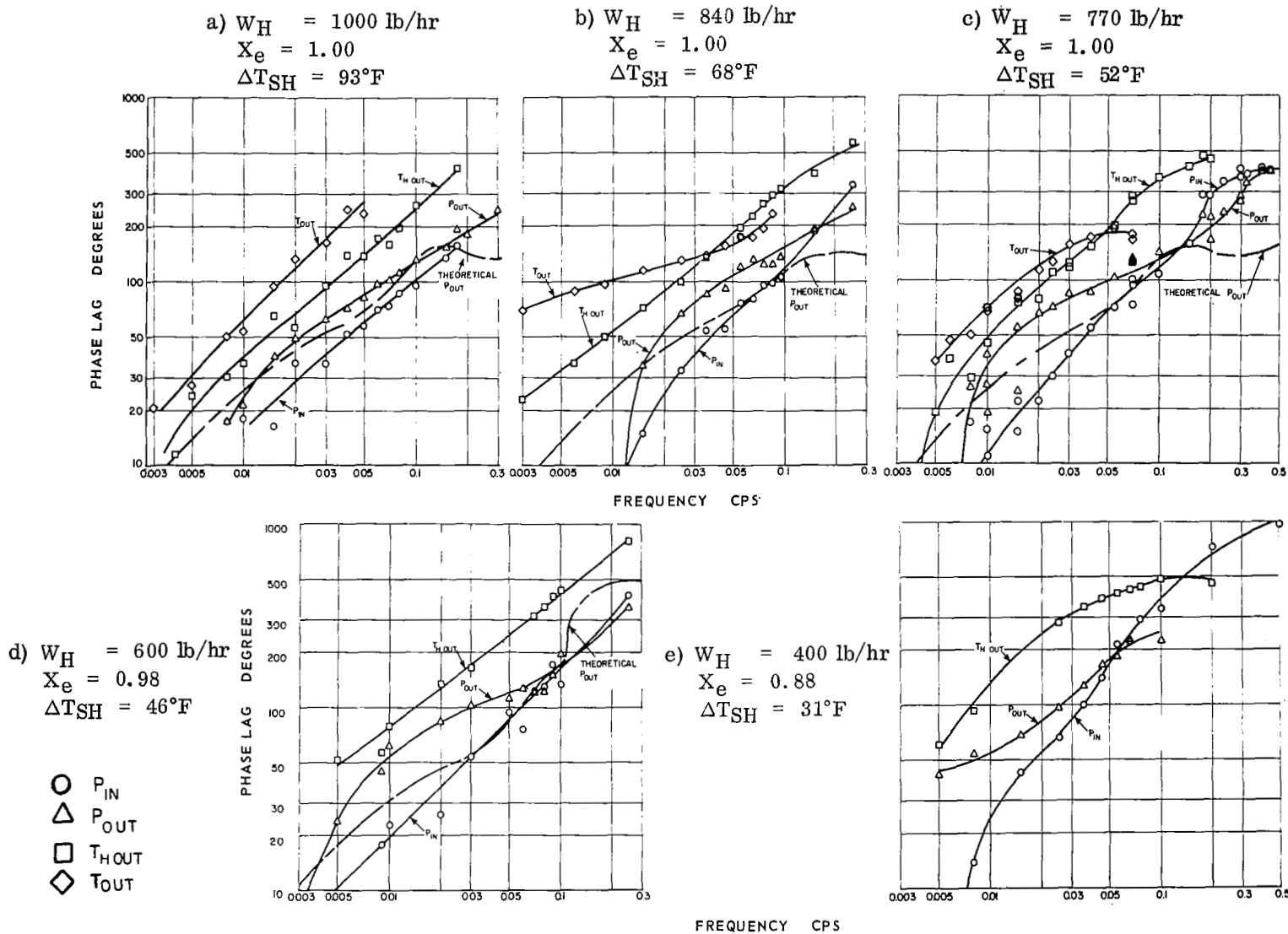
Figure 26   Frequency Response Test Results. Phase Lag vs Frequency at Various Heating-Fluid
Flow Rates. W = 45 lb/hr, $T_{H\ in}$ = 410°F, T_{in} = 140°F, T.S. valve at nominal setting

3. Effect of Heating-Fluid Inlet Temperature

The frequency responses for various values of heating-fluid inlet temperature T_{Hin} are shown in Figures 27 and 28. The individual graphs in these figures are arranged in order of decreasing value of heating-fluid inlet temperature with the 430°F case representing a dry superheated boiling fluid exit condition and the 360°F case representing a wet nonequilibrium exit condition.

In comparing the frequency responses at the different test conditions shown in Figures 27 and 28 it can be seen that the normalized-amplitude and phase-lag curves tend to shift to the left as $T_{H\,in}$ is decreased.

The normalized amplitude of the P_{in} frequency response exhibits a resonance at the 360°F condition. The normalized amplitude of the P_{out} frequency response displays a slight resonance for values of $T_{H\,in}$ below 420°F. The normalized amplitude of the T_{Hout} frequency response also develops a resonance at the 420°F condition. This resonance becomes more pronounced as $T_{H\,in}$ is decreased and nonequilibrium exit conditions are achieved.

At the 360°F condition the phase-lag curve of the T_{Hout} frequency response is drawn as a dotted line in the frequency range between 0.01 and 0.03 cps. This was done because the exact shape of the curve in this region is not known. Since there was no readable variation in the amplitude of the T_{Hout} response in this region, it was not possible to determine the phase lag from the oscillograph recording.

4. Effect of Boiling-Fluid Exit Pressure

The frequency responses for various values of the mean boiling-fluid exit pressure P_{out} are shown in Figures 29 and 30. The individual graphs in these figures are arranged in order of increasing value of P_{out}, with the 50 psia case representing a dry superheated boiling fluid exit condition and the 130 psia case representing a wet nonequilibrium condition.

In comparing the frequency responses at the different conditions shown in Figures 29 and 30 it can again be seen that all normalized-amplitude and phase-lag curves shift to the left as P_{out} is increased, producing a decrease in boiling-fluid superheat and exit quality. In addition, the maximum value of the normalized amplitude of the P_{in} frequency response is observed to decrease as P_{out} is increased.

The normalized amplitude of the P_{out} frequency response develops a slight resonance near the nominal condition of 65 psia. However, the resonance is not significant at other conditions. The normalized amplitude of the T_{Hout} frequency response exhibts a resonance at all values of P_{out}. This resonance is seen to

a) $T_{H \text{ in}} = 430°F$
$X_e = 1.00$
$\Delta T_{SH} = 105°F$

b) $T_{H \text{ in}} = 420°F$
$X_e = 1.00$
$\Delta T_{SH} = 84°F$

c) $T_{H \text{ in}} = 410°F$
$X_e = 1.00$
$\Delta T_{SH} = 52°F$

d) $T_{H \text{ in}} = 390°F$
$X_e = 0.96$
$\Delta T_{SH} = 37°F$

e) $T_{H \text{ in}} = 360°F$
$X_e = 0.84$
$\Delta T_{SH} = 3°F$

○ P_{IN}
△ P_{OUT}
□ $T_{H \text{ OUT}}$
◇ T_{OUT}
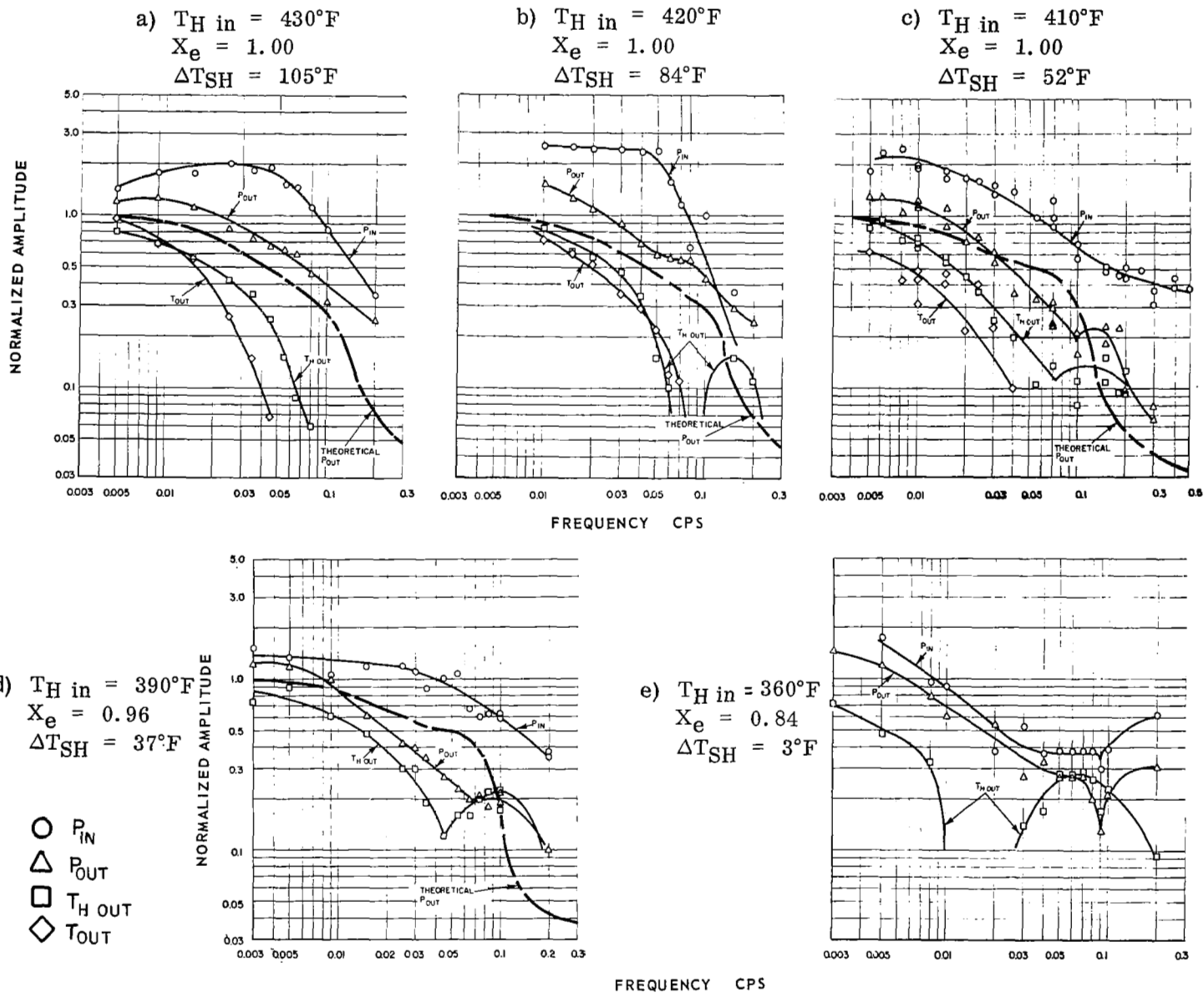
FREQUENCY   CPS

Figure 27   Frequency Response Test Results. Normalized Amplitude vs Frequency at Various Heating-Fluid Inlet Temperatures. W = 45lb/hr, W_H = 770 lb/hr, T_{in} = 140°F, T.S. valve at nominal setting
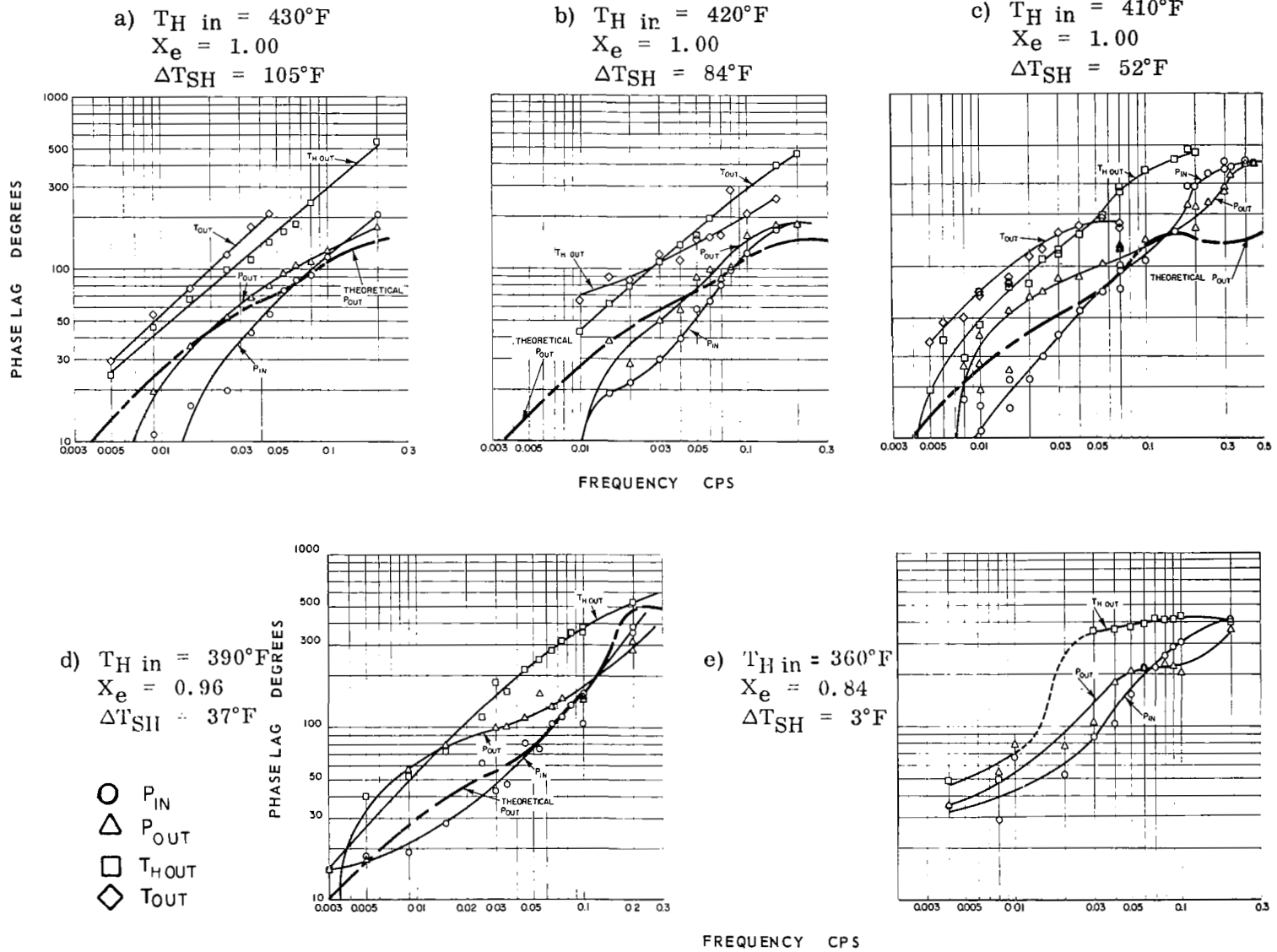
Figure 28   Frequency Response Test Results. Phase Lag vs Frequency at Various Heating-Fluid Inlet Temperatures. W = 45 lb/hr, W_H = 770 lb/hr, T_{in} = 140°F, T.S. valve at nominal setting

a) $\overline{P}_{out}$ = 50 psia
X_e = 1.00
ΔT_{SH} = 112°F

b) $\overline{P}_{out}$ = 60 psia
X_e = 1.00
ΔT_{SH} = 82°F

c) $\overline{P}_{out}$ = 65 psia
X_e = 1.00
ΔT_{SH} = 52°F

d) $\overline{P}_{out}$ = 100 psia
X_e = 0.93
ΔT_{SH} = 22°F

○ P_{IN}
△ P_{OUT}
□ $T_{H\ OUT}$
◇ T_{OUT}

e) $\overline{P}_{out}$ = 130 psia
X_e = 0.88
ΔT_{SH} = 5°F
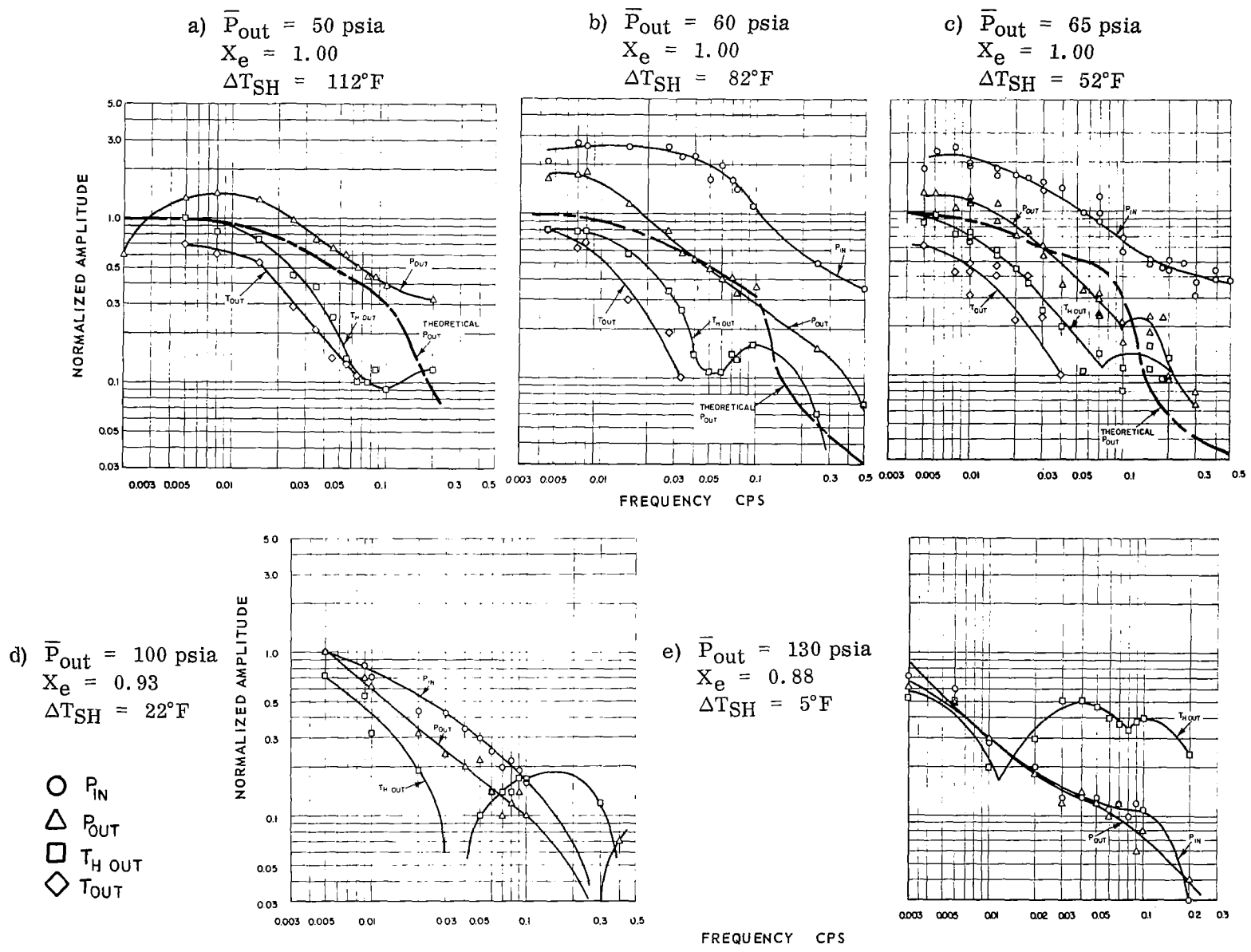
Figure 29   Frequency Response Test Results. Normalized Amplitude vs Frequency at Various Boiling-
Boiling-Fluid Exit Pressures. W = 45 lb/hr, W_H = 770 lb/hr, T_{in} = 140°F, $T_{H\ in}$ = 410°F

a) $\overline{P}_{out} = 50$ psia
$X_e = 1.00$
$\Delta T_{SH} = 112°F$

b) $\overline{P}_{out} = 60$ psia
$X_e = 1.00$
$\Delta T_{SH} = 82°F$

c) $\overline{P}_{out} = 65$ psia
$X_e = 1.00$
$\Delta T_{SH} = 52°F$

d) $\overline{P}_{out}$ 100 psia
X_e 0.93
ΔT_{SH} 22°F

○ P_{IN}
△ P_{OUT}
□ $T_{H\ OUT}$
◇ T_{OUT}

e) $\overline{P}_{out} = 130$ psia
$X_e = 0.88$
$\Delta T_{SH} = 5°F$
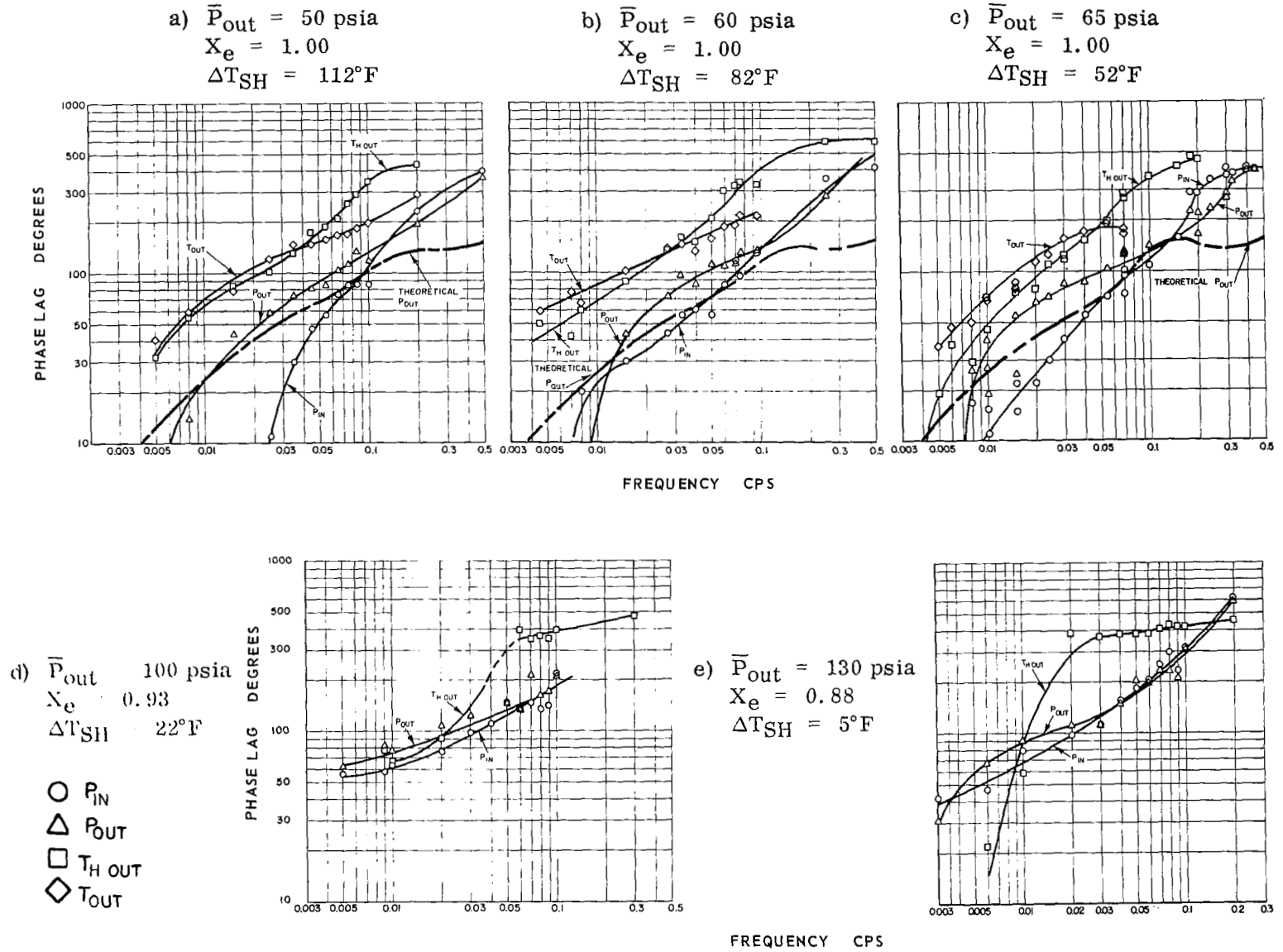
Figure 30   Frequency Response Test Results.   Phase Lag vs Frequency at Various Boiling-Fluid
Exit Pressures.   W = 45 lb/hr, W_H = 770 lb/hr, T_{in} = 140°F, $T_{H\ in}$ = 410°F

become more pronounced and a second resonance is seen to develop as P_{out} is increased, producing nonequilibrium conditions at the boiling-fluid exit.

In Figure 29a it can be seen that no normalized-amplitude curve is plotted for the P_{in} frequency response for the 50 psia case. The reason for this can be seen by examining Figure 33 which is a plot of the steady-state normalizing data, $\Delta P_{in}/\Delta W$ versus P_{out}. The normalizing data is seen to approach zero as P_{out} approaches 50 psia. This steady-state behavior results from the fact that the decrease in pressure drop in the boiler with an increase in flow rate nearly equals the increase in pressure upstream of the choked valve with an increase in flow rate. When this data is used to normalize the amplitude of the frequency response for the 50 psia case, values approaching infinity result and the normalized amplitude is no longer a convenient parameter to describe the boiler dynamics.

If the actual amplitude of the frequency response in this region is studied instead of the normalized amplitude, an interesting effect is noticed. Figure 34 shows a plot of actual amplitudes for the P_{in} response at three different exit pressure conditions. The actual amplitudes are almost identical over most of the frequency range for all three conditions. This occurs despite significant differences in the normalized amplitude. This indicates that, although there are advantages in presenting frequency-response data by normalizing variations to their steady-state values, in some cases dynamic similarities may be obscured in the normalizing process.

5. Effect of Boiling-Fluid Inlet Temperature

The frequency response for various values of the boiling-fluid inlet temperature T_{in} are shown in Figures 31 and 32. The individual graphs on these figures are arranged in order of decreasing value of T_{in} which also represents the order of decreasing boiling-fluid superheat.

In comparing the frequency responses at these different conditions, there appears to be very little difference between the frequency responses at each condition. However there is some tendency for the normalized-amplitude and phase-lag curves to shift to the left as T_{in} decreases.

6. Theoretical Transfer Function

Figures 23 through 32 also contain curves representing the theoretical values for the P_{out} transfer function as predicted by the analysis of boiler dynamics presented in Section VII of this report. These curves permit a point-by-point comparison between the theoretical and experimental values for the P_{out} normalized amplitudes and phase lags. Additional comparisons between the theory and the experimental data together with a detailed discussion of these comparisons are presented in Section VII.

a) T_{in} = 185°F
    X_e = 1.00
    ΔT_{SH} = 60°F

b) T_{in} = 160°F
    X_e = 1.00
    ΔT_{SH} = 55°F

c) T_{in} = 140°F
    X_e = 1.00
    ΔT_{SH} = 52°F

d) T_{in} = 120°F
    X_e = 1.00
    ΔT_{SH} = 50°F

e) T_{in} = 95°F
    X_e = 1.00
    ΔT_{SH} = 49°F

○ P_{IN}
△ P_{OUT}
□ $T_{H\ OUT}$
◇ T_{OUT}
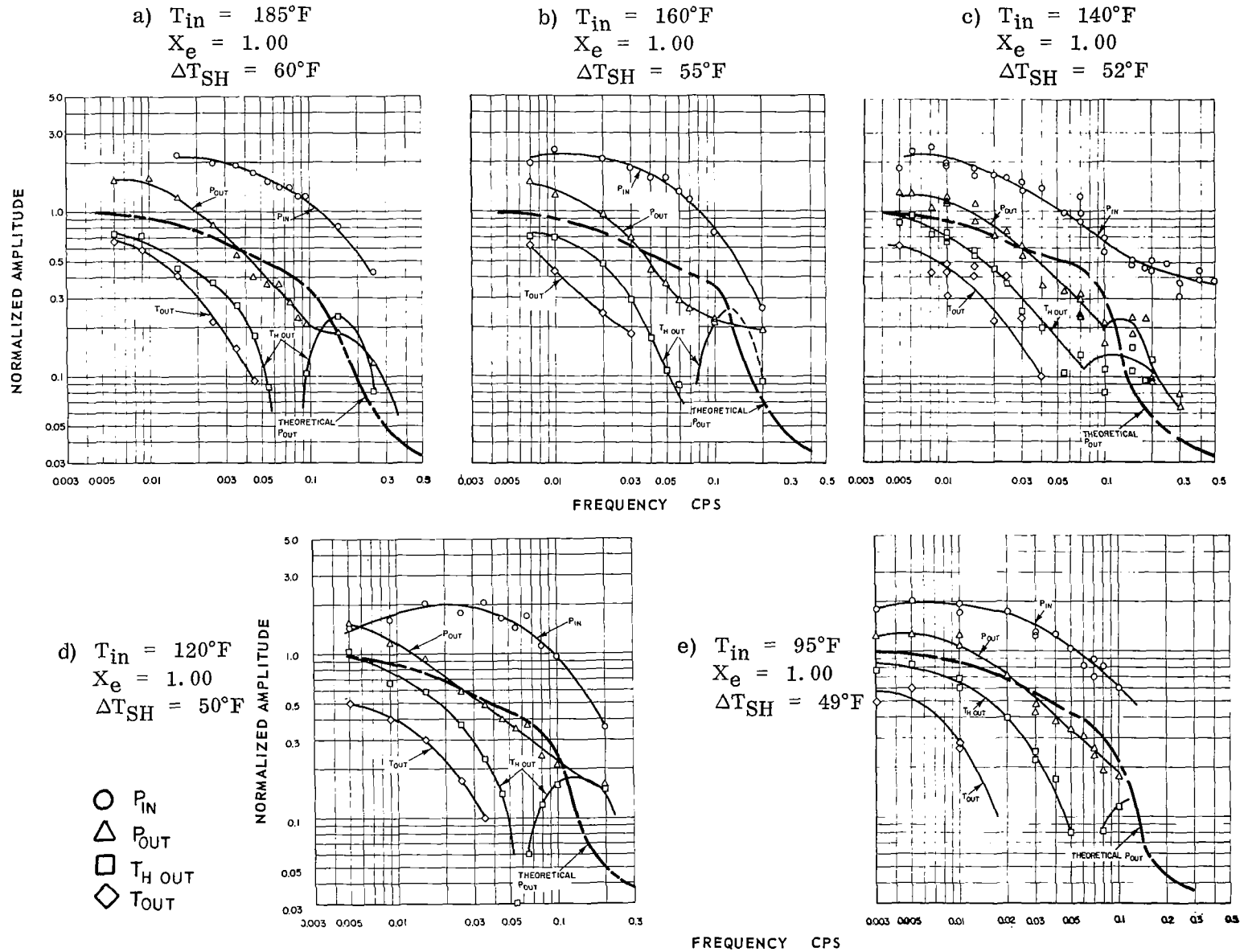
Figure 31   Frequency Response Test Results. Normalized Amplitude vs Frequency at Various Boiling-Fluid
Inlet Temperatures. W = 45 lb/hr, W_H = 770 lb/hr, $T_{H\ in}$ = 410°F, T.S. valve at nominal setting
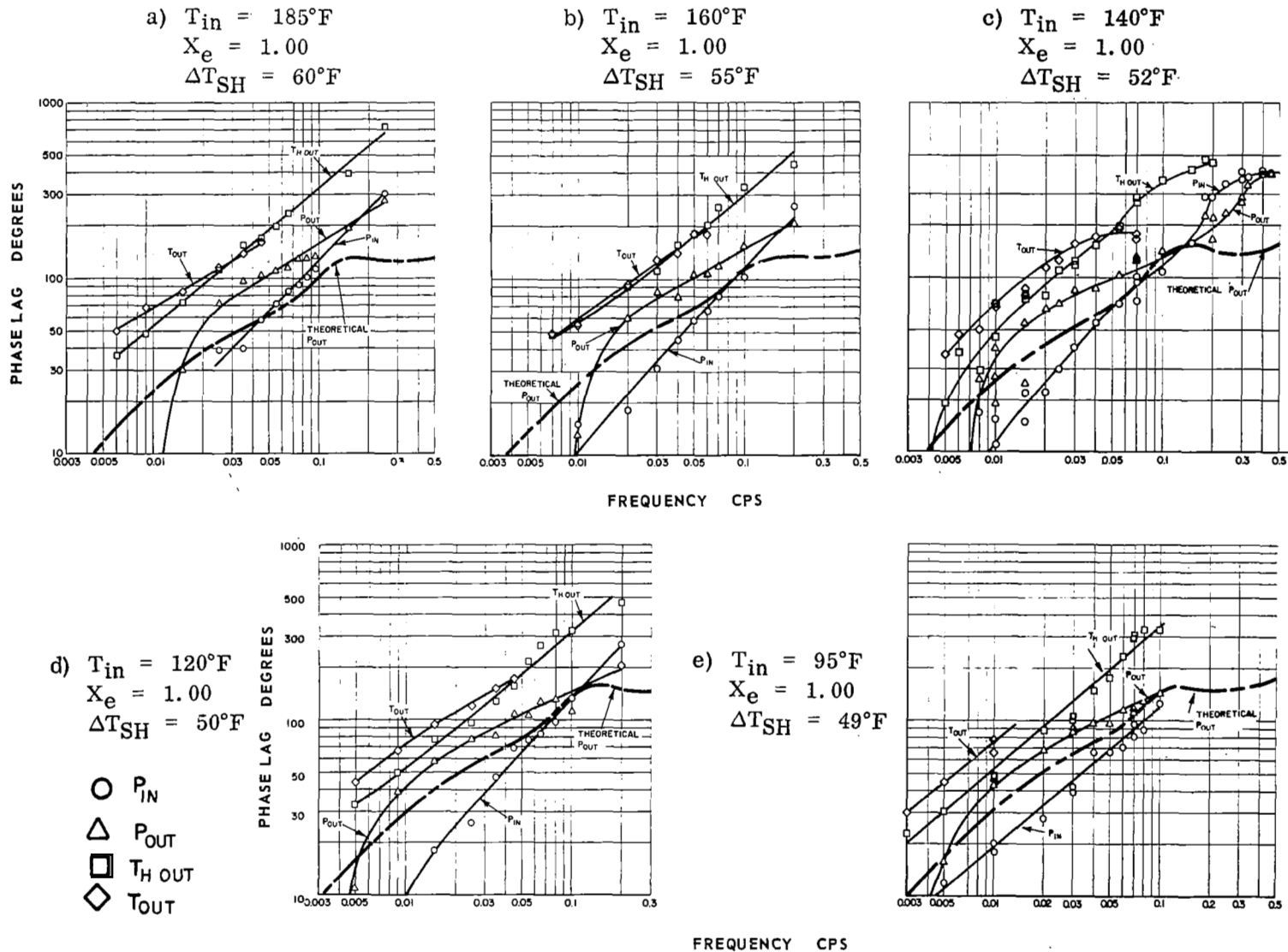
Figure 32   Frequency Response Test Results. Phase Lag vs Frequency at Various Boiling-Fluid Inlet
Temperatures. W = 45 lb/hr, W_H = 770 lb/hr, $T_{H\,in}$ = 410°F, T.S. valve at nominal setting
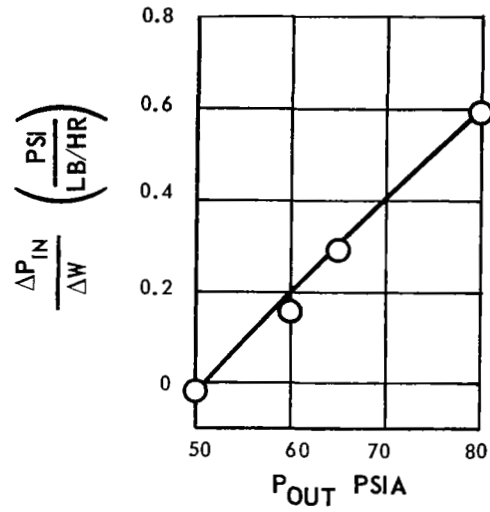
Figure 33   Normalizing Data vs Boiling-Fluid Exit Pressure P_{out}

FREQUENCY ~ CPS
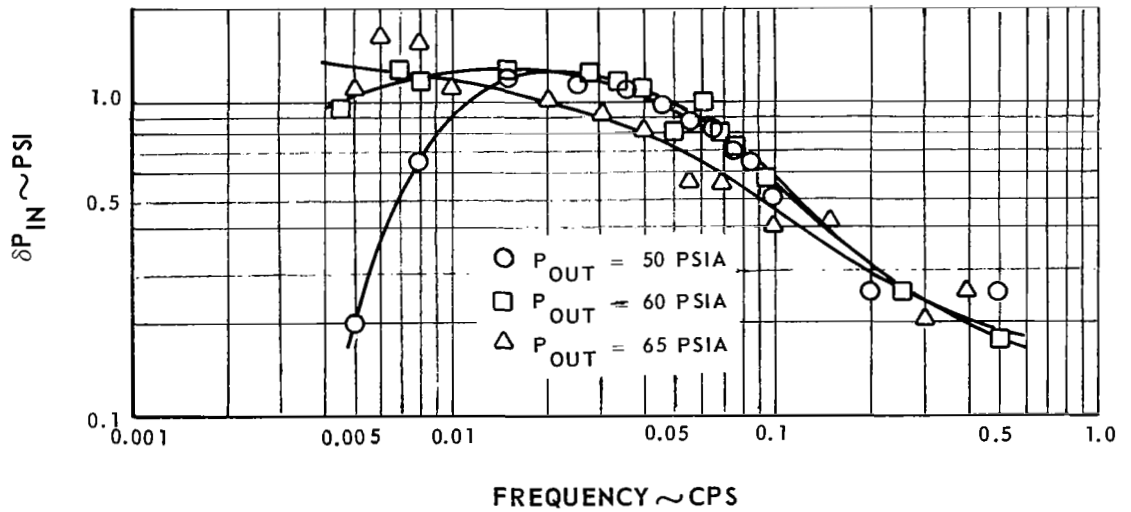
Figure 34   Amplitude of Boiling-Fluid Inlet Pressure Response δP_{in} to Sinusoidal Flow Perturbation of ± 3.0 lb/hr

C. Step-Response Characteristics of Boiler

At each operating condition specified in Table 5 step-response tests were conducted following the procedures described in Section III of this report. The main purpose of the step-response tests was to determine whether resonances were present at higher frequencies than could be obtained in the frequency-response tests. Examination of the oscillograph recordings of the pressure and temperature responses revealed no high-frequency resonances. A photograph of an oscillograph record of the initial portion of one test is presented in Figure 35. In this test a 12 percent step increase in flow rate at the boiler inlet was made starting at a steady-state condition with 60 psia boiler exit pressure. The initial and final positions of the recorded boiler-exit pressure trace are shown with dotted lines in the figure to make the form of the response more apparent. The boiler-exit pressure response is seen to consist of a pure delay of about 2 seconds, followed by an approximately exponential rise with a time constant of about 10 seconds. The responses of the boiler inlet pressure, exit temperature and the heating-fluid exit temperature also tend towards a delay followed by an exponential change, but are less clear-cut. In particular, the boiler inlet pressure underwent readjustments up to 15 minutes after the step change. These readjustments were small in absolute magnitude (less than 1 psi) but relatively large compared to the total change induced by the flow step.

The other steady-state operating conditions at which superheated vapor was produced at the boiler exit showed the same type of responses to a step change in flow rate.
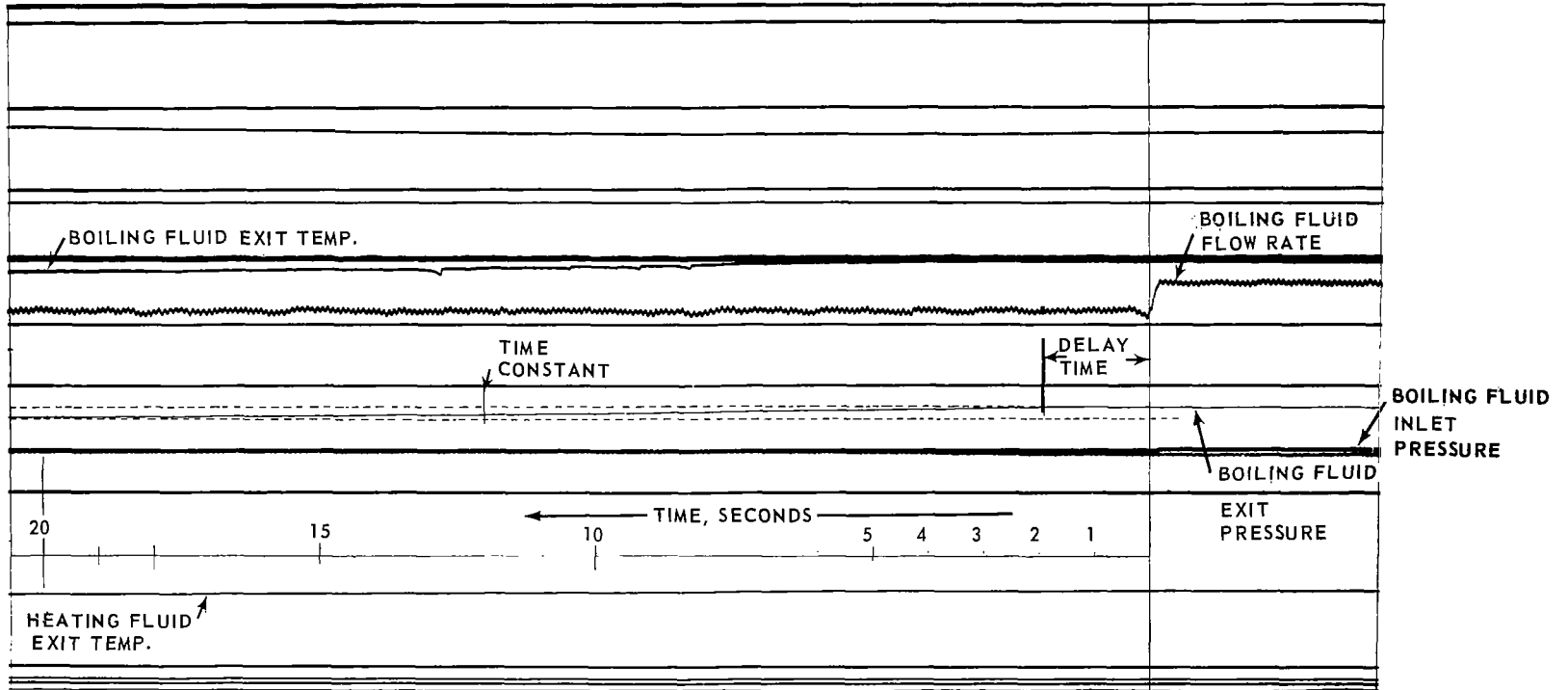
Figure 35 Oscillograph Recording of Response to Step Change in Boiling-Fluid Flow Rate

VI. BOILER STABILITY

During the course of the testing required under the contract, two areas of unstable boiler operation were observed. These instabilities were characterized by sustained oscillations in boiling fluid pressure. This section discusses the possible causes of these instabilities in terms of the types of instability known to occur in boiling systems.

A. Types of Boiler Instability

Instability in boiling systems has been observed by a multitude of investigators. The causes for these instabilities are not, as yet, completely understood. They do appear to be closely related to the specific test system configurations employed by each investigator. As a consequence, numerous types of different boiler instability have been cited in the literature. As indicated in Reference 1, the job of classifying and understanding the different types of instability is still in its early stages.

The following paragraphs discuss the types of instability that are pertinent to the boiling system of this study. For purposes of discussion these instabilities will be classified in terms of those that result from interactions between the boiler and the feed system and those that result from dynamic interactions within the boiler itself.

1. Feed System-Boiler Instability

The frequency response of the boiler inlet pressure indicates the dynamic head-flow characteristics that are required in the power-loop pump in order to avoid unstable system interactions. A simplified stability criterion for matching the pump and boiler for a typical Rankine-cycle system is presented as follows. The coupling between boiler inlet pressure and pump exit pressure, and between boiler-inlet flow rate and pump-exit flow rate is represented schematically below, using control notation. It will be assumed in the following discussion that the pump exit pressure-versus-flow rate characteristics are linear, that there are no additional impedances between the pump and the boiler, and that there are no time delays between changes in flow rate in the pump and pump exit pressure. This condition is approximated in a powerplant when the pump inlet pressure is held constant, as was done with the test system in this study.

65
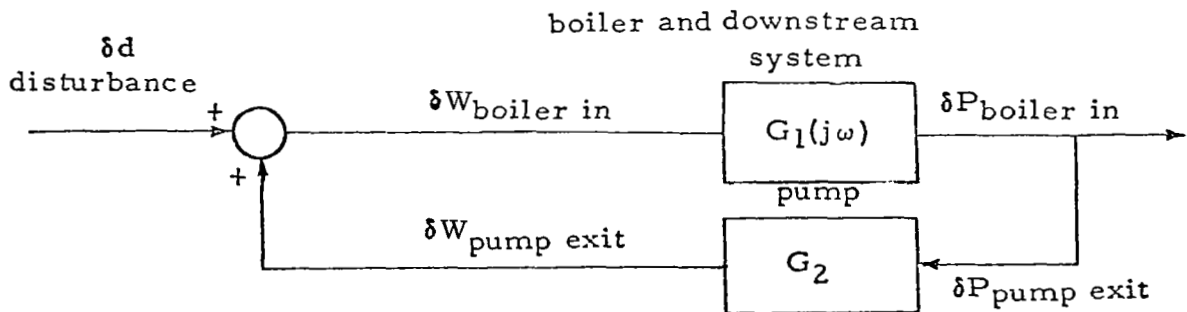
Since the fluid between the pump exit and boiler inlet is in a liquid state and lengths involved are small, the effects of fluid compressibility and momentum are small. The pressure and flow rate are, therefore, approximately equal at the pump exit and boiler inlet. Assuming that a disturbance is introduced into this coupled system, the response of the boiler inlet pressure to the disturbance δd may be written

$$\delta P_{boiler\ in} = \frac{G_1\ (j\omega)}{1 - G_1\ (j\omega)\ G_2}\ \delta d \qquad (2)$$

The terms $G_1\ (j\omega)$ and G_2 represent the transfer functions of the boiling-fluid inlet pressure, and the pump exit pressure respectively. $G_1\ (j\omega)$ is defined by the relation

$$G_1\ (j\omega) = \frac{\delta P_{in}}{\delta W_{in}}\ (j\omega) \qquad (3)$$

The experimental values of $G_1\ (j\omega)$ obtained from the P_{in} frequency-responses are presented in Figures 23 through 32. Actual amplitudes can be calculated by multiplying the normalized amplitudes presented in these figures by the corresponding values of $\Delta P_{in}/\Delta W$ presented in Table 11.

If it is assumed that the boiler is stable when operated in an open loop, then the closed-loop system diagrammed would be unstable when the following condition is incurred

$$G_1\ (j\omega)\ G_2 \geq 1 \qquad (4)$$

From the assumed linear pump characteristics

$$P_{pump\ exit} = C_1 - C_2\ W_{pump\ exit} \qquad (5)$$

It follows that $\quad G_2 = \dfrac{\delta W_{pump\ exit}}{\delta P_{pump\ exit}} = -\dfrac{1}{C_2} \qquad (6)$

Consequently this simplified analysis indicates that the system is unstable when

$$\left| G_1\ (j\omega) \right| \geq \left| -\ C_2 \right| \qquad (7)$$

66

According to Equation (7) pump-boiler instabilities will occur under two possible conditions:

a) The amplitude of the boiler transfer function is negative at zero frequency and less than the pump slope, C_2, as shown in Equation (8) below:

$$G_1 (0) = \left(\frac{\Delta P_{in}}{\Delta W} \right) < - C_2 \qquad (8)$$

b) The amplitude of the boiler transfer function is greater than or equal to C_2 at a phase angle of 180 degrees (or an odd multiple of 180 degrees).

The first condition is frequently referred to as a static instability since it results from the static, rather than the dynamic characteristics of the boiler. The static instability results in an unattainable operating point, and system excursions from this point to a stable point. This type of instability is discussed widely in the literature[6].

The pump-boiler combination for the test system of this study is statically stable. This occurs in spite of the negative slope of the curve of boiler pressure loss versus flow rate, and results from the fact that as the boiling-fluid flow rate is increased, the increase in P_{out} resulting from the flow through the choked restriction more than compensates for the reduction in ΔP due to the negative slope. This is illustrated in Figure 36 where it can be seen that P_{in} increases with flow rate over the range of the conditions tested. The term $(\Delta P_{in}/\Delta W)$ is therefore positive and the system is statically stable.
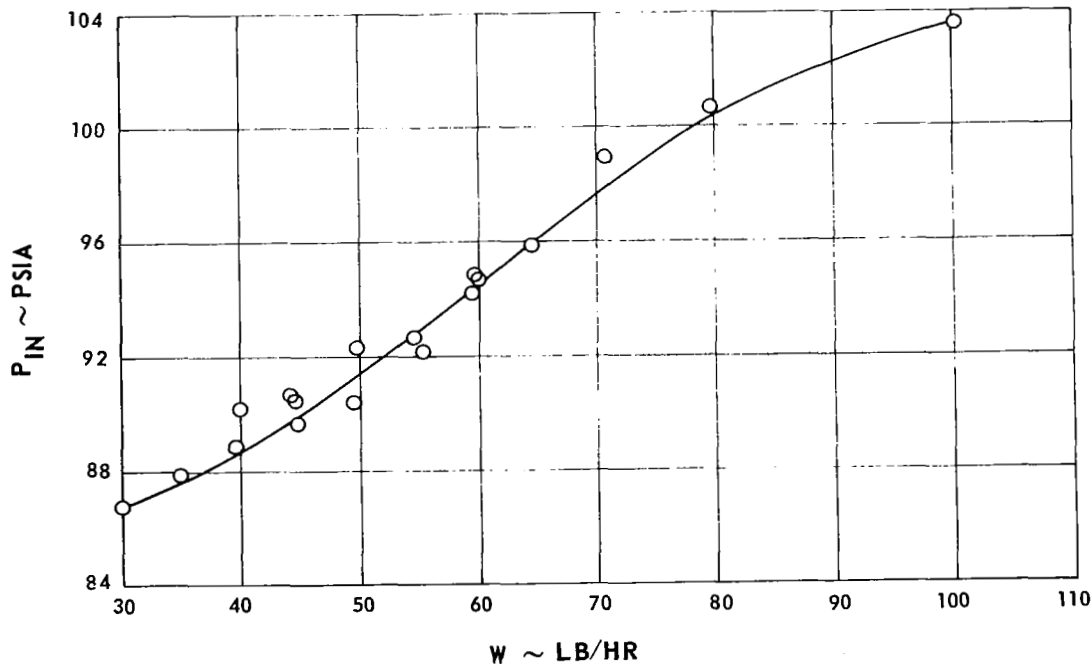
Figure 36   Boiling-Fluid Inlet Pressure vs Boiling-Fluid Flow Rate

67

The second condition results in an instability which involves the dynamic characteristics of the boiler and the feed system. Under this condition flow rates and pressures are observed to oscillate at the frequency at which the 180-degree phase shift occurs. From examination of Figures 23 through 32, in light of Equation (7), it is evident that dynamic instability is possible in the operation of the test boiler. For many of the conditions tested, the P_{in} transfer function has a relatively large amplitude at the frequency where the 180-degree phase lag occurs. Whether or not such instabilities will occur at a given operating point will then depend upon the pressure-versus-flow characteristics of the feed system.

2. Internal Instability

Internal instabilities arise from the dynamic interactions between the thermal and hydraulic processes occurring within the boiler. The complexity of these interactions can be appreciated by reviewing the analysis of the boiler dynamics discussed in Section VII and Appendix 2.

Several different types of internal instability are possible for the counterflow boiler configuration of the study. One of the more frequently observed internal instabilities results from a transition between different flow regimes. Considering a once-through boiler which produces superheated vapor, the boiling fluid undergoes several transitions between two-phase flow regimes as it passes through the boiler. These regimes include:

1) Bubbly flow
2) Plug-slug flow
3) Annular flow
4) Annular mist transition flow
5) Mist flow

Other transitions are also possible. These include the transition between laminar and turbulent flow and between nucleate and film boiling.

According to Berenson[7], the transitions between: a) bubble, plug, and annular flow; b) laminar and turbulent flow; and c) nucleate and film boiling can all give rise to instabilities. These instabilities include pressure variations, transient pressure drop and recovery, and sustained oscillations.

Closely related to the flow regime transition instabilities is the density wave instability observed by Stenning and Veziroglu[8]. This type of instability involves the dynamic interaction between the flow rate, the two-phase density distribution, and the pressure gradient distribution within the boiler. A detailed discussion of this type of instability is presented in the reference.

A third type of internal instability is possible due to the feed-back characteristics of the counterflow boiler configuration. Temperature fluctuations in the boiling fluid will affect the local heat-transfer rate. This, in turn, will affect both the local rate of vapor generation and the temperature of the heating fluid.

It is possible for a boiling fluid temperature and pressure disturbance originating near the pinch point to propagate down the length of the boiler. This would produce a disturbance in the heating-fluid temperature which would propagate in the opposite direction due to the counter flow of the heating fluid. If this disturbance reached the pinch point 180 degrees out of phase with the initial disturbance, an unstable condition could result. This type of instability would be particularly significant under those conditions where the pinch point temperature difference was relatively small.

B. Areas of Unstable Operation

Oscillatory instabilities were encountered at two operating conditions. The first instability was encountered during steady-state testing when the boiling-fluid flow rate was slightly less than 30 lb/hr with the other primary variables at their nominal values. Neutral or constant-amplitude oscillations occurred with a frequency of approximately 0.9 cps. This unstable condition was first encountered with the electrohydraulic valve at the boiler inlet in the integral flow control mode. An oscillograph recording taken at that time is shown in Figure 37a. The same condition was then set with the electrohydraulic valve in a fixed position, and the oscillograph recording shown in Figure 37b resulted. A comparison of the two records shows that when the valve was put in a fixed position the oscillations had about the same frequency as before, and the amplitude of variation of P_{in}, P_{out}, T_{Hout}, and T_{out} remained about the same. The flow rate trace with a fixed valve position was nearly sinusoidal, while with the valve operating as a flow control, most of the flow variation occurred in about 1/5 of the cycle, and the amplitude of the variation was about 1/3 less. Apparently the flow control system, as set up for these tests, was not sufficiently fast to respond to the frequency of 0.9 cps.

To investigate this instability further, additional tests were made in this unstable region. It was then found that by closing the bypass around the power-loop pump (see Figure 4), the oscillations could be eliminated. Consequently, the cause for this instability was a boiler-feed system coupling. A possible explanation of this phenomenon is presented below.

Using Equation (7), feed system-boiler instabilities can be predicted if the characteristics of the feed system are known and data showing the frequency response of the boiling-fluid inlet pressure to a variation in boiling-fluid flow rate are available up to the threshold of the unstable region. Figures 23a and 24a show that as the boiling-fluid flow rate was reduced towards the threshold of the unstable region (i.e., to 35 lb/hr), the P_{in} frequency response
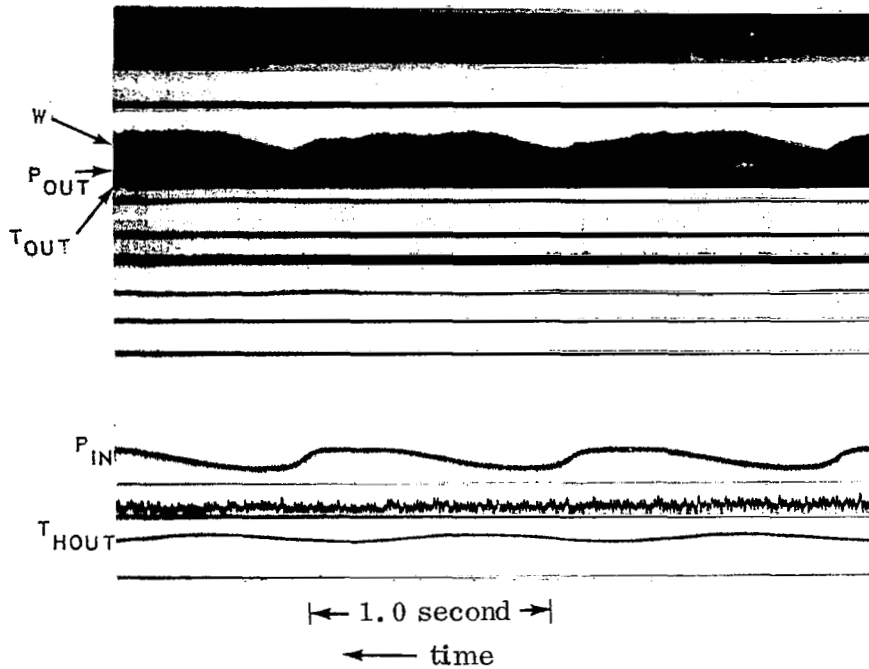
Limits of Variation

W – 25.3 to 26.7 lb/hr
P_{in} – 67.0 to 75.5 psia
P_{out} – 23.0 to 27.5 psi
T_{out} – 410 to 412°F
$T_{H\ out}$ – 376 to 379°F

|← 1.0 second →|

←——— time

a) Flow Control Valve in Integral Flow Control Mode
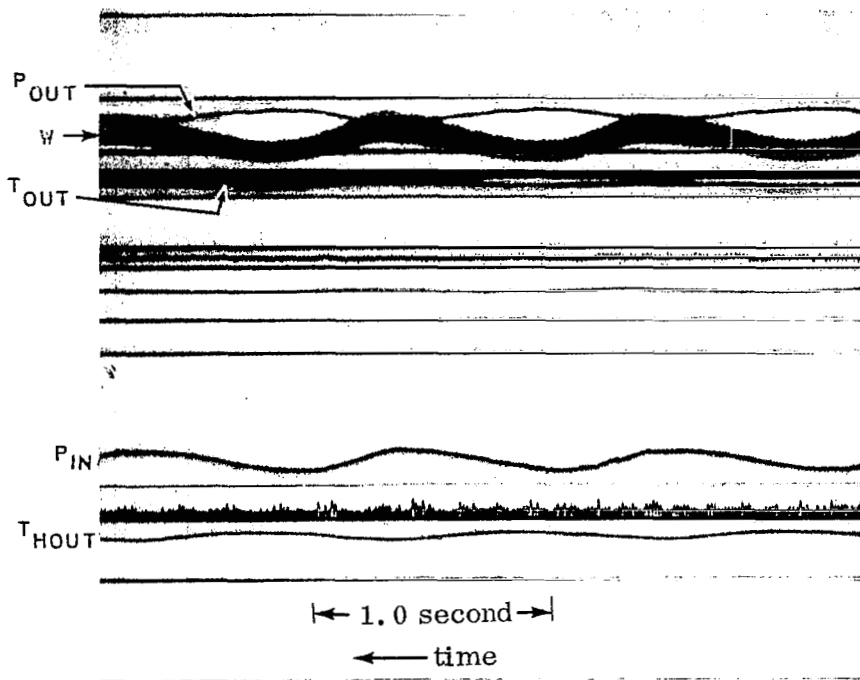
Limits of Variation

W – 25 to 27 lb/hr
P_{in} – 67.0 to 75.5 psia
P_{out} – 23.0 to 27.5 psi
T_{out} – 410 to 412°F
$T_{H\ out}$ – 376 to 379°F

|← 1.0 second →|

←——— time

b) Flow Control Valve in Fixed Position

Figure 37   Oscillograph Recording of Instability at Boiling–Fluid Flow Rate
of 30 lb/hr

70

became extremely erratic and displayed several sharp resonances near the frequency at which the 180-degree phase lag occurred.

Figure 38 shows the pressure-versus-flow characteristics of the feed system for the two settings of the bypass valve. The slope of the pressure versus flow curve has a value of -0.1820 psi/lb/hr with the bypass open and a value of -1.40 psi/lb/hr, with the bypass closed.

The observed instability could be explained if the amplitude of the P_{in} frequency response at the 180-degree phase lag point was greater than 0.182 psi/lb/hr, but less than 1.40 psi/lb/hr for flow rates just below 30 lb/hr. The system would then be unstable with the bypass open and stable with the bypass closed. This could happen if one of the resonances shown in Figure 23a increased in amplitude as the boiling-fluid flow rate was reduced from 35 to 30 lb/hr.

If the above explanation were valid, it would be expected that the system would oscillate at the frequency where the 180-degree phase lag occurred. Figure 39 shows this frequency as a function of boiling-fluid flow rate. Extrapolating the data to a flow rate of 30 lb/hr indicates that the 180-degree phase lag could indeed occur near a frequency of 0.9 cps, the frequency at which the system was observed to oscillate.

The second oscillatory instability was observed to occur at a heating-fluid flow rate of 400 lb/hr and at a boiling-fluid flow rate of 47 lb/hr. Since this condition was not set during steady-state testing, the instability was not noted until the frequency response test at W_H = 400 lb/hr was made. In this test low amplitude oscillations with a frequency of approximately 0.24 cps were found on the P_{in} and P_{out} oscillograph traces during the high-flow portion of the inlet flow rate variation cycle. This only occurred when the frequency was low enough (less than 0.01 cps) to allow the oscillations to develop during the high-flow portion of the cycle. Also, at a frequency of 0.085 cps the response of the P_{in} and P_{out} occurred at a frequency of 0.24 cps, a harmonic of the input frequency.

Figure 40 is a photograph of the oscillograph record for the frequency-response test at the 400 lb/hr condition and for a frequency of 0.002 cps. Oscillations occur only in P_{in} and P_{out}, and not in the inlet flow rate or any of the other variables. Consequently it seems fairly certain that this instability does not involve coupling with the boiler feed system.

The second instability occurred when the exit quality was less than 90 percent and the subcooled length was relatively long, in contrast to the first instability when the subcooled and boiling lengths were very short and the superheat was near the maximum attainable. In the light of the low-amplitude irregular pressure fluctuations that were often encountered when an appreciable amount of liquid was present at the boiler exit (see Figure 21b), it seems likely that the second instability was a resonant state involving variations in the two-phase flow patterns either at the boiler exit or internally. Since the amplitude of the

oscillations was small, it is questionable whether this kind of oscillation should be considered detrimental to boiler operation.
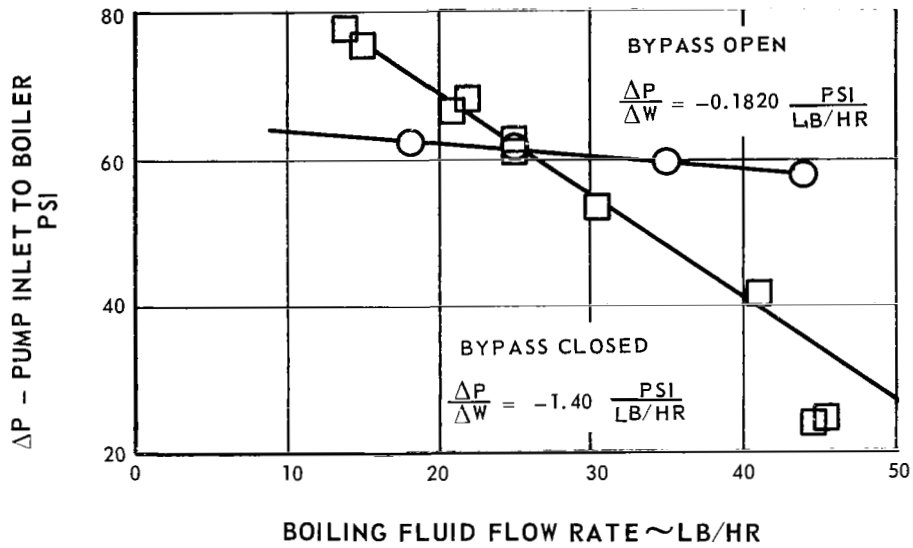
Figure 38   Feed System Pressure vs Flow Characteristics
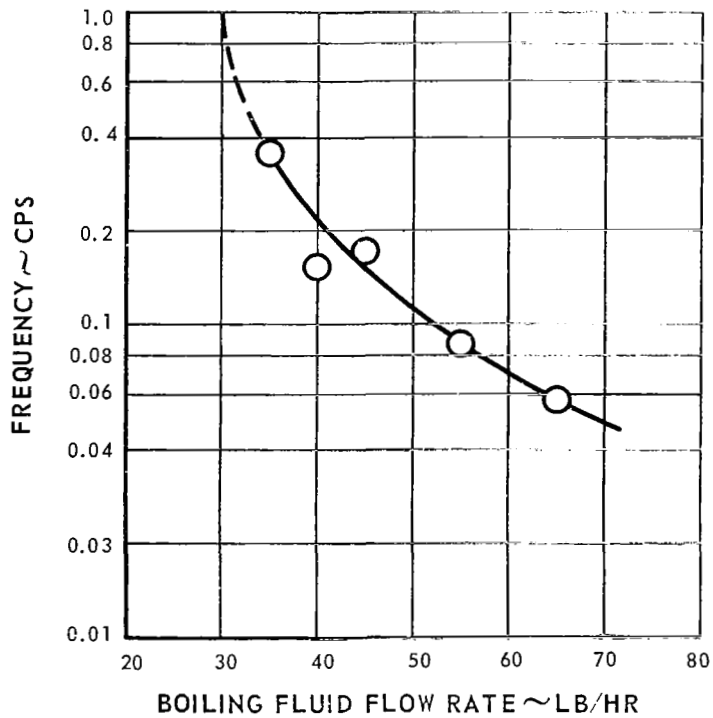
Figure 39   Frequency at which 180 Degrees Phase Lag Occurs for P_{in} Frequency Response
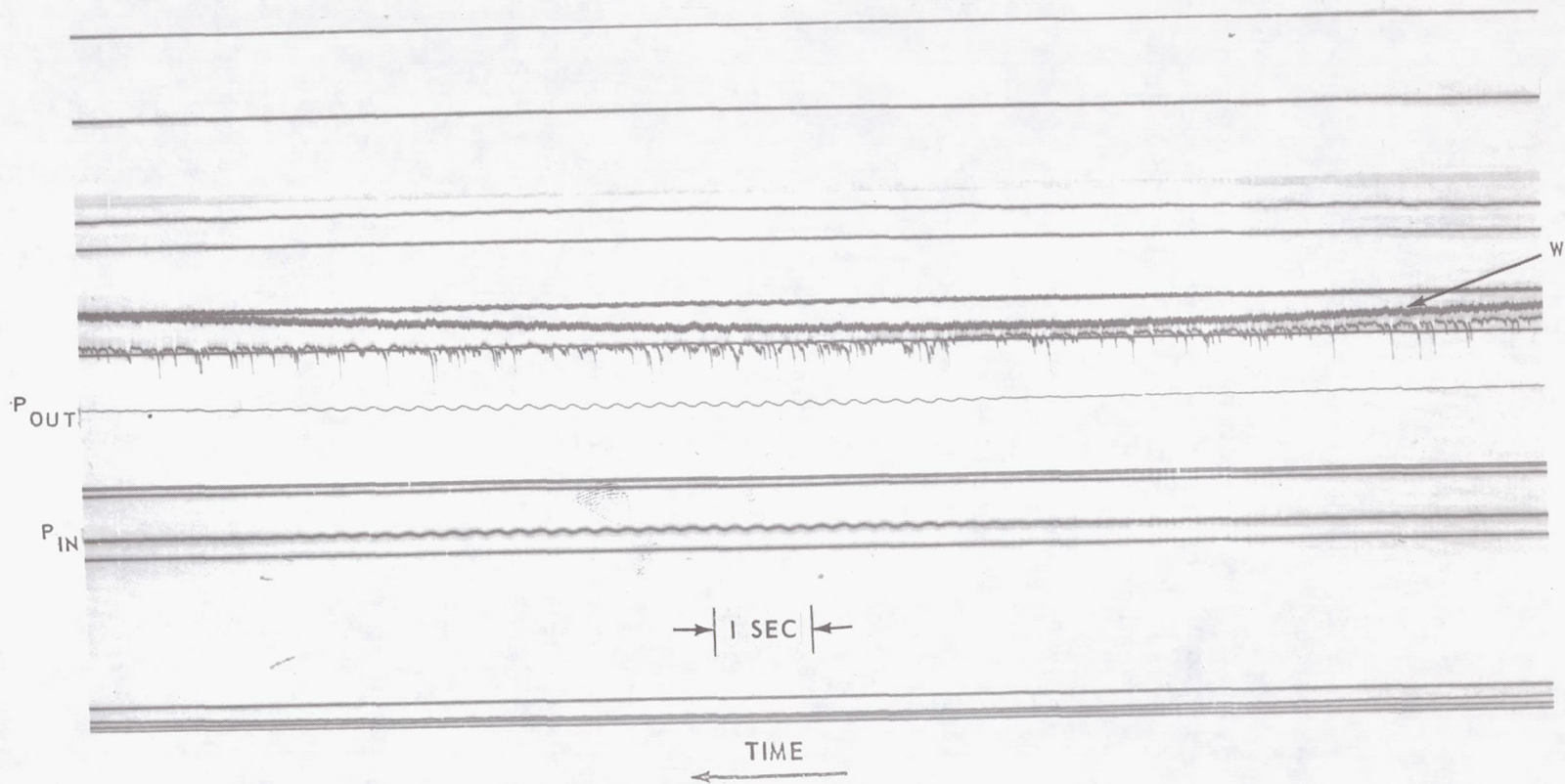
Figure 40   Oscillograph Record of Frequency-Response Test at W_H = 400 lb/hr
and ω = 0.002 cps Showing Pressure Oscillations

VII. THEORETICAL ANALYSIS OF BOILER DYNAMICS

An analysis of the boiler dynamics was performed to derive a theoretical rela-
tion for predicting the P_{out} transfer function. The purpose of this analysis was
to determine whether a theoretical transfer function could be formulated that
showed sufficiently good agreement with the experimental data of this study so
that it could be employed in predicting the dynamic performance of boilers in
Rankine-cycle space powerplants.

This analysis employed linearized relationships and a simplified model of the
boiler. The distributed-parameters approach was employed wherever possible
in analyzing components of the boiler. The resulting equation for the transfer
function was a complicated relationship between 22 parameters.

A comparison was made between the theoretical transfer function obtained from
this analysis and the experimental transfer function obtained from the frequency-
response data. In calculating the theoretical transfer function, values for the
22 parameters were determined from the experimental data obtained from the
steady-state tests.

This section contains a brief description of the derivation of the expression for
the theoretical transfer function and a discussion of the comparison between the
theoretical and experimental transfer functions. A detailed description of the
derivation is presented in Appendix 2.

A. Description of Derivation

The geometry of the boiler considered for the analysis is described in Section III
above. The boiler can be classified as a single-tube counterflow heat exchanger
designed to produce superheated vapor and having a choked restriction downstream
of the boiling fluid exit. Provision was made in the analysis to account for the
effects of the spiralled plug inserted in the boiler tube.

The boiler was divided into three regions: subcooled, boiling, and superheated,
each of which was analyzed separately. These regions correspond to the
regions observed in the steady-state data described in Section IV above. For
simplicity however, it was assumed that the evaporation process was completed
in the boiling region so that the boiling fluid entered the superheat region as a
dry saturated vapor. This assumption is justified by the lack of specific know-
ledge of the rate of droplet evaporation in the nonequilibrium-superheat region

of the actual boiler. Dynamic equations were derived for these three regions and for the boiler as a whole. The equations include:

Overall Equations

continuity equation of the boiling fluid
pressure-drop equation for the boiling fluid
choked valve equation

Subcooled Region

energy equation of the boiling fluid
energy equation of the plug wall

Boiling Region

energy equation of heating fluid
energy equation of shell wall
energy equation of the boiling fluid

Superheated Region

energy equation of the boiling fluid

The basic approach followed in the derivation was to linearize these equations for small perturbations around a steady-state point and take the Laplace transforms of the perturbed variables.

Simplifications were introduced into the analysis, where required, in an effort to keep the analysis reasonably manageable. The principal simplifying concept was made in the derivation of the continuity and pressure drop equations where it was assumed that the density change of the boiling fluid occurred at one discrete location in the boiler. The fluid density and flow rate were, therefore, considered to be independent of axial position and equal to the inlet values everywhere upstream of this location. Similarly, the fluid density and flow rate are considered to be independent of axial position and equal to the exit values everywhere downstream of this location. The location at which the density change was assumed to occur is the point at which a liquid-vapor interface would be present if all the liquid in the boiler at any instant, filled the flow passage starting from the inlet (see Figure 41). It was further assumed that the movement of this point is simply related by a proportionality constant to the movement of the pinch point. This was done to provide a common reference point for the continuity, pressure drop and energy equations.

75
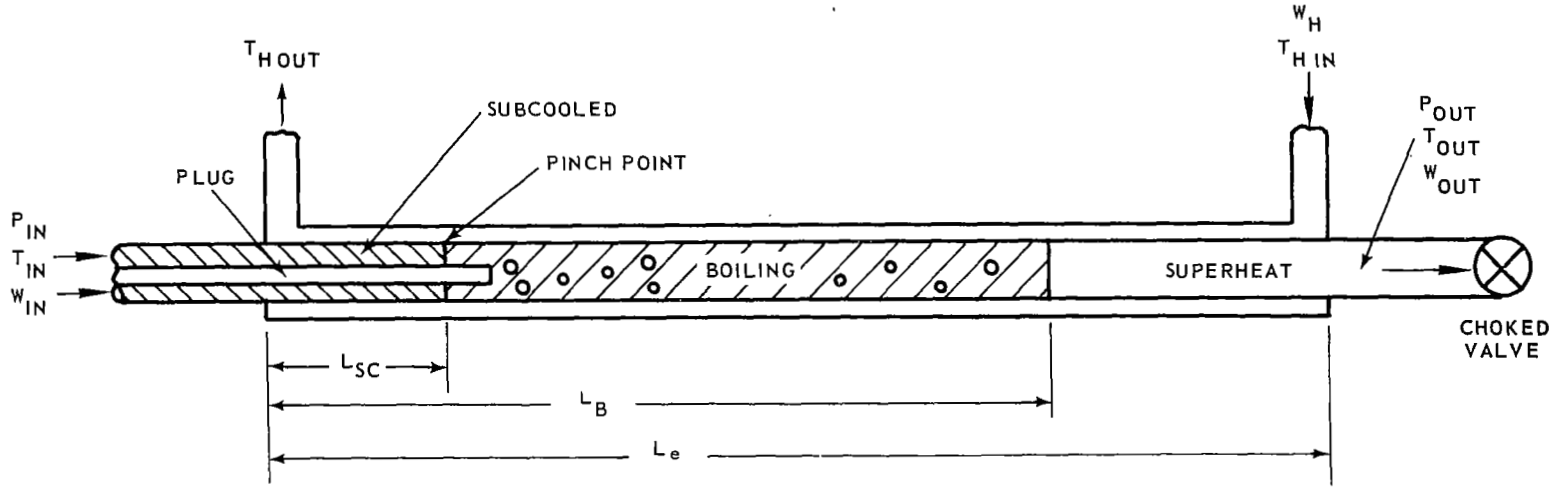
BOILER CONFIGURATION
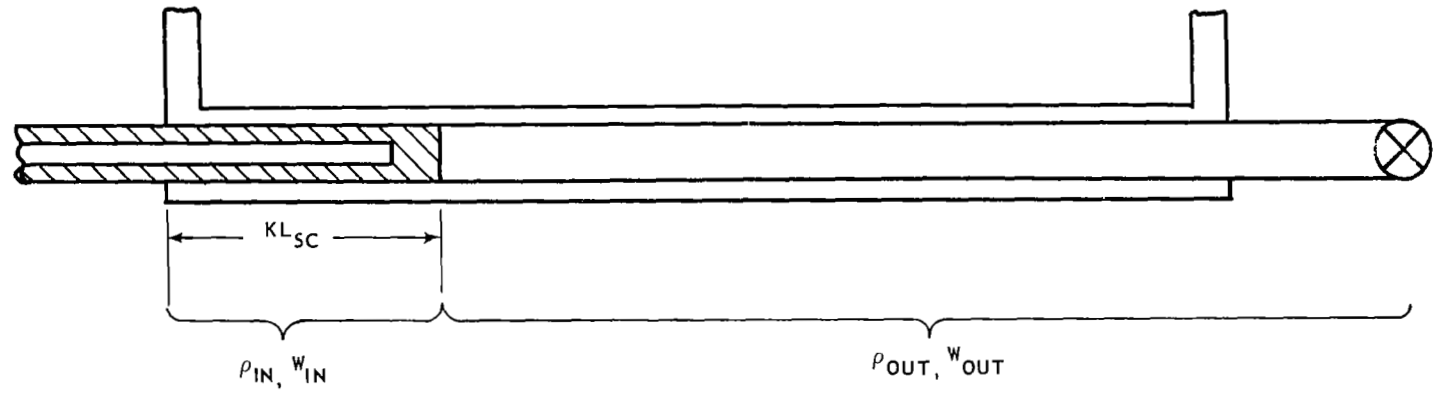
LUMPED DENSITY CHANGE MODEL

Figure 41   Lumped Density Change Model

In the derivation of the energy equations the distributed-parameters concept was employed wherever practical. This was possible in the derivation of five of the six individual energy equations where partial differential equations were derived with time and axial distance as the independent variables. These equations were then linearized, transformed and solved for the variation in the axial direction.

The solution to the partial differential equation for the boiling fluid in the boiling region, however, proved to be too complicated for the purposes of this analysis. In its place a quasidynamic equation was written with coefficients evaluated by means of steady-state relationships, and with transport time lags superimposed. The transport times appear in the equation in the form they would take in an approximate solution to a single-phase partial differential energy equation. The transport times in the boiling region are referred to the time it takes a liquid particle to travel the length of the boiling region.

In deriving these individual energy equations a fixed frame of reference was used, although the locations of the boundaries of both the subcooled and boiling regions fluctuate with time. The energy equations of the three regions were connected in a fixed reference frame by employing linearized perturbations about the steady-state boundaries in the boundary conditions of the equations.

The energy equations for the boiling and subcooled regions were combined into a single equation. The resulting five basic equations are tabulated below*.

Choked valve

$$\frac{\widehat{P}_{out}}{P_{out,o}} = \frac{\widehat{W}_{out}}{W_o} + \frac{\widehat{T}_{out}}{2T_{out,o}} \tag{9}$$

Pressure drop

$$\frac{\widehat{P}_P}{P_{P,o}} = \frac{\widehat{P}_{out}}{P_{out,o}} + \left(\frac{\partial\,(\Delta P_B/P_{P,o})}{\partial\,(L_{SC}/L_{SC,o})}\right)\left(\frac{\widehat{L}_{SC}}{L_{SC,o}}\right) \tag{10}$$

Continuity

$$\frac{\widehat{W}_{in}}{W_o} - \frac{\widehat{W}_{out}}{W_o} = K\tau_{SC}S\,\frac{\widehat{L}_{SC}}{L_{SC,o}} + \tau_V S\,\frac{\widehat{P}_{out}}{P_{out,o}} \tag{11}$$

*Symbols are defined in the nomenclature, in Figure 41, and in Appendix 2

Combined energy equation

$$\frac{\hat{L}_{SC}}{L_{SC,o}} = \textcircled{A}\,\frac{\hat{w}_{in}}{w_o} + \textcircled{B}\,\frac{\hat{P}_P}{P_{P,o}} + \textcircled{C}\,\frac{\hat{w}_{out}}{w_o} \qquad (12)$$

Energy equation of superheated region

$$\frac{\hat{T}_{out}}{2T_{out,o}} = \textcircled{D}\,\frac{\hat{P}_P}{P_{P,o}} + \textcircled{E}\,\frac{\hat{w}_{out}}{w_o} + \textcircled{F}\,\frac{\hat{P}_{out}}{P_{out,o}} + \textcircled{G}\,\frac{\hat{L}_{SC}}{L_{SC,o}} \qquad (13)$$

Equations (9) through (12) were combined into a single expression for the transfer function between boiling-fluid exit pressure and boiling-fluid inlet flow rate.

$$\frac{\hat{P}_{out}/P_{out,o}}{\hat{w}_{in}/w_o} = \frac{\left[1-\beta_3\textcircled{B}\right]\left[1+\dfrac{\hat{T}_{out}/2T_{out,o}}{\hat{w}_{in}/w_o}\right] - SK\tau_{SC}\left[\textcircled{A} - \textcircled{C}\,\dfrac{\hat{T}_{out}/2T_{out,o}}{\hat{w}_{in}/w_o}\right]}{\left[1+\tau_V S\right]\left[1-\beta_3\textcircled{B}\right] + SK\tau_{SC}\left[\textcircled{B}+\textcircled{C}\right]} \qquad (14)$$

Where S is the complex operator and where the term $\dfrac{\hat{T}_{out}/2T_{out,o}}{\hat{w}_{in}/w_o}$

is obtained from the following expression which results from the combination of Equations (9) through (13).

$$\frac{\hat{T}_{out}/2T_{out,o}}{\hat{w}_{in}/w_o} = \frac{-\gamma_{22} + \dfrac{\gamma_{21}\left[\left[1-\beta_3\textcircled{B}\right] - SK\tau_{SC}\textcircled{A}\right]}{\left[1+\tau_V S\right]\left[1-\beta_3\textcircled{B}\right] + SK\tau_{SC}\left[\textcircled{B}+\textcircled{C}\right]}}{1 - \dfrac{\gamma_{21}\left[1-\beta_3\textcircled{B} + SK\tau_{SC}\textcircled{C}\right]}{\left[1+\tau_V S\right]\left[1-\beta_3\textcircled{B}\right] + SK\tau_{SC}\left[\textcircled{B}+\textcircled{C}\right]}} \qquad (15)$$

Normalizing at zero frequency (i.e., at S = 0) the result is

$$\left(\frac{\hat{P}_{out}}{\hat{w}_{in}}\right)_{normalized} = \frac{\left(\dfrac{\hat{P}_{out}}{\hat{w}_{in}}\right)_{(s)}}{\left(\dfrac{\hat{P}_{out}}{\hat{w}_{in}}\right)_{(s=0)}} = \frac{(\hat{P}_{out}/\hat{w}_{in})}{\dfrac{P_{out,o}}{w_o}\left[1+\left(\dfrac{\hat{T}_{out}/2T_{out,o}}{\hat{w}_{in}/w_o}\right)_{(s=0)}\right]} \qquad (16)$$

Combining Equations (14) and (16) the normalized transfer function becomes

$$\left(\frac{\hat{P}_{out}}{\hat{w}_{in}}\right)_{normalized} = \frac{\left[1-\beta_3\textcircled{B}\right]\left[1+\dfrac{\hat{T}_{out}/2T_{out,o}}{\hat{w}_{in}/w_o}\right] - SK\tau_{SC}\left[\textcircled{A} - \textcircled{C}\,\dfrac{\hat{T}_{out}/2T_{out,o}}{\hat{w}_{in}/w_o}\right]}{\left[1+\left(\dfrac{\hat{T}_{out}/2T_{out,o}}{\hat{w}_{in}/w_o}\right)_{(s=0)}\right]\left[\left[1+\tau_V S\right]\left[1-\beta_3\textcircled{B}\right] + SK\tau_{SC}\left[\textcircled{B}+\textcircled{C}\right]\right]}$$

$$(17)$$

The equation for the theoretical transfer function is a very large complicated expression employing complex variables. At the initiation of this study it was desired to obtain a relatively simple expression for the transfer function. It was hoped that such an expression might indicate, by cursory inspection, the important parameters which affect the boiler dynamics and give insight into the manner in which they interact to produce the effects observed. However, due to the complexity of the boiler geometry and the multitude of different regions and processes affecting the boiler dynamics, no simple relation was possible. In fact, Equation (17) itself is highly simplified over the relation that would have resulted if the approximations discussed above and in Appendix 2 had not been made.

The details of the complete analysis are presented in Appendix 2.

B. <u>Comparison between Theoretical and Experimental Data</u>

The theoretical transfer function predicted by the analysis of the boiler dynamics was evaluated as a function of frequency for the boiler operating conditions at which the frequency-response tests were conducted. The theoretical normalized amplitudes and phase lags were compared with their corresponding experimental values. The following paragraphs contain a brief discussion of the calculation of the theoretical transfer function and a discussion of the comparison between the theoretical and experimental results.

1. <u>Calculation of Theoretical Transfer Function</u>

To calculate the theoretical transfer function it was first necessary to evaluate the 22 parameters required by Equation (17). This was done using the results of the steady-state tests described in Section IV of this report. The methods used to evaluate these parameters from the steady-state test data are discussed in Appendix 3. This appendix also contains a set of curves showing these parameters as functions of the primary variables. The complexity of these parameter curves, as demonstrated by the sharp breaks displayed as boiler exit conditions change, indicates the need for thoroughly understanding the steady-state performance of the boiler in order to predict its dynamic performance.

The normalized amplitude and phase lag were calculated as a function of frequency using Equation (17) and the parameter curves of Appendix 3. This was done for the boiler operating conditions at which frequency-response tests had been conducted. Since Equation (17) was derived for the boiler operating conditions where a superheat region existed, the theoretical transfer function was not calculated for those test conditions which did not exhibit a nonequilibrium-superheat region at the exit of the boiler.

2. Description of Comparison between Theoretical and Experimental Data

The results of the above calculations were plotted on the same Bode diagrams as the corresponding experimental values for the P_{out} transfer function. These plots are shown in Figures 23 through 32 in Section IV and in Figures 42 through 46 in this section. Figures 23 through 32 permit a direct point-by-point comparison between the theoretical and experimental transfer functions at each boiler operating condition. Figures 42 through 46 show the manner in which both theoretical and experimental transfer functions are affected by the primary variables.

In examining these figures, it can be seen that the theory predicts the same general trends for the P_{out} transfer function as shown in the experimental data. For example, the normalized amplitudes predicted by the theory attenuate in the same manner as those of the experimental data. In addition, Figures 42 through 46 show that the experimental data tends to bracket the theoretical normalized amplitudes. The phase lags predicted by the theory also tend to increase with frequency in the same manner as those of the experimental data. This agreement is an indication of the validity of the basic approach taken in the linearized analysis of the boiler dynamics.

However, while the theory and the experimental data show similar trends, the magnitudes of the normalized amplitude and phase lag predicted by the theory are not always in close agreement with the experimental data over the full range of frequencies. For example, it can be seen in Figures 42a through 46a that at the lower frequencies the theory does not predict normalized amplitudes greater than 1.0 as observed in the experimental data. Figures 42b through 46b also show that the phase lags of the experimental data tend to be somewhat higher than predicted by the theory, particularly in the middle frequency range.

Figures 42 through 46 also indicate that closer agreement between the theory and the data is achieved under those conditions where the boiling fluid emerges as a dry superheated vapor. For example, Figure 43 shows excellent agreement for a heating-fluid flow rate of 1000 lb/hr, where the boiling fluid is superheated by 93°F, as opposed to the poorer agreement shown for the 600 lb/hr case where the boiling fluid emerges in a nonequilibrium condition. This is probably a result of the fact that the assumptions concerning the superheating of the boiling fluid made in the analysis of the boiler dynamics become less valid as nonequilibrium conditions become pronounced.

a)

b)
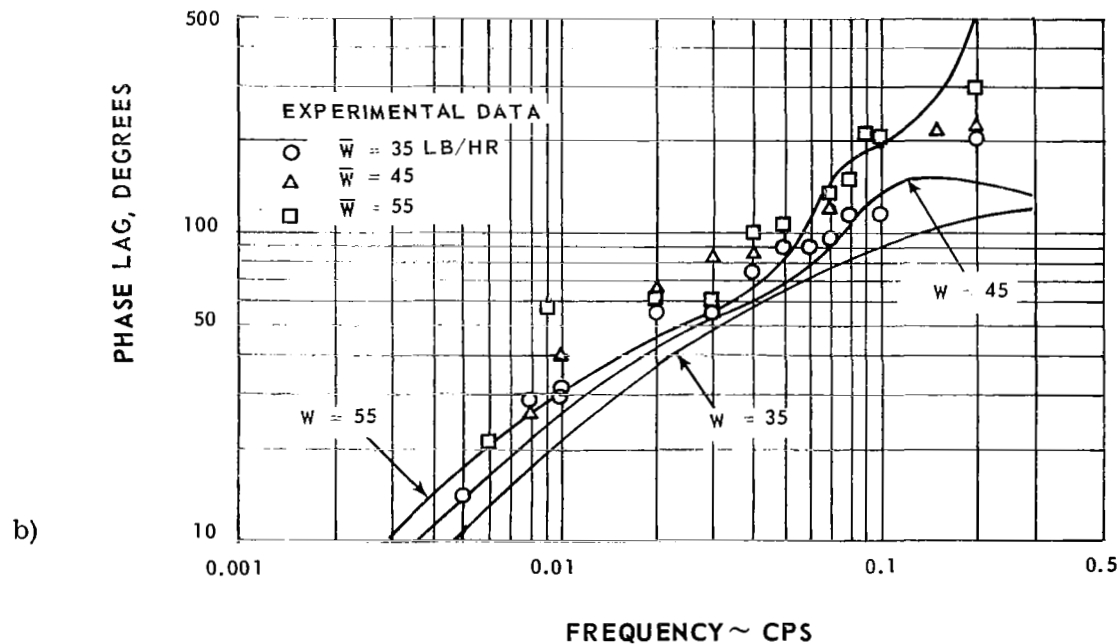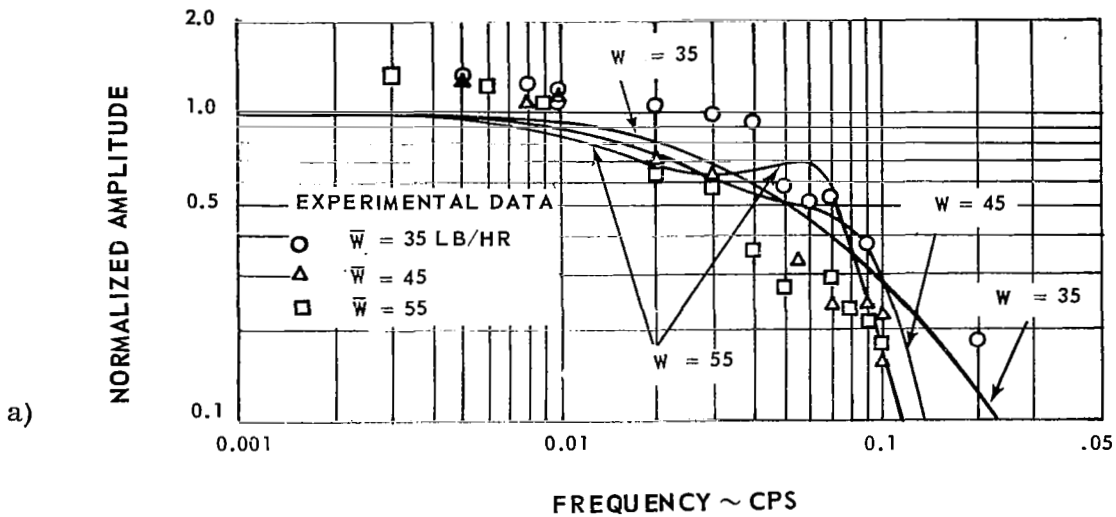
Figure 42   Comparison between Theoretical Transfer Function and Experimental Values of P_{out} Frequency Response for Various Values of Boiling-Fluid Flow Rate

81
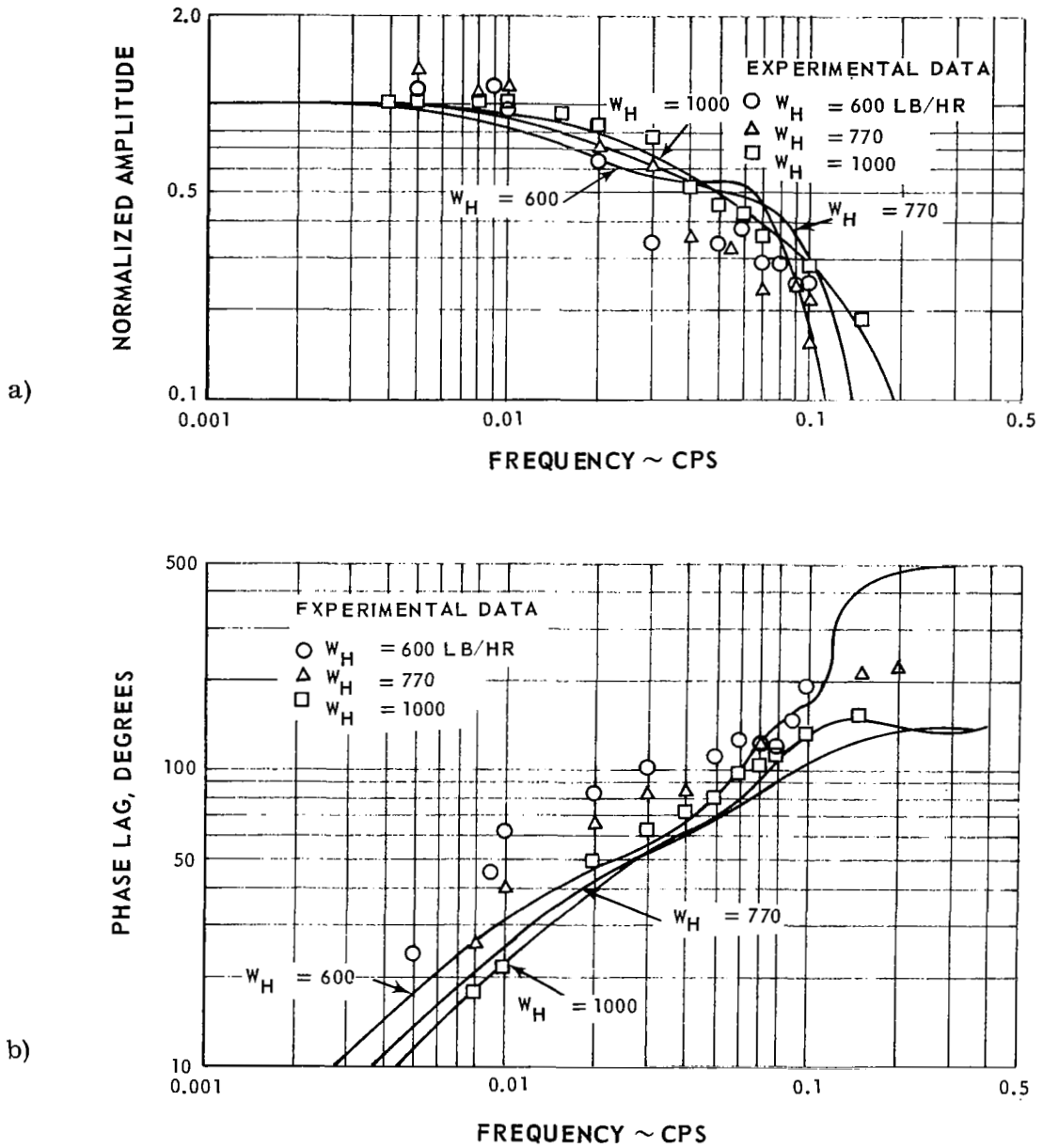
Figure 43   Comparison between Theoretical Transfer Function and Experimental Values of P_{out} Frequency Response for Various Values of Heating-Fluid Flow Rate

a)

b)
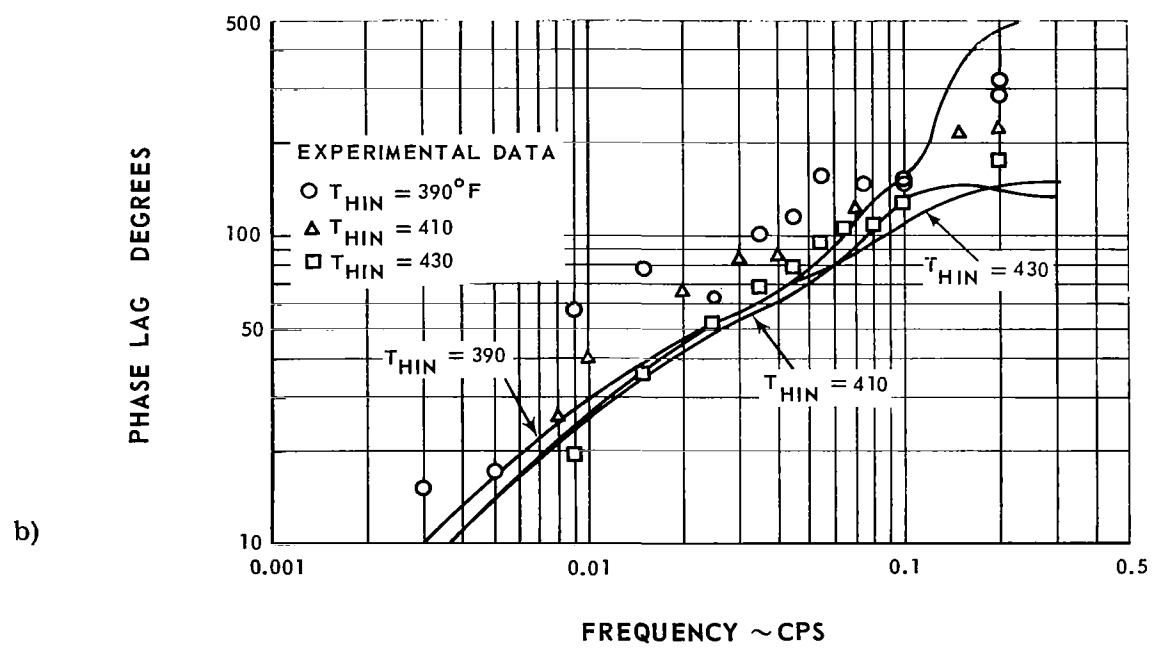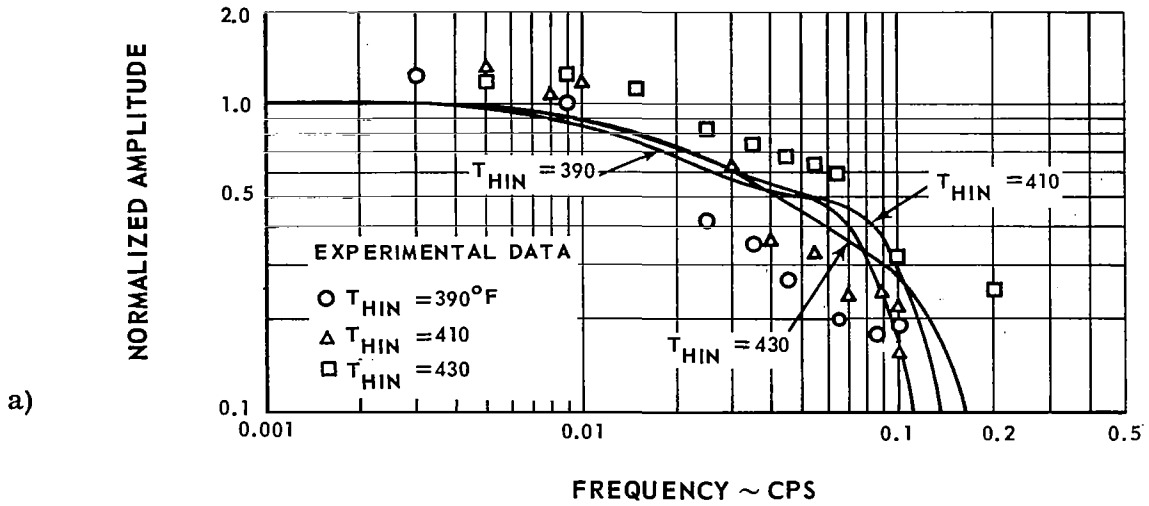
Figure 44   Comparison between Theoretical Transfer Function and Experimental Values of P_{out} Frequency Response for Various Values of Heating–Fluid Inlet Temperature
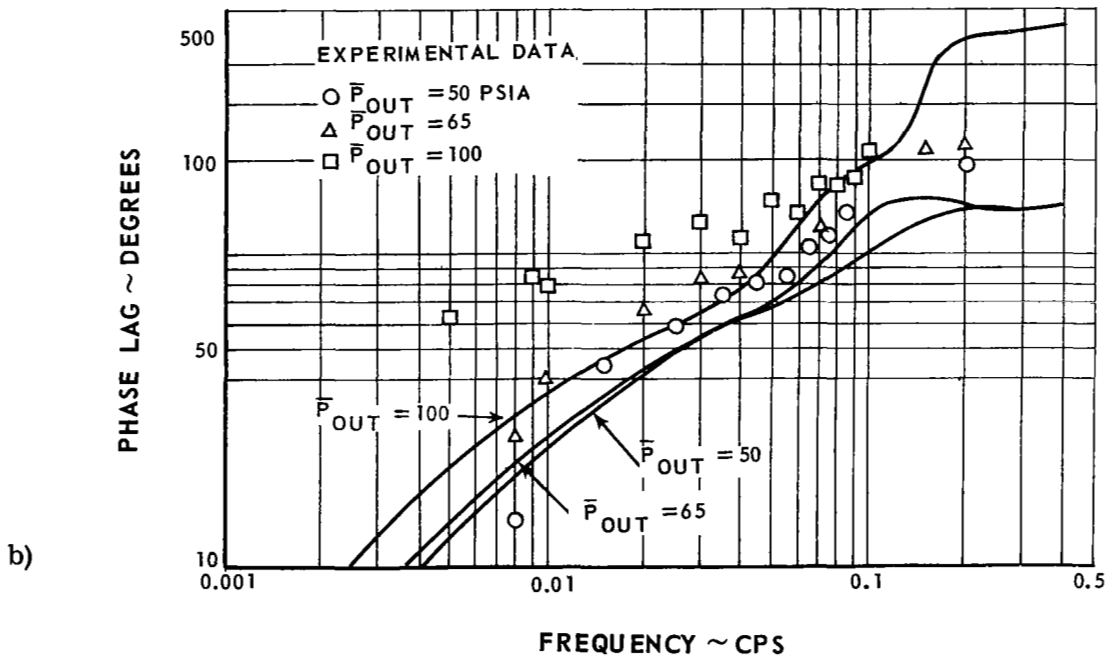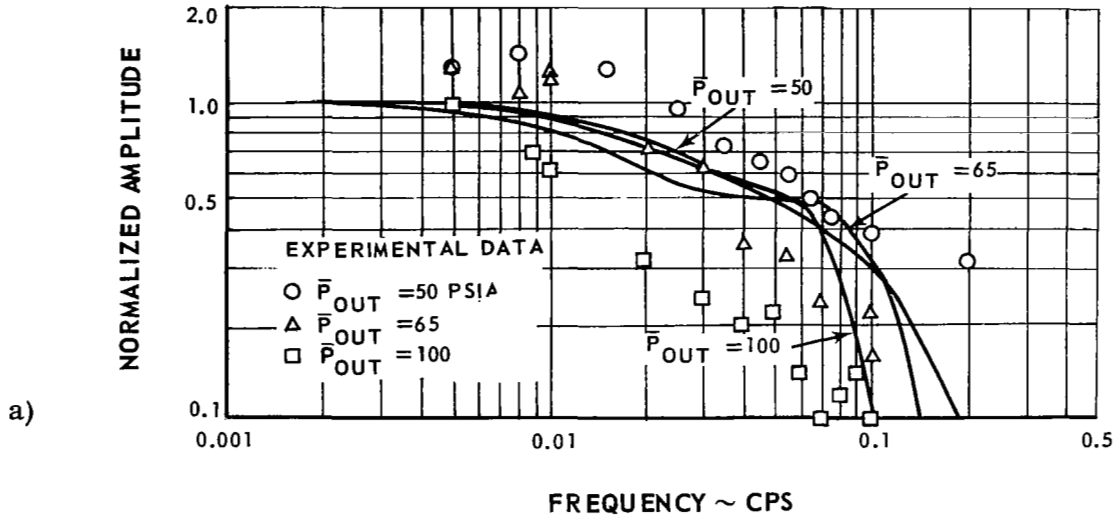
Figure 45 Comparison between Theoretical Transfer Function and Experimental Values of P_{out} Frequency Response for Various Values of Boiling-Fluid Exit Pressure
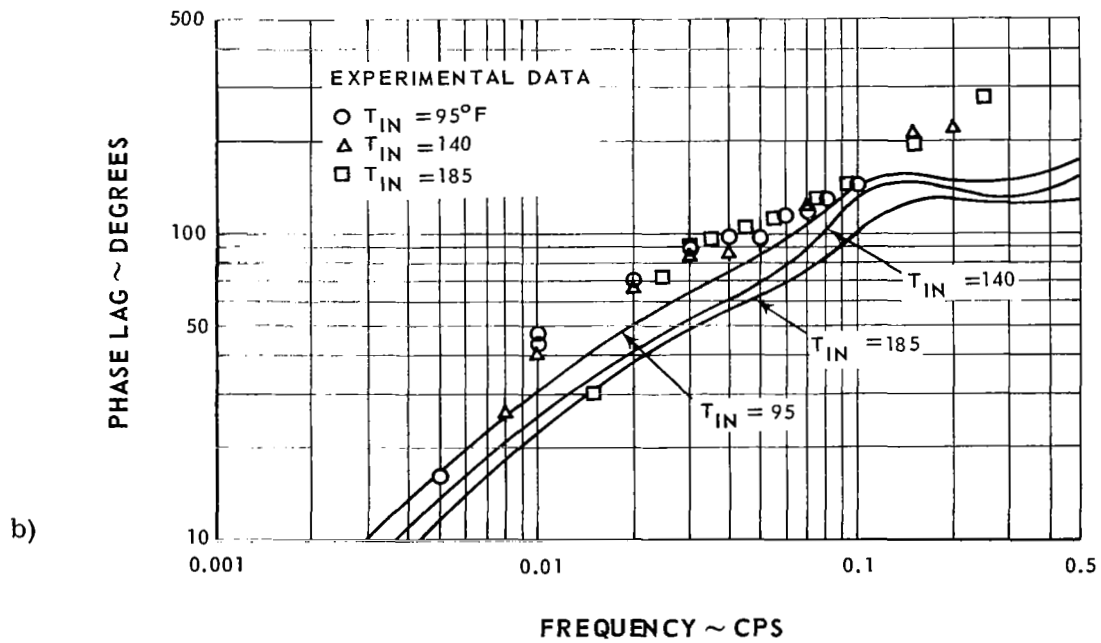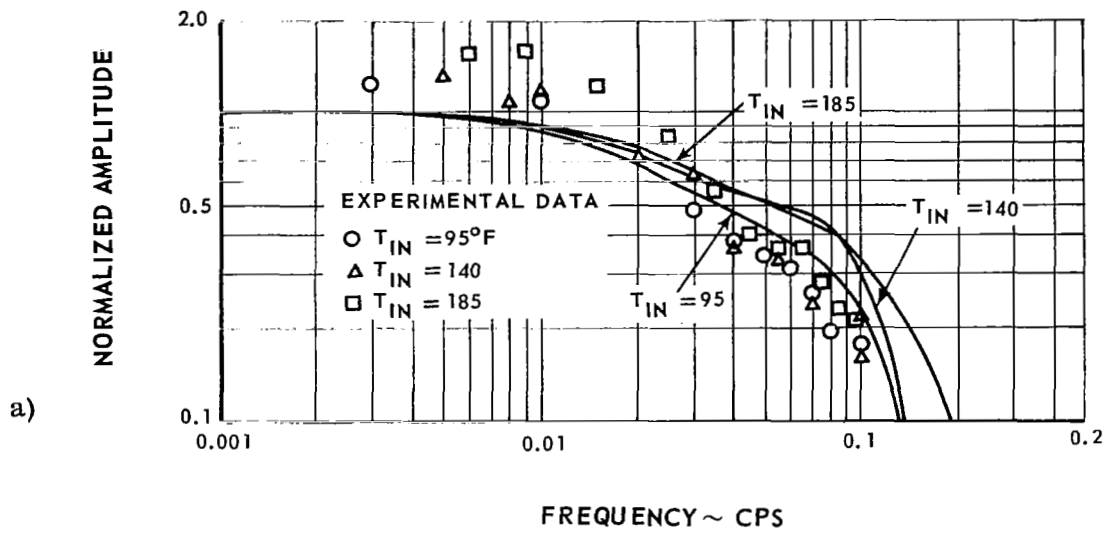
Figure 46   Comparison between Theoretical Transfer Function and Experimental Values of P_{out} Frequency Response for Various Values of Boiling-Fluid Inlet Temperature

Close scrutiny of Figures 23 through 32 indicates that the best agreement between the theory and the experimental data occurs in the middle frequency range, usually between 0.01 and 0.1 cps. Below these frequencies the normalized amplitudes of the experimental data tend to be greater than the value of 1.0 predicted by the theory. Above these frequencies there is little agreement between the phase lags of the theory and those of the experimental data.

In studying the stability of the interactions between the boiler and the feed system of a Rankine-cycle space powerplant, the amplitude of the transfer function of the boiler at a phase lag of 180 degrees is a very important consideration. Since, in most of the cases considered, the phase lag of 180 degrees occurs at frequencies above 0.10 cps, caution should be exercised in applying Equation (17) to predict the stability of the interactions between the feed system and the boiler.

3. Evaluation of Comparison Between Theoretical and Experimental Data

In evaluating the results of this comparison, it should be remembered that the analysis presented in this section represents an initial effort to analyze the dynamics of an extremely complex nonlinear device. The degree of agreement that was achieved between the theory and the data is an indication of the validity of the basic approach of performing a separate linearized analysis for each section of the boiler. However, in order to develop a more useful tool for predicting boiler stability, modifications to this analysis are required in order to achieve closer agreement between the theory and the data at the higher frequencies. This can probably be accomplished by refining the analysis to remove several of the simplifying assumptions. The following modifications to the analysis are recommended:

1) A more exact description of the distribution of the boiling fluid mass within the boiler and the manner in which this mass responds to perturbations in the flow rate.

2) Replacement of the quasi-dynamic relation employed as the energy equation of the boiling fluid in the boiling region, with a relation based on the distributed-parameters approach.

3) Inclusion of the effects of the heat capacities of the tube, the shell, and spiralled plug insert in all sections of the boiler.

VIII. CONCLUSIONS

The following conclusions have been reached on the basis of the results presented in this report.

1. The condition of the boiling fluid at the exit of the boiler is a significant characteristic in describing the steady-state and dynamic behavior of the boiler. This is seen in the sharp breaks, rather than smooth transitions, displayed by many of the steady-state performance and boiler parameter curves as the boiler exit conditions change from a dry superheated vapor to a nonequilibrium mist and from a nonequilibrium mist to a wet saturated condition. This is also seen in the general shift of the experimental frequency-response curves as the boiler exit conditions vary in the direction from dry superheated vapor to wet saturated conditions.

2. For small perturbations of the boiling-fluid flow rate, the boiler can be treated as a linear element over much of the operating range investigated. This is shown by the linear responses observed in the oscillograph traces for the boiling-fluid inlet and exit pressures and the heating-fluid exit temperature over virtually the entire range of conditions tested. In studying the response of the boiling-fluid exit temperature, the linear approximation is valid only for dry boiling-fluid exit conditions.

3. The boiling system of this study is statically stable in spite of the negative slope of the curve of boiling-fluid pressure drop versus flow. This is shown by the positive slope of the curve of boiling-fluid inlet pressure versus flow which results from the effects of the choked restriction downstream of the boiler exit.

4. The boiling system of this study can undergo dynamic instabilities. The possibility of dynamic instabilities arising from the dynamic interactions between the feed system and the boiler is indicated by the experimental frequency-response curves. In these curves it can be seen that the P_{in} transfer function has a relatively large amplitude at the 180-degree phase lag point for many of the cases studied. This type of instability was experienced at one point in the test program. A second type of instability which can probably be attributed to dynamic interactions within the boiler itself was also observed during testing.

5. The basic linearized approach taken in the analysis of the boiler dynamics appears to be valid in view of the agreement found between the trends of the experimental and theoretical values for the P_{out} transfer function. Further work in this area appears desirable in order to develop a more useful analytical tool for predicting the stability of the dynamic interactions between the boiler and the feed system.

NOMENCLATURE

A	cross-sectional area, ft^2
$\circledA$	defined by Equation (98), dimensionless
$\circledB$	defined by Equation (99), dimensionless
C_p	specific heat at constant pressure, Btu/lb$_m$ - °F
C	arbitrary constant
$\copyright$	defined by Equation (100), dimensionless
$\circledD$	defined by Equation (121), dimensionless
d_h	hydraulic diameter, ft
d_i	tube inside diameter, ft
d_m	tube mean diameter, ft
d_o	tube outside diameter, ft
$\circledE$	defined by Equation (122), dimensionless
e	base of natural logarithms
$\circledF$	defined by Equation (123), dimensionless
f	friction factor, dimensionless
$\circledG$	defined by Equation (124), dimensionless
g	acceleration due to gravity, ft/hr^2
G	mass flux, lb$_m$/hr-ft^2
G_1	transfer function defined in Section VI
G_2	transfer function defined in Section VI
G_3	mass flux after expansion, lb$_m$/hr-ft^2
h	convective heat transfer coefficient, Btu/hr-ft^2-°F
H_{fg}	heat of vaporization, Btu/lb$_m$
j	$\sqrt{-1}$
k	thermal conductivity, Btu/hr-ft-°F
K	defined by Equation (34), dimensionless
l	axial distance, ft
L	axial distance from boiler inlet, ft
M	fluid mass, lb$_m$
N	number of 90-degree bends
n	defined by $U \propto V^n$, dimensionless
p	heat transfer perimeter, ft
P	pressure, psia
Pr	Prandtl number
q	heat flux, Btu/hr-ft^2
Q	heat transferred, Btu/hr
R	gas constant, ft-lb$_f$/lb$_m$-°R
R_b	flow resistance due to bends, dimensionless
R_g	vapor fraction of two-phase flow, dimensionless
R_l	flow resistance due to length, dimensionless
R_L	liquid fraction of two-phase flow, dimensionless

R_t	total flow resistance, dimensionless
Re	Reynolds number
S	complex operator, hr^{-1}
t	time, hr
t_h	tube thickness, ft
T	temperature, °F
U	overall heat transfer coefficient, Btu/hr-ft^2-°F
v	specification volume, ft^3/lb_m
V	fluid velocity, ft/hr
Vol	volume, ft^3
W	mass flow rate, lb_m/hr
x	axial distance, ft
X	quality
$(L/D)_{eq}$	equivalent length-to-diameter ratio
ΔP_B	pressure drop of boiling fluid across boiler, psi
ΔT_{LM}	logarithmic mean temperature difference, °F
ΔT_M	arithmetic mean temperature difference, °F
ΔT_P	difference between heating and boiling fluid temperatures at pinch point, °F
ΔT_{SH}	superheat at boiling fluid exit, °F
$\Delta P_{in}/\Delta W$	amplitude of P_{in} frequency response at zero frequency, psi-hr/lb_m
$\Delta P_{out}/\Delta W$	amplitude of P_{out} frequency response at zero frequency, psi-hr/lb_m
$\Delta T_{H\ out}/\Delta W$	amplitude of T_{Hout} frequency response at zero frequency, °F hr/lb_m
$\Delta T_{out}/\Delta W$	amplitude of T_{out} frequency response at zero frequency, °F hr/lb_m

α	defined in Appendix 3, dimensionless
$\beta 1$	defined by Equation (57), dimensionless
$\beta 2$	defined by Equation (116), dimensionless
$\beta 3$	defined by Equation (126), dimensionless
γ	ratio of specific heats C_p/C_v, dimensionless
γ_1	defined by Equation (59), dimensionless
γ_2	defined by Equation (60), dimensionless
γ_3	defined by Equation (61), dimensionless
γ_4	defined by Equation (83), dimensionless
γ_5	defined by Equation (84), dimensionless
γ_{11}	defined by Equation (132), dimensionless
γ_{12}	defined by Equation (133), dimensionless
γ_{13}	defined by Equation (134), dimensionless
γ_{21}	defined by Equation (137), dimensionless
γ_{22}	defined by Equation (138), dimensionless
θ	defined by Equation (38), hr^{-1}

θ_1	defined by Equation (38), hr^{-1}
θ_2	defined by Equation (42), hr^{-1}
θ_B	defined by Equation (63), hr^{-1}
θ_{B1}	defined by Equation (64), hr^{-1}
θ_{B2}	defined by Equation (69), hr^{-1}
θ_{SH}	defined by Equation (102), hr^{-1}
ρ	density, lb_m/ft^3
σ	ratio of initial to expanded flow area, dimensionless
γ	transport time of fluid in subscripted region, hr
ϕ_1	defined by Equation (56), dimensionless
ϕ_2	defined by Equation (78), dimensionless
ϕ_3	defined by Equation (92), dimensionless
ϕ_4	defined by Equation (114), dimensionless
ϕ_5	defined by Equation (117), dimensionless
ω	frequency of disturbance, cps

Subscripts

B	boiling region of boiler
e	boiling fluid exit
H	heating fluid
Hin	heating fluid entering boiler
Hout	heating fluid leaving boiler
HP	heating fluid at pinch point
in	boiling fluid entering boiler
L	liquid
o	steady-state condition
out	boiling fluid leaving boiler
P	boiling fluid at pinch point
PM	plug metal
SAT	boiling-fluid saturation condition at pinch point
SAT OUT	boiling-fluid saturation condition at boiler exit pressure
SC	subcooled region of boiler
SF	swirl flow
SH	superheat region of boiler
SM	shell metal
SV	dry saturated vapor
T	tube
TPF	two-phase flow
V	vapor

Note: Non-subscripted variables refer to boiling fluid

Superscripts

$(\hat{\ })$	Laplace transform of linearized variable
$(\bar{\ })$	mean value

REFERENCES

1. "Two-Phase Gas-Liquid Flow Oscillations: Preliminary Survey", by S.W. Gouse, Jr., Report DSR 8734-5, Massachusetts Institute of Technology, July 1964

2. "Frequency Response of Forced-Flow Single Tube Boiler", by E.A. Krejsa, J.H. Goodykoontz, and G.H. Stevens, NASA TN D-4039, June 1967

3. "Frequency Response of a Forced-Flow Single-Tube Boiler", by R.G. Dorsch, NASA TM X-52306, 1967

4. "Steady-State and Dynamic Operating Characteristics of a Simulated Three-Loop Space Rankine-Cycle Powerplant" by J.R. Hooper, NASA CR-625, November 1966

5. "Analysis of Pressure Drop Function in Rankine Space Power Boilers with Discussion of Flow Maldistribution Implications", by A. A. Schoenberg and D. R. Packe, NASA TN-D-4498, April 1968

6. "Analysis and Measurement of Flow Oscillations", by E.R. Quandt, Chemical Engineering Progress Symposium Series, No. 32, Vol. 57, pp 111-126, 1961

7. "Flow Stability in Multitube Forced-Convection Vaporizers", by P.J. Berenson, Technical Documentary Report No. APL TDR 64-117, Air Force Aero Propulsion Laboratory, Wright Patterson Air Force Base, Ohio 1964

8. "Flow Oscillation Modes in Forced-Convection Boiling", by A.H. Stenning and T.N. Veziroglu, Proceedings of the 1965 Heat Transfer and Fluid Mechanics Institute, Stanford University Press, 1965

9. "Heat Transmission, Second Edition", by H.W. McAdams, p. 168, McGraw-Hill, New York, 1942

10. "Heat Transfer and Pressure-Drop Characteristics of Wire-Coil Type Turbulence Promoters", by Eldor W. Sams, Lewis Flight Propulsion Laboratory, NACA Cleveland, Ohio. Presented at the Reactor Heat Transfer Conference, Nov. 1, 1956, Hotel Statler, New York City

11. "Flow of Fluids", Crane Technical Paper No. 410, Crane Corp., Chicago. pps. 2-12, A-27, (Primary ref. - K. H. Beij, Pressure Losses for fluids in 90° pipe Bends, J. of Res. of NBS, Vol. 21, July 1938)

12. "Prediction of Pressure Drop during Forced-Circulation Boiling of Water", by R. C. Martinelli and D. B. Nelson, Trans. ASME, Aug 1948, pps 695-702

13. "Two-Phase Pressure Loss across Abrupt Contractions and Expansions, Steam-Water at 600 to 1400 psi", by E. Janssen, Proceedings of the Third International Heat Transfer conference, Aug. 7-12, 1966, Chicago, Vol. IV, pp. 12-23

APPENDIX 1

Boiler Design Calculation

The boiler design is described in detail in Section III. This appendix contains a brief description of the thermal and hydraulic analyses which served as the basis for this design. Since the actual computations are long and complex, this appendix will be limited to a description of the basic relations and assumptions employed in the analyses and a comparison between the predicted and the measured performance of the boiler.

In analyzing the thermal and hydraulic performance, it was necessary to divide the boiler into six different sections which were analyzed spparately. These sections, designated by the station numbers illustrated in Figure 47, are classified by the state of the boiling fluid flow as shown below:

Section	Station Numbers
1) Subcooled flow through the plug	0 – 1
2) Boiling flow through the plug	1 – 2
3) Sudden expansion at the end of the plug	2 – 3
4) Boiling flow from end of plug to 80.9% quality	3 – 4
5) Boiling flow from 80.9% quality to 100% quality	4 – 5
6) Superheating of the vapor flow	5 – 6

The boiling fluid was maintained in a swirl-flow pattern throughout the length of the boiler to enhance its heat-transfer coefficient. In Sections 1 and 2 of the boiler, the swirl-flow pattern was induced using a spiral-flow channel formed between the machined plug and the tube wall. In the remaining sections of the boiler the swirl-flow pattern was maintained by means of a wire coil brazed to the tube wall. The effects of these swirl-inducing devices were included in the analysis. During the course of the analysis a number of assumptions were made. These were particularly necessary since little is known about heat transfer and fluid friction for the types of swirl flow encountered in this boiler design. These assumptions are stated in the discussion that follows wherever they are applied.

HEATING
FLUID
OUT

HEATING
FLUID
IN

PLUG

THERMOCOUPLE
PROBE

SUBCOOLED
WATER IN

SUPERHEATED
STEAM OUT

STATION
NUMBERS   0   1 23   4   5   6
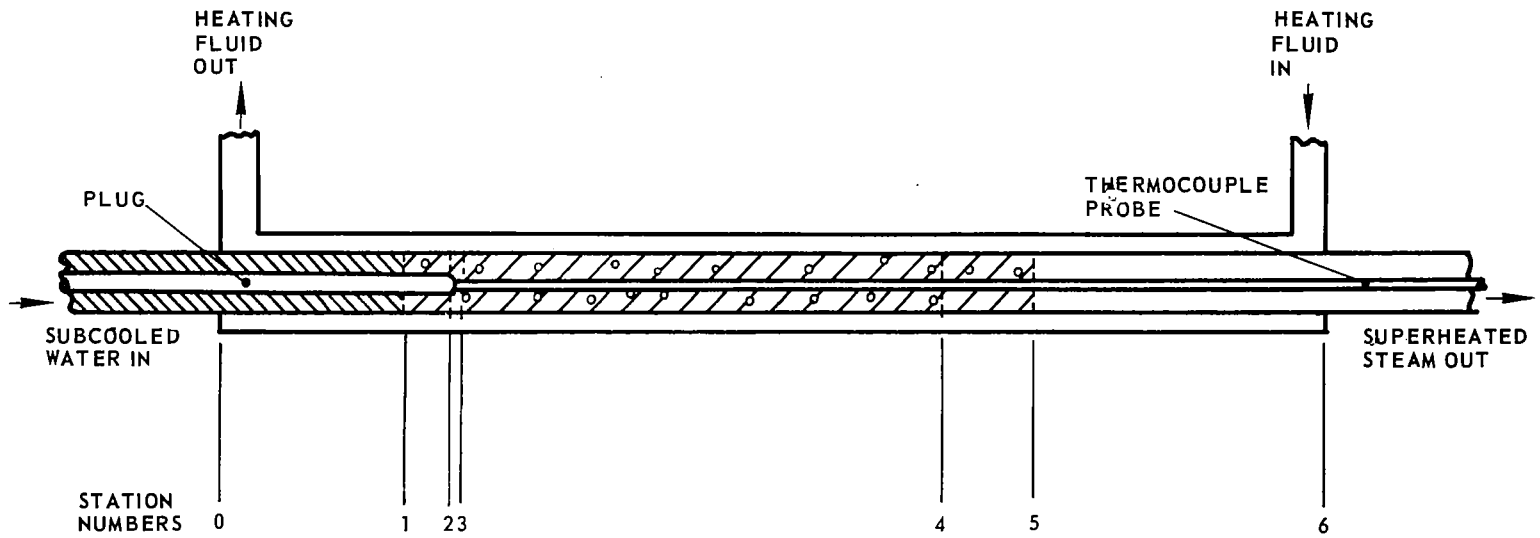
Figure 47   Boiler Configuration Showing Sections

The relations used to calculate the heat-transfer coefficients in the different sections of the boiler are discussed below. The heat-transfer coefficient of the heating fluid in all sections of the boiler was predicted using the relation

$$h = 0.023 \frac{k}{d_H} (Re)^{0.8} (Pr)^{0.4} \tag{18}$$

This is the familiar McAdams relation[9] for predicting the heat-transfer coefficient for the turbulent flow of a single-phase fluid through a channel.

The heat-transfer coefficient for the boiling fluid in Sections 1 and 6 of the boiler where single-phase flow occurred was predicted using the relation

$$h = 0.023 \frac{k}{d_H} (Re)^{0.8} (Pr)^{0.4} \left(\frac{h_{SF}}{h_{SC}} \right) \tag{19}$$

Equation (19) is the McAdams equation multiplied by the factor (h_{SF}/h_{SC}) to account for the increase in heat-transfer coefficient resulting from the swirl flow of the fluid. In determining this factor, it was assumed that the swirl-flow data of Sams[10] could be applied to the cases at hand. This data was taken for the swirl flow of air induced by a wire coil inside of a tube.

Since the swirl flow of superheated vapor through Section 6 of the boiler closely resembled the flow configuration of Reference 10, the factor (h_{SF}/h_{SC}) was determined directly from Figure 10 of the reference.

In Section 1 of the boiler, however, the swirl-flow pattern was induced using a spiral-flow channel rather than a coil inside of a tube. Since no heat transfer data could be found for this type of flow configuration, it was assumed that the relationship between heat-transfer coefficient and friction factor in the data of Reference 10 could be applied to the spiral flow case. To relate the heat-transfer coefficient and the friction factor, the following approximate relation was fitted to the data taken at a coil pitch-to-wire diameter ratio of 10.

$$\left(\frac{h_{SF}}{h_{SC}} \right) = \left(\frac{f_{SF}}{f_{SC}} \right)^{0.28} \tag{20}$$

In evaluating the ratio of the friction factors, the following relationship was assumed to apply

96

$$\frac{f_{SF}}{f_{SC}} = \frac{\Delta P_{SF}}{\Delta P_{SC}} \tag{21}$$

where ΔP_{SF} is the pressure loss for the flow through the spiral channel calculated using Equations (23) and (24) below, and ΔP_{SC} is the pressure loss for an equivalent straight channel having the same flow rate and linear and cross-sectional dimensions as the spiral channel.

Due to the lack of adequate boiling heat transfer data for the swirl–flow configurations of this boiler, it is necessary to assume values for the boiling heat transfer coefficient. For Sections 2 and 4 of the boiler the bulk boiling coefficient was assumed to be constant at a value of 6,000 Btu/hr - ft^2 - °F. For Section 5, where film boiling was assumed to take place, the heat transfer was assumed to vary linearly with boiling fluid quality from the bulk boiling coefficient to the vapor coefficient. This is shown in the following equation.

$$h = 6000 - \left(\frac{6000 - h_{SV}}{0.191}\right) \ (X - 0.809) \tag{22}$$

The term h_{SV} in Equation (22) represents the heat transfer coefficient of the dry saturated vapor at Station 5. Equation (19) was used to calculate h_{SV}.

The relations used to calculate the boiling fluid pressure losses are discussed below. The momentum pressure drop of the boiling fluid from the inlet to the exit was estimated to be only 0.2 psi. As a consequence, only frictional losses were considered.

Pressure losses for the single–phase flow of the boiling fluid were calculated using two different methods depending upon the location in the boiler. For Section 1 of the boiler, where the fluid flows in a spiral path, the following equations were used to calculate the pressure loss

$$\Delta P = 4f\left(\frac{L}{D}\right)_{eq} \frac{G^2}{2g\,\rho} \tag{23}$$

where

$$\left(\frac{L}{D}\right)_{eq} = R_t + (N-1)\left(R_1 + \frac{R_b}{2}\right) \tag{24}$$

These equations are based on the method presented in Reference 11 for flow through a spiral tube. Values for R_t, R_1, and R_b can be obtained from Figure 48.
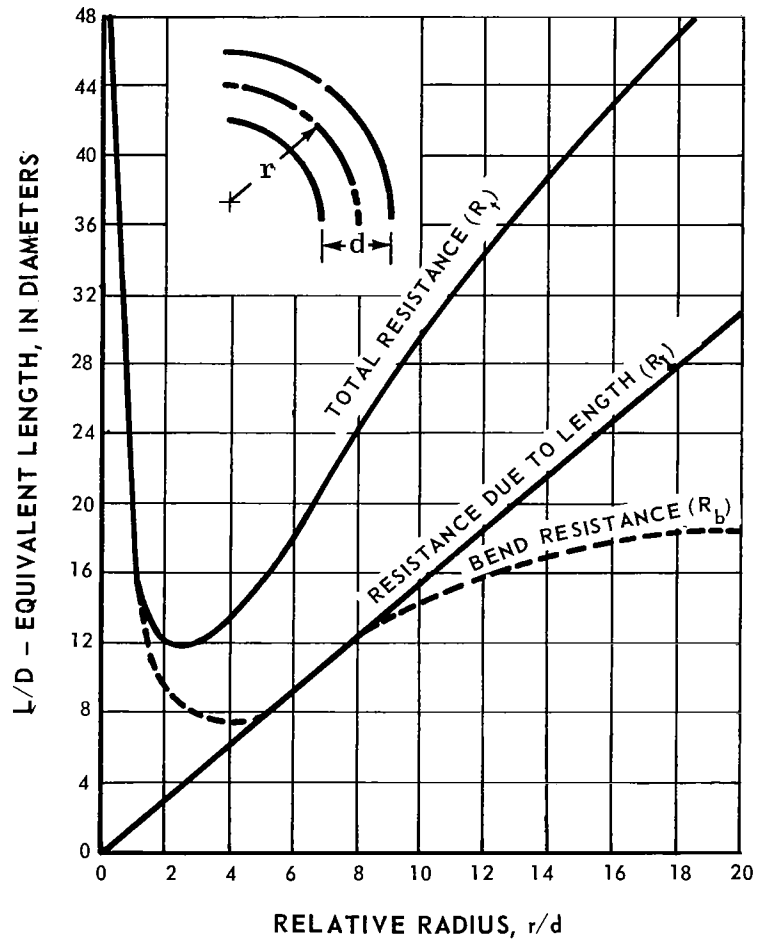
Figure 48   Equivalent Resistances for Flow Through Pipe Bends

For Section 6 of the boiler where the swirl flow is maintained by a wire coil brazed inside the tube, the pressure loss calculations were based on the method presented by Sams[10].

$$\Delta P = 4f \frac{1}{d_H} \left(\frac{f_{SF}}{f_{SC}}\right) \frac{G^2}{2g\rho} \tag{25}$$

The term (f_{SF}/f_{SC}) was determined by an extrapolation of the data of Reference 10.

For Sections 2, 4, and 5 of the boiler, where two-phase flow occurred, the method of Martinelli and Nelson[12] was employed for calculating pressure losses.

$$\frac{dP}{dl} = \frac{\left(\frac{dP}{dl}\right)_{TPF}}{\left(\frac{dP}{dl}\right)_L} \left(\frac{dP}{dl}\right)_L \tag{26}$$

The parameter $(dP/dl)_{TPF}/(dP/dl)_L$ can be obtained from Figure 3 of Reference 12 as a function of boiling-fluid quality and pressure. The term $(dP/dl)_L$ in Equation (26) is the frictional pressure gradient that would exist if the flow were entirely liquid. This term was calculated for the different sections of the boiler using the following relations:

Section 2

$$- \left(\frac{dP}{dl}\right)_L = 4f \frac{\left(\frac{L}{D}\right)_{eq}}{l_{actual}} \frac{G^2}{2g\rho} \tag{27}$$

Sections 4 and 5

$$-\left(\frac{dP}{dl}\right)_L = \frac{4f}{d_h} \left(\frac{f_{SF}}{f_{SC}}\right) \frac{G^2}{2g\rho} \tag{28}$$

Equations (27) and (28) represent differentiated forms of Equations (23) and (25) respectively.

The pressure drop for the two-phase sudden expansion that takes place in Section 3 of the boiler was calculated using the following equation which was presented by Jansen[13]

$$\Delta P = \frac{G_3^2 \, v_L}{g \, \sigma} \left[\frac{v_V}{v_L} \frac{x^2}{Rg} (1-\sigma) \right] \tag{29}$$

The vapor fraction R_g was determined using the correlation found in Figure 5 of Reference 12.

The thermodynamic performance of Sections 1 and 6 of the boiler was calculated using the log mean temperature difference method

$$Q = U A \Delta T_{LM} \tag{30}$$

where
$$U = \frac{1}{\dfrac{d_o}{h d_i} + \dfrac{t_H d_o}{k d_m} + \dfrac{1}{h_H}}$$

These sections are the subcooled and superheated regions where no change of phase is assumed to occur. In these sections, the rate at which the boiling fluid temperature increases with length is directly dependent upon the local rate of heat transfer. For these conditions Equation (30) provides a reasonable description of heat-exchanger performance. In Sections 2, 4 and 5 where boiling occurred, the boiling fluid was assumed to be saturated. Under these conditions, boiling fluid temperature becomes directly dependent upon the boiling-fluid pressure, rather than the local rate of heat transfer. As a consequence, the following differential equations were derived to describe the heat exchange process in Sections 2, 4 and 5 of the boiler.

$$\frac{dX}{dl} = \frac{q \pi d_o}{W h_{fg}} \tag{31}$$

where $q = U \Delta T$

$$\frac{d(\Delta T)}{dl} = \left[\frac{W H_{fg}}{W_H C_{PH}} \frac{dX}{dl} - \left(\frac{dT}{dP} \right)_{sat} \left(\frac{dP}{dl} \right) \right] \tag{32}$$

Equation (31) relates the rate of change in boiling fluid quality to the local heat flux q which in turn is dependent upon the local temperature difference between the two fluids ΔT. The first term on the right hand side of Equation (32) relates the rate of change of the heating-fluid temperature to the rate of change in the boiling-fluid quality, while the second term relates the rate of change of the boiling-fluid temperature to the boiling-fluid pressure gradient.

For each of the boiler sections under consideration, Equations (30) through (32) were combined with the appropriate relations for heat-transfer coefficients and pressure gradient, and solved using numerical integration.

The design calculations were based on the following set of conditions as specified in Task I of the contract.

1) Boiling-fluid flow rate   W   50 lb/hr

2) Heating-fluid flow rate W_H 650 lb/hr

3) Boiling-fluid inlet temperature T_{in} 140°F

4) Heating-fluid inlet temperature $T_{H\ in}$ 402°F

5) Boiling-fluid inlet pressure P_{out} 85 psia

The values calculated for the important thermodynamic variables at each station shown in Figure 47 are tabulated below:

Station No.	Axial Length L, ft	Boiling Fluid Pressure P, psia	Boiling Fluid Quality X	Boiling Fluid Temperature T, °F	Heating Fluid Temperature T_H °F
0	0	85.0	Subcooled	140	323
1	1.25	83.8	0	316	336
2	2.15	76.0	0.068	308	339
3	2.15	76.0	0.068	308	339
4	6.65	72.2	0.809	305	387
5	7.55	70.6	1.00	304	400
6	10.00	67.7	Superheated	377	402

In addition, a comparison between the calculated performance of the boiler and that which was experimentally determined by running the boiler at the design conditions is presented below:

	Calculated	Measured
Total heat transferred Q	54,000 Btu/hr	51,000 Btu/hr
Pinch point temperature difference ΔT_p	20°F	19°F
Boiling-fluid pressure drop ΔP	17.3 psi	16.2 psi
Boiling-fluid exit temperature T_{out}	377°F	338°F
Boiling-fluid superheat ΔT_{SH}	76°F	37°F

	Calculated	Measured
Boiling-fluid exit quality X_e	1.00	0.949
Heating-fluid exit temperature $T_{H\ out}$	323°F	330°F

This analysis was able to predict the total heat transferred within 6 percent, the pinch-point temperature difference within 1°F, and the pressure drop of the boiling fluid within 1.1 psi. However, since the dynamics of the two-phase flow was not considered, the analysis was not able to predict the nonequilibrium exit conditions observed for the boiling fluid. Instead of emerging as a dry vapor superheated by 76°F as predicted by the analysis, the boiling fluid emerged as a mist containing, by weight, 94.9 percent vapor superheated by 37°F and 5.1 percent droplets of saturated liquid.

In order to eliminate liquid at the boiler exit during testing, the nominal design operating conditions were changed to those presented in Section III.

APPENDIX 2

Derivation of Theoretical Transfer Function

The details of a derivation of a transfer function between boiler exit pressure and boiler inlet flow rate are presented in this appendix. The configuration considered is a single-tube counterflow boiler using a liquid heating fluid, designed to produce superheated vapor and having a choked restriction at its exit. A complete description of this boiler is presented in Section III of this report. Provisions was made in the analysis to account for the effects of the swirl-inducing plug inserted in the boiling fluid stream at the inlet end of the boiler.

In the analysis, the boiler was divided into three regions: subcooled, boiling, and superheated, each of which was analyzed separately. These regions correspond to those observed in the steady-state data which are described in Section IV of this report. For simplicity however, it was assumed that the evaporation process was completed in the boiling region so that the boiling fluid entered the superheat region as a dry saturated vapor. This assumption is justified by the lack of specific knowledge of the rate of droplet evaporation in the nonequilibrium-superheat region of the actual boiler.

Dynamic equations were derived for these three regions and for the boiler as a whole. These equations include:

Overall Equations

Continuity equation of the boiling fluid
Pressure-drop equation for the boiling fluid
Choked valve equation

Subcooled Region

Energy equation of the boiling fluid
Energy equation of the plug wall

Boiling Region

Energy equation of heater-loop fluid
Energy equation of shell wall
Energy equation of the boiling fluid

Superheated Region

Energy equation of the boiling fluid

The basic approach followed in the derivation was to linearize these equations for small perturbations around a steady-state point and take the Laplace transforms of the perturbed variables.

Simplifications have been introduced into the analysis, where required, in an effort to keep the transfer function reasonably manageable. The principal simplifying concept is that in the derivation of the continuity and pressure-drop equations, the density change of the boiling fluid is assumed to occur at one discrete location in the boiler. The fluid density and flow rate are, therefore, considered to be independent of axial position and equal to the inlet values everywhere upstream of this location. Similarly, the fluid density and flow rate are considered to be independent of axial position and equal to the exit values everywhere downstream of this location. The location at which the density change is assumed to occur is the point at which a liquid-vapor interface would be present if all the liquid in the boiler at any instant filled the flow passage starting from the inlet (see Figure 41).

The boiler-fluid inlet temperature, the heating-fluid inlet temperature, the heating-fluid flow rate and the size of the choked restriction are assumed constant in this analysis. Additional assumptions are stated whenever they are used in the derivation.

<u>Overall Equations</u>

For flow through a choked restriction the total pressure of the flow entering the restriction is proportional to the mass flow rate and the square root of the total temperature.

$$P_{out} \propto W_{out} \cdot \sqrt{T_{out}}$$

Linearizing this expression for small perturbations about a steady-state point and transforming the variables, the result is

$$\frac{\hat{P}_{out}}{P_{out,\,o}} = \frac{\hat{W}_{out}}{W_o} + \frac{\hat{T}_{out}}{2T_{out,\,o}} \tag{33}$$

The continuity equation was written to account for changes in the location of the point where density change is assumed to occur and changes in the vapor density due to changes in exit pressure. The distance from the boiler inlet to the density change point is assumed to be proportional to the length of the subcooled region. This simplification avoids the necessity of describing analytically the dynamic two-phase flow mechanisms. It is a reasonable approximation to the

extent that most of the mass of the boiler fluid resides in the subcooled and very low quality regions. The resulting differential equation is presented below.

$$W_{in} - W_{out} = K (\rho_L - \rho_V) A_{SC} \left(\frac{dL_{SC}}{dt}\right) + \left(\frac{Vol_V}{RT_{out}}\right)\left(\frac{dP_{out}}{dt}\right)$$

The proportionality constant K is defined by the relation

$$K = \frac{\partial \left[\int_0^{L_e} \rho\, A\, dx\right]}{\partial \left[\rho_L A_{SC} L_{SC}\right]} \tag{34}$$

and can be evaluated from the steady-state experimental test data in which W was varied.

Linearizing the equation for small perturbations about a steady-state point and transforming the variables the result is

$$\frac{\hat{W}_{in}}{W_o} - \frac{\hat{W}_{out}}{W_o} = K\tau_{SC}s \frac{\hat{L}_{SC}}{L_{SC,o}} + \tau_V s \frac{\hat{P}_{out}}{P_{out,o}} \tag{35}$$

where
$$\tau_{SC} = \frac{(\rho_L - \rho_V) A_{SC} L_{SC}}{W_o}$$

$$\tau_V = \frac{P_{out}\, Vol_V}{W_o}$$

In keeping with the concept of a sudden density change at a discrete point, the pressure drop between the end of the subcooled region and the boiler exit is expressed in the form of a single-phase pressure drop, i. e., proportional to length and to flow rate squared, and inversely proprotional to density.

$$(P_{out} - P_P) \propto \frac{W_{out}^2\, length}{\rho_{out}} \tag{36}$$

Since most of the pressure drop in the boiler is due to the vapor phase, the boiler exit density and flow rate are used. When the pressure-drop equation is written in this form, the length cannot be taken as a literal length because of flow-area changes caused by inserts inside the boiler tube. Consequently, changes in the fictitious length are approximately related to changes in the subcooled length by means of the empirical coefficient

$$\beta_3 = \frac{\partial (\Delta P_B / P_{P,o})}{\partial (L_{SC}/L_{SC,o})}$$

Combining Equations (33) and (36) with the perfect gas law, the result is

$$(P_{out} - P_P) \propto (P_{out}) \text{(length)}$$

Linearizing, transforming, and relating a perturbation in the fictitious length to a perturbation in subcooled length, the result is

$$\frac{\hat{P}_P}{P_{P,o}} = \frac{\hat{P}_{out}}{P_{out,o}} + \left(\frac{\partial (\Delta P_B/P_{P,o})}{\partial (L_{SC}/L_{SC,o})}\right)\left(\frac{\hat{L}_{SC}}{L_{SC,o}}\right) \tag{37}$$

The combined energy equation incorporates the five individual energy equations written for different portions of the subcooled and boiling regions into a single relation. This combined equation describes perturbations in the length of the subcooled region as a function of the perturbations of the inlet flow rate, exit flow rate and exit pressure of the boiling fluid.

Four of the five energy equations were derived using the distributed-parameter approach whereby a partial differential equation was derived with time and axial distance as the independent variables. The solution to the partial differential equation for the boiling fluid in the boiling region, however, proved to be too complicated for the purposes of this analysis. In its place a quasi-dynamic equation was written with coefficients evaluated by means of steady-state relationships, and with transport time lags superimposed. The transport times appear in the equation in the form they would take in an approximate solution to a single-phase partial differential energy equation. The transport times in the boiling region are referred to the time it takes a liquid particle to travel the length of the boiling region.

In deriving these energy equations a fixed frame of reference was used, although the locations of the boundaries of both the subcooled and boiling regions fluctutate with time. The energy equations of the two regions were connected in a fixed reference frame by employing linearized perturbations about the steady-state boundaries in the boundary conditions of the equations.

Subcooled Region

In deriving the energy equation in the subcooled region the following basic assumptions were made:

1) No change in heating-fluid temperature takes place due to heat transfer in the subcooled region. Consequently, the only heating-fluid temperature changes are those which are transported into the subcooled region due to changes with time at the pinch point.

2) Heat storage occurs in the plug metal but not in the tube metal or shell metal. Infinite thermal conductivity of the plug metal in the radial direction and zero conductivity in the axial direction are assumed in calculating heat transfer from plug metal to boiling fluid.

3) The overall heat-transfer coefficient between heating fluid and boiler fluid changes (for small perturbations about a point) with boiling fluid velocity to the n_{SC} power. The boiling-fluid heat-transfer coefficient is considered constant for the purpose of calculating heat transfer from plug metal to boiling fluid.

4) Average properties in the region are used for both fluids.

heating fluid

$$U_{sc}\, \mathcal{P}\, (T_H - T)\, \Delta x$$

$(\rho_L A_{sc} C_\rho V T)_{IN}$ → → $(\rho_L A_{sc} C_\rho V T)_{OUT}$ boiling fluid

$h_{sc}\mathcal{P}_{PM}(T_{PM}-T)\Delta x$

plug metal

Δx
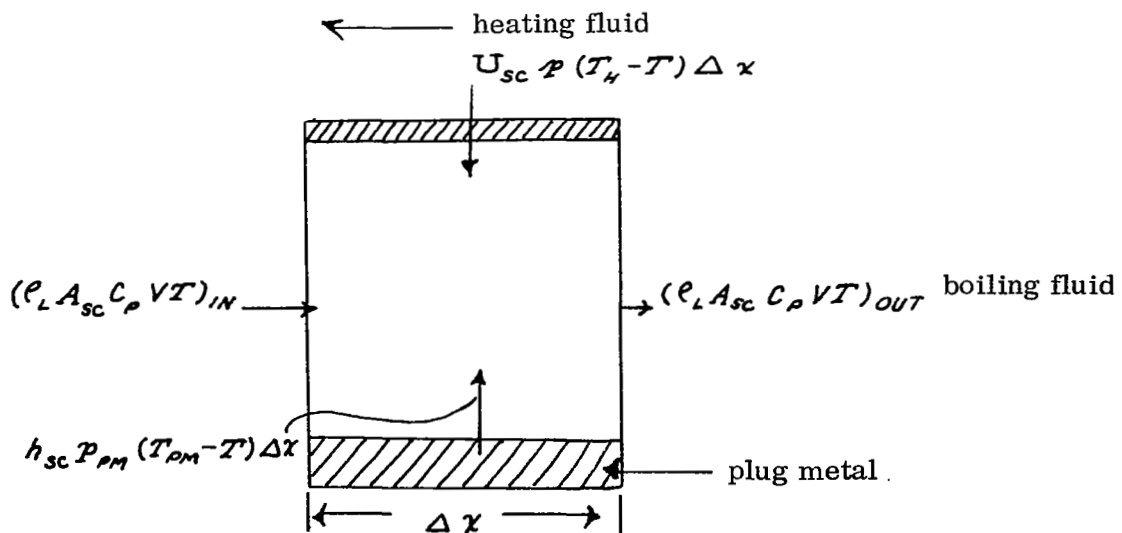
Taking an energy balance on a differential element of the boiling fluid

$$\text{energy in} = \text{energy out} + \text{energy stored}$$

$$(\rho_L A_{sc} C_p V T)_{IN} + U_{sc}\, P_T (T_H - T)\, \Delta x + h_{sc} P_{PM} (T_{PM} - T)\Delta x = (\rho_L A_{sc} C_p V T)_{OUT} + \rho_L A_{sc} C_p \frac{\partial T}{\partial t}$$

$$\rho_L A_{sc} C_p V \left[T - \frac{\partial T}{\partial x}\frac{\Delta x}{2}\right] + U_{sc} P (T_H - T)\Delta x + h_{sc} P_{PM} (T_{PM} - T)\Delta x =$$

$$\rho_L A_{sc} C_p V \left[T + \frac{\partial T}{\partial x}\frac{\Delta x}{2}\right] + \rho_L A_{sc} C_p \frac{\partial T}{\partial t}$$

$$\frac{\partial T}{\partial t} + V\frac{\partial T}{\partial x} = \Theta (T_H - T) + \Theta_1 (T_{PM} - T) \tag{38}$$

where $\quad \Theta = \dfrac{U_{sc} P_T}{\rho_L A_{sc} C_p}\quad$ (U_{SC} is assumed variable)

$$\Theta_1 = \frac{h_{sc} P_{PM}}{\rho_L A_{sc} C_p}\quad (h_{SC} \text{ is assumed constant})$$

Linearizing for small perturbations about a steady point and transforming the variables the result is:

$$s\hat{T} + V_o \frac{d\hat{T}}{dx} + \hat{V}\frac{\partial T_o}{\partial x} = \hat{\Theta}(T_{Ho} - T_o) + \Theta_o (\hat{T}_H - \hat{T}) + \Theta_1 (\hat{T}_{PM} - \hat{T}) \tag{39}$$

Steady-State Equation

$$V_o \frac{\partial T_o}{\partial x} = \Theta (T_{Ho} - T_o)$$

Steady-State Solution $\tag{40}$

$$T_o = T_{Ho} - (T_{Ho} - T_{IN})\, e^{-\frac{\Theta_o}{V_o} x}$$

$$\frac{\partial T_o}{\partial x} = \frac{\Theta_o}{V_o} (T_{Ho} - T_{IN})\, e^{-\frac{\Theta_o}{V_o} x} \tag{41}$$

Energy Equation of Plug Metal in Subcooled Region

Taking a heat balance on a differential element of the plug metal

$$\text{energy in } = \text{ energy stored}$$

$$- h_{sc} \, \mathcal{P}_{PM} \, (T_{PM} - T) \, \Delta x = \rho_{PM} \, A_{PM} \, C_{P_{PM}} \, \Delta x \, \frac{\partial T_{PM}}{\partial t}$$

$$\frac{\partial T_{PM}}{\partial t} = - \Theta_2 \, (T_{PM} - T) \tag{42}$$

$$\text{where} \quad \Theta_2 = \frac{h_{sc} \, \mathcal{P}_{PM}}{\rho_{PM} \, A_{PM} \, C_{P_{PM}}}$$

Linearizing and transforming the variables the result is

$$S \hat{T}_{PM} = - \Theta_2 \, (\hat{T}_{PM} - \hat{T}) \tag{43}$$

Solution of Differential Equations

On the basis of the first basic assumption

$$T_{H_2O} = T_{H_2O_0} \quad , \quad \therefore \quad \frac{\partial T_H}{\partial x} = 0 \tag{44}$$

$$\hat{T}_H = \hat{T}_{HP} \, e^{- \frac{S(L_{sc,0} - x)}{V_H}} \tag{45}$$

On the basis of the third basic assumption

$$\Theta = C V^{n_{sc}} \, , \quad \therefore \quad \hat{\Theta} = \frac{\Theta_0}{V_0} \, n_{sc} \, \hat{V} \tag{46}$$

Combining Equations (39), (40), (41), (43), (44), (45), and (46) the result is

$$\frac{d\hat{T}}{dx} + \left[\frac{S + \Theta_o - \Theta_1 \left(\frac{\Theta_2}{S + \Theta_2} - 1 \right)}{V_o} \right] \hat{T} = -\frac{\Theta_o}{V_o^2} (1 - \eta_{sc}) (T_{HPO} - T_{IN}) e^{-\frac{\Theta_o}{V_o}x} \hat{V}$$

$$+ \frac{\Theta_o}{V_o} e^{-\frac{s(L_{sc,o} - x)}{V_H}} \hat{T}_{HP} \qquad (47)$$

The general solution to Equation (47) is

$$\hat{T} = e^{-[\quad]x} \left[\int \left(-\frac{\Theta_o}{V_o^2} (1 - \eta_{sc})(T_{HPO} - T_{IN}) e^{-\frac{\Theta_o}{V_o}x} \hat{V} \right. \right.$$

$$\left. \left. + \frac{\Theta_o}{V_o} e^{-s\left(\frac{L_{sc,o} - x}{V_H}\right)} \hat{T}_{HP} \right) e^{+[\quad]x} dx + c \right]$$

which upon integration becomes

$$\hat{T} = -\frac{\frac{\Theta_o}{V_o} (1 - \eta_{sc}) (T_{HPO} - T_{IN})}{S - \Theta_1 \left(\frac{\Theta_2}{S + \Theta_2} - 1 \right)} e^{-\frac{\Theta_o}{V_o}x} \hat{V} \quad +$$

$$\frac{\frac{\Theta_o}{V_o} e^{-s \tau_{Hsc}} e^{\frac{sx}{V_H}}}{\left\{ \frac{S + \Theta_o - \Theta_1 \left(\frac{\Theta_2}{S + \Theta_2} - 1 \right)}{V_o} + \frac{s}{V_H} \right\}} \hat{T}_{HP} + c\, e^{-\left[\frac{S + \Theta_o - \Theta_1 \left(\frac{\Theta_2}{S + \Theta_2} - 1 \right)}{V_o} \right]x}$$

$$(48)$$

110

Applying the boundary condition $\hat{T} = 0$ at $x = 0$ the result is

$$\hat{T} = -\frac{\frac{\Theta_o}{V_o}(1-\eta_{sc})(T_{HP,O}-T_{IN})}{S-\Theta_1\left(\frac{\Theta_2}{S+\Theta_2}-1\right)}\left[e^{-\frac{\Theta_o}{V_o}x}-e^{-\left\{\frac{S+\Theta_o-\Theta_1\left(\frac{\Theta_2}{S+\Theta_2}-1\right)}{V_o}\right\}x}\right]\hat{V}$$

$$+\frac{\frac{\Theta_o}{V_o}e^{-S\tau_{HSC}}}{\left\{\frac{S+\Theta_o-\Theta_1\left(\frac{\Theta_2}{S+\Theta_2}-1\right)}{V_o}+\frac{S}{V_H}\right\}}\left[e^{\frac{Sx}{V_H}}-e^{-\left\{\frac{S+\Theta_o-\Theta_1\left(\frac{\Theta_2}{S+\Theta_2}-1\right)}{V_o}\right\}x}\right]\hat{T}_{HP}$$

$$\tag{49}$$

at $x = L_{sc,o}$; $\hat{T} = \hat{T}_P$ and

$$\hat{T}_P = -(1-\eta_{sc})\left[\frac{\Theta_o}{V_o}(T_{HP,O}-T_{IN})e^{-\Theta_o\tau_{sc}}\right]\left[\frac{1-e^{-\left\{S-\Theta_1\left(\frac{\Theta_2}{S+\Theta_2}-1\right)\right\}\tau_{sc}}}{S-\Theta_1\left(\frac{\Theta_2}{S+\Theta_2}-1\right)}\right]\frac{\hat{W}_{IN}}{\rho_L A_{sc}}$$

$$+\frac{\frac{\Theta_o}{V_o}}{\left\{\frac{S+\Theta_o-\Theta_1\left(\frac{\Theta_2}{S+\Theta_2}-1\right)}{V_o}+\frac{S}{V_H}\right\}}\left[1-e^{-\left\{S+\Theta_o-\Theta_1\left(\frac{\Theta_2}{S+\Theta_2}-1\right)\right\}\tau_{sc}-S\tau_{HSC}}\right]T_{HP}$$

$$\tag{50}$$

where $\quad\dfrac{L_{sc,O}}{V_o} = \tau_{sc}$ $\tag{51}$

$$\frac{L_{sc,O}}{V_H} = \tau_{HSC} \tag{52}$$

$$V = \frac{W_{IN}}{\rho_L A_{sc}} \quad;\quad \therefore\quad \hat{V} = \frac{\hat{W}_{IN}}{\rho_L A_{sc}} \tag{53}$$

Boundary Condition at Pinch Point

Defining the subcooled length as the distance from the boiler inlet required for the boiling fluid to reach the saturation temperature, small perturbations of the subcooled length around steady-state value can be expressed by the following equation

$$\hat{L}_{sc} = \frac{\hat{T}_P - \hat{T}_{SAT}}{-\left(\frac{\partial T_o}{\partial x}\right)_{x=L_{sc,o}}} \tag{54}$$

And Equation (50) becomes

$$\hat{L}_{sc} = (1-\eta_{sc})\left(\frac{1-e^{-\left[s-\Theta_1\left(\frac{\Theta_2}{s+\Theta_2}-1\right)\right]\tau_{sc}}}{s-\Theta_1\left(\frac{\Theta_2}{s+\Theta_2}-1\right)}\right)\hat{W}_{IN}\left(\frac{L_{po}}{W_o\,\tau_{sc}}\right)$$

$$-\left(\frac{L_{sc,o}}{(T_{HP,o}-T_{IN})\,e^{-\Theta_o\,\tau_{sc}}}\right)\left(\frac{1-e^{-\left[s+\Theta_o-\Theta_1\left(\frac{\Theta_2}{s+\Theta_2}-1\right)\right]\tau_{sc}-s\,\tau_{HSC}}}{\left[s+\Theta_o-\Theta_1\left(\frac{\Theta_2}{s+\Theta_2}-1\right)\right]\tau_{sc}+s\,\tau_{HSC}}\right)\hat{T}_{HP}$$

$$+\frac{\hat{T}_{SAT}}{\frac{\Theta_o}{V_o}\left[T_{HP_o}-T_{IN}\right]e^{-\Theta_o\,\tau_{sc}}} \tag{55}$$

For x = L$_{sc, 0}$ Equation (40) becomes

$$e^{\Theta_o\,\tau_{sc}} = \frac{T_{HP,o}-T_{IN}}{\Delta T_{P_o}} \equiv \phi_1 \tag{56}$$

112

For small perturbations

$$
\frac{\hat{T}_{SAT}}{\Delta T_{\rho o}} = \left[\frac{\partial \left(T_{SAT} / \Delta T_{\rho o} \right)}{\partial \left(P / P_{\rho o} \right)} \right]_{L_{SC,0}} \frac{\hat{P}_{\rho}}{P_{\rho o}} = \beta_1 \quad \frac{\hat{P}_{\rho}}{P_{\rho o}} \tag{57}
$$

Combining equations (55), (56) and (57) and noting that

$$
\left[\frac{\Theta_2}{s + \Theta_2} - 1 \right] = \frac{s \Theta_2}{s^2 - \Theta_2^2} - \frac{s^2}{s^2 - \Theta_2^2}
$$

The result is:

$$
\frac{\hat{L}_{SC}}{L_{SC,0}} = \frac{\gamma_1}{s \, T_{SC}} \frac{\hat{W}_{IN}}{W_o} - \gamma_2 \frac{\hat{T}_{HP}}{\Delta T_{\rho o}} + \gamma_3 \frac{\hat{P}_{\rho}}{P_{\rho o}} \tag{58}
$$

where

$$
\gamma_1 = \left[\frac{1 - \left[e^{-\left(\frac{\Theta_1 s^2}{s^2 - \Theta_2^2} \right) T_{SC}} \right] e^{-s \left(1 - \frac{\Theta_1 \Theta_2}{s^2 - \Theta_2^2} \right) T_{SC}}}{1 - \frac{\Theta_1 \Theta_2}{s^2 - \Theta_2^2} + s \left[\frac{\Theta_1}{s^2 - \Theta_2^2} \right]} \right] (1 - \eta_{SC}) \tag{59}
$$

$$
\gamma_2 = \frac{1 - \left[\left(\frac{1}{\phi_1} \right) e^{-\left(\frac{\Theta_1 s^2}{s^2 - \Theta_2^2} \right) T_{SC}} \right] e^{-s \left[\left(1 - \frac{\Theta_1 \Theta_2}{s^2 - \Theta_2^2} \right) T_{SC} + T_{HSC} \right]}}{\left[\ln \phi_1 + \left(\frac{\Theta_1 s^2}{s^2 - \Theta_2^2} \right) T_{SC} \right] + s \left[\left(1 - \frac{\Theta_1 \Theta_2}{s^2 - \Theta_2^2} \right) T_{SC} + T_{HSC} \right]} \tag{60}
$$

$$
\gamma_3 = \frac{\beta_1}{\ln \phi_1} \tag{61}
$$

113

Boiling Region

In deriving the energy equations in the boiling region the following basic assumptions were made:

1) Heat storage occurs in the shell metal but not in the tube metal or probe metal. Infinite thermal conductivity of the shell metal in the radial direction and zero conductivity in the axial direction are assumed.

2) All heat-transfer coefficients are constant and independent of the boiling-fluid flow rate.

3) The saturation temperature is independent of axial distance and equal to the value determined by the pinch-point pressure.

4) The transport time of a liquid particle in the boiling region is the principal dynamic element in the boiling-fluid energy relationships.
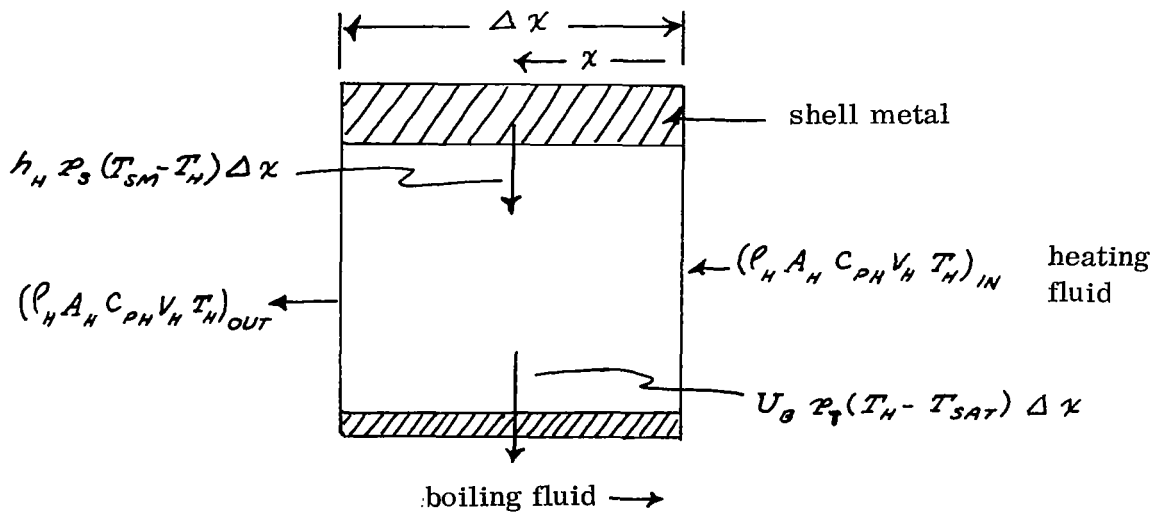
Taking x in the direction of the heating fluid flow, an energy balance on a differential element of the heater loop fluid becomes

$$\text{energy in} = \text{energy out} + \text{energy stored}$$

$$(\rho_H A_H C_{PH} V_H T_H)_{IN} + h_H P_{SM}(T_{SM} - T_H)\Delta x = U_B P_T(T_H - T_{SAT})\Delta x +$$

$$(\rho_H A_H C_{PH} V_H T_H)_{OUT} + \rho_H A_H C_{PH}\frac{\partial T_H}{\partial t}\Delta x$$

$$\rho_{_H} A_{_H} C_{_{PH}} \frac{\partial T_{_H}}{\partial t} \Delta x + \rho_{_H} A_{_H} C_{_{PH}} V_{_H} \left[T_{_H} + \frac{\partial T_{_H}}{\partial x} \frac{\Delta x}{2} \right] = \rho_{_H} A_{_H} C_{_{PH}} V_{_H} \left[T_{_H} - \frac{\partial T_{_H}}{\partial x} \frac{\Delta x}{2} \right]$$

$$+ U_B P_T (T_{SAT} - T_{_H}) + h_{_H} P_{SM} (T_{SM} - T_{_H})$$

$$\frac{\partial T_{_H}}{\partial t} + V_{_H} \frac{\partial T_{_H}}{\partial x} = \Theta_B (T_{SAT} - T_{_H}) + \Theta_{B_1} (T_{SM} - T_{_H}) \qquad (62)$$

where

$$\Theta_B = \frac{U_B P_T}{\rho_{_H} A_{_H} C_{_{PH}}} \qquad (63)$$

$$\Theta_{B_1} = \frac{h_{_H} P_{SM}}{\rho_{_H} A_{_H} C_{_{PH}}} \qquad (64)$$

Linearizing for small perturbations about a steady point and taking the Laplace transforms of the perturbed variables the result is

$$\frac{d \hat{T}_{_H}}{d x} + \frac{s}{V_{_H}} \hat{T}_{_H} = \frac{\Theta_B}{V_{_H}} \left(\hat{T}_{SAT} - \hat{T}_{_H} \right) + \frac{\Theta_{B_1}}{V_{_H}} \left(\hat{T}_{SM} - \hat{T}_{_H} \right) \qquad (65)$$

Steady–State Equation

$$V_{_H} \frac{\partial T_{_{H,o}}}{\partial x} = - \Theta_B (T_{_{H,o}} - T_{SAT,o})$$

Steady–State Solution

$$T_{_{H,o}} = T_{SAT,o} + (T_{_{H,IN}} - T_{SAT,o}) e^{-\frac{\Theta_B}{V_{_H}} x} \qquad (66)$$

$$\frac{\partial T_{_{H,o}}}{\partial x} = - \frac{\Theta_B}{V_{_H}} (T_{_{H,IN}} - T_{SAT,o}) e^{-\frac{\Theta_B}{V_{_H}} x} \qquad (67)$$

115

Energy Equation of the Shell Metal in the Boiling Region

Assuming no heat loss to the surroundings the heat balance for a differential element of the shell metal becomes

$$\text{energy in} = \text{energy stored}$$

$$h_H \, \mathcal{P}_{SM} \, (T_H - T_{SM}) \, \Delta x = \rho_{SM} \, C_{P_{SM}} \, A_{SM} \, \frac{\partial T_{SM}}{\partial t} \, \Delta x$$

or

$$\frac{\partial T_{SM}}{\partial t} = - \Theta_{B_2} \, (T_{SM} - T_H) \tag{68}$$

where

$$\Theta_{B_2} = \frac{h_H \, \mathcal{P}_{SM}}{\rho_{SM} \, C_{P_{SM}} \, A_{SM}} \tag{69}$$

Linearizing and transforming the variables the result is

$$s \, \hat{T}_{SM} = - \Theta_{B_2} \, (\hat{T}_{SM} - \hat{T}_H) \tag{70}$$

Solution of the Differential Equations

Combining Equations (65) and (70) the result is

$$\frac{d\hat{T}_H}{dx} + \left[\frac{s + \Theta_B - \Theta_{B_1}\left(\frac{\Theta_{B2}}{s + \Theta_{B2}} - 1 \right)}{V_H} \right] \hat{T}_H = \frac{\Theta_B}{V_H} \hat{T}_{SAT} \qquad (71)$$

On the basis of the third basic assumption

$$\hat{T}_{SAT} = \hat{T}_{SAT,P} \neq f(x)$$

The general solution to Equation (71) is then

$$\hat{T}_H = e^{-[\ ]x} \left[\int \frac{\Theta_B}{V_H} \hat{T}_{SAT} \, e^{[\ ]x} \, dx + c \right] \qquad (72)$$

which upon integration becomes

$$\hat{T}_H = \frac{\Theta_B}{s + \Theta_B - \Theta_{B_1}\left(\frac{\Theta_{B2}}{s + \Theta_{B2}} - 1 \right)} \hat{T}_{SAT} + c \, e^{-\left[\frac{s + \Theta_B - \Theta_{B_1}\left(\frac{\Theta_{B2}}{s + \Theta_{B2}} - 1 \right)}{V_H} \right]x} \qquad (73)$$

Applying the boundary condition

$$\hat{T}_H = \left(\frac{\partial T_{HO}}{\partial x} \right)_{x=0^+} \hat{L}_B \qquad (74)$$

$$AT \quad x = 0^+$$

117

which relates small perturbations in the heating-fluid temperature to small perturbations in the location of the end of the boiling region. The result is

$$
\hat{T}_H = \left[\frac{1 - e^{-\left[\frac{s + \Theta_B - \Theta_{B_1} \left(\frac{\Theta_{B_2}}{s + \Theta_{B_2}} - 1 \right)}{V_H} \right] x}}{s + \Theta_B - \Theta_{B_1} \left(\frac{\Theta_{B_2}}{s + \Theta_{B_2}} - 1 \right)} \right] \Theta_B \hat{T}_{SAT} +
$$

$$
\left(\frac{\partial T_{H,0}}{\partial x} \right)_{x=0} \hat{L}_B \, e^{-\left[\frac{s + \Theta_B - \Theta_{B_1} \left(\frac{\Theta_{B_2}}{s + \Theta_{B_2}} - 1 \right)}{V_H} \right] x} \tag{75}
$$

At the pinch point $x = (L_{B,O} - L_{sc,O})$, $\hat{T}_H = \hat{T}_{HP}$ and Equation (75) becomes

$$
\hat{T}_{HP} = \left[\frac{1 - e^{-\left[s + \Theta_B - \Theta_{B_1} \left(\frac{\Theta_{B_2}}{s + \Theta_{B_2}} - 1 \right) \right] \tau_{HB}}}{s + \Theta_B - \Theta_{B_1} \left(\frac{\Theta_{B_2}}{s + \Theta_{B_2}} - 1 \right)} \right] \Theta_B \hat{T}_{SAT} +
$$

$$
\left(\frac{\partial T_{H,0}}{\partial x} \right)_{x=0} \hat{L}_B \, e^{-\left[s + \Theta_B - \Theta_{B_1} \left(\frac{\Theta_{B_2}}{s + \Theta_{B_2}} - 1 \right) \right] \tau_{HB}} \tag{76}
$$

118

where

$$\tau_{HB} = \frac{L_{B,o} - L_{SC,o}}{V_H} \tag{77}$$

At the pinch point Equation (66) becomes

$$e^{\Theta_B \tau_{HB}} = \frac{T_{H,IN} - T_{SAT,o}}{\Delta T_{Po}} \equiv \phi_2 \tag{78}$$

while at x = 0 Equation (67) becomes

$$\left(\frac{\partial T_{H,o}}{\partial x}\right)_{x=o} = -\frac{\Theta_B}{V_H}\left(T_{H,IN} - T_{SAT,o}\right) \tag{79}$$

Combining Equations (77), (78), and (79) the result is

$$\left(\frac{\partial T_{H,o}}{\partial x}\right)_{x=o} = -\frac{\ln \phi_2 \, \Delta T_{Po}}{(L_{B,o} - L_{sc,o})} \, e^{\Theta_B \tau_{HB}} \tag{80}$$

Combining Equations (76), (78), and (80)

$$\frac{\hat{T}_{HP}}{\Delta T_{Po}} = \ln \phi_2 \left[\frac{1 - \left(\frac{1}{\phi_2}\right) e^{-\left[s - \Theta_{B1}\left(\frac{\Theta_{B2}}{s + \Theta_{B2}} - 1\right)\right]\tau_{HB}}}{\ln \phi_2 + \left[s - \Theta_{B1}\left(\frac{\Theta_{B2}}{s + \Theta_{B2}} - 1\right)\right]\tau_{HB}} \right] \frac{\hat{T}_{SAT}}{\Delta T_{Po}} -$$

$$(\ln \phi_2) \, e^{-\left[s - \Theta_{B1}\left(\frac{\Theta_{B2}}{s + \Theta_{B2}} - 1\right)\right]\tau_{HB}} \frac{\hat{L}_B}{(L_{B,o} - L_{sc,o})} \tag{81}$$

Combining Equations (57) and (81) and noting that

$$\left[\frac{\Theta_{B2}}{S + \Theta_{B2}} - 1 \right] = \frac{S\,\Theta_{B2}}{S^2 - \Theta_{B2}^2} - \frac{S^2}{S^2 - \Theta_{B2}^2}$$

the result is

$$\frac{\hat{T}_{HP}}{\Delta T_{Po}} = \gamma_4 \frac{\hat{P}_P}{P_{Po}} - \gamma_5 \frac{\hat{L}_B}{(L_{B,o} - L_{SC,o})} \tag{82}$$

where

$$\gamma_4 = \beta_1 \, \ln \phi_2 \left[\frac{1 - \left(\frac{1}{\phi_2}\right) e^{-\left[\frac{\Theta_{B1} S^2}{S^2 - \Theta_{B2}^2}\right] T_{HB}} e^{-S\left[1 - \frac{\Theta_{B1}\,\Theta_{B2}}{S^2 - \Theta_{B2}^2}\right] T_{HB}}}{\left[\ln \phi_2 + \frac{\Theta_{B1} S^2 T_{HB}}{S^2 - \Theta_{B2}^2}\right] + S\left[1 - \frac{\Theta_{B1}\,\Theta_{B2}}{S^2 - \Theta_{B2}^2}\right] T_{HB}} \right]$$

$$\tag{83}$$

$$\gamma_5 = \left[(\ln \phi_2)\, e^{-\left[\frac{\Theta_{B1} S^2}{S^2 - \Theta_{B2}^2}\right] T_{HB}} \right] e^{-S\left[1 - \frac{\Theta_{B1}\,\Theta_{B2}}{S^2 - \Theta_{B2}^2}\right] T_{HB}}$$

$$\tag{84}$$

120

Energy Equation of the Boiling Fluid in the Boiling Region

Assuming that changes in L_B can be described using a chain rule type of equation where the independent variables are subject to time lags, the result is

$$\frac{d L_B}{d t} = \left(\frac{\partial L_B}{\partial W_{OUT}}\right) \frac{d\left[W_{OUT}(t - T_B/2)\right]}{d t} + \left(\frac{\partial L_B}{\partial L_{SC}}\right) \frac{d\left[L_{SC}(t - T_B)\right]}{d t} +$$

$$\left(\frac{\partial L_B}{\partial P_P}\right) \frac{d\left[P_P(t - T_B)\right]}{d t} + \left(\frac{\partial L_B}{\partial T_{HP}}\right) \frac{d\left[T_{HP}(t - T_B)\right]}{d t}$$

$$(85)$$

where T_B is the time required for a liquid particle to travel the length of the boiling region.

Linearizing about a steady point and transforming the variables the result is

$$\hat{L}_B = \left(\frac{\partial L_B}{\partial W_{OUT}}\right)_o \hat{W}_{OUT} \, e^{-\frac{s T_B}{2}} + \left(\frac{\partial L_B}{\partial L_{SC}}\right)_o \hat{L}_{SC} \, e^{-s T_B} +$$

$$\left(\frac{\partial L_B}{\partial P_P}\right)_o \hat{P}_P \, e^{-s T_B} + \left(\frac{\partial L_B}{\partial T_{HP}}\right)_o \hat{T}_{HP} \, e^{-s T_B}$$

$$(86)$$

Taking a steady-state energy balance over the entire boiling region the result is

$$Q_B = W_o H_{fg} - W_H C_{PH} (T_{H,IN} - T_{HP})$$ (87)

Assuming that the heat transferred in the boiling region can be described using an arithmetic mean temperature difference, the result is

$$Q_B = U_B P_T (L_B - L_{SC}) \Delta T_M$$ (88)

where $$\Delta T_M = \frac{(T_{H,IN} - T_{SAT}) + (T_{HP} - T_{SAT})}{2}$$

$$= \left(\frac{T_{H,IN} + T_{HP}}{2} \right) - T_{SAT}$$

Combining Equations (87) and (88) the result is

$$L_B = \frac{W_o H_{fg}}{U_B P_T \Delta T_M} + L_{SC}$$ (89)

Differentiating Equation (89) the result is

$$\frac{\partial L_B}{\partial W_{OUT}} = \frac{H_{fg}}{U_B P_T \Delta T_M} = \frac{L_{B,O} - L_{SC,O}}{W_o}$$ (90)

$$\frac{\partial L_B}{\partial L_{sc}} = 1 = \frac{T_{Hsc}}{T_{HB}} \cdot \left(\frac{L_{B,o} - L_{sc,o}}{L_{sc,o}} \right) \tag{91}$$

$$\frac{\partial L_B}{\partial P_P} = \left(\frac{\partial L_B}{\partial \Delta T_M} \right) \left(\frac{\partial \Delta T_M}{\partial T_{SAT}} \right) \left(\frac{\partial T_{SAT}}{\partial P_P} \right)$$

$$= -\left(\frac{W_o H_{fg}}{U_B P_T \Delta T_M^2} \right) (-1) \left(\frac{\partial T_{SAT}}{\partial P_P} \right)$$

Combining the above equation with Equation (89) and the definition of β_1 the result is

$$\frac{\partial L_B}{\partial P_P} = \frac{L_{B,o} - L_{sc,o}}{\Delta T_M} \quad \frac{\Delta T_{Po}}{P_{Po}} \quad \beta_1$$

or

$$\frac{\partial L_B}{\partial P_P} = \frac{(L_{B,o} - L_{sc,o})}{P_{Po}} \phi_3 \beta_1 \tag{92}$$

where

$$\phi_3 = \frac{\Delta T_{Po}}{\Delta T_M}$$

$$\frac{\partial L_B}{\partial T_{HP}} = \left(\frac{\partial L_B}{\partial \Delta T_M} \right) \left(\frac{\partial \Delta T_M}{\partial T_{H,P}} \right)$$

$$= \left(-\frac{W_o H_{fg}}{U_B P_T \Delta T_M^2} \right) \left(\frac{1}{2} \right)$$

123

Combining with Equation (89)

$$\frac{\partial L_B}{\partial T_{HP}} = - \frac{(L_{B,o} - L_{sc,o})}{2 \Delta T_M} \tag{93}$$

Combining Equations (86), (90), (91), (92), and (93) the result is

$$\frac{\hat{L}_B}{L_{B,o} - L_{sc,o}} = \frac{\hat{W}_{ouT}}{W_o} e^{-\frac{sT_B}{2}} + \left(\frac{T_{HSC}}{T_{HB}}\right) \frac{\hat{L}_{sc}}{L_{sc,o}} e^{-sT_B}$$

$$+ \phi_3 \beta_1 \frac{\hat{P}_P}{P_{Po}} e^{-sT_B} - \frac{\phi_3}{2} \frac{\hat{T}_{HP}}{\Delta T_{PO}} e^{-sT_B} \tag{94}$$

Combined Energy Equation

Combining Equations (58) and (82) the result is

$$\frac{\hat{L}_{sc}}{L_{sc,o}} = \frac{\gamma_1}{s T_{sc}} \frac{\hat{W}_{IN}}{W_o} + \left[\gamma_3 - \gamma_2 \gamma_4\right] \frac{\hat{P}_P}{P_{P,o}} + \gamma_2 \gamma_5 \frac{\hat{L}_B}{L_{B,o} - L_{sc,o}} \tag{95}$$

Combining Equations (82) and (94) the result is

$$\left[1 - \gamma_5 \frac{\phi_3}{2} e^{-sT_B}\right] \frac{\hat{L}_B}{L_{B,o} - L_{sc,o}} = e^{-\frac{sT_B}{2}} \frac{\hat{W}_{ouT}}{W_o}$$

$$+ \frac{T_{HSC}}{T_{HB}} e^{-sT_B} \frac{\hat{L}_{sc}}{L_{sc,o}} - \phi_3 \left[\frac{\gamma_4}{2} - \beta_1\right] e^{-sT_B} \frac{\hat{P}_P}{P_{P,o}} \tag{96}$$

124

Combining Equations (95) and (96) the result is

$$\frac{\hat{L}_{sc}}{L_{sc,o}} = \boxed{A}\ \frac{\hat{W}_{IN}}{W_o} + \boxed{B}\ \frac{\hat{P}_P}{P_{P,o}} + \boxed{C}\ \frac{\hat{W}_{OUT}}{W_o} \qquad (97)$$

where

$$\boxed{A} = \left[\frac{\gamma_1 / s\,\tau_{sc}}{1 - \dfrac{\gamma_2\,\gamma_5 \left(\dfrac{\tau_{Hsc}}{\tau_{HB}}\right) e^{-s\tau_B}}{\left\{1 - \dfrac{\gamma_5\phi_3}{2} e^{-s\tau_B}\right\}}} \right] \qquad (98)$$

$$\boxed{B} = \left[\frac{\gamma_3 - \gamma_2\,\gamma_4 - \dfrac{\gamma_2\,\gamma_5\,\phi_3 \left(\dfrac{\gamma_4}{2} - \beta_1\right) e^{-s\tau_B}}{1 - \dfrac{\gamma_5\phi_3}{2} e^{-s\tau_B}}}{1 - \dfrac{\gamma_2\,\gamma_5 \left(\dfrac{\tau_{Hsc}}{\tau_{HB}}\right) e^{-s\tau_B}}{\left\{1 - \dfrac{\gamma_5\phi_3}{2} e^{-s\tau_B}\right\}}} \right] \qquad (99)$$

$$\boxed{C} = \left[\frac{\dfrac{\gamma_2\,\gamma_5\, e^{-s\frac{\tau_B}{2}}}{1 - \dfrac{\gamma_5\phi_3}{2} e^{-s\tau_B}}}{1 - \dfrac{\gamma_2\,\gamma_5 \left(\dfrac{\tau_{Hsc}}{\tau_{HB}}\right) e^{-s\tau_B}}{\left\{1 - \dfrac{\gamma_5\phi_3}{2} e^{-s\tau_B}\right\}}} \right] \qquad (100)$$

125

## Energy Equation in the Superheated Region

The energy equation for the superheated region is written to account for the perturbations in the boiling-fluid outlet temperature resulting from perturbations in the boiling-fluid outlet flow rate and pressure as well as perturbations in the boiling length L_B. The equation is based on the solution of the partial differential energy equation of the boiling fluid, subject to the following assumptions:

1) No change in heating-fluid temperature takes place due to heat transfer in the superheat region. Consequently, the temperature is constant at the value of the heating-fluid inlet temperature.

2) Negligible heat storage occurs in all metal volumes.

3) The overall heat transfer coefficient between heating fluid and boiling fluid varies (for small perturbations around a point), with boiling fluid velocity to the n_{SH} power.

4) The density of the superheated vapor is considered constant at its value at the boiler exit.

5) The steady-state value of the boiling-fluid temperature entering the superheated region is equal to the saturation temperature determined by the steady-state value of the outlet pressure $P_{out,o}$.

Energy Equation of the Boiling Fluid in the Superheated Region
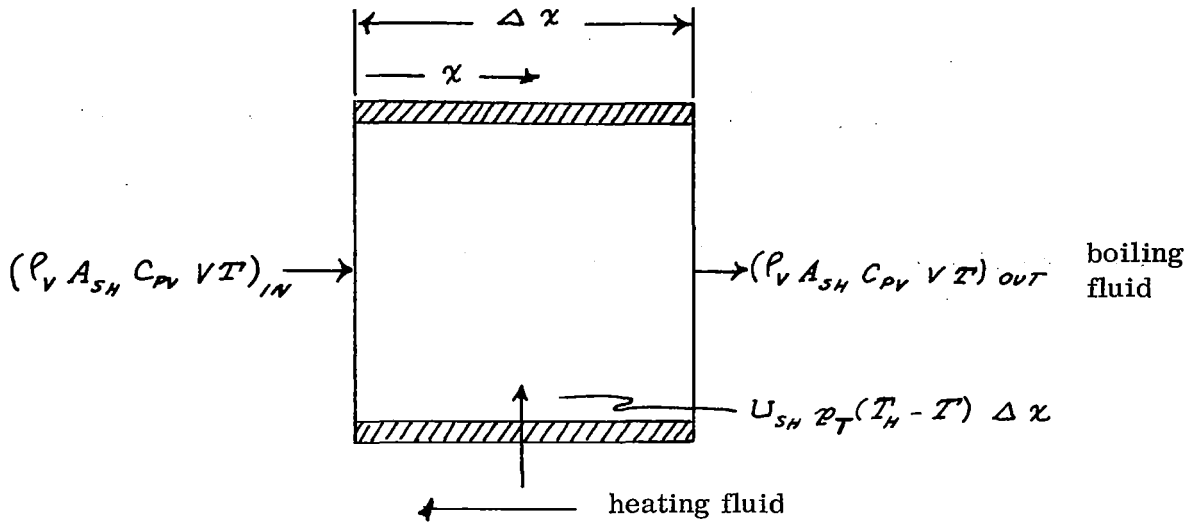
Taking an energy balance on a differential element of the boiling fluid the result is

$$\text{energy in } = \text{energy out } + \text{ energy stored}$$

$$(\rho_v \, A_{SH} \, C_{PV} \, V_v \, T)_{IN} + U_{SH} \, \mathcal{P}_T (T_{H\,IN} - T) \, \Delta x = (\rho_v A_{SH} \, C_{PV} \, V_v \, T)_{OUT}$$

$$+ \rho_v \, C_{PV} \, A_{SH} \, \Delta x \, \frac{\partial T}{\partial t}$$

$$\rho_v \, C_{PV} \, A_{SH} \, \Delta x \, \frac{\partial T}{\partial x} + \rho_v \, A_{SH} \, C_{PV} \, V_v \left[T + \frac{\partial T}{\partial x} \, \frac{\Delta x}{2} \right] = \rho_v \, A_{SH} \, C_{PV} V_v \left[T - \frac{\partial T}{\partial x} \, \frac{\Delta x}{2} \right]$$

$$+ \, U_{SH} \, \mathcal{P}_T \left[T_{H\,IN} - T \right] \Delta x$$

$$\frac{\partial T}{\partial t} + V_V \frac{\partial T}{\partial x} = \Theta_{SH} (T_{HIN} - T) \tag{101}$$

where

$$\Theta_{SH} = \frac{U_{SH} \, \mathscr{P}_T}{\rho_V \, C_{PV} \, A_{SH}} \qquad (\text{U}_{SH} \text{ is a variable}) \tag{102}$$

Linearizing for small perturbations around a steady point and transforming the perturbed variables, the result is

$$s \hat{T} + V_{V,o} \frac{\partial \hat{T}}{\partial x} + \hat{V}_V \frac{\partial T_o}{\partial x} = \hat{\Theta}_{SH} (T_{HIN} - T_o) - \Theta_{SH,o} \hat{T} \tag{103}$$

Steady-State Equation

$$V_{V,o} \frac{\partial T_o}{\partial x} = \Theta_{SH,o} (T_{HIN} - T_o)$$

Steady-State Solution

$$T_o = T_{HIN} - (T_{HIN} - T_{SAT,o \atop OUT}) \, e^{- \frac{\Theta_{SH,o}}{V_{V,o}} x} \tag{104}$$

$$\frac{\partial T_o}{\partial x} = \frac{\Theta_{SH,o}}{V_{V,o}} (T_{HIN} - T_{SAT,o \atop OUT}) \, e^{- \frac{\Theta_{SH,o}}{V_{V,o}} x} \tag{105}$$

On the basis of the third basic assumption

$$\Theta_{SH} = C V_V^{n_{SH}}$$

or

$$\hat{\Theta}_{SH} = \frac{\Theta_{SH,o}}{V_{V,o}} n_{SH} \hat{V}_V \qquad (106)$$

Combining Equations (103) and (106) and rearranging the result is

$$\frac{\partial \hat{T}}{\partial x} + \frac{(s + \Theta_{SH,o})}{V_{V,o}} \hat{T} = -(1 - n_{SH}) \frac{\Theta_{SH,o}}{V_{V,o}^2} (T_{HIN} - T_{SAT,o}^{OUT}) e^{-\frac{\Theta_{SH,o}}{V_{V,o}} x} (\hat{V}_V) \qquad (107)$$

The general solution to Equation (107) is

$$\hat{T} = e^{-\left(\frac{s + \Theta_{SH,o}}{V_{V,o}}\right) x} \left[\int - (1 - n_{SH}) \frac{\Theta_{SH,o}}{V_{V,o}^2} (T_{HIN} - T_{SAT,o}^{OUT}) e^{\frac{s}{V_{V,o}} x} \hat{V}_V \, dx + c\right]$$

which upon integration becomes

$$\hat{T} = e^{-\left(\frac{s + \Theta_{SH,o}}{V_{V,o}}\right) x} \left[- (1 - n_{SH}) \frac{\Theta_{SH,o}}{s V_{V,o}} (T_{HIN} - T_{SAT,o}^{OUT}) e^{\frac{s}{V_{V,o}} x} \hat{V}_V + c\right] \qquad (108)$$

Applying the boundary condition which accounts for perturbations of saturation temperature and the boiling length

$$\hat{T} = \left(\frac{\partial T_{SAT}}{\partial P}\right) \hat{P}_{OUT} - \left(\frac{\partial T_o}{\partial x}\right)_{x=o} \hat{L} \qquad (109)$$

at $x = 0$

129

and introducing Equation (105), Equation (108) becomes

$$\hat{T} = -(1-\eta_{SH})\,\Theta_{SH,o}\,(T_{HIN}-T_{\substack{SAT,o\\OUT}})\,e^{-\frac{\Theta_{SH,o}}{V_{V,o}}x}\,\frac{\left(1-e^{-\frac{S}{V_{V,o}}x}\right)}{S}\,\frac{\hat{V}_V}{V_{V,o}} +$$

$$\left(\frac{\partial T_{SAT}}{\partial P}\right)e^{-\left(\frac{S+\Theta_{SH,o}}{V_{V,o}}\right)x}\hat{P}_{OUT} - \frac{\Theta_{SHO}}{V_{V,o}}(T_{HIN}-T_{\substack{SAT,o\\OUT}})\,e^{-\left(\frac{S+\Theta_{SHO}}{V_{V,o}}\right)x}\hat{L}_{\beta} \tag{110}$$

$$\text{let} \qquad T_{SH} \equiv \frac{(L_{SH,o}-L_{\beta,o})}{V_{V,o}} \tag{111}$$

From continuity considerations

$$\frac{\hat{V}_V}{V_{V,o}} = \frac{\hat{W}_{OUT}}{W_o} \tag{112}$$

At the boiler exit x = (L$_{SH,0}$ – L$_{B,0}$). Introducing Equations (111) and (112) and evaluating Equation (110) at the boiler exit the result is

$$\hat{T}_{OUT} = -(1-\eta_{SH})(\Theta_{SH,o}\,T_{SH})(T_{HIN}-T_{\substack{SAT,o\\OUT}})\,e^{-\Theta_{SH,o}\,T_{SH}}\,\frac{(1-e^{-S\,T_{SH}})}{S\,T_{SH}}\,\frac{\hat{W}_{OUT}}{W_o}$$

$$+ \left(\frac{\partial T_{SAT}}{\partial P}\right)e^{-(S+\Theta_{SH,o})\,T_{SH}}\hat{P}_{OUT} -\Theta_{SH,o}\,T_{SH}\,(T_{HIN}-T_{\substack{SAT,o\\OUT}})\,e^{-(S+\Theta_{SHO})\,T_{SH}}\,\frac{\hat{L}_{\beta}}{L_{SH,o}-L_{B,o}} \tag{113}$$

130

Evaluating Equation (104) at x = ($L_{SH,0} - L_{B,0}$) the result is

$$e^{-\theta_{SH,0} \, T_{SH}} = \frac{\Delta T_{OUT}}{T_{HIN} - T_{SAT,0 \atop OUT}} \equiv \phi_4 \qquad (114)$$

where

$$\Delta T_{OUT} = T_{HIN} - T_{OUT,0} \qquad (115)$$

defining

$$\beta_2 \equiv \frac{\partial \left(\dfrac{T_{SAT}}{\Delta T_{OUT}} \right)}{\partial \left(\dfrac{P}{P_{OUT,0}} \right)} \qquad (116)$$

$$\phi_5 \equiv \frac{\Delta T_{OUT}}{2 T_{OUT,0}} \qquad (117)$$

Combining Equations (113), (114), (116) and (117)

$$\frac{\hat{T}_{OUT}}{2 T_{OUT,0}} = (1-\eta_{SH}) \, \phi_5 \, \ell n \, \phi_4 \left(\frac{1-e^{-s T_{SH}}}{s T_{SH}} \right) \frac{\hat{W}_{OUT}}{W_0} +$$

$$\beta_2 \, \phi_4 \, \phi_5 \, e^{-s T_{SH}} \, \frac{\hat{P}_{OUT}}{P_{OUT,0}} + \phi_5 \, \ell n \, \phi_4 \, e^{-s T_{SH}} \, \frac{\hat{L}_B}{L_{SH,0} - L_{B,0}} \qquad (118)$$

Combining Equations (82) and (94) the result is

$$\left[1 - \frac{\gamma_5 \, \phi_3}{2} \, e^{-s\tilde{\tau}_B} \right] \frac{\hat{L}_B}{(L_{B,o} - L_{sc,o})} = \frac{\hat{W}_{OUT}}{W_o} \, e^{-\frac{s\tau_B}{2}} + \left(\frac{\tau_{HSC}}{\tau_{HB}} \right) e^{-s\tilde{\tau}_B} \frac{\hat{L}_{sc}}{L_{sc,o}}$$

$$+ \phi_3 \left[\beta_1 - \frac{\gamma_4}{2} \right] e^{-s\tilde{\tau}_B} \frac{\hat{P}_P}{P_{P,o}} \qquad (119)$$

Combining Equations (118) and (119) and noting that

$$\left[\frac{L_{B,o} - L_{sc,o}}{L_{sH,o} - L_{B,o}} \right] = \frac{\tau_{HB}}{\tau_{HSH}}$$

the result is

$$\frac{\hat{T}_{OUT}}{2 \, T_{OUT,o}} = \textcircled{D} \, \frac{\hat{P}_P}{P_{P,o}} + \textcircled{E} \, \frac{\hat{W}_{OUT}}{W_o} + \textcircled{F} \, \frac{\hat{P}_{OUT}}{P_{OUT,o}} + \textcircled{G} \, \frac{\hat{L}_{sc}}{L_{sc,o}}$$

$$(120)$$

where

$$\textcircled{D} = \frac{\phi_3 \, \phi_5 \, \ln \, \phi_4 \left(\frac{\tau_{HB}}{\tau_{HSH}} \right) \left[\beta_1 - \frac{\gamma_4}{2} \right] e^{-s(\tilde{\tau}_{SH} + \tilde{\tau}_B)}}{\left[1 - \frac{\gamma_5 \, \phi_3}{2} \, e^{-s\tilde{\tau}_B} \right]} \qquad (121)$$

132

$$\textcircled{E} = \phi_5 \ \ln \ \phi_4 \left[(1-m_{SH}) \left(\frac{1-e^{-s\tau_{SH}}}{s\tau_{SH}} \right) + \frac{\left(\frac{\tau_{HB}}{\tau_{HSH}} \right) e^{-s \left(\tau_{SH} + \frac{\tau_B}{2} \right)}}{\left(1 - \frac{\gamma_5 \ \phi_3}{2} \ e^{-s\tau_B} \right)} \right] \tag{122}$$

$$\textcircled{F} = \beta_2 \ \phi_4 \ \phi_5 \ e^{-s\tilde{\tau}_{SH}} \tag{123}$$

$$\textcircled{G} = \frac{\phi_5 \ \ln \ \phi_4 \left(\frac{\tau_{HSC}}{\tau_{HSH}} \right) e^{-s(\tilde{\tau}_{SH} + \tilde{\tau}_B)}}{\left[1 - \frac{\gamma_5 \ \phi_3}{2} \ e^{-s\tilde{\tau}_B} \right]} \tag{124}$$

133

Transfer Function Between Boiling-Fluid Exit Pressure and Boiling-Fluid Inlet Flow Rate

Equations (33), (35), (37) and (97) are now combined to obtain a normalized transfer function between boiler exit pressure and boiler-inlet flow rate in terms including the transfer function between boiler exit temperature and boiler-inlet flow rate. Consequently, this latter transfer function may be eliminated when it is not significant or it may be evaluated from experimental data or an analytical expression derived below when it is significant.

Combining Equations (33), (37) and (97)

$$\left[1 - \textcircled{B} \beta_3\right] \frac{\hat{L}_{sc}}{L_{sc,o}} = \textcircled{A} \frac{\hat{W}_{IN}}{W_o} + \left[\textcircled{B} + \textcircled{C}\right] \frac{\hat{P}_{OUT}}{P_{OUT,o}} - \textcircled{C} \frac{\hat{T}_{OUT}}{2 T_{OUT,o}} \tag{125}$$

where

$$\beta_3 = \left[\frac{\partial\left(\Delta P_B/P_{P,o}\right)}{\partial\left(L_{sc}/L_{sc,o}\right)}\right] \tag{126}$$

Combining Equations (33) and (35) the result is

$$\frac{\hat{L}_{sc}}{L_{sc,o}} = \frac{\dfrac{\hat{W}_{IN}}{W_o} - (1 - \mathcal{T}_V S) \dfrac{\hat{P}_{OUT}}{P_{OUT,o}} + \dfrac{\hat{T}_{OUT}}{2 T_{OUT,o}}}{K \mathcal{T}_{sc} S} \tag{127}$$

Combining Equations (125) and (127) the result is

$$\frac{\hat{P}_{OUT}/P_{OUT,o}}{\hat{W}_{IN}/W_o} = \frac{\left[1 - \beta_3 \textcircled{B}\right]\left[1 + \dfrac{\hat{T}_{OUT}/2 T_{OUT,o}}{\hat{W}_{IN}/W_o}\right] - S K \mathcal{T}_{sc}\left[\textcircled{A} - \textcircled{C} \dfrac{\hat{T}_{OUT}/2 T_{OUT,o}}{\hat{W}_{IN}/W_o}\right]}{\left[1 + \mathcal{T}_V S\right]\left[1 - \beta_3 \textcircled{B}\right] + S K \mathcal{T}_{sc}\left[\textcircled{B} + \textcircled{C}\right]} \tag{128}$$

134

Normalizing at zero frequency (i.e., at S = 0)

$$\left(\frac{\hat{P}_{out}}{\hat{W}_{IN}}\right)_{NORMALIZED} = \frac{\left(\frac{\hat{P}_{OUT}}{\hat{W}_{IN}}\right)(s)}{\left(\frac{\hat{P}_{OUT}}{W_{IN}}\right)_{(s=0)}} = \frac{\left(\hat{P}_{out}/\hat{W}_{IN}\right)}{\frac{P_{OUT,o}}{W_o}\left[1 + \left(\frac{\hat{T}_{OUT}/2T_{OUT,o}}{\hat{W}_{IN}/W_o}\right)_{s=0}\right]} \qquad (129)$$

Combining Equations (128) and (129) the result is

$$\left(\frac{\hat{P}_{out}}{\hat{W}_{IN}}\right)_{NORMALIZED} = \frac{\left[1 - \beta_3 \circled{B}\right]\left[1 + \frac{\hat{T}_{OUT}/2T_{OUT,o}}{\hat{W}_{IN}/W_o}\right] - SK\,\tau_{sc}\left[\circled{A} - \circled{C}\,\frac{\hat{T}_{OUT}/2T_{OUT,o}}{\hat{W}_{IN}/W_o}\right]}{\left[1 + \left(\frac{\hat{T}_{OUT}/2T_{OUT,o}}{\hat{W}_{IN}/W_o}\right)_{s=0}\right]\left[\left(1 + \tau_v s\right)\left(1 - \beta_3 \circled{B} + SK\,\tau_{sc}\left(\circled{B} + \circled{C}\right)\right)\right]}$$

$$(130)$$

Transfer Function Between Boiling-Fluid Outlet Temperature and Boiling-Fluid Inlet Flow Rate

In this section Equations (33), (35), (37), (120) and (128) are combined to obtain a theoretical expression for the transfer function between the boiling-fluid outlet temperature and the boiling-fluid inlet flow rate for use with Equation (130).

Combining Equations (37) and (120) the result is

$$\frac{\hat{T}_{OUT}}{2\,T_{OUT,o}} = \gamma_{11}\,\frac{\hat{W}_{OUT}}{W_o} + \gamma_{12}\,\frac{\hat{P}_{OUT}}{P_{OUT,o}} + \gamma_{13}\,\frac{\hat{L}_{SC}}{L_{SC,o}} \tag{131}$$

where

$$\gamma_{11} \equiv \boxed{E} \tag{132}$$

$$\gamma_{12} \equiv \left[\boxed{D} + \boxed{F} \right] \tag{133}$$

$$\gamma_{13} \equiv \left[\beta_3 \boxed{D} + \boxed{G} \right] \tag{134}$$

Combining Equations (131) and (35) the result is

$$\frac{\hat{T}_{OUT}}{2\,T_{OUT,\,o}} = \left[\gamma_{12} - \frac{\tau_V\,S}{K\,\tau_{SC}\,S}\,\gamma_{13} \right] \frac{\hat{P}_{OUT}}{P_{OUT,o}} + \frac{\gamma_{13}}{K\,\tau_{SC}\,S}\,\frac{\hat{W}_{IN}}{W_o} +$$

$$\left[\gamma_{11} - \frac{\gamma_{13}}{K\,\tau_{SC}\,S} \right] \frac{\hat{W}_{OUT}}{W_o} \tag{135}$$

Combining Equations (135) and (33) the result is

136

$$\frac{\hat{T}_{OUT}}{2 T_{OUT,o}} = \gamma_{21} \frac{\hat{P}_{OUT}}{P_{OUT,o}} - \gamma_{22} \frac{\hat{W}_{IN}}{W_{OUT}} \tag{136}$$

where

$$\gamma_{21} \equiv \frac{\gamma_{13}(1 + T_v S) - SK T_{sc}(\gamma_{11} + \gamma_{12})}{\gamma_{13} - SK T_{sc}(1 + \gamma_{11})} \tag{137}$$

$$\gamma_{22} \equiv \frac{\gamma_{13}}{\gamma_{13} - SK T_{sc}(1 + \gamma_{11})} \tag{138}$$

Combining Equations (128) and (136) the result is

$$\frac{(\hat{T}_{OUT}/2 T_{OUT,o})}{(\hat{W}_{IN}/W_o)} = \frac{-\gamma_{22} + \dfrac{\gamma_{21}\left[\left(1 - \beta_3 \circled{B}\right) - SK T_{sc} \circled{A}\right]}{\left[\left(1 + T_v S\right)\left(1 - \beta_3 \circled{B}\right) + SK T_{sc}\left(\circled{B} + \circled{C}\right)\right]}}{1 - \dfrac{\gamma_{21}\left[\left(1 - \beta_3 \circled{B}\right) + SK T_{sc}\circled{C}\right]}{\left[\left(1 + T_v S\right)\left(1 - \beta_3 \circled{B}\right) + SK T_{sc}\left(\circled{B} + \circled{C}\right)\right]}} \tag{139}$$

APPENDIX 3

Boiler Parameters

In order to calculate values for the theoretical transfer function derived in Appendix 2, it was necessary to evaluate the 22 parameters listed in Table 12. These parameters were calculated using the steady-state test data described in Section IV of this report. The method of calculating most of the parameters in Table 12 is obvious from their definition. However, the definitions of several of these parameters are not sufficiently explicit that the exact methods of calculating them from the experimental data are apparent without further explanation. This appendix contains two parts. The first part describes the methods of calculating those parameters which require further explanation while the second part presents curves of the parameters as a function of the primary variables.

Calculation of Boiler Parameters

In the derivation of the theoretical transfer function the boiler was divided into several sections which were analyzed separately. Inherent in this division is the assumption that a clearly-defined boundary existed between the boiling and superheat regions. Examination of the steady-state test data, described in Section IV of this report, indicated that there was no abrupt transition between saturated boiling conditions and superheating of the vapor. Instead, an intermediate condition existed in which superheating of the vapor and evaporation of the liquid took place simultaneously. The boiling fluid during this transition consisted of a mist containing superheated vapor and droplets of saturated liquid. Therefore it was not possible to discern a clearly-defined boundary between the region where only boiling took place and the region where the fluid was superheated as a dry vapor. For the purposes of calculating the boiler parameters, it was therefore necessary to define an artificial boundary.

The most obvious criterion for defining this boundary would have been to select the point at which the temperature of the boiling fluid departed from the saturation conditions. However, there were not sufficient temperature measurements within the boiler to establish this point with any accuracy. As a consequence, the following procedure was adopted.

Using the internal temperature measurements and local heat balances within the boiler, an estimate was made of the boiling-fluid quality distribution along the length of the boiler. The results were plotted as shown in Figure 49. A straight line was then drawn from the point of zero quality, the pinch point, to the point of 80 percent quality. This line was then extended to 100 percent quality. The point where the straight line reached 100 percent quality was taken
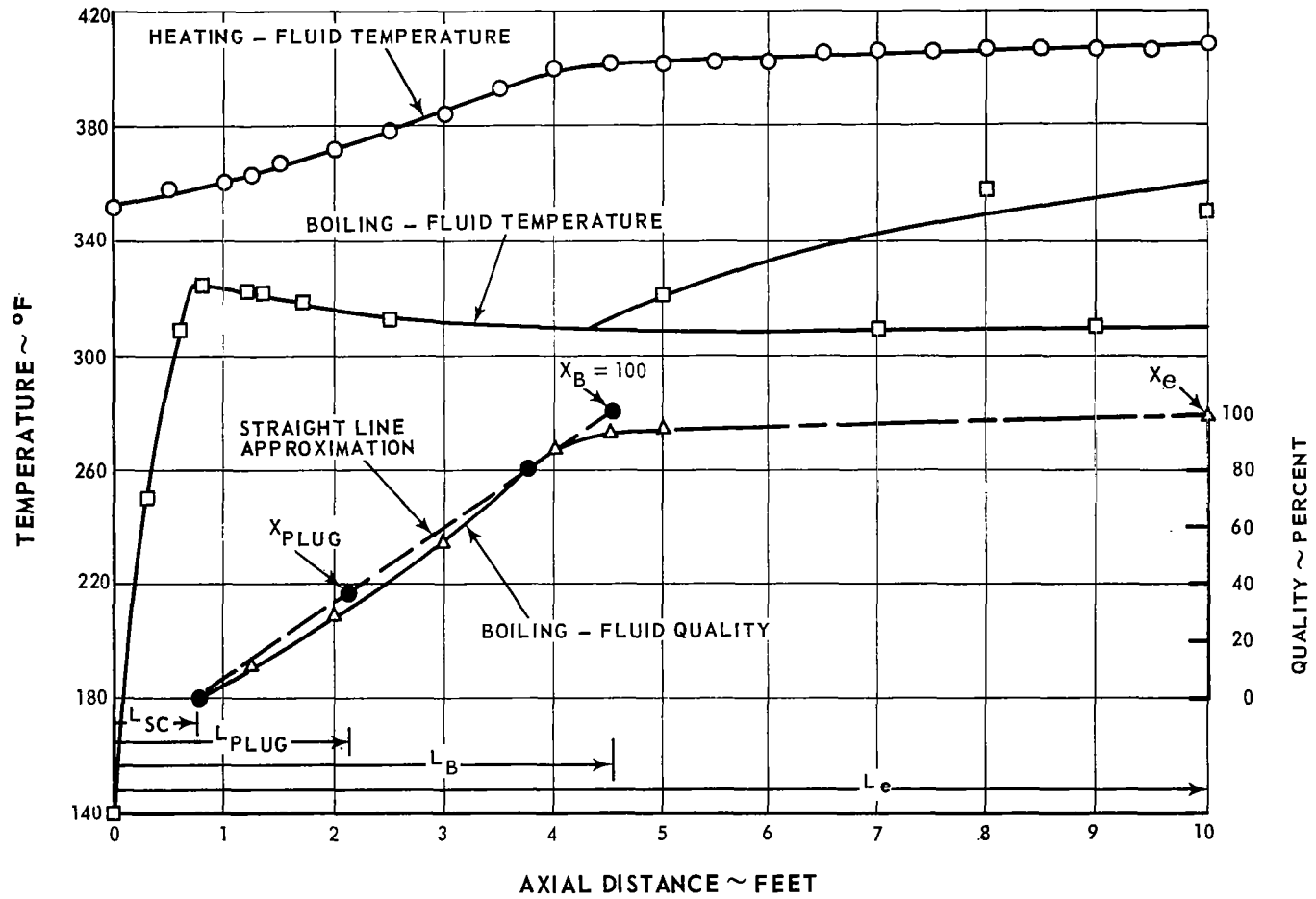
Figure 49 Straight Line Approximation of Boiling-Fluid Quality Distribution at Nominal Operating Conditions

as the boundary between the two regions as shown in Figure 49. The axial distance between the boiling fluid inlet and this point was defined as the boiling length L_B. For those cases where the straight line did not reach 100 percent quality before the end of the boiler, no appreciable superheating of the vapor was observed and L_B was taken as equal to the length of the boiler.

Calculation of K

The parameter K is defined by the relation

$$K = \frac{\partial \left(\int_0^{L_e} \rho \, A \, d\ell \right)}{\partial \left(\rho_L A_{SC} L_{SC} \right)} = \frac{\partial M_{total}}{\partial M_{SC}} \tag{140}$$

which relates the total mass of the boiling fluid in the boiler M_{total} to the mass of boiling fluid in the subcooled region M_{SC}.

In evaluating the total mass of the boiling fluid, it was assumed that the mass of the vapor in the boiler was negligible compared to the mass of the liquid. As a consequence, only the subcooled and boiling regions needed to be considered in the integral, and the density of the fluid in the boiling region could be approximated by the relation

$$\rho = R_L \rho_L \tag{141}$$

The term R_L in Equation (141) is the liquid fraction of the two-phase flow. Incorporating the above assumption in the integral to calculate M_{total} the result is

$$M_{total} = \int_0^{L_e} \rho \, A \, d\ell = \int_0^{L_{sc}} \rho_L A_{plug} \, d\ell + \int_{L_{sc}}^{L_{plug}} \rho_L R_L A_{plug} \, d\ell + \int_{L_{plug}}^{L_b} \rho_L R_L A_{probe} \, d\ell \tag{142}$$

The terms A_{plug} and A_{probe} refer to the cross-sectional areas of the flow passages on a plane perpendicular to the boiler axis.

In evaluating the second term on the right-hand side of Equation (142) it was assumed that boiling-fluid quality varied linearly with length according to the relation

$$X = \frac{X_B}{L_B - L_{SC}} \left(\ell - L_{SC} \right) \qquad (143)$$

Equation (143) describes the straight-line relationship used to define L_B. As can be seen in Figure 49 this relation gives a reasonable approximation to the quality variation.

Differentiating Equation (143) and rearranging the result is

$$d\ell = \left(\frac{L_B - L_{SC}}{X_B} \right) dX \qquad (144)$$

The liquid fraction R_L was determined using the following relationship which was fitted as an approximation of the liquid fraction data of Martinelli and Nelson, Reference 12.

$$R_L = e^{\alpha X^{1/3}} - e^{\alpha} \qquad (145)$$

The parameter α is a function of pressure and is tabulated below

P, psia	α
14.7	− 4.78
60.0	− 4.21
200.0	− 3.51

Equations (142), (144) and (145) were combined with the result

$$M_{total} = \int_0^{L_{SC}} \rho_L A_{plug} \, d\ell + \int_{X=0}^{X=X_{plug}} A_{plug}\rho_L \frac{\left(L_B - L_{SC}\right)}{X_B} \left[e^{\alpha X^{1/3}} - e^{\alpha}\right]dX$$

$$(146)$$

$$+ \int_{X=X_{plug}}^{X=X_B} A_{probe}\,\rho_L \frac{\left(L_B - L_{SC}\right)}{X_B} \left[e^{\alpha X^{1/3}} - e^{\alpha}\right]dX$$

The term X_{plug} in the limits of integration is the quality at the end of the plug as determined by the linear approximation (see Figure 49).

Equation (146) was integrated numerically using values of L_{SC}, L_B, X_{plug} and X_B determined from the steady-state test data. The results were plotted as a function of the mass of the boiling fluid in the subcooled region $M_{SC} = \rho_L A_{plug} L_{SC}$. A single line was drawn through the data as shown in Figure 50. The parameter K was then determined as a function of M_{SC} by taking slopes of the curve in Figure 50. The results are shown in Figure 51. K was then evaluated by determining M_{SC} for each steady-state test point and then reading the value from Figure 51.

Calculation of τ_B

τ_B is defined as the time required for a liquid particle to travel the length of the boiling region. It was calculated by means of the integral

$$\tau_b = \int_{L=L_{SC}}^{L=L_B} \frac{d\ell}{V_L}$$

$$(147)$$

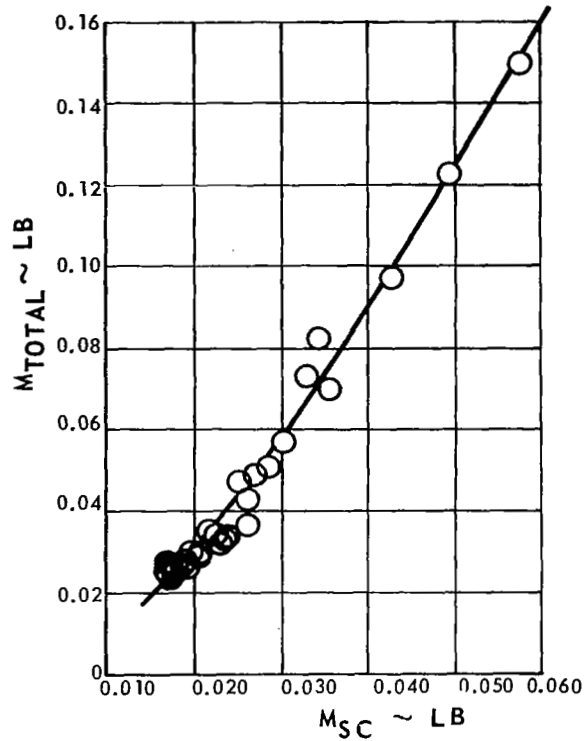where V_L is the axial component of the velocity of the liquid phase.

Figure 50   Total Mass of Boiling Fluid M_{total} vs Mass of Boiling Fluid in Sub-cooled Region M_{SC}
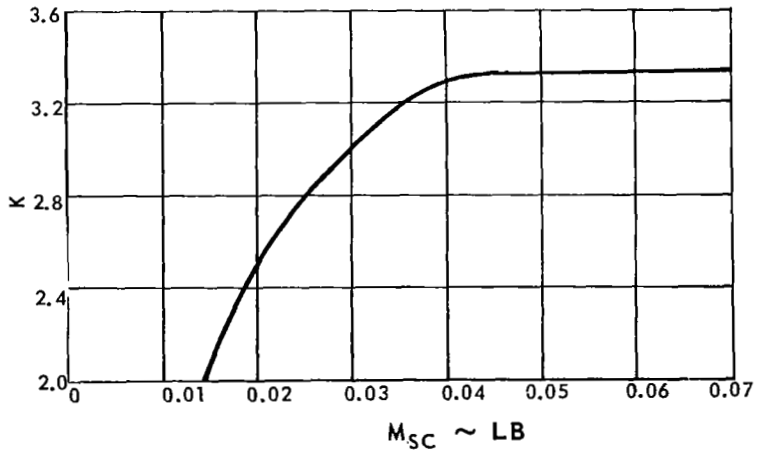

Figure 51   K vs Mass of Boiling Fluid in Subcooled Region M_{SC}

From continuity considerations

$$V_L = \frac{W_L}{\rho_L A_L} \qquad (148)$$

Introducing the boiling fluid quality $X = (W - W_L)/W$ and the liquid fraction R_L Equation (148) becomes

$$V_L = \frac{(1-X)W}{\rho_L R_L A} \qquad (149)$$

where $A = A_{plug}$; $\quad 0 \leq X \leq X_{plug}$

$\qquad A = A_{probe}$; $X_{plug} < X \leq X_B$

Combining Equations (144) for the quality distribution and Equation (145) for liquid fraction with Equations (147) and (149), the result is

$$\tau_b = \int_{X=0}^{X=X_{plug}} \frac{\rho_L A_{plug}}{W} \frac{(L_B - L_{SC})}{X_B} \left[\frac{e^{\alpha X^{1/3}} - e^{\alpha}}{1-X} \right] dX$$

$$+ \int_{X=X_{plug}}^{X=X_B} \frac{\rho_L A_{probe}}{W} \frac{(L_B - L_{SC})}{X_B} \left[\frac{e^{\alpha X^{1/3}} - e^{\alpha}}{1-X} \right] dX \qquad (150)$$

Equation (150) was integrated numerically using values of L_{SC}, L_B, X_{plug} and X_B obtained from the steady-state test data.

Calculation of β_3

The parameter β_3 is defined by the following equation which relates the change in boiling fluid pressure drop to the change in subcooled length that results when the boiling-fluid flow rate is perturbed

144

$$\beta_3 = \frac{\partial \left(\dfrac{\Delta P_B}{P_{P,o}} \right)}{\partial \left(\dfrac{L_{SC}}{L_{SC,o}} \right)} = \left(\frac{\partial \Delta P_B}{\partial L_{SC}} \right) \left(\frac{L_{SC,o}}{P_{P,o}} \right) \tag{151}$$

In calculating the derivative in Equation (151) ΔP_B was plotted as a function of L_{SC} for the steady-state test conditions where boiling-fluid flow rate was varied. A single curve was drawn through the data as shown in Figure 52. The derivative was then determined by taking the slope of this curve at various values of L_{SC}. The results are shown in Figure 53.

In calculating β_3 from Equation (151), it was assumed that the boiling fluid pressure at the pinch point $P_{P,o}$ was equal to the boiling-fluid inlet pressure obtained from the steady-state data. The subcooled length L_{SC} was also obtained from the steady-state data while the derivative was obtained as a function of L_{SC} from Figure 53.

Calculation of n_{SC} and n_{SH}

The exponent n_{SC} was defined by the equation

$$U_{SC} = c V_{SC}^{n_{SC}} \tag{152}$$

which relates the boiling-fluid velocity in the subcooled region V_{SC} to the overall heat-transfer coefficient of that region U_{SC}. From continuity considerations, V_{SC} is proportional to the boiling-fluid flow rate W, with the result that Equation (152) can be re-expressed in the form

$$U_{SC} = C_3 W^{n_{SC}} \tag{153}$$

Taking logarithms of both sides of Equation (153) and rearranging the result is
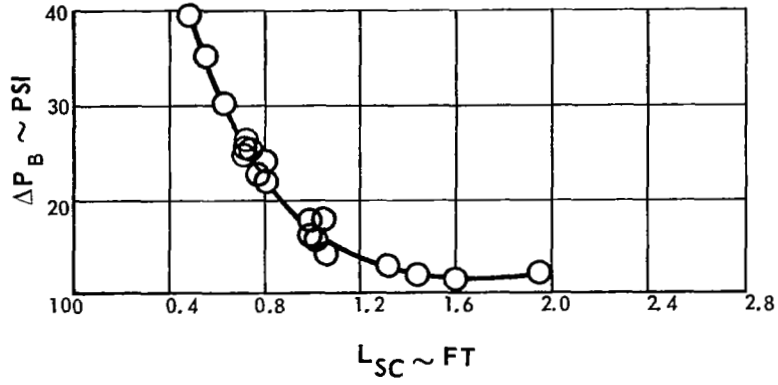
$$n_{SC} = \frac{\ln U_{SC} - \ln C_3}{\ln W} \tag{154}$$

145

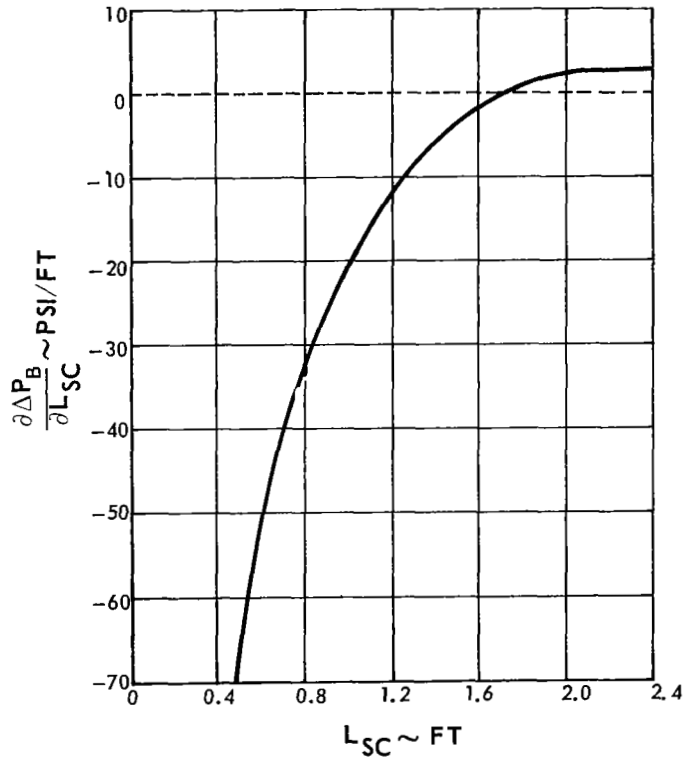Figure 52   Boiling-Fluid Pressure Drop ΔP_B vs Subcooled Length L_{SC}

Figure 53 $\dfrac{\partial \Delta P_B}{\partial L_{SC}}$ vs Subcooled Length L_{SC}

146

which in differential form becomes

$$n_{SC} = \frac{d \, (\ln U_{SC})}{d \, (\ln W)}$$ (155)

The overall heat-transfer coefficient was calculated using the equation

$$U_{SC} = \frac{1}{\dfrac{d_o}{h_{SC} \, d_i} + \dfrac{t_h d_o}{k \, d_m} + \dfrac{1}{h_{H \, SC}}}$$ (156)

where the heat-transfer coefficients of the two fluids were determined using the methods described in Appendix 1.

The heat-transfer coefficient of the boiling fluid h_{SC} was calculated as a function of W using Equations (19), (20) and (21) while the heat-transfer coefficient of the heating fluid h_{SC} was calculated using Equation (18). These values were then employed to calculate U_{SC} from Equation (156). The results were plotted on log-log graph paper as shown in Figure 54. The exponent n_{SC} was then determined on the basis of Equation (155) by taking the slopes of the curves of constant W_H plotted in Figure 54. The results are shown as a function of W and W_H in Figure 55.

The exponent n_{SH} was defined by the relation

$$U_{SH} = c V_{SH}^{n_{SH}}$$ (157)

which relates the boiling-fluid velocity in the superheat region to the overall heat-transfer coefficient of that region. The exponent was calculated using the same methods described above for determining n_{SC} except that the data of Reference 10 was employed in place of Equations (20) and (21). The results indicated that for the conditions under study, n_{SC} was independent of W and W_H and equal to a constant value of 0.751.
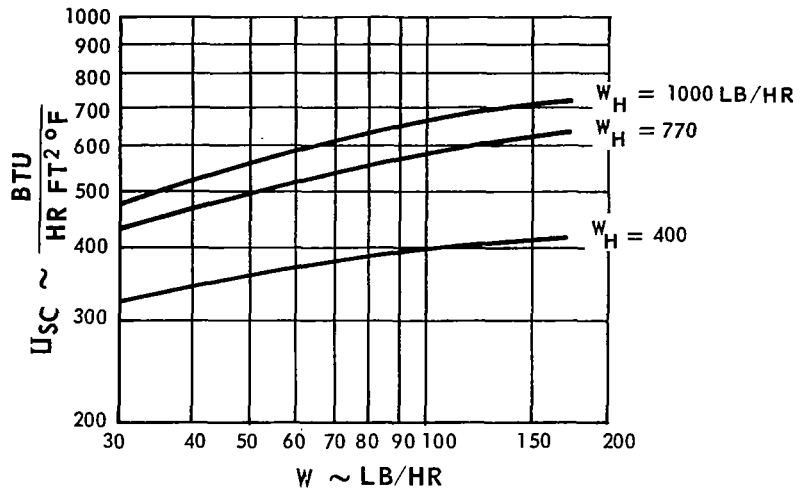
Figure 54 Variation of Overall Heat Transfer Coefficient U_{SC} with Boiling-Fluid Flow Rate and Heating-Fluid Flow Rate
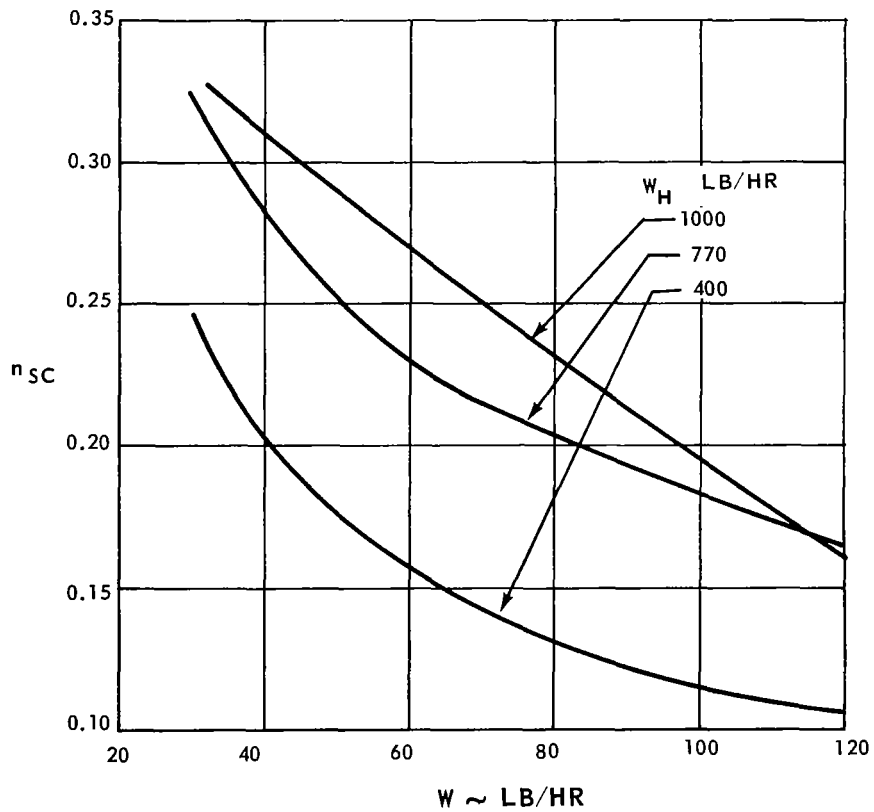

Figure 55 Variation of n_{SC} with Boiling-Fluid Flow Rate and Heating-Fluid Flow Rate

Curves of the Boiler Parameters

The following pages present curves of the boiler parameters as functions of the primary variables. These parameters were calculated on the basis of the steady-state test results described in Section IV of this report. These curves were employed in the calculation of the theoretical transfer function described in Section VII of the report.
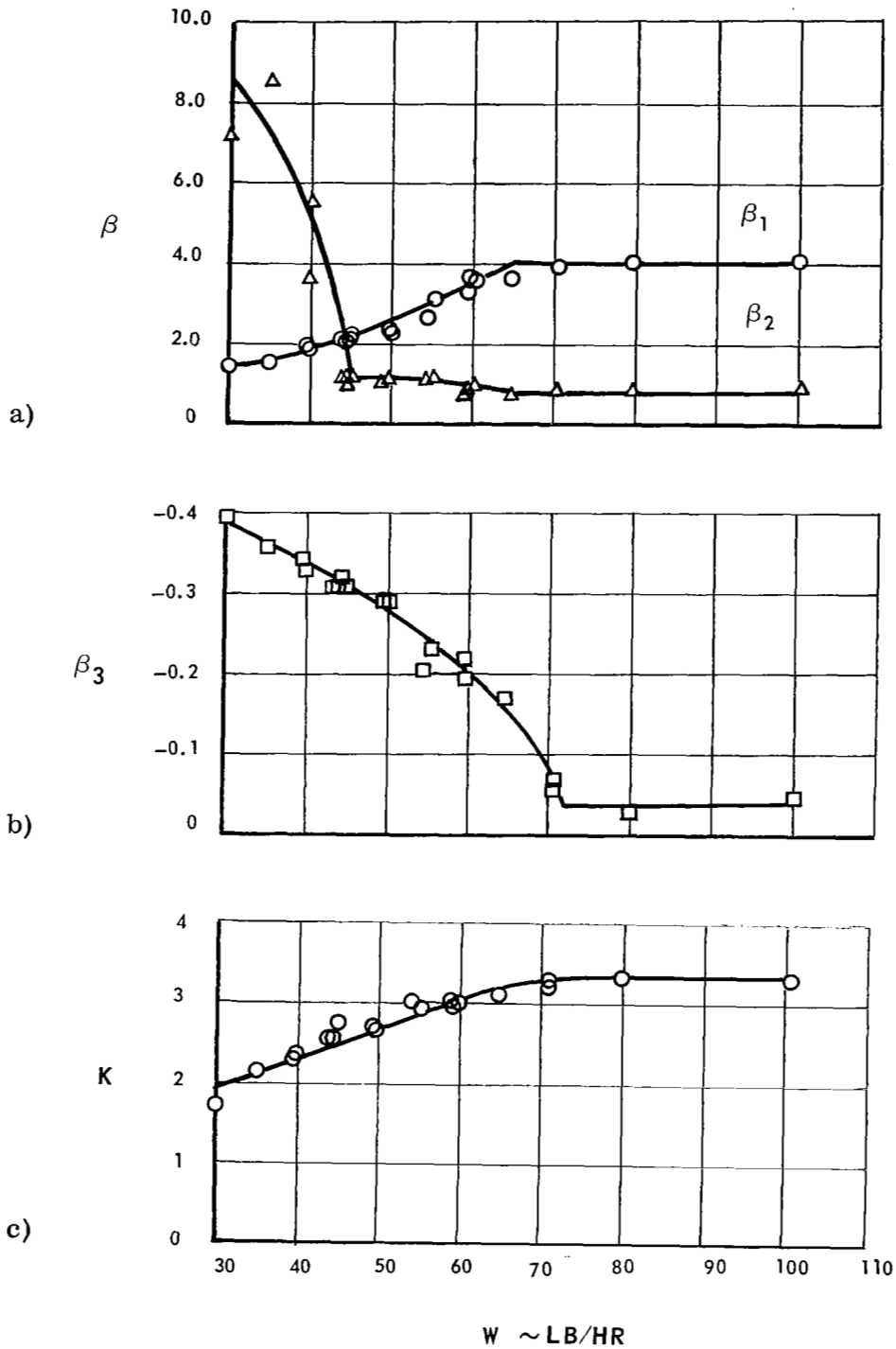
Figure 56 Variation of Boiler Parameters with Boiling-Fluid Flow Rate
$T_{in} = 140°F$ T.S. valve at $W_H = 770$ lb/hr $T_{H\ in} = 410°F$
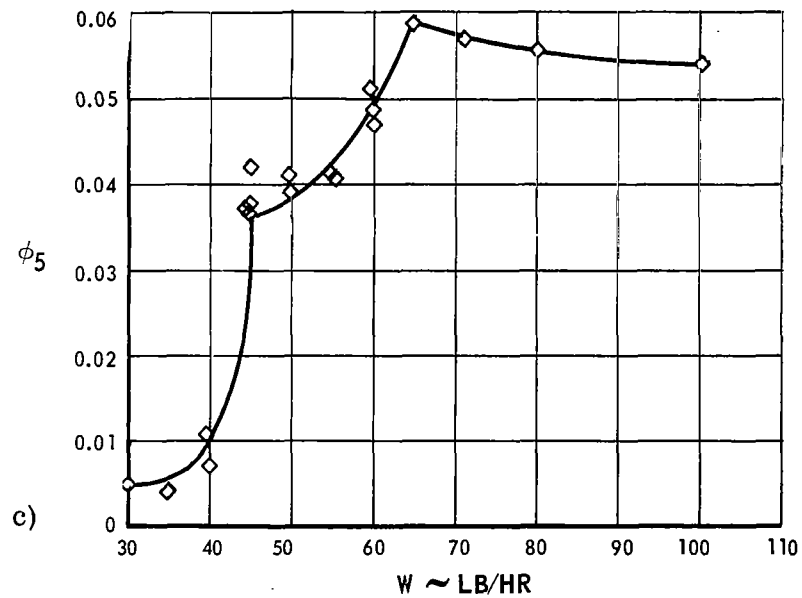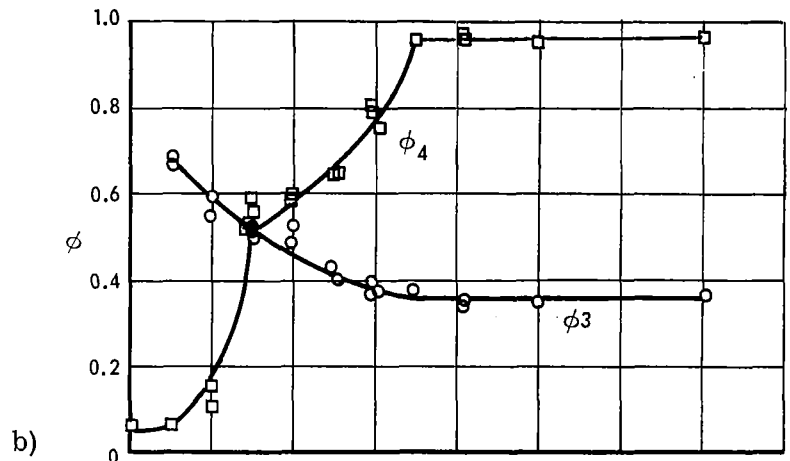nominal setting

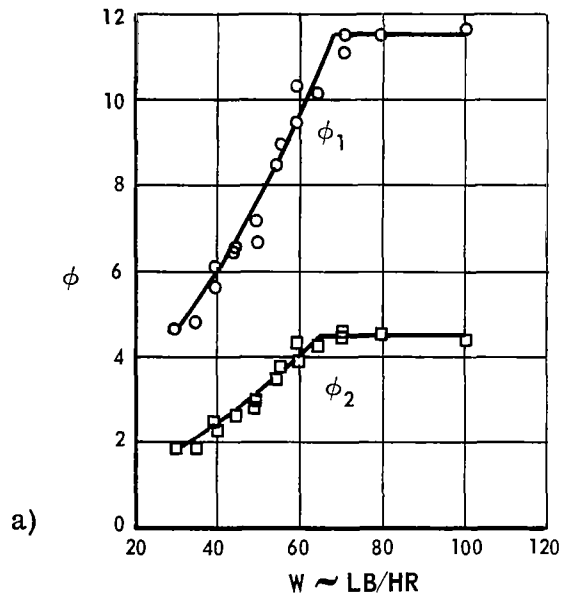Figure 57   Variation of Boiler Parameters with Boiling-Fluid Flow Rate
$T_{in} = 140°F$ T.S. valve at nominal setting $W_H = 770$ lb/hr $T_{H\ in} = 410°F$

Figure 58 Variation of Boiler Parameters with Boiling-Fluid Flow Rate
$T_{in} = 140°F$ T.S. valve at nominal setting $W_H = 770$ lb/hr $T_{H in} = 410°F$
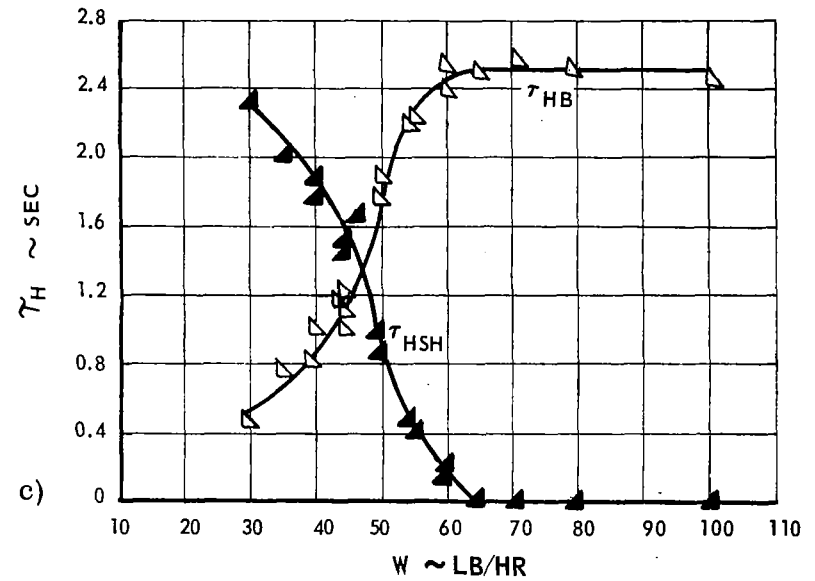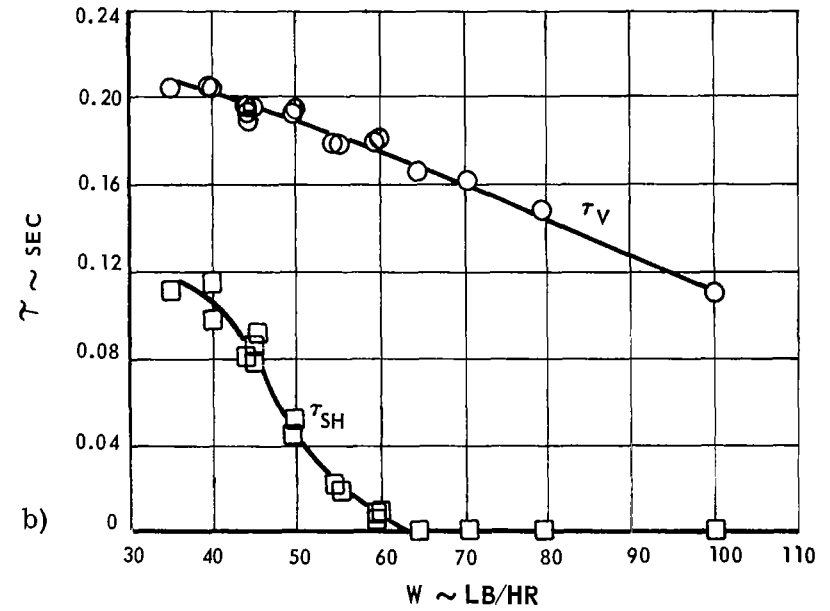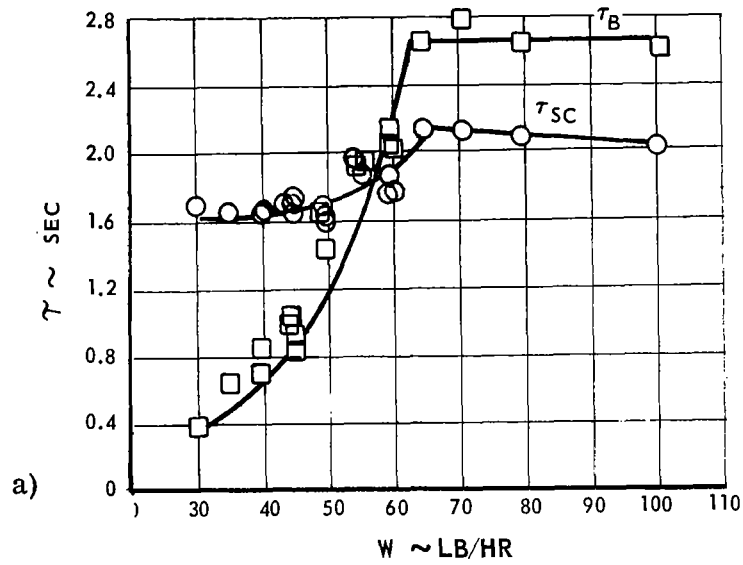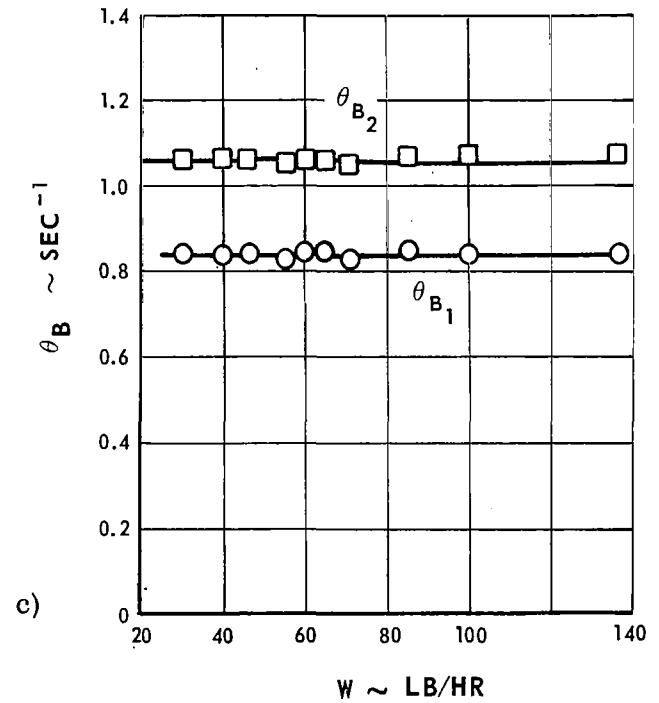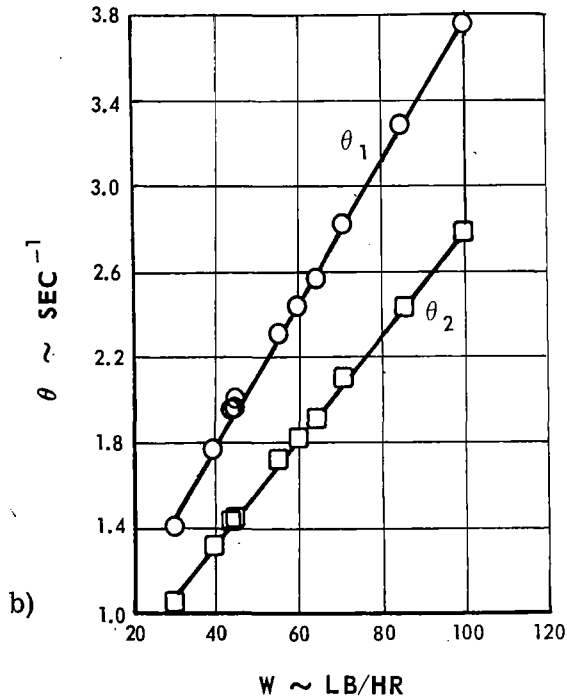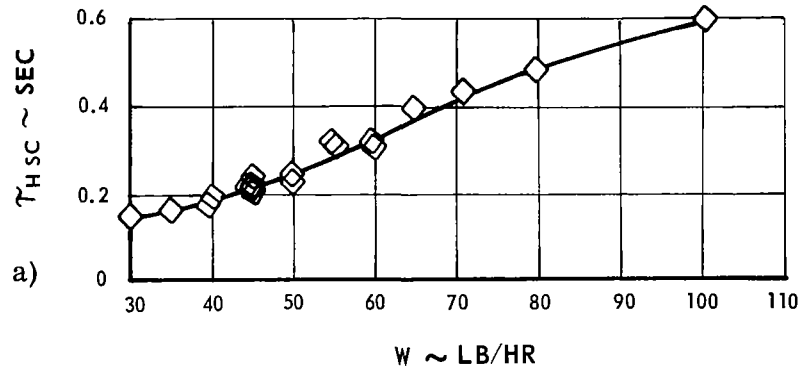
Figure 59 Variation of Boiler Parameters with Boiling-Fluid Flow Rate
$T_{in} = 140°F$ T.S. valve at nominal setting $W_H = 770$ lb/hr $T_{H\ in} = 410°F$
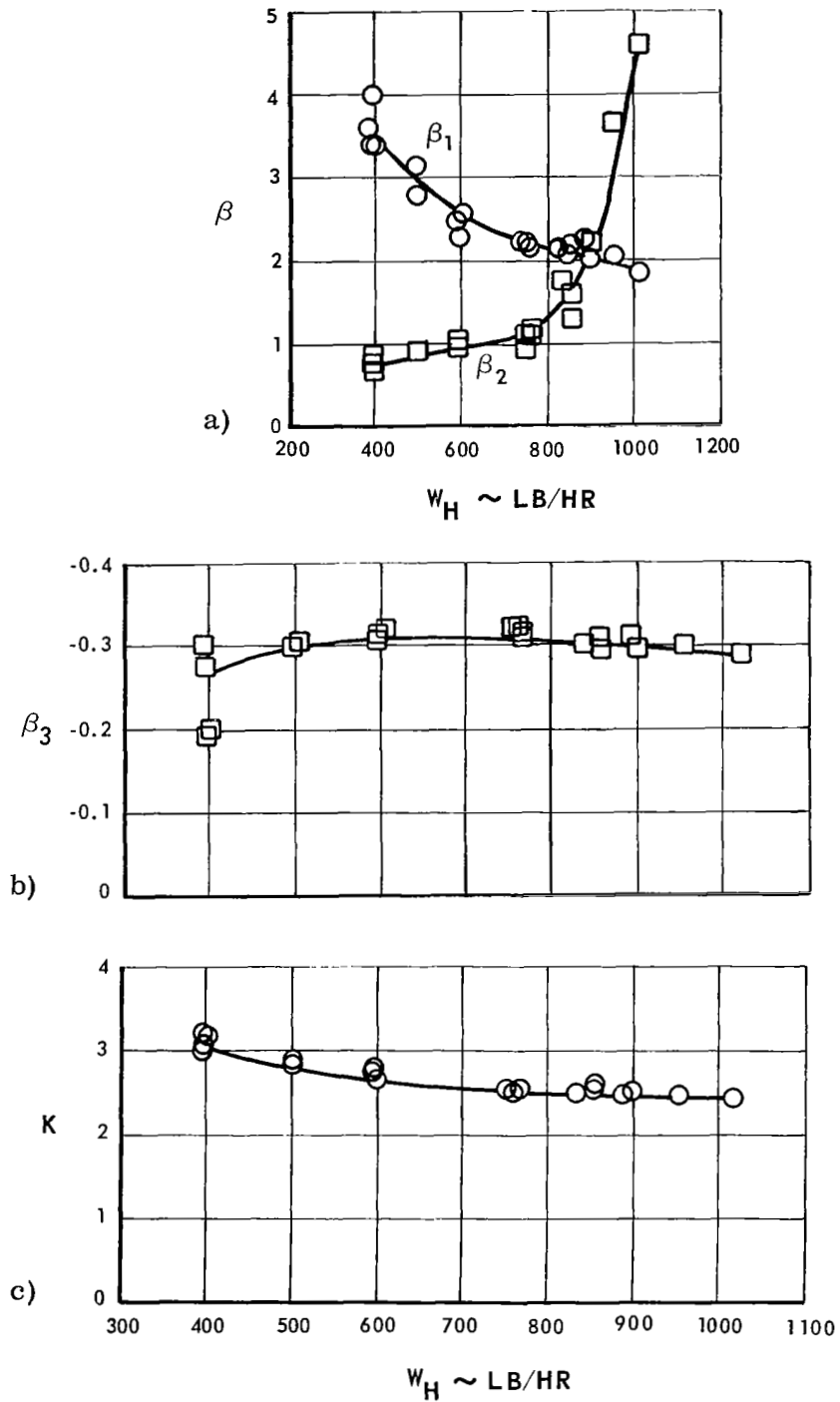
Figure 60 Variation of Boiler Parameters with Heating-Fluid Flow Rate
W = 45 lb/hr $T_{H\ in}$= 410°F T_{in} = 140°F T.S. valve at nominal setting
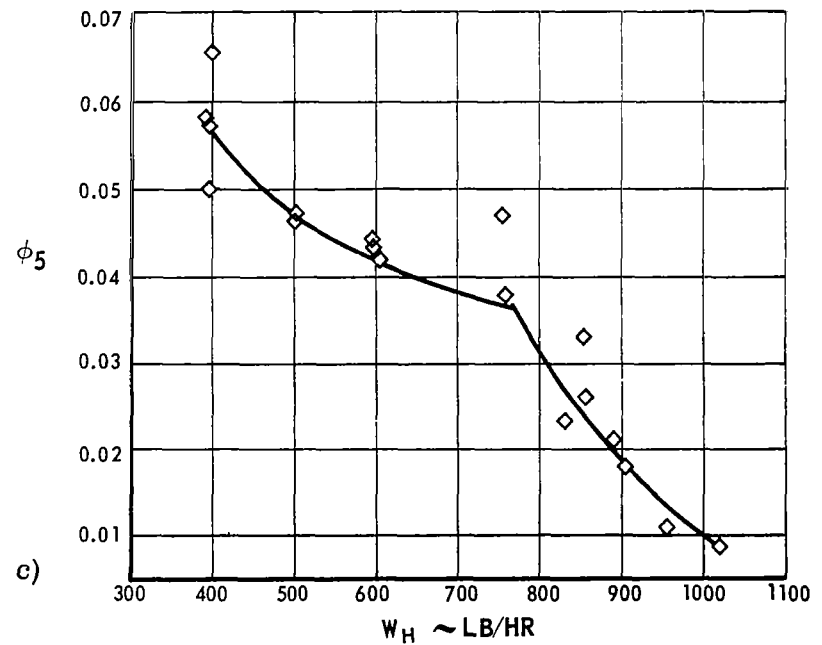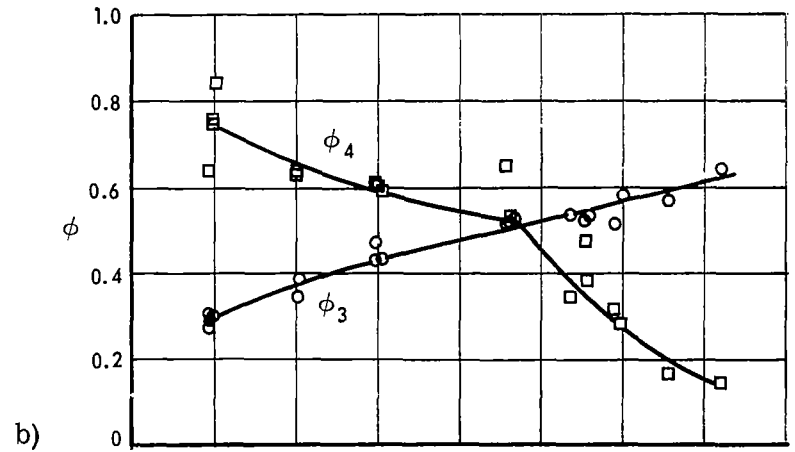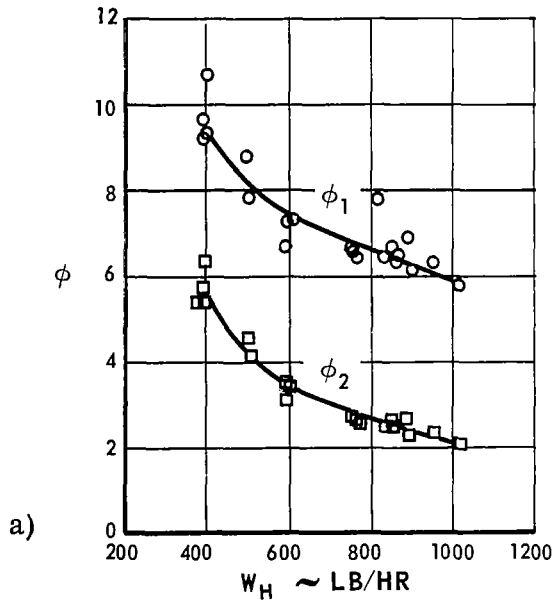
Figure 61 Variation of Boiler Parameters with Heating-Fluid Flow Rate

W = 45lb/hr $T_{H\ in}$= 410°F T_{in} = 140°F   T.S. valve at nominal setting
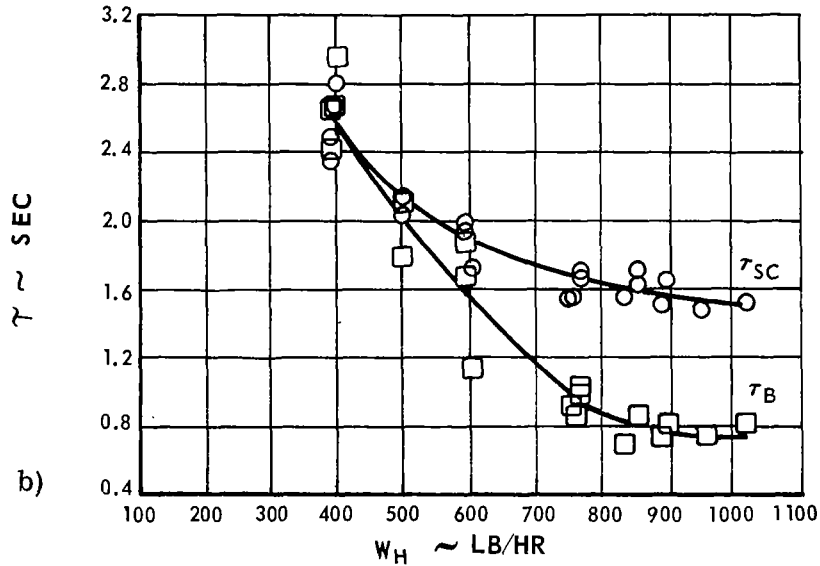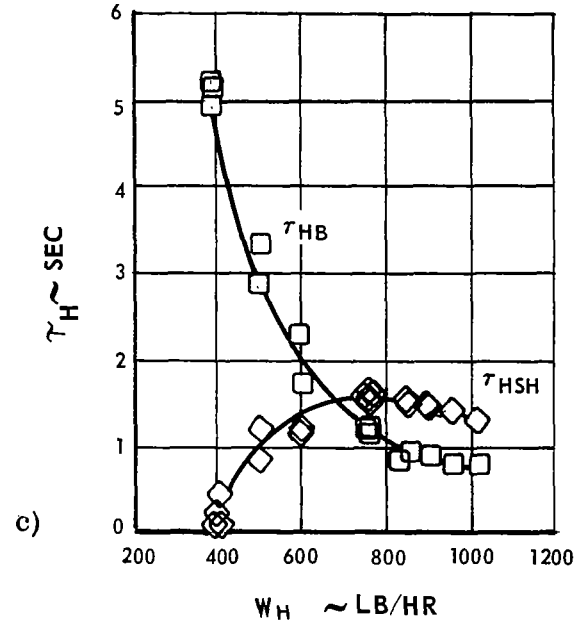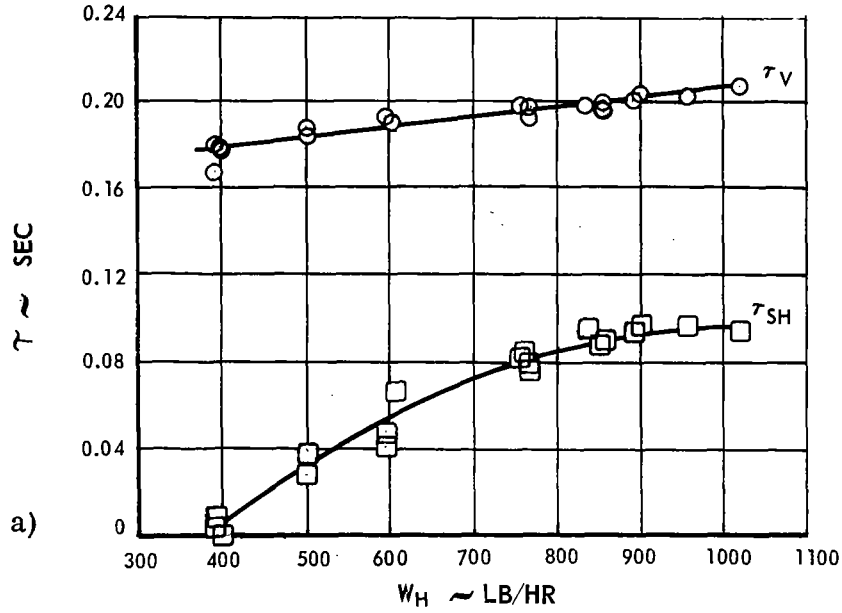
Figure 62   Variation of Boiler Parameters with Heating-Fluid Flow Rate

W = 45 lb/hr $T_{H\ in}$= 410°F T_{in} = 140°F   T.S. valve at nominal setting
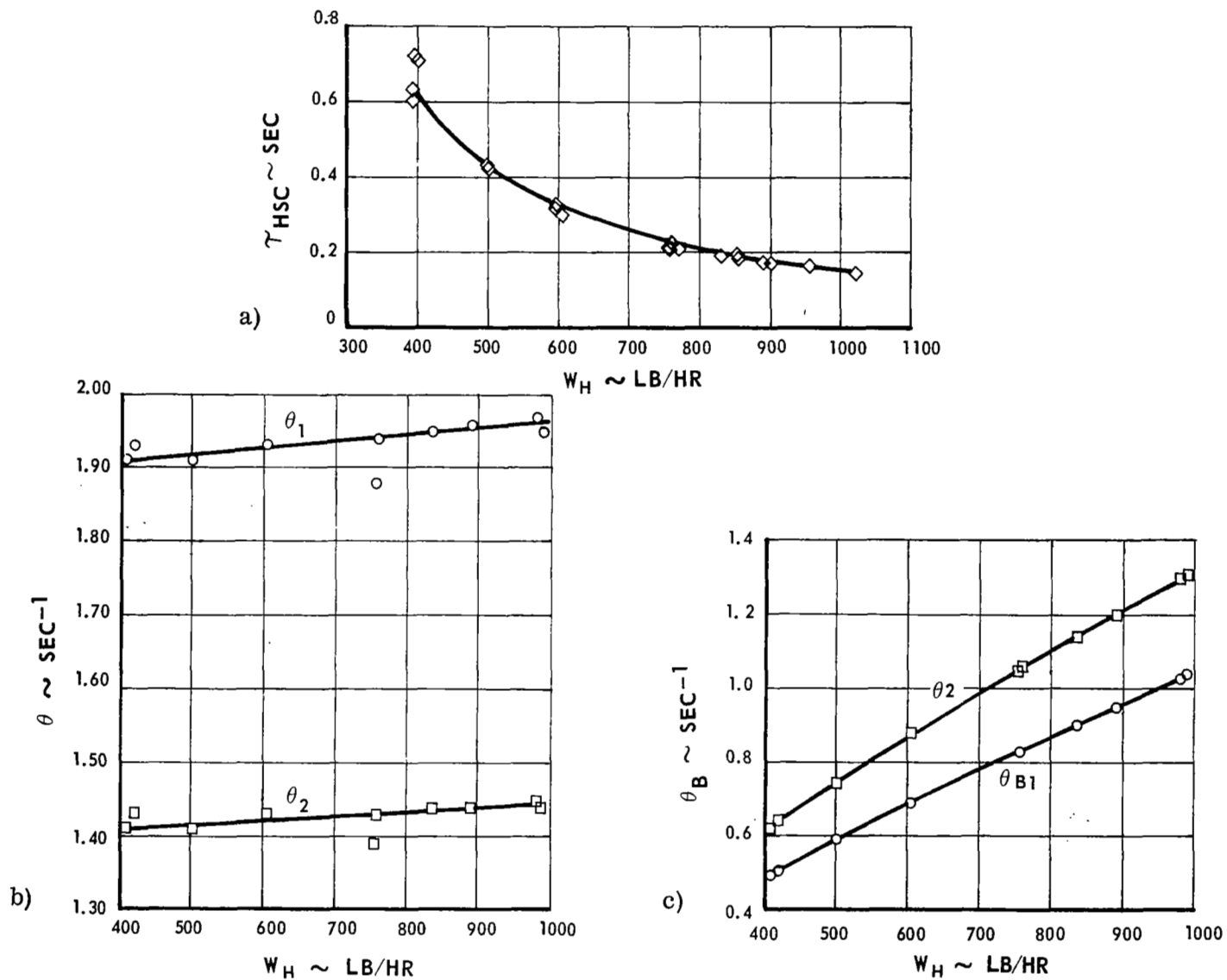
Figure 63 Variation of Boiler Parameters with Heating-Fluid Flow Rate

W = 45 lb/hr $T_{H\ in} = 410°F$ $T_{in} = 140°F$ T. S. valve at nominal setting
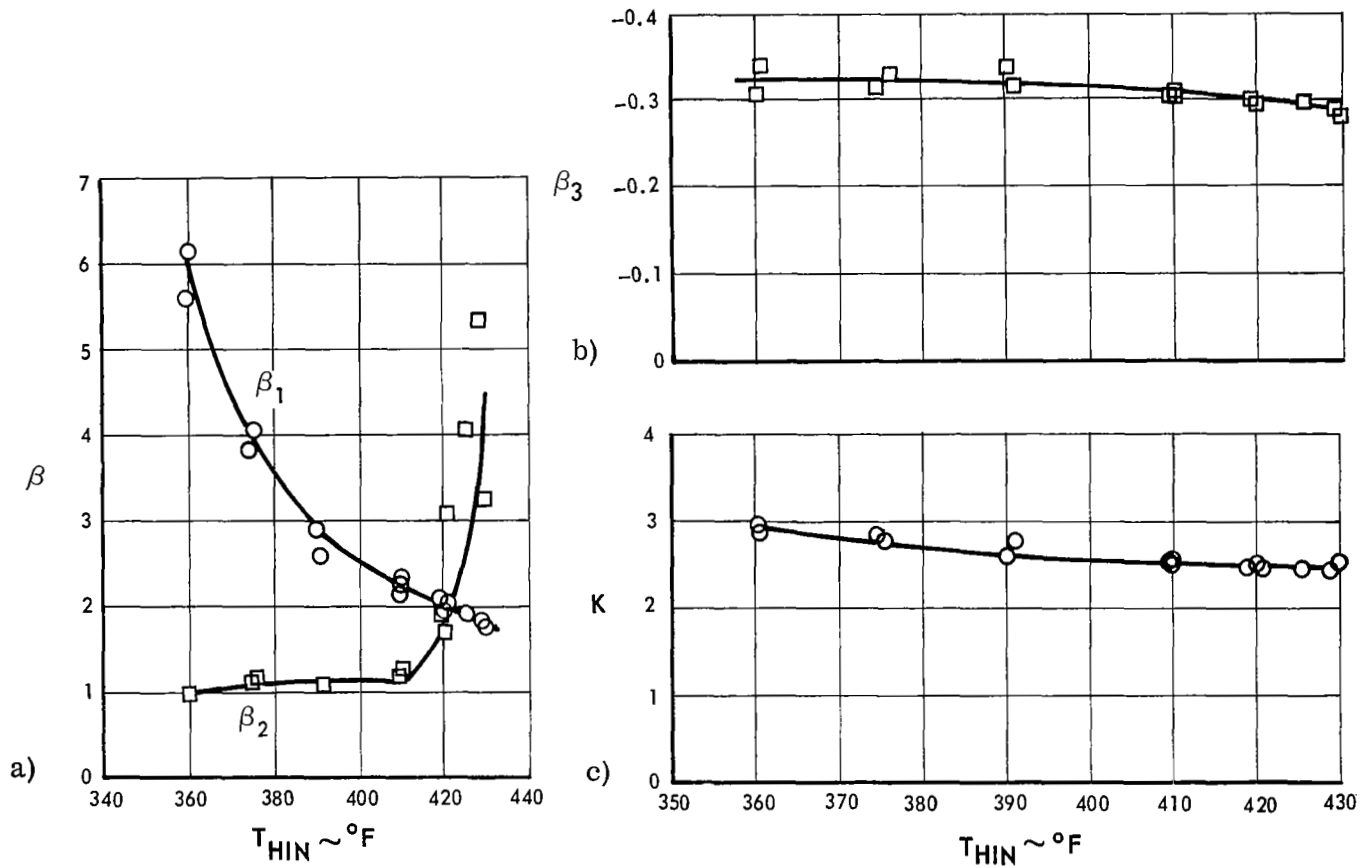
Figure 64   Variation of Boiler Parameters with Heating-Fluid Inlet Temperature

W . = 45 lb/hr T_{in} = 140°F W_H = 770 lb/hr   T.S. valve at nominal setting
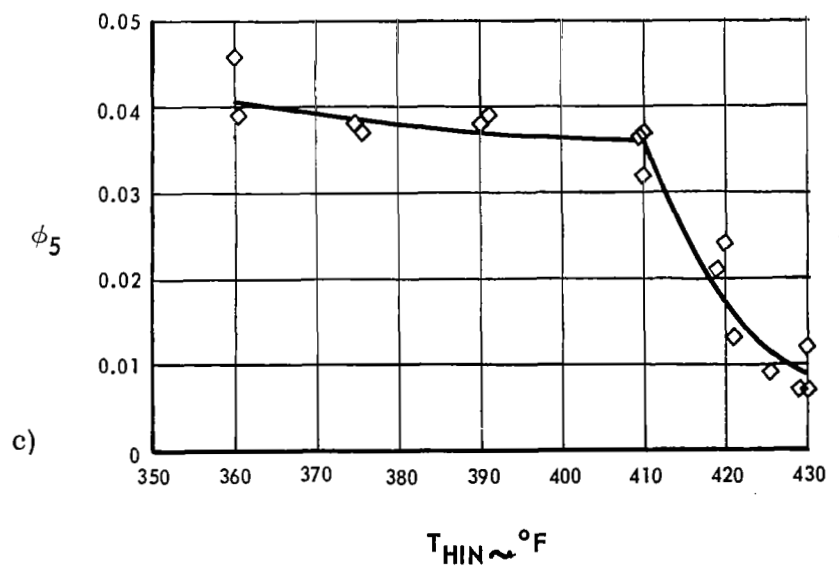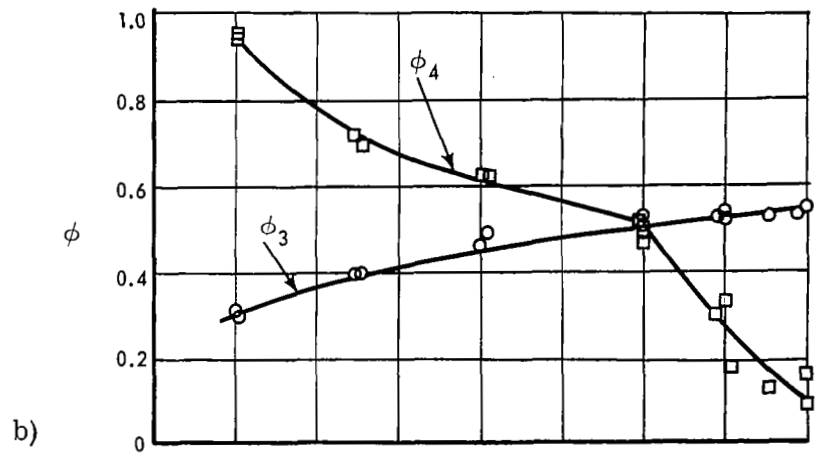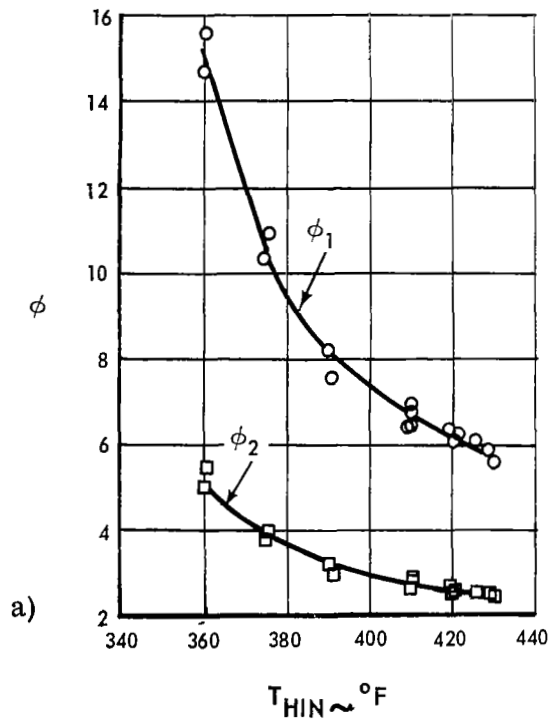
Figure 65 Variation of Boiler Parameters with Heating-Fluid Inlet Temperature
W = 45 lb/hr T_{in} = 140°F W_H = 770 lb/hr   T.S. valve at nominal setting.
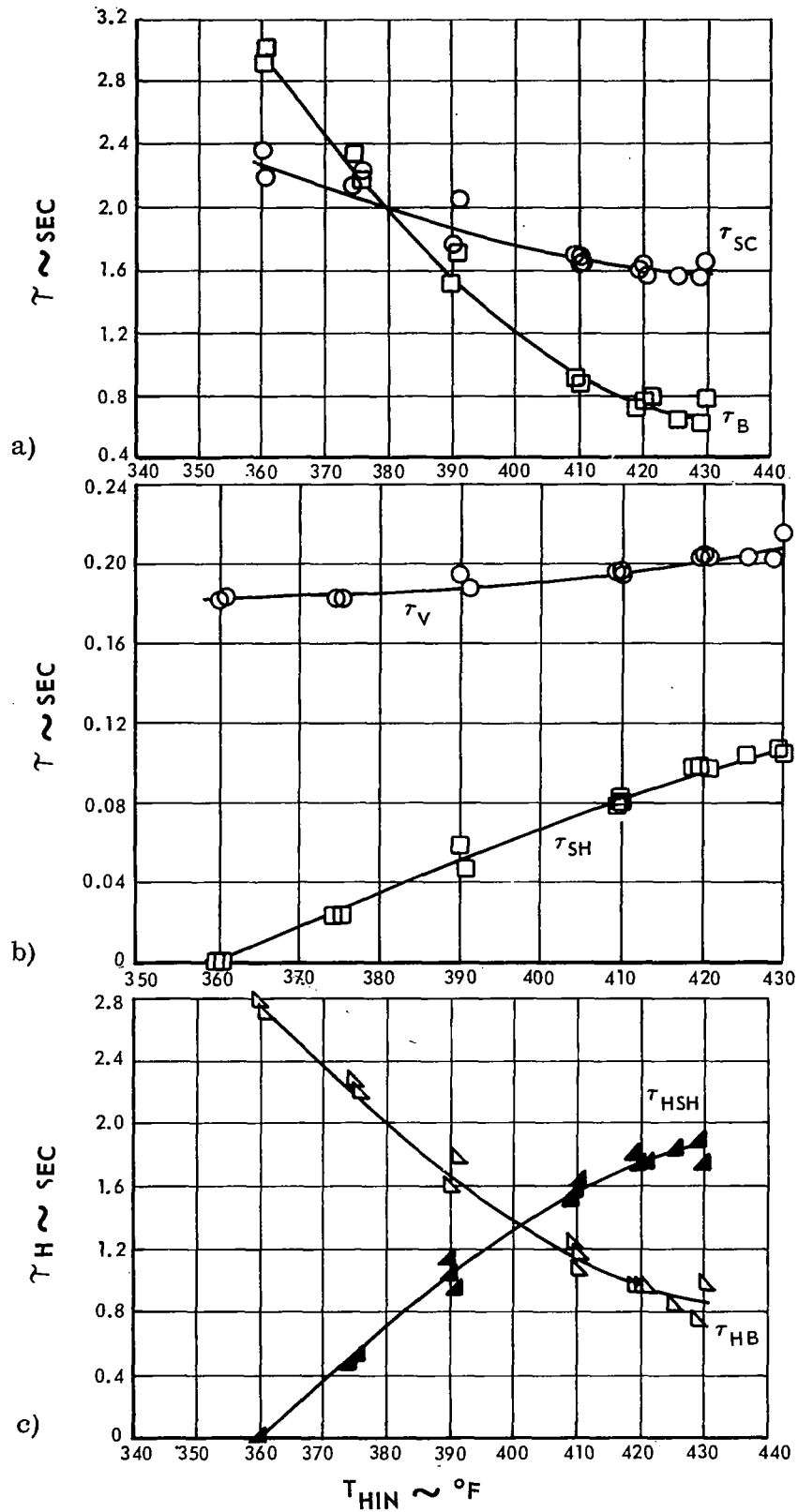
Figure 66   Variation of Boiler Parameters with Heating-Fluid Inlet Temperature
$W = 45 \text{ lb/hr}$ $T_{in} = 140°F$ $W_H = 770 \text{ lb/hr}$ T.S. valve at
nominal setting
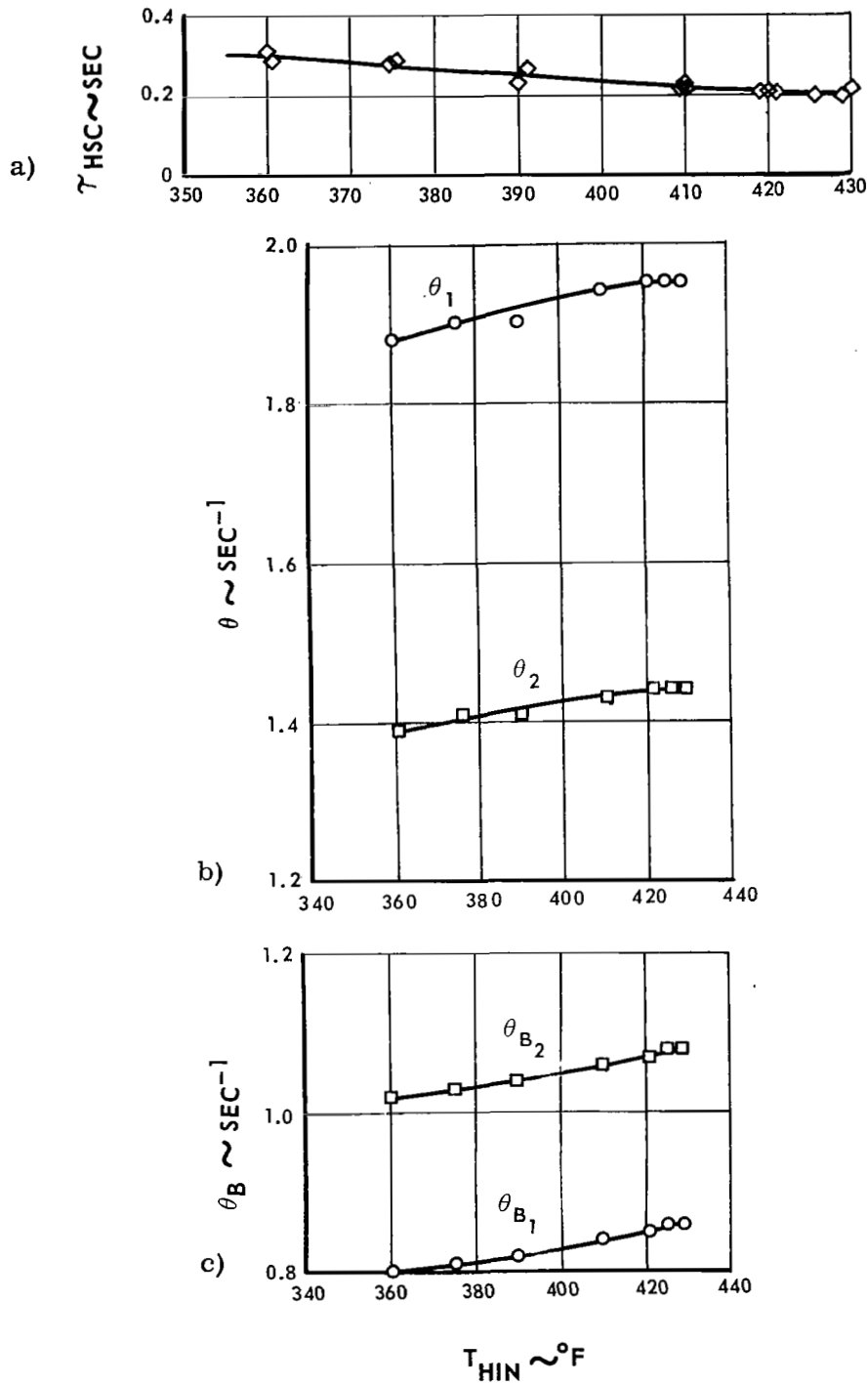
Figure 67 Variation of Boiler Parameters with Heating-Fluid Inlet Temperature

W = 45 lb/hr T_{in} = 140°F W_H = 770 lb/hr T.S. valve at
nominal setting
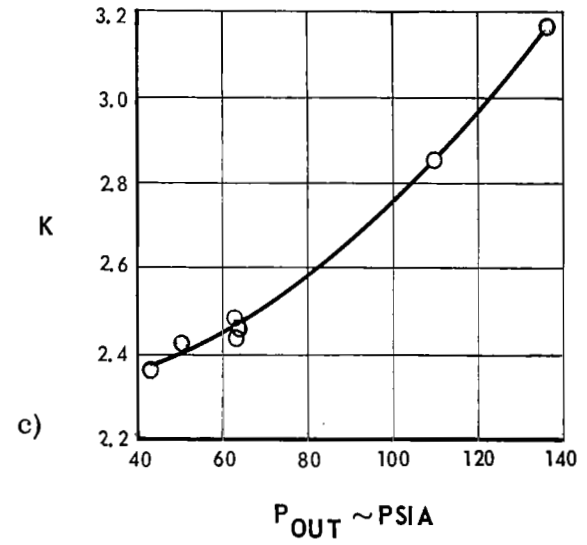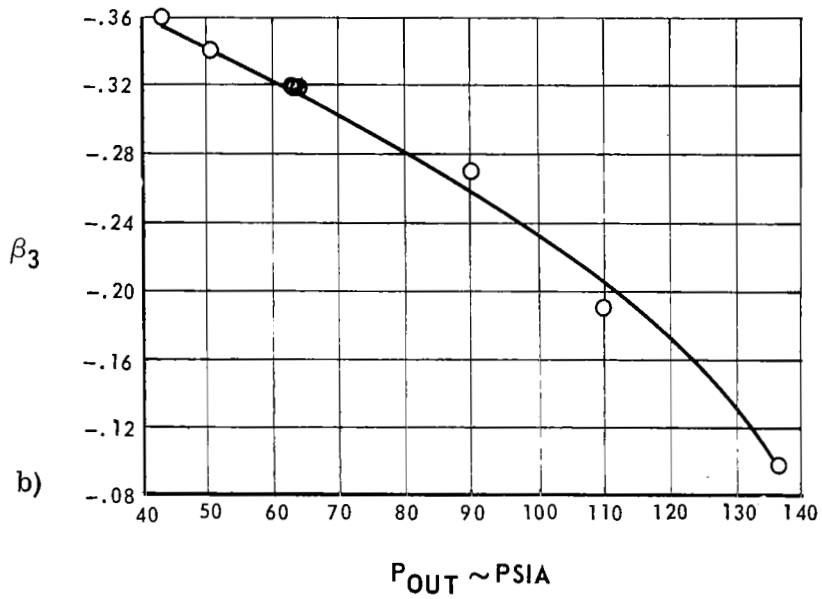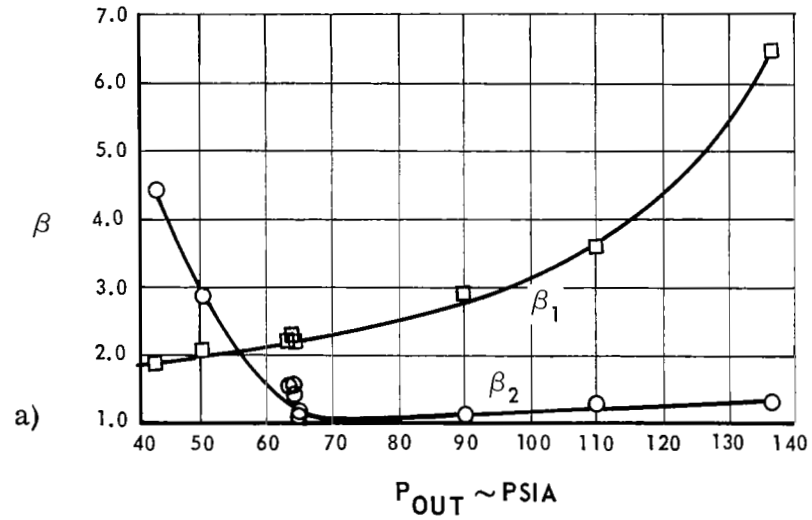
Figure 68 Variation of Boiler Parameters with Boiling-Fluid Exit Pressure

W = 45 lb/hr T_{in} = 140°F W_H = 770 lb/hr T_H in= 410°F
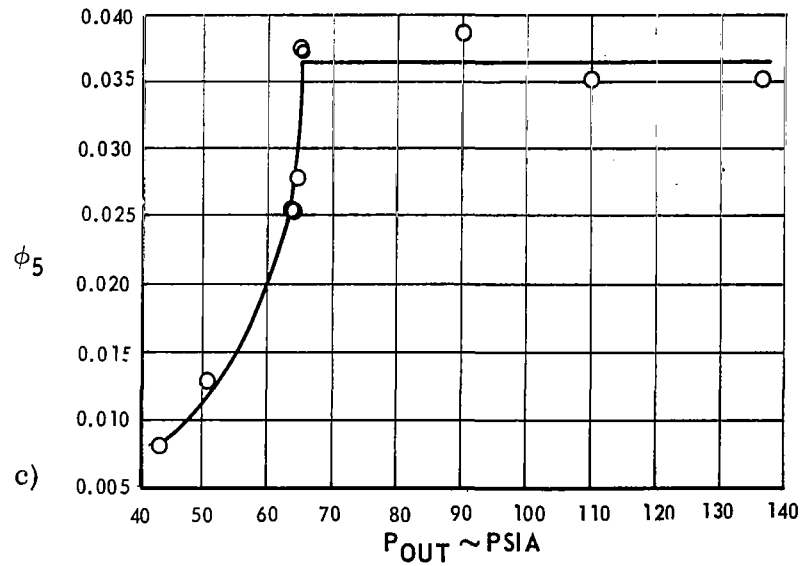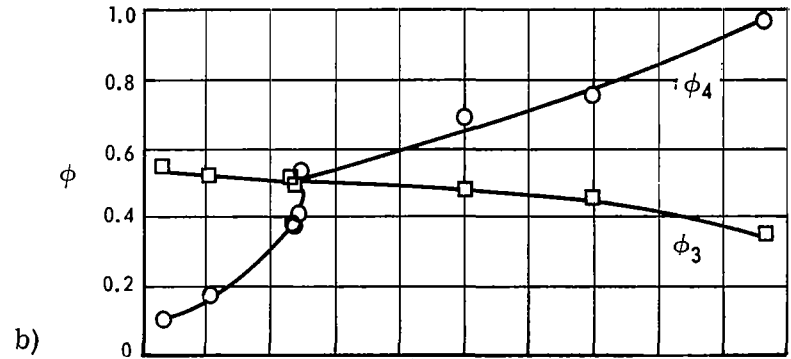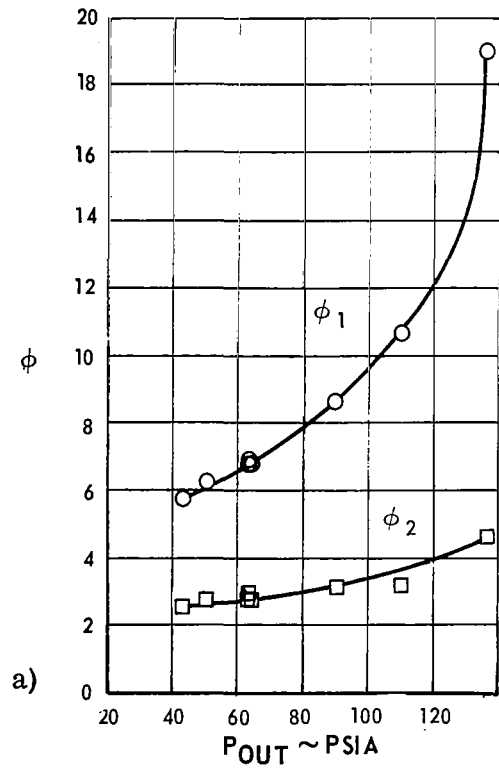
Figure 69   Variation of Boiler Parameters with Boiling-Fluid Exit Pressure

W = 45 lb/hr T_{in} = 140°F W_H = 770 lb/hr $T_{H\ in}$= 410°F
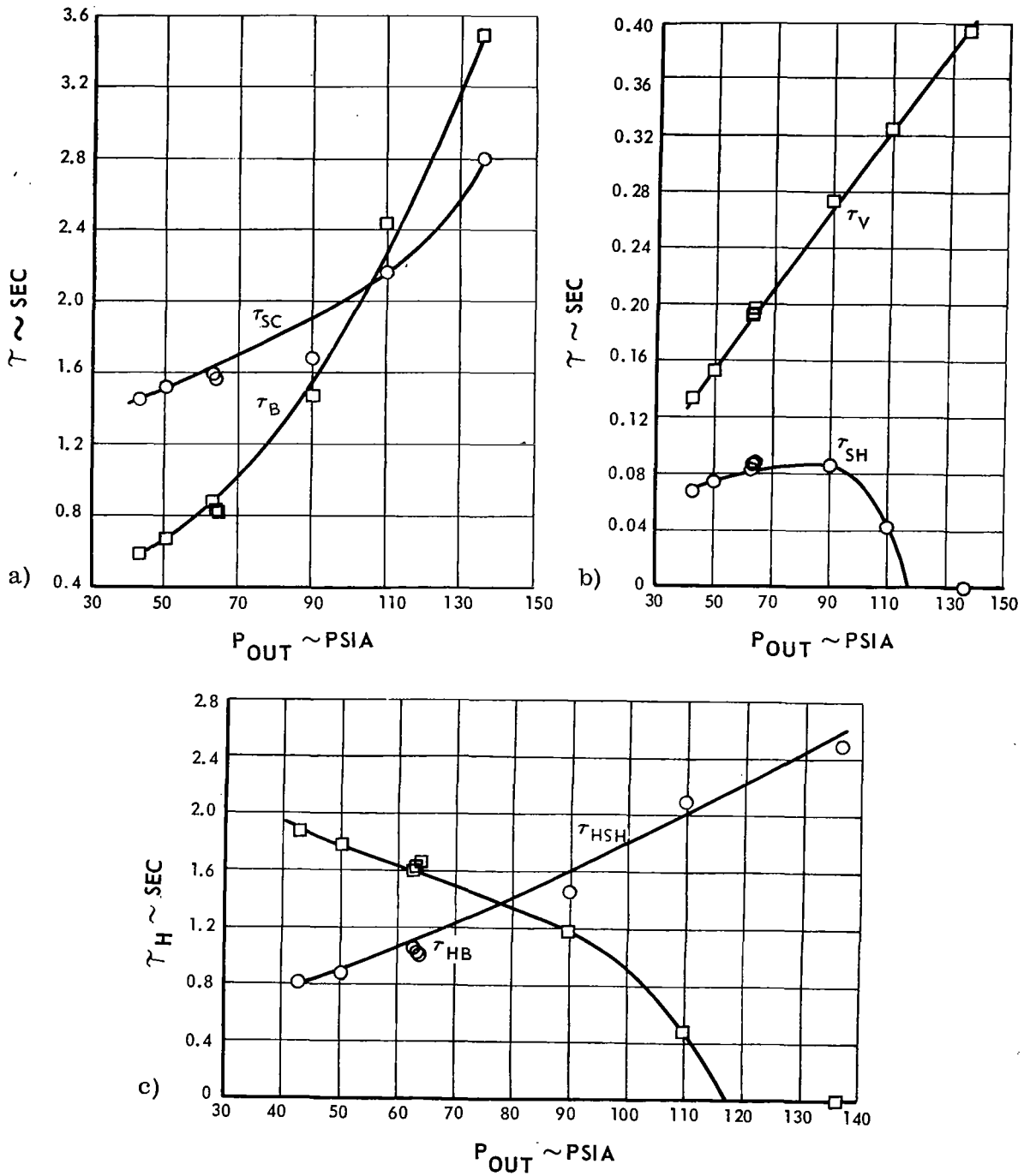
Figure 70 Variation of Boiler Parameters with Boiling-Fluid Exit Pressure

$W = 45$ lb/hr $\qquad$ $T_{in} = 140°F$ $\qquad$ $W_H = 770$ lb/hr $\qquad$ $T_{H\ in} = 410°F$
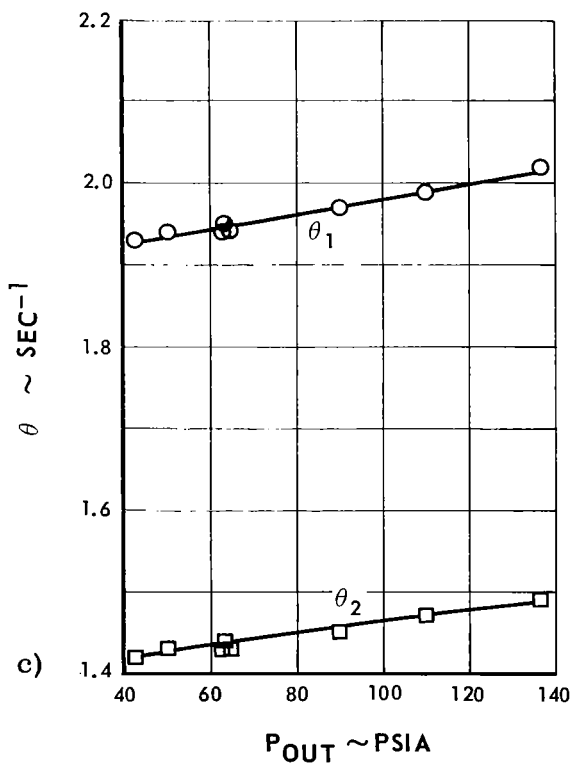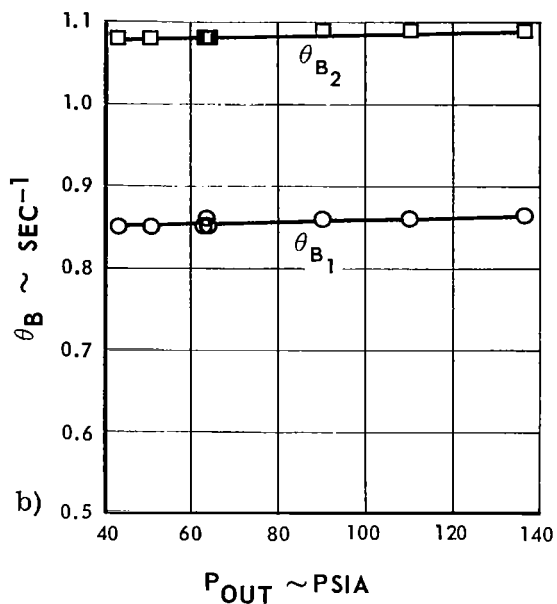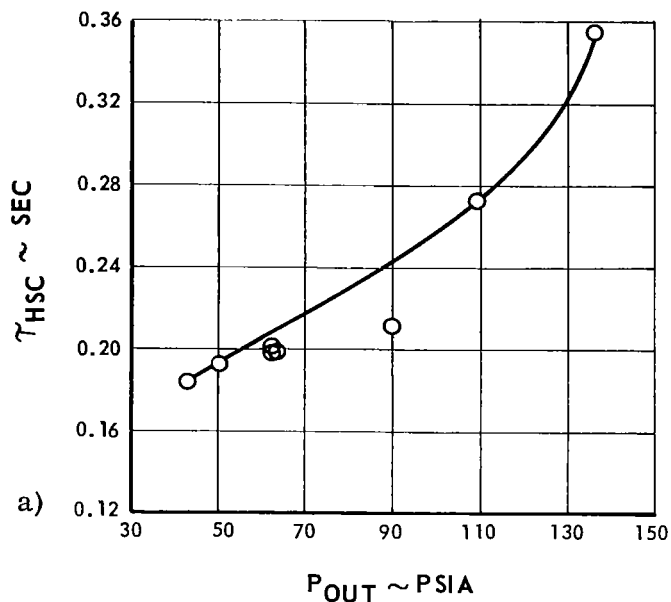
Figure 71 Variation of Boiler Parameters with Boiling-Fluid Exit Pressure

W = 45 lb/hr T_{in} = 140 °F W_H = 770 lb/hr $T_{H\ in}$ = 410°F
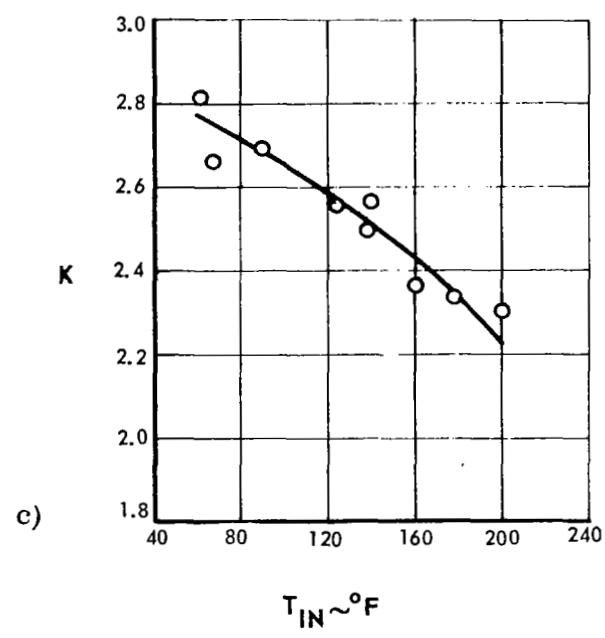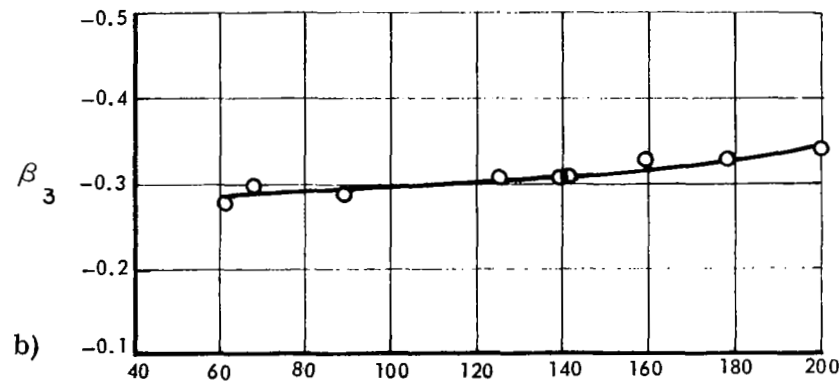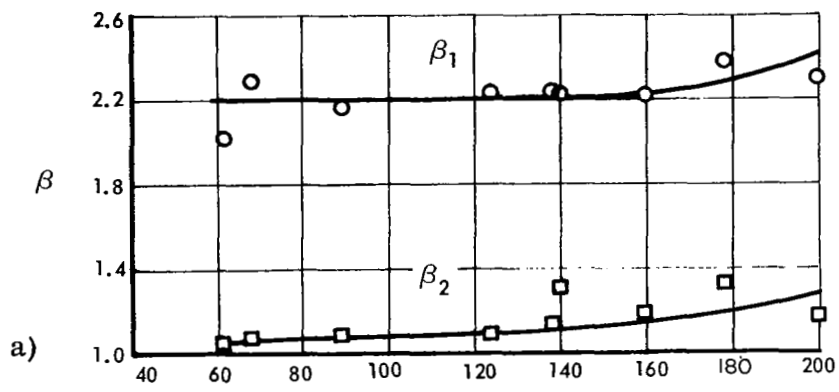
Figure 72 Variation of Boiler Parameters with Boiling-Fluid Inlet Temperature

W = 45 lb/hr W_H = 770 lb/hr   T.S. valve at T_H in= 410°F
nominal setting
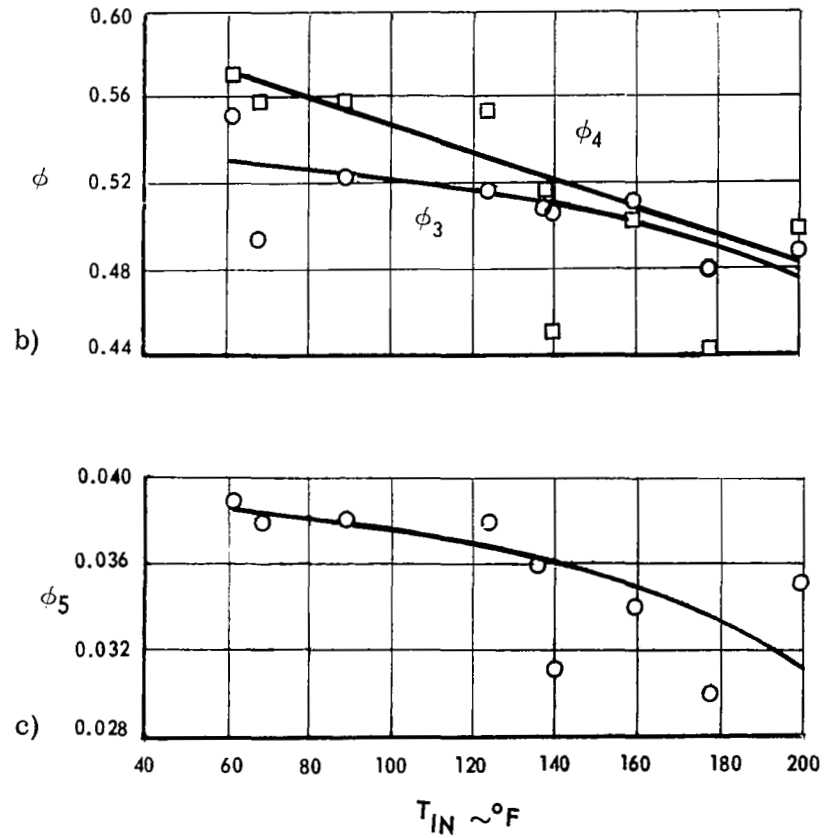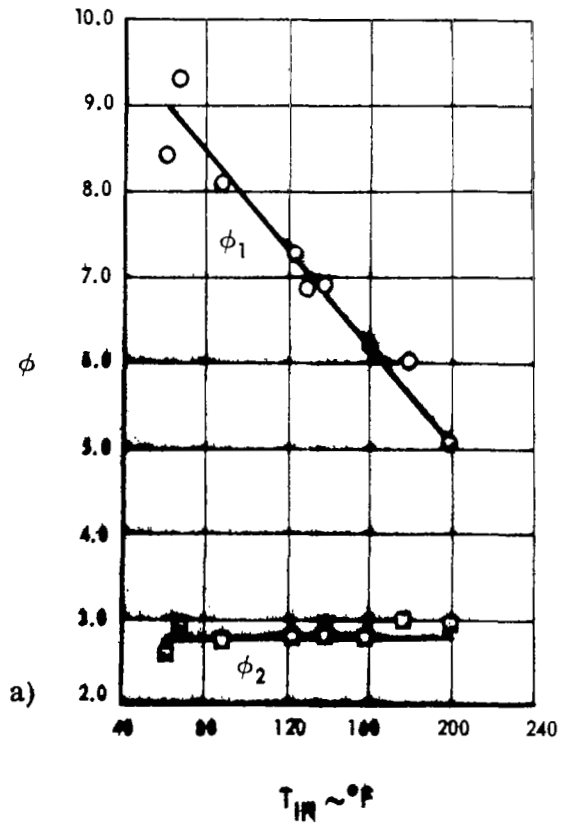
Figure 73 Variation of Boiler Parameters with Boiling-Fluid Inlet Temperature

W = 45 lb/hr W_H = 770 lb/hr   T.S. valve at nominal setting $T_{H\ in}$ = 410°F
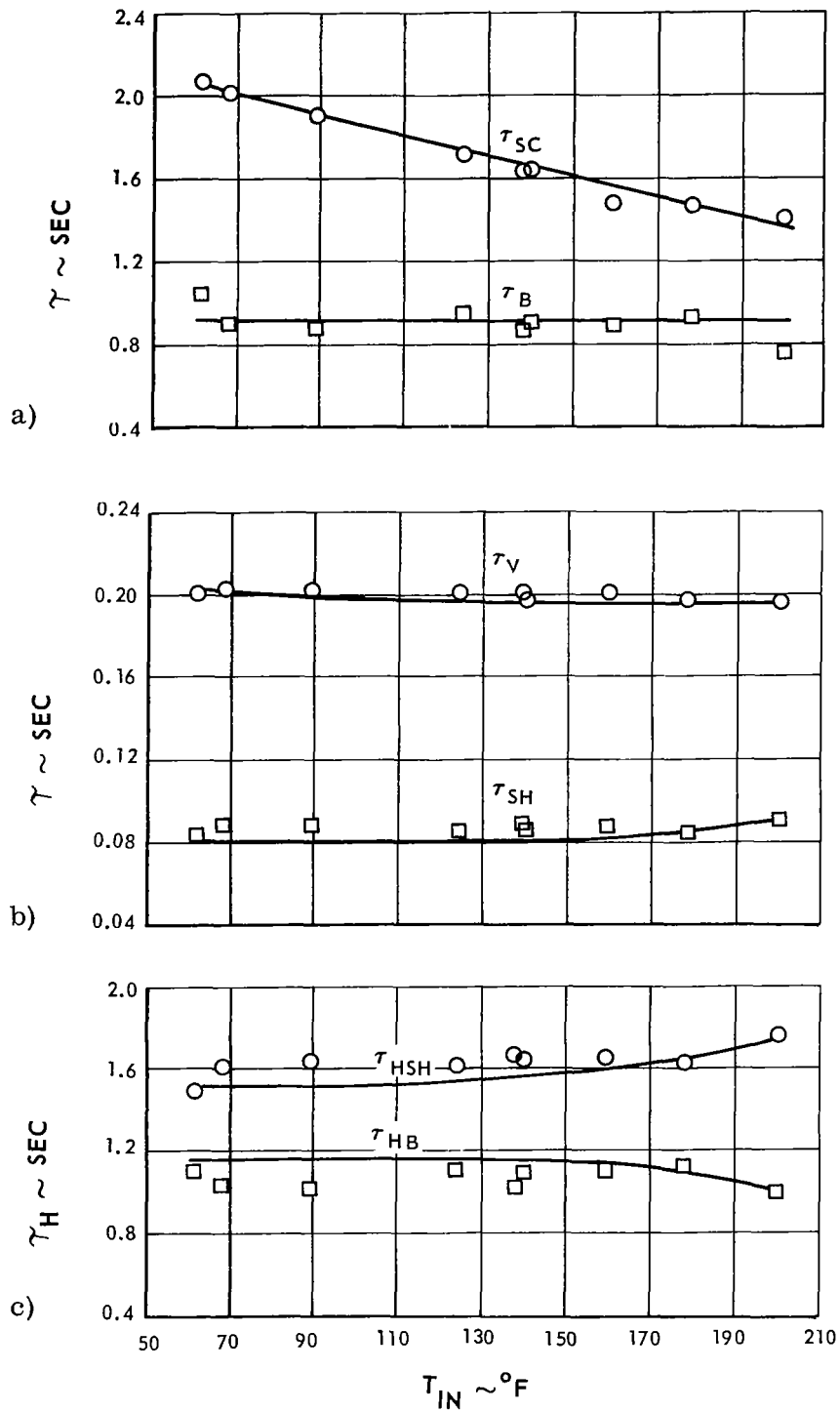
Figure 74 Variation of Boiler Parameters with Boiling-Fluid Inlet Temperature

W $= 45$ lb/hr   W $_H$ $= 770$ lb/hr   T.S. valve at T_H in$= 410°F$
                                                nominal setting
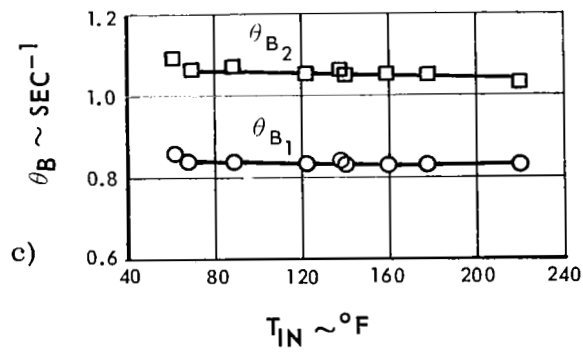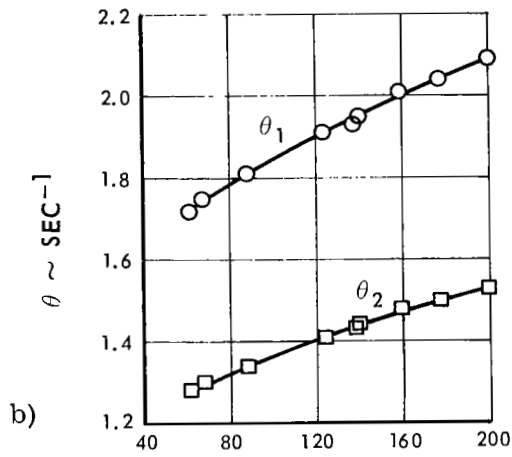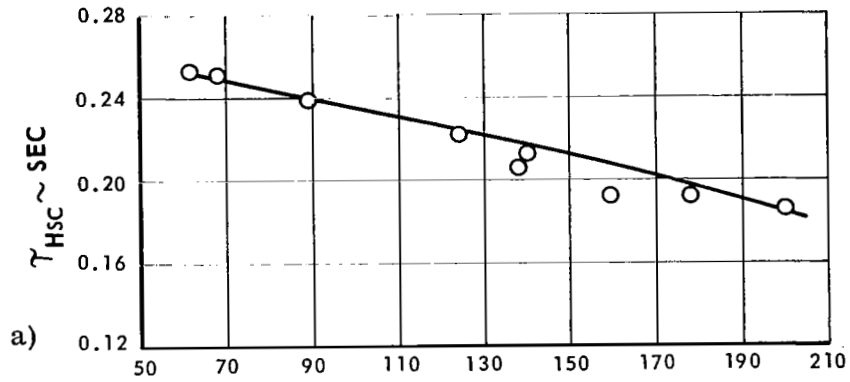
Figure 75 Variation of Boiler Parameters with Boiling-Fluid Inlet Temperature

W = 45 lb/hr W_H = 770 lb/hr   T.S. valve at $T_{H\ in}$ = 410°F
                                       nominal setting

APPENDIX 4

Tables

TABLE 1

Boiler Thermocouple Locations

Boiler Shell

Thermocouple Number	*Distance, Inches	Thermocouple Number	Distance, Inches
1	6	11	60
2	12	12	66
3	15	13	72
4	18	14	78
5	24	15	84
6	30	16	90
7	36	17	96
8	42	18	102
9	48	19	108
10	54	20	114

Boiler Plug Insert

1	3.6	5	14.4
2	7.2	6	16.3
3	9.6	7	20.4
4	12.0	8	22.8

Thermocouple Probe

1	30
2	60
3	84
4	96
5	108

*Axial distances from base of spiralled plug insert

TABLE 2

Test System Instrumentation

	Location	Type	Make and Model	Range	Estimated Accuracy	Estimated Time Constant
	(See Figure 4) T_6, T_7, T_8, T_9, T_{10}, T_{11}, T_{12}, T_{13}, T_{14}	thermocouple	1/16" chromel-alumel sheathed sealed junction	–	±1.5°F	100 millisec.
Temperatures	T_2 T_4	thermocouple	0.020" chromel-alumel sheathed exposed junction	–	±1.5°F	40 millisec.
	T_3	thermocouple	0.20" chromel-alumel sheathed sealed junction	–	±1.5°F	200 millisec.
	T_1 T_5	thermocouple	1/32" chromel-alumel sheathed sealed junction	–	±1.5°F	75 millisec.
Pressures A. Transients	P_{t1}	strain gage transducer	CEC Model 4-316-0001	0~150 psig	±1.3% F.R.	1 millisec.
	P_{t2}	strain gage transducer	CEC Model 4-316-0001	0~150 psig	±1.0% F.R.	1 millisec.
	P_{t3}	strain gage transducer	CEC Model 4-326-0003	0~40 psig	±1.5% F.R.	1 millisec.
	P_{t4}	strain gage transducer	CEC Model 4-312-0001	±25 psid	±1.0% F.R.	–
	P_1	Bourdon-tube gage	Heise 16" with Auto Thermal Compensator	0~200 psig	±0.1% F.R.	–
	P_2	Bourdon-tube gage	Heise 16" with Auto Thermal Compensator	0~150 psig	±0.1% F.R.	–
B. Steady State	P_3, P_4	Bourdon-tube gage	Helicoid Type 410 4-1/2"	-30"-30 psig	±1.5% F.R.	–
	P_5	Bourdon-tube gage	Helicoid Type 410 4-1/2"	0~200 psig	±1.5% F.R.	–
	P_6, P_8	Bourdon-tube gage	Barton Instrument 5-1/2"	0-15 psid	±1.5% F.R.	–
	P_7	Bourdon-tube gage	Barton Instrument 3"	0-70 psid	±2.0% F.R.	–
	P_9, P_{10}	Bourdon-tube gage	Helicoid Type 410 4-1/2"	0~1000 psig	±1.5% F.R.	–
	P_{11}	Bourdon-tube gage	Helicoid Type 410 4-1/2"	0~200 psig	±1.5% F.R.	–
Flows	F_1, F_2	turbine flowmeter	Potter, Model 60-4115 Micro Flowmeter	20-200 pph	±0.25% repeatability ±1.0% F.R. linearity	5 millisec.
	F_3, F_4	turbine flowmeter	Fischer & Porter, Model 10C 1505, 1/2 - 4	100-5000 pph	±1.5% F.R.	
	O_1	orifice	P & WA	45 lb/hr at 0.5 psi		
	O_2	orifice	P & WA	1100 lb/hr at 15 psi		
	O_3	orifice	P & WA	400 lb/hr at 60 psi		
Auxiliary Equip.	1	flowmeter frequency translator	P&WA Model 1158-004	0-200 & 0-1000 pph	±1.0% F.R.	20-25 millisec.
		thermocouple translator	P&WA Model 851-1	150°F ref.	±2.0% F.R.	
		pressure pickup power supply	P&WA Model 840-20	0-12 vdc		
		frequency generator	Wavetek Model 112	0.0015 Hz-10 KHz	0.5% F.R.	
		recording oscillograph	CEC., 50 Channel Model T5-119		3.0% absolute 1.0% variation	
		T.C. readout potentiometer	Brown Model 156 Vertical Scale	0-600°F	±0.2% F.R.	

TABLE 3

Operating Conditions for Steady-State Tests

Heating-Fluid Inlet Temperature, °F	Heating-Fluid Flow Rate, lb/hr	Boiling-Fluid Flow Rate, lb/hr	Boiling-Fluid Inlet Temperature, °F	Boiling-Fluid Exit Pressure, psia
360	770	45	140	*
375	770	45	140	*
390	770	45	140	*
420	770	45	140	*
425	770	45	140	*
430	770	45	140	*
410	400	45	140	*
410	500	45	140	*
410	600	45	140	*
410	840	45	140	*
410	910	45	140	*
410	1000	45	140	*
410+	770+	25+	140+	*+
410	770	30	140	*
410	770	40	140	*
410**	770**	45**	140**	65**
410	770	55	140	*
410	770	60	140	*
410	770	65	140	*
410	770	70	140	*
410	770	80	140	*
410	770	100	140	*

TABLE 3 (CONTINUED)

Operating Conditions for Steady-State Tests

Heating-Fluid Inlet Temperature, °F	Heating-Fluid Flow Rate, lb/hr	Boiling-Fluid Flow Rate, lb/hr	Boiling-Fluid Inlet Temperature, °F	Boiling-Fluid Exit Pressure, psia
410	770	45	60	*
410	770	45	90	*
410	770	45	120	*
410	770	45	160	*
410	770	45	180	*
410	770	45	200	*
410	770	45	140	40
410	770	45	140	50
410	770	45	140	60
410	770	45	140	90
410	770	45	140	110
410	770	45	140	130

*Value determined by setting of turbine simulator valve at nominal operating conditions
**Nominal operating conditions
+Unstable operating region (see Section VI of report)

TABLE 4

Variables Recorded by Oscillograph

Variable	Range
boiling-fluid flow rate W	13-72 lb/hr
boiling-fluid inlet pressure P_{in}	0-120 psig
boiling-fluid exit pressure P_{out}	0-150 psig
boiling-fluid inlet temperature T_{in}	60-220°F
boiling-fluid exit temperature T_{out}	320-430°F
electrohydraulic valve position	0-100% of full stroke
power-loop orifice pressure drop	0-10 psid
heating-fluid flow rate W_H	240-1000 lb/hr
heating-fluid inlet temperature $T_{H\,in}$	320-430°F
heating-fluid exit temperature $T_{H\,out}$	320-430°F
boiling-fluid condenser inlet temperature	250-400°F
boiling-fluid condenser exit temperature	65-200°F
boiling-fluid condenser inlet pressure	0-40 psig
condenser coolant flow rate	120-800 lb/hr
condenser coolant inlet temperature	30-75°F
condenser coolant exit temperature	80-200°F

TABLE 5

Operating Conditions for Dynamic Tests

Heating-Fluid Inlet Temperature, °F	Heating-Fluid Flow Rate, lb/hr	Boiling-Fluid Flow Rate (mean), lb/hr	Boiling-Fluid Inlet Temperature, °F	Boiling-Fluid Exit Pressure (mean), psia	Screening Test Runs
360	770	45	140	*	no
390	770	45	140	*	no
420	770	45	140	*	no
430	770	45	140	*	no
410	400	45	140	*	yes
410	600	45	140	*	yes
410	840	45	140	*	no
410	1000	45	140	*	no
410	770	35	140	*	yes
410	770	40	140	*	yes
410	770	55	140	*	yes
410	770	65	140	*	yes
410	770	45	95	*	no
410	770	45	120	*	no
410	770	45	160	*	no
410	770	45	185	*	no
410	770	45	140	50	yes
410	770	45	140	60	yes
410**	770**	45**	140**	65**	yes
410	770	45	140	100	yes
410	770	45	140	130	yes

*Value determined by setting of turbine simulator valve at nominal operating conditions
**Nominal operating conditions

TABLE 6

Steady-State Test Results – Variation of Boiling-Fluid Flow Rate

Point No.	Boiling-Fluid Flow Rate, lb/hr W	Heating-Fluid Flow Rate, lb/hr W_H	Boiling-Fluid Inlet Temp., °F T_{in}	Heating-Fluid Inlet Temp., °F $T_{H\,in}$	Boiling-Fluid Exit Pressure, psia P_{out}	Boiling-Fluid Pressure Drop, psi ΔP_B	Boiling-Fluid Exit Temp., °F T_{out}	Heating-Fluid Exit Temp., °F $T_{H\,out}$	Pinch-Point Temp. Difference, °F ΔT_P	Boiling-Fluid Superheat, °F ΔT_{SH}	Boiling-Fluid Exit Quality X_e	Heat Balance Btu/hr × 10⁻³ Q Boiler Shell	Q Cond Shell	Length of Subcooled Region, ft L_{SC}	Distance to End of Boiling Region, ft L_B
1	30	762	140	410	47.4	39.4	401.5	369.5	50	124	1.000	33.1	32.7	0.48	2.08
2	35	767	140	409.5	52.7	35.2	402	364	48	117	1.000	37.6	38.0	0.55	3.07
3	39.7	765	140	410	60	28.9	392	356	36	99	1.000	44.2	43.3	0.62	3.46
4	40	764.8	140	410	60.1	30.1	398	357	40	105	1.000	43.4	44.2	0.63	3.96
5	44.1	767.5	139	410	64.5	26.2	350.5	351	34	53	1.000	48.7	49.6	0.72	4.65
6	44.5	767	139	409.5	64.7	25.8	350	352.5	34	52	0.982	47.0	47.0	0.72	4.80
7	44.6	765	140	411	64.5	24.8	343	351.5	34	46	1.000	48.7	47.3	0.71	4.62
8	44.8	765	140	411	64.4	25.3	350	352	33	53	1.000	48.3	47.4	0.74	4.26
9	44.8	765	140	410	64.9	24.1	347	350	32	50	1.000	49.1	48.5	0.80	4.62
10	49.6	760.8	140	410	68.4	22	344	344	30	43	1.000	53.4	52.4	0.80	7.00
11	49.8	770.8	140	410	69.7	22.6	347	347	32	44	0.963	51.8	53.8	0.77	6.60
12	54.5	760	140	409.5	74.7	18	343	340	25	35.4	0.965	56.8	58.5	1.05	8.43
13	55.3	762	142	409	74.5	17.7	343	339	23	36	0.951	56.8	57.3	0.99	8.63
14	59.4	767.8	140	410	78.4	15.8	330	335	20	20	0.948	61.0	60.4	1.00	9.43
15	59.6	770.8	140	410	80.8	14.1	333	337	22	20	0.920	59.8	61.5	1.06	9.50
16	60	765	141.5	410	79	15.7	335	335	20	24	0.932	60.7	59.9	1.01	9.34
17	64.6	765	142	409.5	83	12.9	318	332	20	3.5	0.892	63.1	61.9	1.32	10.00
18	70.7	767.5	141	410	87.1	11.9	320.5	331	18.5	2.5	0.819	64.6	65.9	1.44	10.00
19	79.7	770.8	141	410	89.3	11.4	323	330.5	18	4	0.712	65.3	66.3	1.60	10.00
20	100.2	760.8	140	410	91.6	12	325	327.5	18	3.0	0.542	67.1	66.9	1.95	10.00

TABLE 7

Steady-State Test Results – Variation Of Heating-Fluid Flow Rate

Point No.	Boiling-Fluid Flow Rate, lb/hr	Heating-Fluid Flow Rate, lb/hr	Boiling-Fluid Inlet Temp., °F	Heating-Fluid Inlet Temp., °F	Boiling-Fluid Exit Pressure, psia	Boiling-Fluid Pressure Drop, psi	Boiling-Fluid Exit Temp., °F	Heating-Fluid Exit Temp., °F	Pinch-Point Temp. Difference, °F	Boiling-Fluid Superheat, °F	Boiling-Fluid Exit Quality	Heat Balance $B_{tu}/hr \times 10^{-3}$		Length of Subcooled Region, ft	Distance to End of Boiling Region, ft
	W	W_H	T_{in}	$T_{H\ in}$	P_{out}	ΔP_B	T_{out}	$T_{H\ out}$	ΔT_P	ΔT_{SH}	X_e	Q Boiler Shell	Q Cond Shell	L_{SC}	L_B
21	44.5	391.4	140	410	56.2	12.6	331	311	20	43	0.843	41.2	44.2	1.00	9.25
22	44.0	391.8	139	411	58.2	11.0	321	308.5	19	30.3	0.888	42.6	45.9	1.05	9.70
23	44.7	395	140	410	60	9.5	321	307	17	28.3	0.914	44.3	45.1	1.20	10.0
24	44.5	400	139	411	58.7	11.0	310	310	20	18.4	0.880	42.8	44.7	1.20	10.0
25	44.5	500	140.5	409	61.4	14.8	336	324	22	42	0.941	45.2	46.2	0 91	7.36
26	44.5	501	140	411.5	60.7	15.6	336	325	25	42.5	0.962	46.1	47.6	0.91	8.10
27	44.5	594	140	409	61.6	19.4	340	336	31	45.0	0.962	46.2	46.7	0.82	7.28
28	44.5	596	141.5	409	61.2	19.7	338	336	28	44.2	0.958	45.9	48.4	0.85	6.78
29	44.6	604	141	410	62.1	20.1	342	337.5	28	47	0.976	46.7	46.7	0.78	5.43
30	44.6	755	138	410.5	64.1	27.0	336	352	33	36	0.991	47.5	47.8	0.70	4.65
31	44.5	758	140	409.5	64.2	25.8	349	351	33	50	0.994	47.4	47.7	0.70	4.49
32	44.5	835	141.5	411	65.3	28.6	372	358	34	74	0.975	46.6	48.0	0.69	3.84
33	44.5	853.9	139.5	410	64.4	28.4	356.5	355	33	59.5	1.000	50.6	47.8	0.69	4.20
34	44.5	856	140	409	65.3	28.9	366	355	35	67.7	1.000	49.6	48.5	0.73	4.30
35	44.4	890	142	409.5	65	29.7	374	359	32	76	1.000	48.2	48.4	0.67	3.95
36	44.3	899.9	139.5	410	66.4	29.9	379	359	37	79.6	1.000	49.7	49.2	0.70	4.08
37	44.7	955	139	409	67.2	29.0	390.5	362	36	90.3	1.000	49.9	48.5	0.67	4.00
38	44.3	1019	139	411	68.4	32.3	396	366	40	95	1.000	49.1	49.0	0.65	4.05

TABLE 8

Steady-State Test Results - Variation of Heating-Fluid Inlet Temperature

Point No.	Boiling-Fluid Flow Rate, lb/hr W	Heating-Fluid Flow Rate, lb/hr W_H	Boiling-Fluid Inlet Temp., °F T_{in}	Heating-Fluid Inlet Temp., °F $T_{H\ in}$	Boiling-Fluid Exit Pressure, psia P_{out}	Boiling-Fluid Pressure Drop, psi ΔP_B	Boiling-Fluid Exit Temp., °F T_{out}	Heating-Fluid Exit Temp., °F $T_{H\ out}$	Pinch-Point Temp. Difference, °F ΔT_P	Boiling-Fluid Superheat, °F ΔT_{SH}	Boiling-Fluid Exit Quality X_e	Heat Balance Btu/hr × 10⁻³ Q Boiler Shell	Q Cond Shell	Length of Subcooled Region, ft L_{SC}	Distance to End of Boiling Region, ft L_B
39	44.3	768.3	139.5	360	57.5	9.5	293	309	12	3	0.841	41.0	43.2	1.0	10
40	44.6	774	141.5	360.5	58.2	9.4	294	308	11	23.2	0.875	42.5	42.2	0.93	10
41	44.5	776	141	374.5	59.2	14.4	315	321	18	23.2	0.908	43.8	45.6	0.91	8.37
42	44.3	766	140	375.5	60.2	15.2	318	320	17	25	0.932	44.7	44.2	0.92	8.27
43	44.4	767	140.5	390	61.7	18.3	330	333	24	36	0.971	46.3	45.6	0.75	6.14
44	44.3	773	138	391	61.1	19.4	330	335	27	36.1	0.959	45.8	46.5	0.87	6.77
45	44.6	765	139.5	410	64.6	25.3	350	351	32	53	1.000	48.3	47.1	0.71	4.39
46	44.6	762	141	410	64.8	25.4	357	350.5	31	50	1.000	48.5	48.2	0.71	4.38
47	44.5	759	140	419	66.7	29.0	383	358	35	83.3	1.000	49.1	48.5	0.68	3.84
48	44.5	776.9	141	420	66.2	29.7	379.5	359	37.5	80.5	1.000	51.3	48.6	0.70	3.93
49	44.8	759	140	421	67.5	28.4	399	361	36	99	1.000	49.1	49.1	0.67	4.00
50	44.5	768	139.5	425.5	67.9	30.8	409	365.5	38	108	1.000	49.8	48.9	0.66	3.57
51	44.4	768	141	429	67.9	32.5	416.5	369.5	40	116	1.000	49.5	48.9	0.66	3.44
52	44.3	759.3	139	430	70.8	29.6	409	368	42	105	1.000	50.9	49.6	0.70	3.93

TABLE 9

Steady-State Test Results - Variation of Boiling-Fluid Inlet Temperature

Point No.	Boiling-Fluid Flow Rate, lb/hr W	Heating-Fluid Flow Rate, lb/hr W_H	Boiling-Fluid Inlet Temp., °F T_{in}	Heating-Fluid Inlet Temp., °F $T_{H\,in}$	Boiling-Fluid Exit Pressure, psia P_{out}	Boiling-Fluid Pressure, Drop, psi ΔP_B	Boiling-Fluid Exit Temp., °F T_{out}	Heating-Fluid Exit Temp., °F $T_{H\,out}$	Pinch-Point Temp Difference, °F ΔT_P	Boiling-Fluid Superheat, °F ΔT_{SH}	Boiling-Fluid Exit Quality X_e	Heat Balance Btu/hr $\times 10^{-3}$ Q Boiler Shell	Q Cond Shell	Length of Subcooled Region, ft L_{SC}	Distance to End of Boiling Region, ft L_B
53	44.3	784	61.5	409	65.7	22.0	346	344.5	35	48	1.000	54.0	53.9	0.86	4.74
54	44.2	767	68	409.5	66.0	23.4	348	346.5	31	49	1.000	51.7	51.5	0.84	4.42
55	44.5	769	89	409.5	66.0	23.9	348	348	33	49	1.000	50.6	49.7	0.80	4.34
56	44.6	761	124	409	65.3	24.9	348	350	32	50	0.990	48.1	49.2	0.73	4.50
57	44.2	767	138	410	64.7	26.3	352	353	32	56	0.985	46.8	48.1	0.69	4.23
58	44.6	761	140	409.5	64.4	26.5	359	352.5	32	62	0.966	46.4	46.8	0.70	4.41
59	44.5	758	159.5	409	64.7	26.2	353	353	32	56	0.967	45.5	45.7	0.63	4.36
60	44.5	758	178	410	64.0	27.4	360	355.5	30	63	0.959	44.3	45.5	0.63	4.45
61	44.8	761	200	410	64.6	26.2	353.5	355	31	56	0.998	45.2	43.4	0.61	4.00

TABLE 10

Steady-State Test Results - Variation Of Boiling-Fluid Exit Pressure

Point No.	W	W_H	T_{in}	$T_{H\,in}$	P_{out}	ΔP	T_{out}	$T_{H\,out}$	ΔT_P	ΔT_{SH}	X_e	Q Boiler Shell	Q Cond Shell	L_{SC}	L_B
62	44.7	779	141	410	43.1	40.2	396	351.5	37	124	1.000	48.8	49.2	0.62	3.46
63	44.8	779	139	410	50.3	35.0	388	351	34	107	1.000	49.2	49.6	0.65	3.75
64	44.7	779	140	409	63.0	27.1	367	351	32	71	1.000	48.4	49.0	0.68	4.38
65	45.0	782	140	410	63.7	26.2	368	353	31	73	0.988	47.7	48.6	0.67	4.26
66	44.7	779	139	410	64.1	27.3	364	352.5	32	67	1.000	47.9	49.0	0.67	4.19
67	44.7	782	141	410	89.9	15.0	348	354.5	25	28	0.959	46.5	46.0	0.72	5.86
68	44.8	782	140	410	109.8	9.9	353	356	21	19	0.919	45.2	45.5	0.93	8.30
69	44.8	782	140	410	136.5	5.0	353	358	12	2	0.872	43.6	43.2	1.21	10.0

TABLE 11

Normalizing Data (Amplitudes at Zero Frequency)

Variable	$\Delta P_{in}/\Delta W$ psi/lb/hr	$\Delta P_{out}/\Delta W$ psi/lb/hr	$\Delta T_{H\ out}/\Delta W$ °F/lb/hr	$\Delta T_{out}/\Delta W$ °F/lb/hr
W, lb/hr				
35	0.190	1.30	1.30	1.0
40	0.230	1.15	1.28	3.7
45	0.200	1.05	1.14	5.3
55	0.306	0.93	0.83	---
65	0.385	0.80	0.45	---
W_H, lb/hr				
400	0.212	0.915	1.35	---
600	0.258	1.08	1.42	---
770	0.200	1.05	1.15	5.3
840	0.224	1.12	1.12	5.9
1000	0.275	0.842	0.842	4.5
$T_{H\ in}$, °F				
360	0.226	0.556	0.61	---
390	0.250	0.950	1.10	---
410	0.200	1.05	1.14	5.3
420	0.255	1.05	1.25	7.4
430	0.231	1.08	1.43	3.92
P_{out}, psia				
50	-0.02	0.840	1.15	6.82
60	0.160	0.950	1.16	7.24
65	0.200	1.05	1.14	5.3
100	1.08	1.86	1.18	---
130	1.41	1.81	0.50	---
T_{in}, °F				
95	0.213	0.980	1.24	4.04
120	0.195	0.961	1.17	4.61
140	0.200	1.05	1.14	5.30
160	0.171	0.890	1.11	6.68
185	0.155	0.900	1.02	6.80

TABLE 12

Boiler Parameters Required for Theoretical Transfer Function

$$\beta_1 = \left(\frac{\partial\, T_{SAT} / \Delta T_{P,o}}{\partial\, P / P_{P,o}} \right)$$

$$\beta_2 = \left(\frac{\partial\, T_{SAT} / \Delta T_{OUT}}{\partial\, P / P_{OUT,o}} \right)$$

$$\beta_3 = \left(\frac{\partial\, \Delta P_B / P_{P,o}}{\partial\, L_{SC} / L_{SC,o}} \right)$$

$$\Theta_1 = \frac{h_{SC}\, P_{PM}}{\rho_L\, A_{SC}\, C_P}$$

$$\Theta_2 = \frac{h_{SC}\, P_{PM}}{\rho_{PM}\, A_{PM}\, C_{PPM}}$$

$$\Theta_{B1} = \frac{h_H\, P_{SM}}{\rho_H\, A_H\, C_{PH}}$$

$$\Theta_{B2} = \frac{h_H\, P_{SM}}{\rho_{SM}\, A_{SM}\, C_{PSM}}$$

$$K = \frac{\partial\left(\int_0^{L_e} \rho\, A\, dx \right)}{\partial\left(\rho_L\, A_{SC}\, L_{SC} \right)}$$

$$n_{SC} = \text{DEFINED BY } \mathcal{U}_{SC} \propto V_{SC}^{\,n_{SC}}$$

$$n_{SH} = \text{DEFINED BY } \mathcal{U}_{SH} \propto V_{SH}^{\,n_{SH}}$$

TABLE 12 (continued)

Boiler Parameters Required for Theoretical Transfer Function

$$\phi_1 = \frac{T_{HP,O} - T_{IN}}{\Delta T_{P,O}}$$

$$\phi_2 = \frac{T_{HIN} - T_{SAT,O}}{\Delta T_{P,O}}$$

$$\phi_3 = \frac{\Delta T_{P,O}}{\Delta T_M}$$

$$\phi_4 = \frac{\Delta T_{OUT}}{T_{HIN} - T_{SAT,O}_{OUT}}$$

$$\phi_5 = \frac{\Delta T_{OUT}}{2 T_{OUT,O}}$$

τ_B = transport time of liquid particle in boiling region

τ_{HB} = heating-fluid transport time in boiling region

τ_{HSC} = heating-fluid transport time in subcooled region

τ_{SC} = subcooled liquid transport time

τ_V = vapor transport time

τ_{SH} = vapor transport time in superheat region

τ_{HSH} = heating-fluid transport time in superheat region